U. S. ARMY
TRANSPORTATION RESEARCH COMMAND
FORT EUSTIS, VIRGINIA

TRECOM TECHNICAL REPORT 64-33

A STUDY OF RADIAL-FLOW FANS FOR GEM PROPULSION SYSTEM APPLICATIONS

FINAL REPORT

Task 1D021701A04809
Contract DA 44-177-AMC 886(T)

July 1964

prepared by:

AEROPHYSICS COMPANY
Washington, D. C.

DISCLAIMER NOTICE

When Government drawings, specifications, or other data are used for any purpose other than in connection with a definitely related Government procurement operation, the United States Government thereby incurs no responsibility nor any obligation whatsoever; and the fact that the Government may have formulated, furnished, or in any way supplied the said drawings, specifications, or other data is not to be regarded by implication or otherwise as in any manner licensing the holder or any other person or corporation, or conveying any rights or permission, to manufacture, use, or sell any patented invention that may in any way be related thereto.

* * *

DDC AVAILABILITY NOTICE

Qualified requesters may obtain copies of this report from

Defense Documentation Center
Cameron Station
Alexandria, Virginia 22314

* * *

This report has been released to the Office of Technical Services, U.S. Department of Commerce, Washington 25, D.C., for sale to the general public.

* * *

The findings and recommendations contained in this report are those of the contractor and do not necessarily reflect the views of the U.S. Army Mobility Command, the U.S. Army Materiel Command, or the Department of the Army.

HEADQUARTERS
U S ARMY TRANSPORTATION RESEARCH COMMAND
FORT EUSTIS, VIRGINIA 23604

Existing lift systems for air cushion vehicles (ACVs) display two fundamental weaknesses: excessive internal losses resulting in low system efficiencies and poor adaptability to fluctuations in cushion pressure.

Demonstrated performance of the rotating diffuser (RD) as a basic air mover eliminated the latter objection, although existing applications were designed without the weight considerations for airborne or air-supported operations. The following study analyzes the fan loadings and the configuration constraints for ACVs as they apply to the rotating diffuser and, through scale model tests, determines the internal efficiency of such a system.

The results indicate that consistently high internal efficiencies exceeding the best present ACV lift-system performance by 40-45 percent over a broad range of loadings can be provided by an RD fan system weighing no more than existing fan-duct-nozzle systems.

W. E. Sickles

WILLIAM E. SICKLES
Group Leader
Ground Effect Research Group

APPROVED.

FOR THE COMMANDER:

Larry M. Hewin

LARRY M. HEWIN
Technical Director

FINAL REPORT

Task 1D 021701A 04809
Contract DA 44-177-AMC 886(T)
TRECOM Technical Report 64-33

July 1964

A STUDY OF RADIAL-FLOW FANS FOR GEM PROPULSION SYSTEM APPLICATIONS

Prepared by

AEROPHYSICS COMPANY
Washington, D.C.

for

U.S. ARMY TRANSPORTATION RESEARCH COMMAND
FORT EUSTIS, VIRGINIA

PREFACE

The study presented in this report was undertaken by Aerophysics Company, Washington, D.C. 20036, as the prime contractor and by Joy Manufacturing Company, New Philadelphia, Ohio, as the subcontractor. The study was sponsored by the U.S. Army Transportation Research Command, Fort Eustis, Virginia.

This is the final report prepared under the contract, and it supersedes Phases I, II, III, and VI Reports. It contains the material of the Phase V Report in a slightly abridged form and that of the Phase IV Report (because of its limited interest) in a considerably abridged form. Copies of the Phase IV and Phase V Reports can be obtained on loan from the U.S. Army Transportation Research Command.

The program was carried out under the supervision of Dr. Gabriel D. Boehler. Other participating personnel were Messrs. W. Foshag and J.S. Karwoski of Aerophysics Company, and Messrs. J.A. Balciunas, J.E. Lieser, W.P. Schwanke, and W.W. Olson of Joy Manufacturing Company. The study began in October 1962 and was completed in January 1964. Mr. William Hinshaw was the Project Officer.

The authors are indebted to Mr. D. Winter of the U.S. Navy Bureau of Ships for providing information on the U.S. Navy SKMR-1 craft and to Mr. H. Chaplin for his contribution to the theoretical analysis. The generous help of Etablissements Neu in providing extensive background material on the RD fan is gratefully acknowledged.

CONTENTS

CONTENTS (continued)

CONTENTS (continued)

LIST OF ILLUSTRATIONS

LIST OF TABLES

List of Symbols*

A_o	fan impeller eye area
SHP	shaft horsepower
CFM	volume flow through internal-flow system, cubic feet per minute
g	acceleration of gravity
pt	total pressure rise through the fan
p_{t_i}	weighted-average jet total pressure (gage) measured at the nozzle exit, the pressure at a point being weighted proportional to the normal velocity at that point
q	volume flow through internal-flow system, cubic feet per second
qu	recovery coefficient; ratio of static pressure to total pressure at impeller discharge
R_2	fan blade tip radius
η	overall system efficiency: ratio of air horsepower at the nozzle to fan shaft horsepower
ω	impeller angular velocity
Cd or cd	capacity factor, $q/\omega R_2 A_o$
Cp or cp	pressure coefficient, $pt/(\omega R_2)^2$

* Symbols for Appendixes are shown with each appendix.

SUMMARY

This report presents the overall results of a study of the application of rotating-diffuser centrifugal fans (RD fans) as air movers to peripheral-jet ground effect machines (GEMs), conducted under Contract DA 44-177-AMC-886(T). The overall investigation consists of aerodynamic, structural, fabrication, and design studies.

The RD fan, which consists of a centrifugal impeller with a rotating diffuser, was conceived and developed by Etablissements Neu of Lille, France, around 1950. History of this development is therefore presented. A comparison of the performance characteristics of the RD fan at various stages of development and of other centrifugal fans is made. The main features of the RD fan are explained in the simplest possible way, using Euler's equation and simple flow diagrams. Next, a more complete theory of the RD wheel is suggested; this theory gives a mathematical model of the wheel, in terms of a set of experimentally-to-be-determined hydraulic loss coefficients. The actual method used to predict the performance of an RD wheel, developed by Etablissements Neu, is discussed briefly, within the limits imposed by the need to protect the proprietary interests of Etablissements Neu and of Joy Manufacturing Company.

The advantages of using the RD fan as an air mover for a peripheral-jet GEM are brought to light as the result of a qualitative discussion concerning the general factors that influence the matching of the fan as well as the internal ducting of a GEM, as these factors affect the nozzle, delivery duct, the air intake duct and the fan itself.

The design problems of the duct-RD fan system are discussed. It is proposed that the RD fan be used in the GEM without a conventional volute by using a radial-flow delivery technique. Design of the delivery duct system is therefore of critical importance. The theoretical investigation was therefore backed up by an experimental program; first, an RD fan was installed in a GEM model to simulate a circular planform; then, it was installed in another model to simulate an oval planform; thus, the aerodynamic characteristics of the RD fan could be studied. It was found that high overall internal-flow system efficiencies can be achieved.

A study of environmental, structural, and fabrication problems of RD fans is also reported. In particular a state-of-the-art survey of applied loads for GEMs insofar as they affect the design of an RD fan system is presented. The stress analysis of a 1000-HP impeller was made, and weight estimates are presented for various fabrication approaches. It is shown that lightweight RD fans of large size can be built.

Finally, the results of two design studies, applying the RD fan to two markedly different GEM configurations, are reported. The results provide a vivid illustration of the potential advantages of the application of RD fans to GEMs.

In conclusion, results of the overall investigation indicate that RD fans are well suited to GEM applications because of high aerodynamic efficiency, low weight, and operational advantages, such as sturdiness and quietness.

CONCLUSIONS

It is concluded that:

1. A rotating diffuser fan incorporated as a primary air mover for the internal flow of a ground effect machine has a satisfactory aerodynamic performance. For a full-scale fan (1000 HP), an overall system efficiency of 85 percent has been obtained for a circular configuration. Efficiencies of 70 percent have been obtained for an oval configuration. Additional research should permit the latter figure to be raised. Design of the internal-flow system for a noncircular configuration requires model testing and great attention to detailed flow characteristics. The performance potential of the RD fan appears greater than that of the axial fan for this application.

2. Lightweight RD fans can be built. In most instances, the RD fan can be built as light or lighter than the axial fan designed for the same duty. However, such fans have not yet been built. A development program is necessary in this area to realize the full potential of the RD fan.

3. Combined advantages of high aerodynamic efficiency and low fan weight for a given power plant and total craft weight permit a GEM design with higher payload than that with a corresponding axial fan design. Reduced ducting volume means a higher useful volume to accommodate the additional payload. Additional important advantages of the RD fan to the designer are its sturdiness, leading to safety, and low noise.

4. The RD fan is found to be an efficient air mover which lends itself to uses other than those contemplated under the present contract. A design concept using a multipad plenum chamber GEM concept is discussed briefly in this report. The RD fan also has extensive applications in V-STOL design whenever, due to geometric limitations of certain internal-flow systems, the use of a conical or rectangular diffuser for energy conversion is impossible.

RECOMMENDATIONS

It is recommended that:

1. Theoretical and practical methods of designing and fabricating lightweight RD fans be given expanded interest, since the RD fan may be one of the most efficient ways for diffusing flows in geometry-limited internal-flow systems. This ability to diffuse is achieved at the expense of a larger rotating impeller, since some of the duct is made to rotate; hence, the importance of structural problems.

   It is indicated in this report that an indeterminate structural analysis of the RD fan is available in the literature. This analysis should be applied to the RD fan. Concurrently, a lightweight wheel of moderate size (100 to 150 HP) should be designed, built, and extensively tested.

2. Additional aerodynamic work on GEM configurations of noncircular planform be performed to increase the overall efficiency of the noncircular configuration so that it approaches that of the circular configuration.

3. An experimental program for the detailed survey of the flow within an RD impeller be conducted, since it would be both of great theoretical and of great practical interest. Information gained would permit analytical prediction of the head-capacity curve of an RD fan and analytical design of RD fans for specified missions.

4. Additional study be devoted to the plenum chamber pad concept proposed in this report.

INTRODUCTION

A large variety of air movers has been suggested for peripheral-jet ground effect machines (GEMs). For example, possible air movers listed in Reference 43 include axial-flow fans, centrifugal (or radial-flow) fans, ejectors, turbine engines, tip turbine fans, etc. However, as noted in Reference 43, present-day applications in the United States make almost exclusive use of axial-flow fans. To the contrary, extensive applications of radial-flow fans to GEMs have been made in the United Kingdom.

There is a growing feeling that, for many applications, the radial-flow fan may represent a more practical solution to the air-moving problem of peripheral-jet GEMs than the axial-flow fan. Under Navy sponsorship, the AiResearch Manufacturing Company of Arizona is developing a radial fan called the T-fan (Reference 55). Under Contract DA 44-177-AMC-886(T) with the U.S. Army Transportation Research Command, the Aerophysics Company has been studying the application of rotating-diffuser centrifugal fans (hereinafter called RD fans) to GEMs.

The RD fan concept is not new. RD fans have been developed since the late forties as a proprietary item by Etablissements Neu of Lille, France, and are manufactured under license in the U.S. by Joy Manufacturing Company of Pittsburgh, Pennsylvania and New Philadelphia, Ohio. However, the application of the RD fan to GEMs as an internal-flow air mover presents challenging problems of an aerodynamic, structural and manufacturing nature. These problems were studied under the program which is reported in the following pages. The term "radial-flow fan" is used in the title of this report, but it must be understood that most of the report is concerned with the Joy RD fan, which is a special type of radial-flow fan.

The program discussed in this report consisted of six phases. In Phases II and III, a theoretical study of the Joy rotating-diffuser fans is made; Phase II considers the fan alone, and Phase III considers its use in ground effect. In Phases I and IV, structural and fabrication problems of RD fans for ground effect machine use were studied. In Phase V, an experimental investigation of the aerodynamic characteristics of the Joy RD fan successively installed in two different GEM model configuragions, simulating, respectively, a circular planform and an oval planform GEM, was conducted. Finally, as part of Phase VI, two design studies were made of ground effect machines incorporating internal-flow systems with RD fans. In the first design study, a machine was designed that is similar to the U.S. Navy Bureau of Ships

Hydroskimmer I except that the four axial fans of the Skimmer I were replaced by two RD fans. In the second study, a design was proposed for an Army ground mobility device, which takes full advantage of the high efficiency of the RD internal-flow system.

A summary of the overall work performed under the contract was also required under Phase VI of the contract and is presented herein as the final report under the contract. All elements of the earlier phase reports are incorporated in the report, although the material in the Phase V and Phase IV reports is presented in abridged form.

The work performed under Contract DA 44-177-AMC-886(T), which includes structural, weight, and design studies as well as aerodynamic studies, forms the basis for a comprehensive systems analysis study of GEM internal-flow systems incorporating RD fans. The next step would be an optimization of the fan-internal-flow system. Such an optimization was beyond the scope of the contract. However, the results obtained to date are sufficient to indicate the significant advantages of RD fans in GEMs over either axial or conventional centrifugal fans.

SECTION I

GENERAL CONSIDERATIONS ON THE FAN-DUCT MATCHING PROBLEMS OF A GEM

The general requirements for fan-duct-cushion matching for a ground effect machine using centrifugal fans as air movers have been discussed expertly in References 54 and 55 by Senoo, of the AiResearch Manufacturing Company of Arizona. The discussion of this section will parallel closely that of Senoo, for reasons which are set forth in what follows.

Quite obviously, of the three parameters, fan, duct,and cushion, the only one which can be varied relatively freely is the fan, since, for a given GEM, the size of the internal ducting is determined by the size and the layout of the machine and the aerodynamic characteristics of the air cushion; hence,the flow conditions at the nozzle of the machine are determined by the desired performance of the machine. In other terms, by specifying a GEM mission and a type of machine (such as skirted or unskirted peripheral jet), one pretty well defines the duty of the fan (pressure rise against capacity), and the problem is to design a fan with the highest possible efficiency during most of the mission. Senoo's proposed fan, in the study referred to above, is a radial-flow, helico-centrifugal fan, which was called the T-fan (Reference 55). Its main feature is the claimed ability to deliver very large volume flows of air at the desired pressures of 20 to 200 pounds per square foot gage, which are typical of present-day GEM missions.

In 1961, on the occasion of design studies relating to two design competitions (References 8 and 9), Aerophysics Company faced the same problem of the design of an efficient air mover, to which AiResearch's answer was subsequently to be the T-fan. However, the answer was different. It was concluded that the design from scratch of a new fan might not be warranted, since an intensive search had disclosed the existence and availability of the Joy RD-fan, which, properly modified, appeared to satisfy the requirements of an efficient GEM internal-flow mover. This idea was taken to the U.S. Army Transportation Research Command,and the study discussed in this report resulted.

As a first step, the basic philosophy establishing the compatibility of the RD fan for GEM internal-flow duties is reviewed in this section.

DUCT PRESSURE LOSSES

Pressure losses are either wall friction losses or total pressure losses due to flow separation or stall. In order to reduce wall friction, one should (1) have as low a duct velocity as possible, (2) make the wall surface smooth, and (3) minimize the wall surface area.

Stall is likely to be present in a duct either (1) if an attempt is made to diffuse the flow, or (2) along a bend. Stall losses are therefore reduced if no attempt is made to diffuse the flow and if bends of the duct are minimized.

DESIRABLE DUCT GEOMETRIES

Nozzle

At the exit of the peripheral nozzle of a GEM, the static pressure across the nozzle is not uniform. On the inside, it is equal to the base pressure; on the outside, it is equal to the induced pressure around the GEM created by the external flow. In hovering, the outside static pressure is ambient; the inner side of the jet faces the base pressure, which is considerably higher than the mean static pressure of the jet at the exit. This is combined with the fact that the inside wall of the nozzle is a convex surface and the maximum velocity in the nozzle occurs immediately upstream of the lowest exit velocity. There may likely result a separation of the flow from the inner wall.

Performance of the system may thus be reduced appreciably. In order to avoid flow separation, a low velocity and a high static pressure should be maintained within the duct so that the mean flow is continually accelerated toward the exit of the nozzle.

If a wide nozzle is used, the volume flow is large and the total pressure of the jet is low. In order to keep a relatively high static pressure in the nozzle duct, the velocity in the duct must be very low, and an undesirably large duct is required. If the size of the duct is limited, the velocity in the duct thus increasing in proportion to the flow rate, then the pressure loss in the duct increases in proportion to the square of the velocity. Therefore, the internal efficiency of a wide-nozzle lifting system is inherently low.

The narrow-nozzle system, on the other hand, requires high pressure rises and smaller flow rates. The internal efficiency of a narrow nozzle system is inherently high.

However, conversely, as will be seen in Appendix II, a fairly wide nozzle is desirable from the standpoint of cushion aerodynamics. Since internal-flow efficiency and external-flow efficiency thus go in opposite directions, an optimum must exist.

Delivery Duct (Figure 1)

A general discussion similar to that of References 54 and 55 may be dangerous and misleading in the present case. As will become apparent later in this report, the ducting requirements for a GEM air mover based on the rotating diffuser centrifugal fan concept are substantially different from those for axial-flow fans. Ducting for RD fans is much reduced as compared to axial-flow fans, since some of the functions of the ducting are handled by the fan. For an axial-flow fan system, the ducting does two things: (1) turn the flow 90 degrees, assuming that the axis of the fans is vertical, and (2) diffuse the flow between the fan and the peripheral nozzle to accommodate given nozzle conditions. Both of these things are done by the rotating diffuser centrifugal fan within the fan. Not only can the RD fan be looked upon as a device to raise air pressure, but also as a "rotating duct." However, the function of the duct remains to lead the air from the fan exhaust to

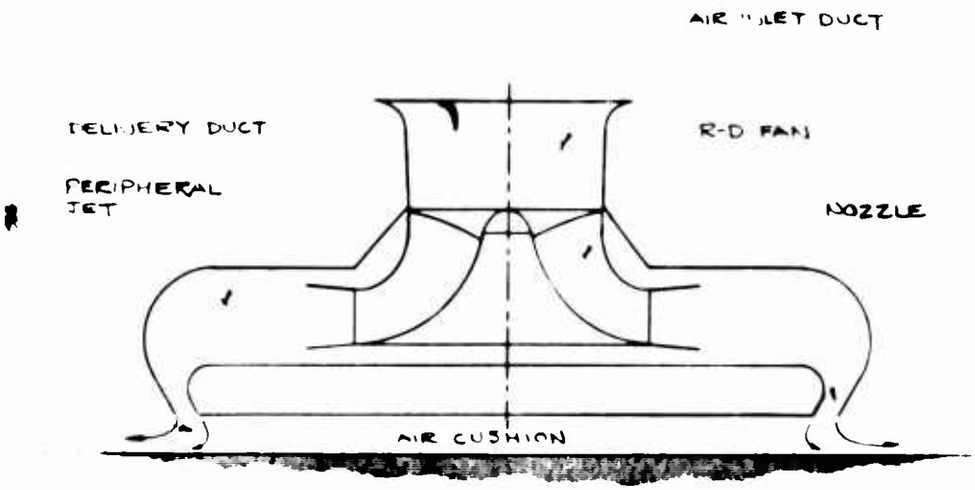

Figure 1: Schematic Representation of a GEM Internal-Flow System

the peripheral nozzle. It is not necessary that this be done while diffusing the flow. A special feature of centrifugal fans, which does not exist for axial fans, is that they do not operate unless they are matched with a casing or a volute. The question must be asked whether a conventional volute must be used or whether the volute can be combined as part of the ducting. The answer to this question is likely to depend upon the planform shape of the GEM; i.e., of its peripheral nozzle. If the planform is circular, an even distribution of the flow to the annular nozzle appears easy, and the problem is reduced to that of finding the equivalent of the cutoff for a centrifugal fan with volute. If the planform is not circular, the additional problem is to insure the proper flow distribution all around the periphery of the nozzle.

Also, as was mentioned in connection with the nozzle, the distribution of static pressure on the periphery of the GEM varies as the GEM speed changes. It is desirable to incorporate a plenum chamber between the fan and the nozzle to act as a "buffer" between the outside flow and the fan. However, if a plenum chamber is installed between the fan and the nozzle, the dynamic pressure at the entrance of the plenum is dissipated in the plenum. Since a low velocity and a high static pressure are required in the duct near the nozzle, a low velocity at the exit of the fan is required.

Air Intake Duct

In order to achieve a high internal efficiency and ram recovery efficiency, the velocity in the intake duct should be decided from the following considerations:

1. The ratio of axial velocity to the speed of the GEM should be larger than a certain critical value which depends upon the intake geometry. For a flush intake with a one-third ring flow-deflector vane, the critical value is 2. (See References 54 and 55.)

2. A small fan and a small duct are preferable to a large fan and a large duct because of space limitations and system weight considerations.

3. The friction loss in a duct is proportional to the fifth power of the hydraulic diameter for a constant mass flow. Since the intake duct is short, the friction loss in the intake duct itself is negligbly small.

GEM FAN REQUIREMENTS

Fan-Duct Compatibility

Exact fan requirements are dictated by the specific requirements of a particular GEM type. In the present study, the emphasis is placed on annular-jet-type machines. Even for such machines, fan requirements can vary from pressures as low as 20 pounds per square foot to pressures as high as 150 pounds per square foot.

Though it is dangerous to generalize, it can be concluded from the previous discussion that a low velocity is desirable at the exit of the fan but a high velocity is preferable at the intake duct. The condition at the exhaust of the fan, that the velocity be low, is more important than the condition at the inlet, that it be high.

By reference to the arguments stated in Section II it becomes evident that the Joy rotating diffuser centrifugal fan fulfills the requirements stated above. The RD fan has a low exhaust velocity, with a very high static pressure recovery. However, it must be pointed out that it is not small in size; specifically, it is much more bulky than the AiResearch T-fan discussed in Reference 55. An evaluation of the weight of the fan and of the fan duct system is given later in this report. As has been explained before, the RD fan fulfills the role of much of the fixed ducting in more conventional fans. Its bulk must therefore be considered in terms of the saving in bulk and weight of the fan-duct combination, not in terms of the changes for the fan alone.

Operational Requirements

A GEM fan must be rugged, self-cleaning and have as low a noise level as possible.

In addition, for operation over water, the head-capacity curve must be flat for the full operation between zero capacity and the design operating point. This is desirable to make possible the lifting of the machine off the water without surging and flow instability. Besides, should the head-capacity curve dip around the zero-capacity point, the proper amount of lift required to lift off the water would only be obtained at the expense of additional installed power.

The Joy RD fan excellently fulfills the two above operational requirements, as will be shown in the subsequent discussion.

SECTION II

DESIGN PROBLEMS OF AN RD FAN SUITABLE FOR A GEM

A schematic representation of a GEM internal-flow system is shown in Figure 1. It can be seen that the system consists of an air inlet duct, an RD fan, a delivery duct, a peripheral jet, and an air cushion. In this section, the aerodynamic characteristics of the RD fan alone and of the delivery duct system are discussed in general terms.

RD FAN

A schematic cross-section of an RD fan is shown in Figure 1. Very briefly, the RD fan is a shrouded centrifugal fan with a conventional impeller, by means of which the flow is turned ninety degrees. The special feature of the fan is that, once the flow is turned, it is decelerated in a bladeless rotating diffuser. An overall view of the 20-inch diameter RD fan, the tests of which are discussed in this report, is shown in Figure 2. The difference between the Joy RD fan and the proposed AiResearch T-fan of Reference 55 is thus that, in the RD fan the flow is first turned and the energy added to it, then diffused; while in the T-fan, turning, energy addition and flow diffusion occur simultaneously.

Figure 2: Overall View of RD 20-Inch Diameter Test Fan

Detailed information on the RD fan is presented in Appendix I, where the history of the development of the RD fan by Etablissements Neu, of Lille, France, is presented. Also shown in Appendix I is a comparison between the performance characteristics of the RD fan at various stages of development and that of other types of centrifugal fans. Next, the main features of the RD fan are explained in the simplest possible way, using Euler's equation and simple flow diagrams. Also, a more complete theory of the RD wheel is suggested. This theory gives a mathematical model of the wheel, in terms of a set of experimentally-to-be-determined hydraulic loss coefficients. Finally, the actual method used to predict the performance of an RD wheel, developed by Etablissements Neu, is discussed briefly in Appendix I, within the limits imposed by the need to protect the proprietary interests of Etablissements Neu and of Joy Manufacturing Company.

DESIGN OF THE DELIVERY DUCT SYSTEM

Air discharged from the fan must be efficiently delivered to the peripheral jet of the GEM. Also, a volute or the equivalent must be provided to insure the proper operation of the RD fan.

Following are three of the many basic duct systems from which to choose:

Volute and Plenum System

The RD fan is installed with a conventional volute, at the exit of which the air is dumped into a large plenum chamber. Air is supplied to the base jet nozzle from the plenum chamber; therefore, flow distortion at the jet nozzle is not transmitted to the fan.

A significant disadvantage of this system is the dumping loss which could be eliminated if the plenum were omitted. In addition, the internal volume of such a configuration is enormous.

Vaneless Duct System

In this configuration, the flow exhausting from the rotating diffuser is directly connected to the nozzle at the periphery of the GEM. Since the flow at the nozzle is not axisymmetric with respect to the center of the fan, the streamlines will adjust themselves in the vaneless duct. The flow at the exit of the fan may not be axisymmetric even at the design condition. Furthermore, without the volute, there is no assurance a priori that the desired aerodynamic characteristics of the fan will be obtained.

The pressure loss in the duct d[illegible] marily upon the relative location of the base nozzles with respect to the [illegible] the base nozzles are distributed relatively uniformly around the fan, a high efficiency may be expected if the problem of the fan cutoff can be taken care of. On the other hand, if the nozzles are concentrated on one side of the fan, the pressure loss will be significant. Special care must be exercised for the flow rate at the peripheral nozzles in order to be reasonably uniform.

The success of this configuration will lie, first, in the ability to find aerodynamic means to replace the volute used in the conventional RD fan. Second, one must be able to minimize duct losses and to insure uniform distribution of the flow at the nozzle periphery. Since theory alone cannot provide an answer to these questions, extensive model investigations were carried out as will be pointed out in greater detail in Section III.

Multiduct System

In this configuration, as for the AiResearch T-fan, many individual ducts are used to connect the fan and the peripheral nozzles. Ideally, at the design condition, the pressure losses in the duct are only friction losses, and a high internal efficiency may be hoped for. The guide vanes also serve as structural members which support the load above the ducts.

The enormous disadvantage of this system is the performance loss that is sure to occur at off-design conditions. As the flow rate or the pressure rise of the fan changes, the direction of flow at the exit of the fan varies, and the air does not flow smoothly into the ducts. A large pressure loss can occur at the duct inlets. Since it was stated that a GEM had to be designed for a wide range of flow conditions, the multiduct approach appears dangerous, unless provisions are incorporated to vary the curvature of the various ducts as a function of the flow conditions.

PROPOSED DELIVERY DUCT SYSTEM

It was realized early in this program that it was impossible to predict theoretically the performance of a given delivery duct configuration and consequently impossible to choose a particular duct configuration for its superior performance over other configurations. It was necessary to rely on judgment and experience for an initial configuration; a test program was established to test extensively a few configurations which appeared most promising.

The first configurations, volute and plenum chamber, never presented much attraction for a conventional peripheral-jet GEM. (It could be attractive for other types of machines, which fall outside the scope of this study.)

A modified form of the third configuration, i.e., a multiduct system, was originally selected for test. Before the test model could be designed, however, consultation with Etablissements Neu and with the Joy Manufacturing Company led to the abandonment of that configuration, on the grounds that it would not permit efficient operation of the GEM through a wide range of operating conditions.

In the past, Etablissements Neu has had limited experience with a vaneless duct system, used in multistage installations in lieu of volute. The duct system is not entirely vaneless, however, but the vanes are located in the nozzle rather than in the duct leading to the nozzle. Such a system was strongly recommended by Neu to Aerophysics, and the decision was made to test such a configuration. The tests were first made on an axisymmetrical GEM of circular planform. Next, an oval model was built, representing one-half of a typical hull-shaped configuration (such as the proposed Bureau of Ships Hydroskimmer II). The purpose of this model was to test the non-uniformity of the flow delivered by the fan along the periphery of the nozzle, and to find ways to correct the nonuniformity by aerodynamic means. For a description of the test models, tests and test results (which were fully successful), the reader is referred to Section IV of this report. It was established that a nearly-vaneless duct system connecting the RD fan and the peripheral nozzle can be designed to carry the flow from the fan to the nozzle with good efficiency over a wide range of flow conditions.

SECTION III

THEORETICAL ANALYSIS

FAN

There does not presently exist a satisfactory theoretical representation of the flow within an RD fan. An attempt at establishing the elements of such a theory is made in Appendix I. The formulation of Appendix I is made in terms of experimental coefficients (hydraulic loss coefficients) which are not presently known with any amount of reliability.

Because of the difficulties of the purely theoretical approach, Etablissements Neu during the past ten years developed a practical method of prediction of RD fan performance. This method is discussed in general terms in Appendix I. The method was applied to prediction of the performance of the 20-inch RD wheel, the tests of which are discussed in Section IV of this report.

A comparison between predicted and actual performance is shown in Figures 12 and 13. The comparison indicates the remarkable accuracy of the Neu performance prediction method.

CUSHION AERODYNAMICS

An extensive discussion of the state of the art of cushion aerodynamics as a determining factor in the determination of the internal-flow requirements of a GEM is made in Appendix II. It is concluded that, at the present time, the "exponential theory" best permits calculating the jet total pressure as a function of the base pressure and of the geometry of the machine. However, jet velocity is best calculated by using Chaplin's recently proposed modified momentum theory, which is discussed in detail in Appendix II.

ESTIMATION OF DUCT LOSSES

As mentioned earlier, the duct losses of any importance are those in the delivery duct. In turn, they can be wall friction losses or flow separation losses.

The proposed delivery duct system was chosen in Section II to be a radial-flow vaneless duct. For a machine of circular planform, the duct has axial symmetry;

for a machine of noncircular planform, it does not, and the flow pattern can hardly be predicted theoretically. This does not make the determination of duct losses any easier!

The prediction of duct losses for a generalized GEM internal-flow ducting system is a very difficult task. Here, the redeeming factor is that the problem is pretty well narrowed down, since one is merely concerned with this radial-flow vaneless duct, a model of which can be built and tested easily. After initial tests, it is possible to effect configuration changes and to reduce the duct losses by trial and error; hence, the need for a comprehensive test program to supplement the findings of the present program. This test program was carried out as Phase V of Contract DA 44-177-AMC-886(T) and is reported in Section IV of this report.

For a reliable estimation of duct losses, one must then rely upon experimental results. However, some general remarks are in order as follows:

As stated above, the duct losses are made up of wall friction losses and flow separation losses.

The wall friction losses are due to a turbulent boundary layer type of flow, directly under the influence of the flow discharged by the fan. They can be minimized by minimizing the interference between the fan exhaust and the wall and minimizing the wall surface roughness. Determination of wall friction losses must be obtained from experimental data on a similar model. The wall friction losses can be minimized, but they cannot be eliminated.

Flow separation losses in general are due to diffusion of the flow and to bends. Since the complete diffusion takes place in the rotating diffuser part of the fan, the delivery duct can be designed so that there is no diffusion in the duct. Also, there are no bends in the delivery duct. Therefore, in principle, the flow separation for a well-designed delivery duct could be very small. Conversely, if the flow pattern of the air exhausting from the fan is allowed to interfere with the walls, for example creating dead-air regions and secondary streams, these losses could be very high. There is a strong incentive to make, in each case, a very careful and detailed experimental study of the delivery duct in order to minimize losses.

Finally, some experimental information is presently available to Etablissements Neu about frictional losses for a flow delivery duct configuration similar to that

used for a typical GEM. This information was used in the numerical example worked out in Appendix I. The validity of these data is checked by comparing the results of the calculated performance shown in Appendix I with the measured performance obtained from the experimental results of Section IV. The reader can verify from Figure 12 that the assumptions made in Appendix I for duct losses are fairly well borne out by testing. It can therefore be concluded that a means to estimate delivery duct losses for a circular configuration is available. The delivery duct losses for a noncircular configuration will always be larger than for a circular one; for a well-designed noncircular planform shape, the duct losses should approach those for the equivalent circular planform shape.

SECTION IV

EXPERIMENTAL INVESTIGATIONS

SCOPE AND OBJECTIVES OF THE TESTS

The objective of the tests was to confirm by experiment from the standpoint of aerodynamic performance, the feasibility of using rotating diffuser fans as air movers for GEM internal-flow systems.

It is not possible or desirable to repeat here all the arguments developed earlier. The conclusions bearing on the test program were essentially two, as follows:

First, centrifugal wheels with or without rotating diffusers are traditionally used with casings, tongue,and volute (see, for example, Reference 64). As discussed in Section I, it would not be advisable to use the RD fan with its conventional volute in a GEM application. Neither would a large plenum chamber downstream of the fan result in a high internal efficiency. The configuration proposed in Section II consists of an RD fan and a radial duct downstream of the fan. The radial duct leads to the peripheral nozzle of the GEM. It is first necessary to prove experimentally that, as suggested earlier in this report, the tongue can be replaced by a system of straightener vanes located in the peripheral nozzle itself, the radial duct being entirely vaneless.

Second, it is shown in Section III that, in a configuration involving an RD fan and a radial duct downstream of the fan, it is impossible to predict accurately the losses in the radial duct. Further, these losses are strongly influenced by the planform shape of the duct's peripheral wall. These losses are expected to be minimum for a planform with axial symmetry and to be maximum for an elongated planform representing a machine with two fans side by side.

In view of the above, two models were built, using the same RD fan and RD fan inlet, to represent the following configurations:

1. One configuration, the RD fan with radial delivery duct and annular nozzle of circular planform (see Figure 4), permits the verification of the effectiveness of nozzle vanes to replace the conventional tongue and to provide a cutoff. Since it is the minimum-

loss configuration, it provides a value for the upper limit of the overall internal efficiency of a GEM utilizing an RD fan. The model was built with a variable-depth delivery duct in order to study the effect of duct depth on performance.

It was indicated in Appendix I that it would be desirable to determine experimentally the streamwise variation of static pressure inside the fan in order to determine whether the largest losses were due to the impeller or to the rotating diffuser. However, obtaining pressure measurements on the rotating wheel, by use of pressure instrumentation within the impeller, was not planned in the original project, and it was not felt wise to add this step because of the limited scope of the present program.

2. The second configuration, the RD fan with pseudo-radial delivery duct and annular nozzle of oval planform (see Figure 16), had the same nozzle area and the same base area as the first one. Since the fan was the same and since it operated at the same speed (1600 rpm), differences in performance between the first and the second model could be attributed to a planform effect. In addition, it was desired to find out whether or not the nozzle vanes were effective with the oval planform and to get a feel for optimization of the oval delivery duct configuration, with a hope that its efficiency could approach that of the circular planform configuration.

DESCRIPTION OF THE TEST STAND INSTRUMENTATION AND CALIBRATION

Description of the Test Stand

A drawing of the test stand is shown in Figure 3. Photographs of various components of the test stand are shown in Figures 5, 6, 7, 8, 14, and 15.

The test was performed in the fan research laboratory of the Department of Mechanical Engineering of the Catholic University of America, Washington 17, D.C., by using an existing 7.5 HP variable-speed D.C. electric motor, which normally drives an axial-flow fan. The motor is mounted on a concrete base block, as shown in Figure 3. A steel angle truss frame was fabricated and bolted on the motor frame; the frame supports the main power train, on which the RD fan is mounted. Power is transmitted from the motor to the power train by mears of a timing belt, with a 2:1 ratio. To the steel frame is also attached a fully-articulated simulated ground board, which is usually vertical; it can be tilted as shown in Figure 7.

BLANK PAGE

A

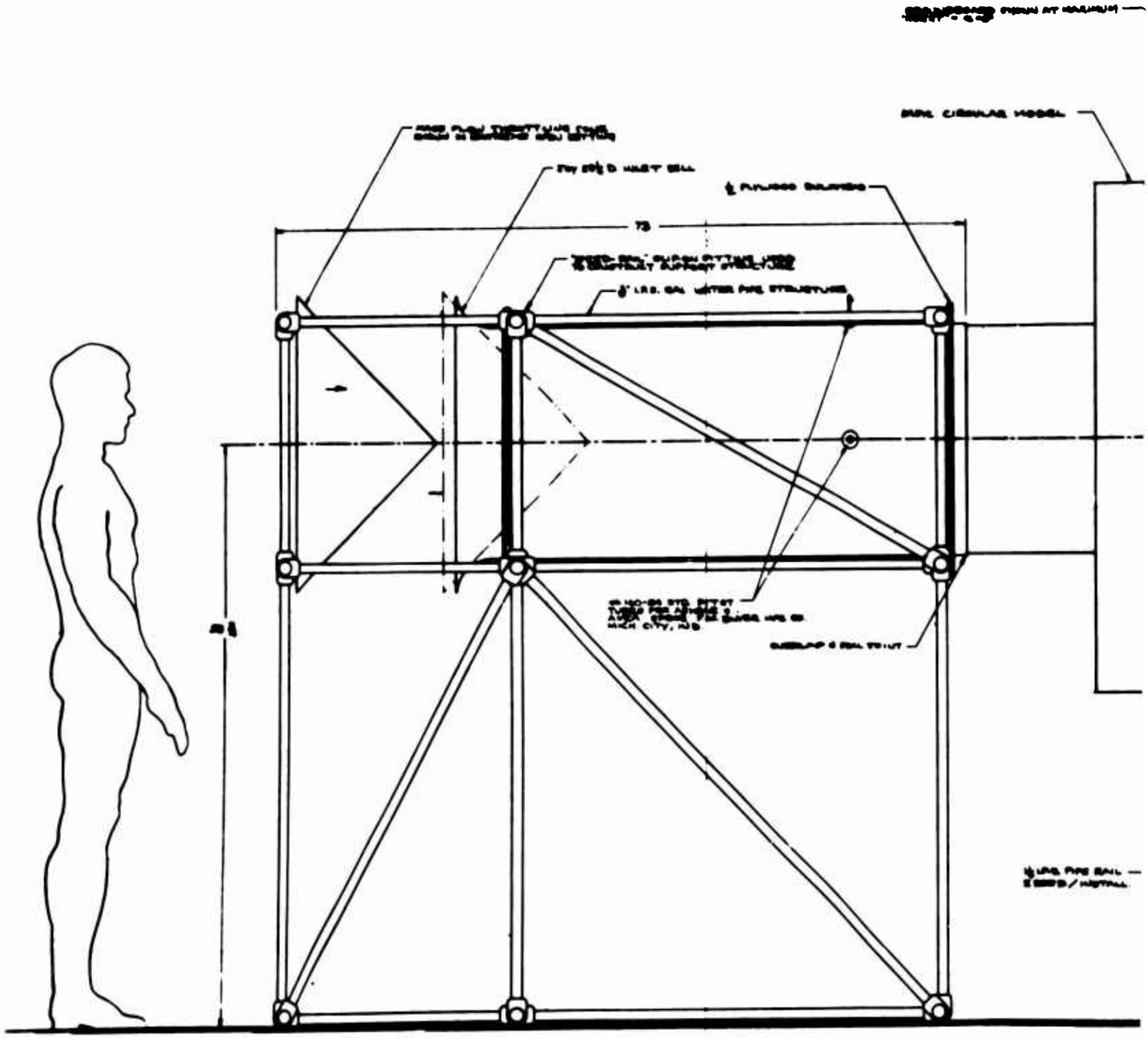

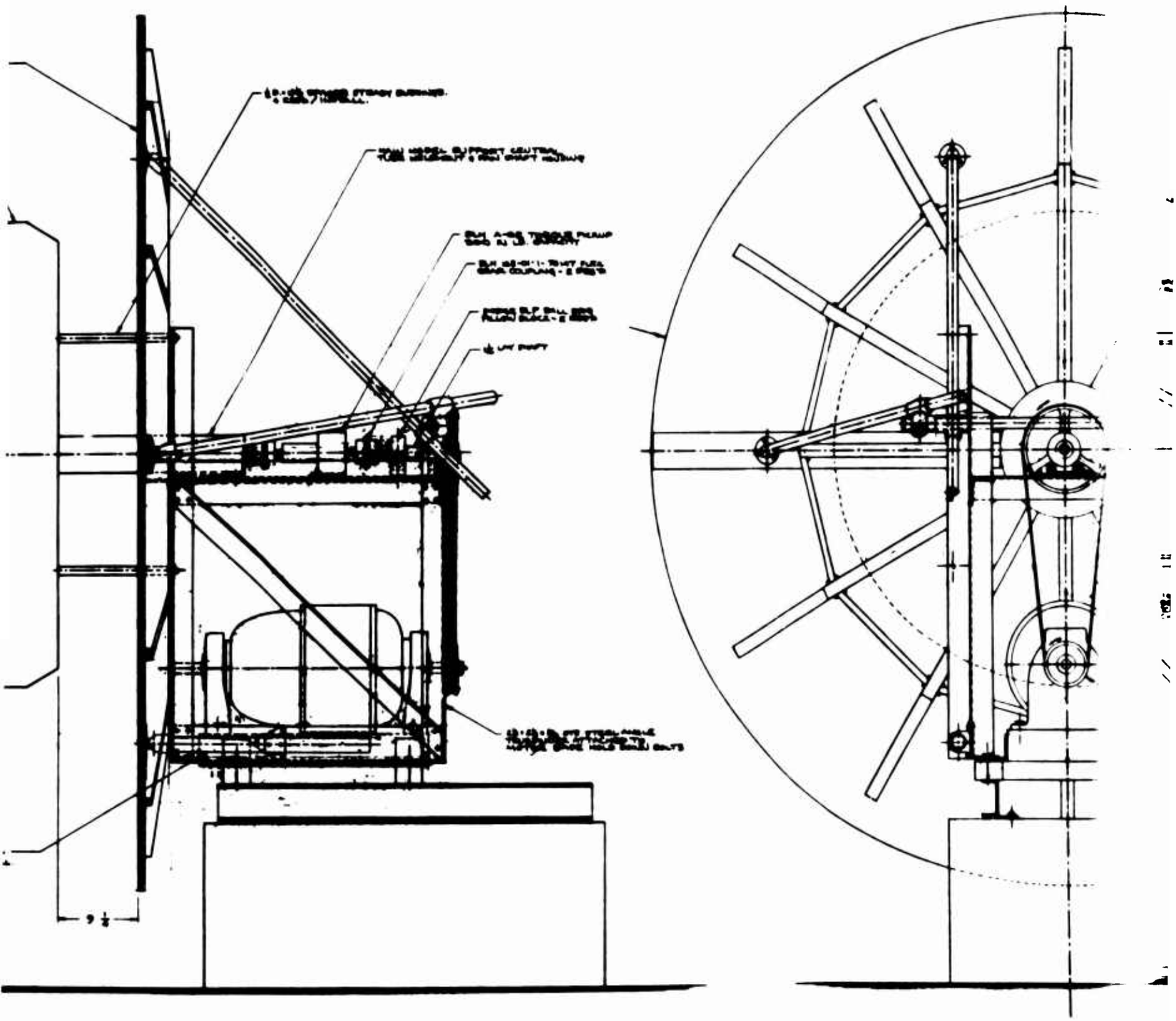

Figure 3: Overall View of Test Setup

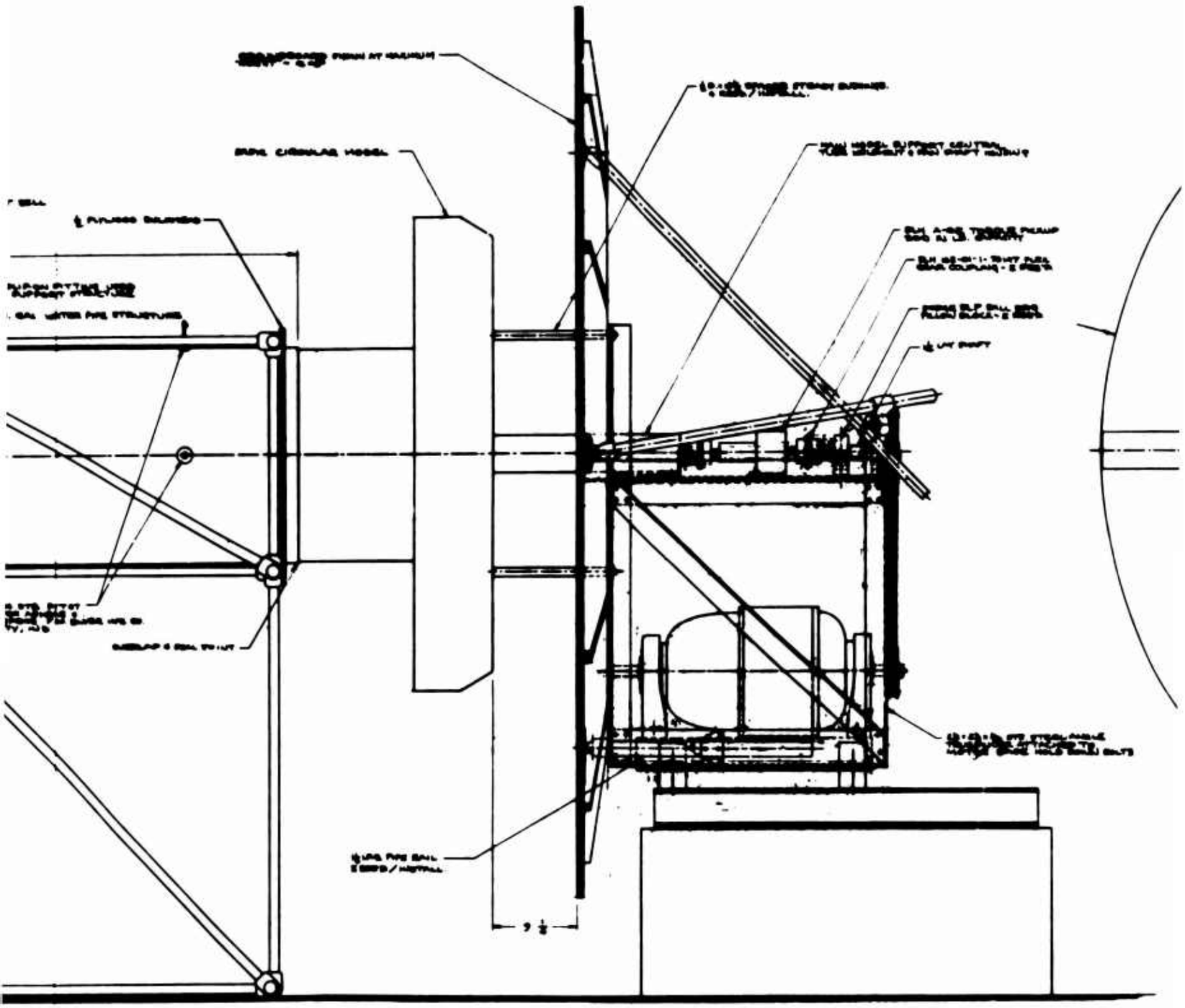

Figure 3: Overall View of Test Setup

B

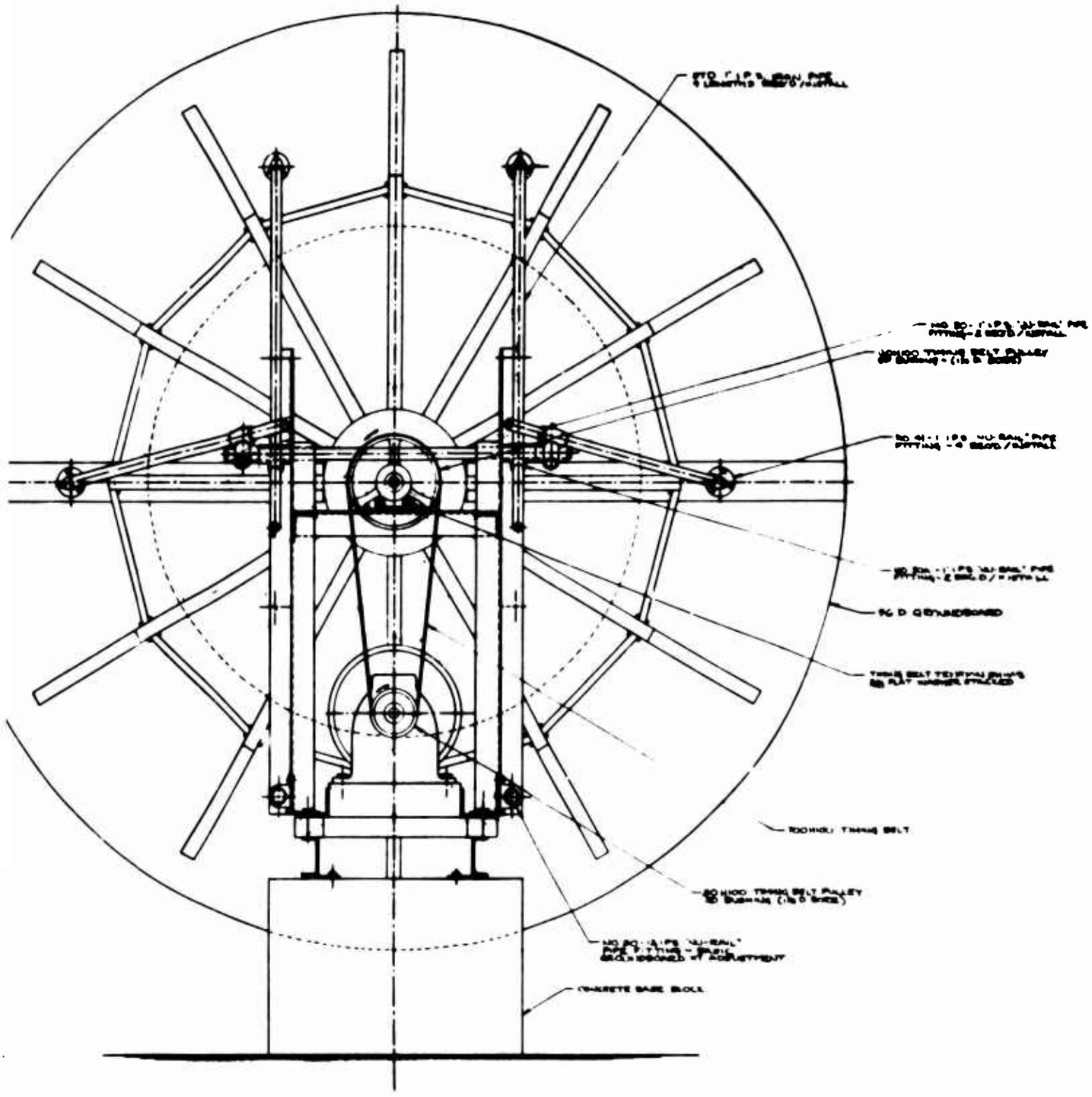

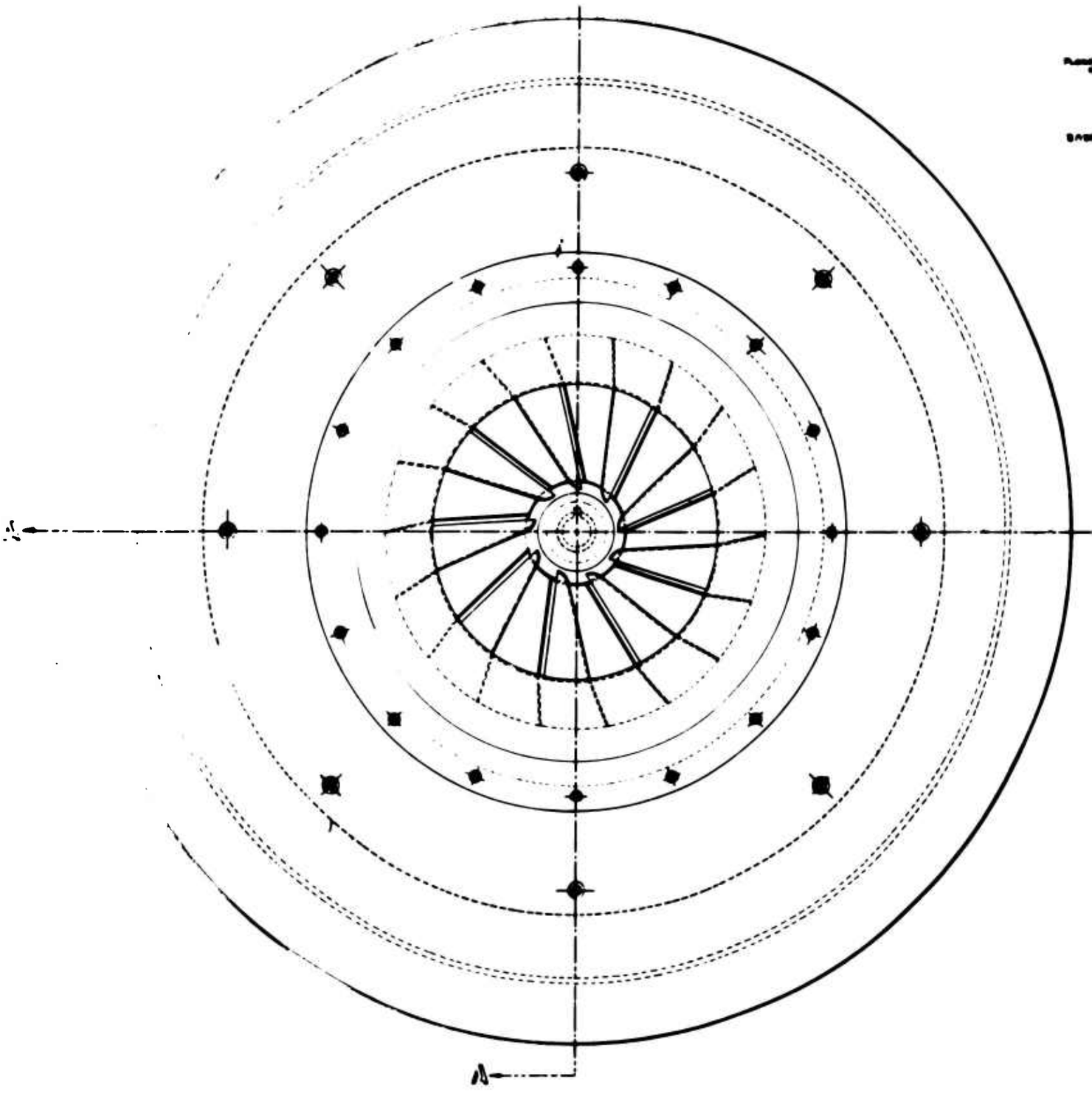

Figure 4: C

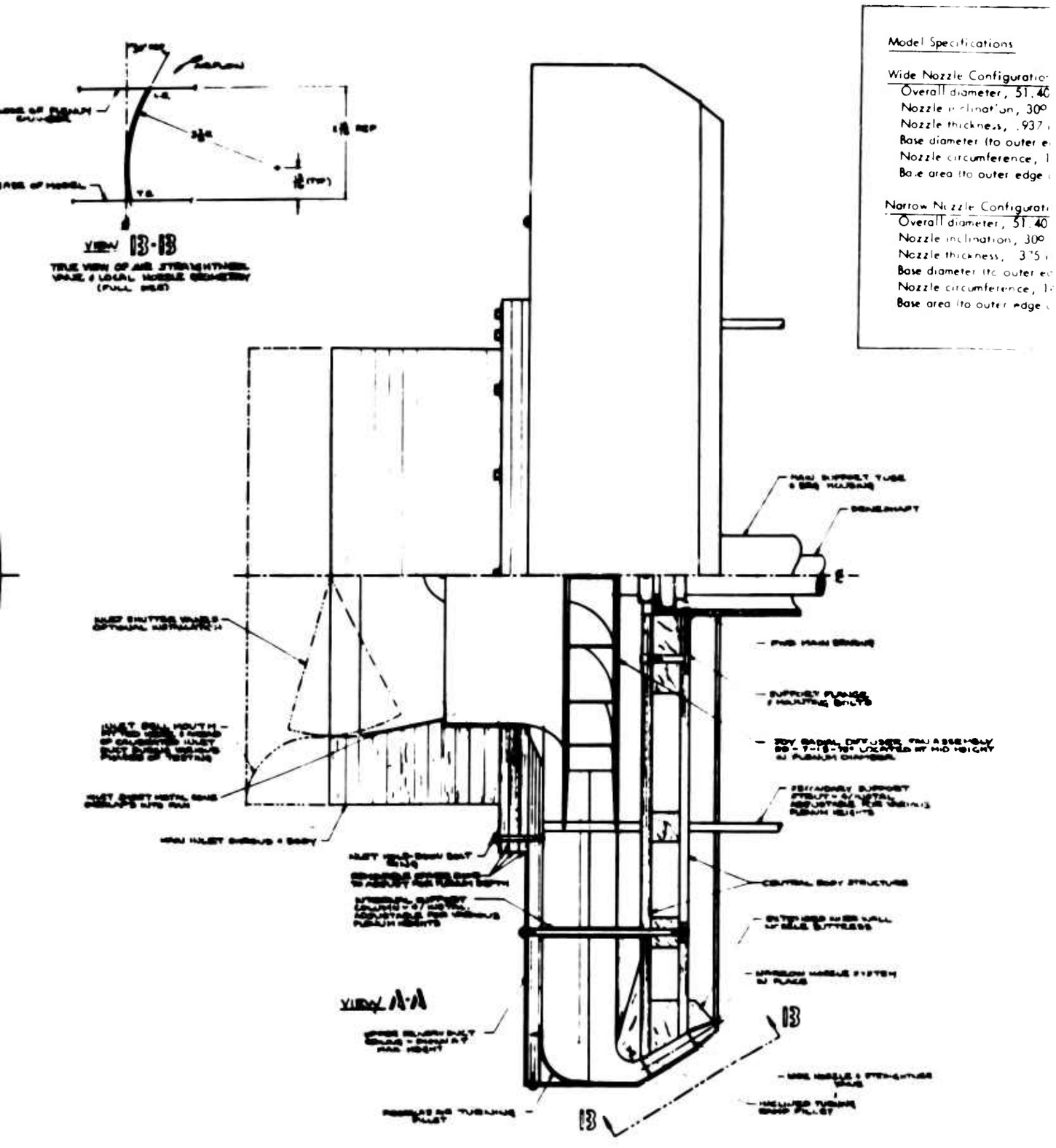

Overall Circular Model Drawing

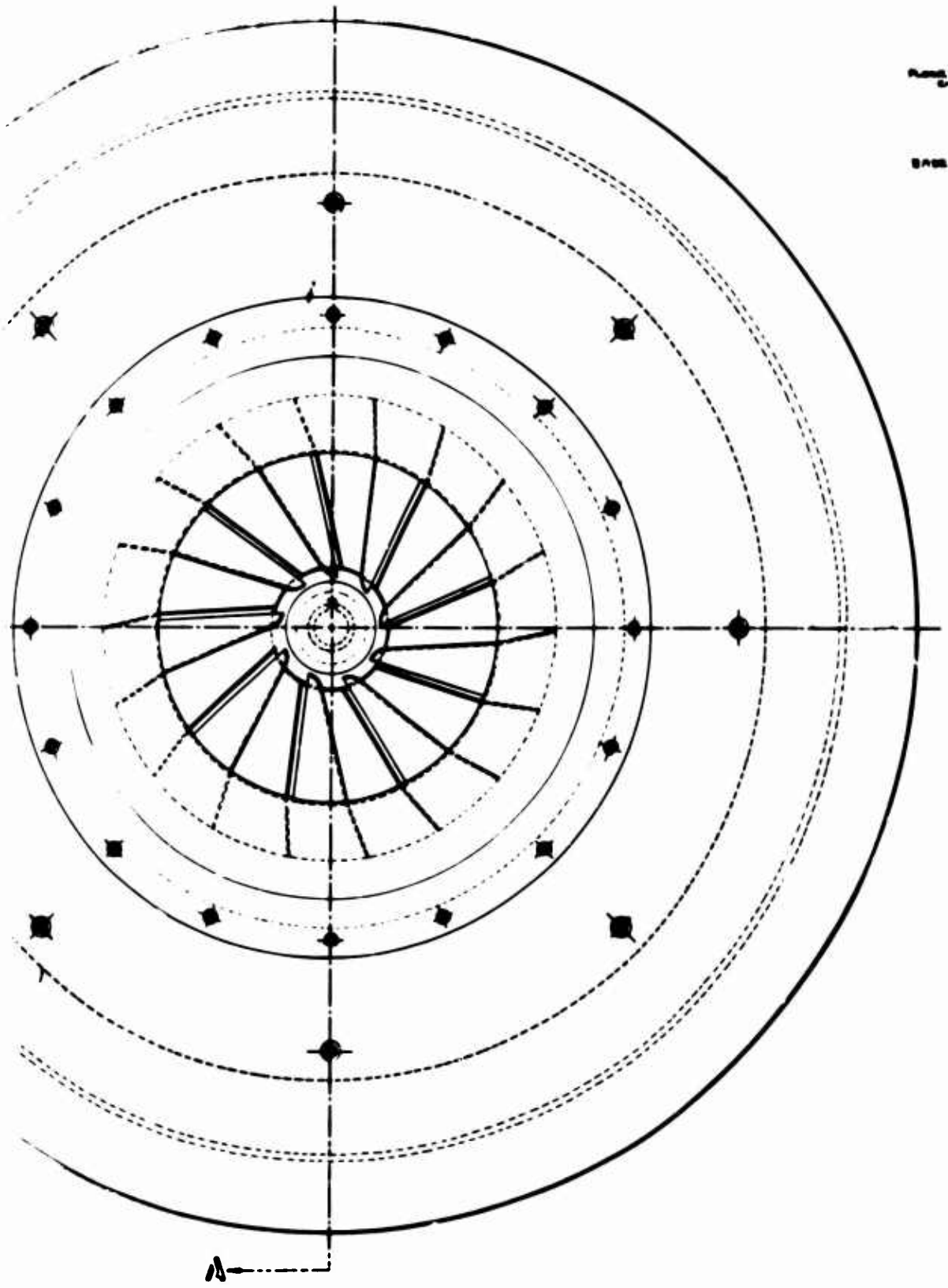

VIEW 13-13

TRUE VIEW OF AIR STEERING NOZZLE VANE & LOCAL NOZZLE GEOMETRY (FULL SIZE)

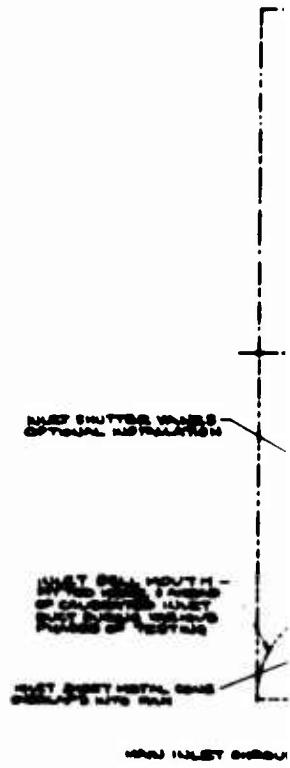

Figure 4: Overall Circular Model D

Model Specifications

Wide Nozzle Configuration
- Overall diameter, 51.40 in., 4.28 ft
- Nozzle inclination, 30°
- Nozzle thickness, .937 in., .078 ft
- Base diameter (to outer edge of nozzle), 47.44 in., 3.95 ft
- Nozzle circumference, 146.08 in., 12.17 ft
- Base area (to outer edge of nozzle), 1767.59 in^2, 12.27 ft^2

Narrow Nozzle Configuration
- Overall diameter, 51.40 in., 4.28 ft
- Nozzle inclination, 30°
- Nozzle thickness, .375 in., 0.31 ft
- Base diameter (to outer edge of nozzle), 45.37 in., 3.78 ft
- Nozzle circumference, 141.37 in., 11.78 ft
- Base area (to outer edge of nozzle), 1616.70 in^2, 11.23 ft^2

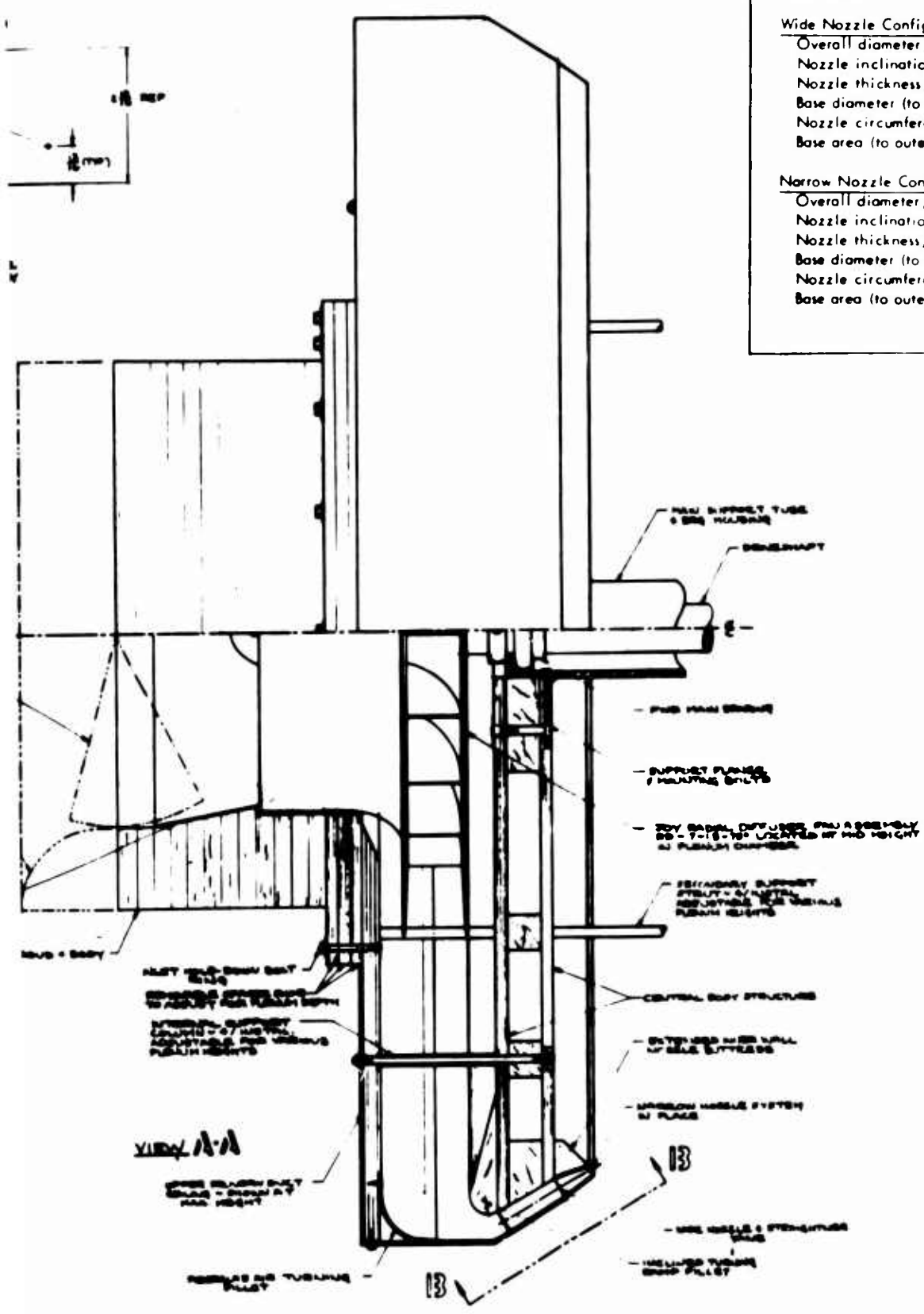

Drawing

BLANK PAGE

Figure 5: Overall View of Test Setup, Circular Model

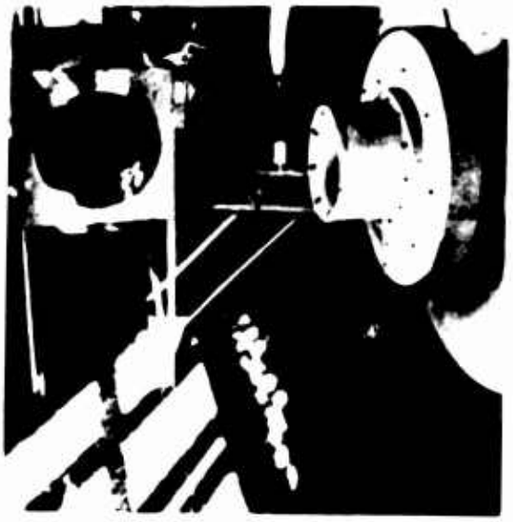

Figure 6: Overall View of Test Setup, Circular Model

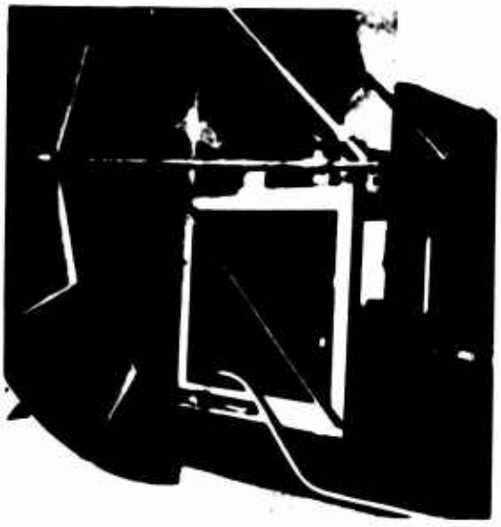

Figure 7: Rear View of Test Setup Showing Tilt Mechanism

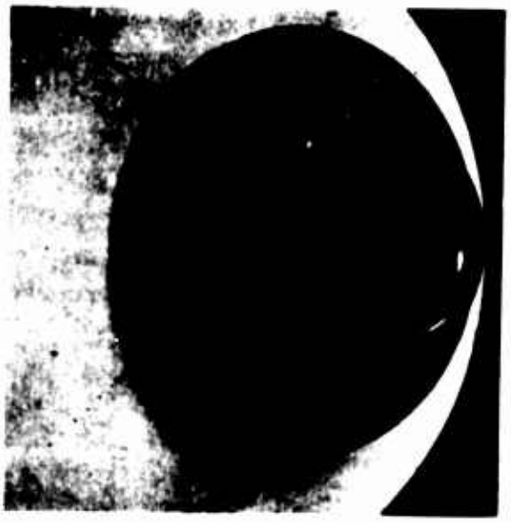

Figure 8: Circular Model and Inlet

The internal-flow model is mounted on the steel frame, as shown in Figure 3, through the ground board, by means of a central tube and of the four spacers mounted as shown on the drawing. The internal-flow models are described schematically in Figure 3. They are described in detail in a later section of this report.

The ground board, being fully adjustable in a direction parallel to the ground, could be positioned as far as 9.25 inches away from the annular nozzle and yet, close enough to close the nozzle completely. When the tests were made at zero capacity, the inlet duct shown in Figure 3 was removed and the inlet bellmouth (not shown in Figure 3, but shown in Figure 4), was adapted against the main inlet shroud, as shown, for example, in Figure 6. For normal runs, the inlet bellmouth was fitted at the forward end of the calibration inlet duct shown schematically in Figure 3. Note that the inlet duct of Figure 3 is not the same as that of Figures 6. In turn, the inlet duct of Figure 6 differs from that of Figures 14 to 16. The reason is that three different inlet ducts were successively constructed and tested. The configuration of Figure 3 was first constructed. It was rapidly found that the mass flow throttling cone shown there was not satisfactory, since it caused a flow distortion in the inlet duct, because of which volume flow measurements were not possible. It was not possible to lengthen the inlet duct appreciably because of the lack of space; therefore, the inlet cone was eliminated. Throttling of the flow was accomplished by means of the ground board.

Next, it was found that the inlet duct area was too large for the volume flow of the system, so that, at moderate capacities, the duct velocity was so small as to be impossible to read accurately. The inlet duct was therefore redesigned and its inlet area reduced by a factor of two.

Instrumentation

The purpose of the tests was to make only a limited number of test runs, but to make them as accurately as possible. It was felt essential, therefore, that the instrumentation be of the highest quality. The tests were made in accordance with the best existing standards. In particular, the Standard Test Code of the Air Moving and Conditioning Association (Reference 1) was adhered to strictly. Efficiency was defined precisely and uniquely. In order to be consistent with the nomenclature of the Appendixes I and II, it was not possible to use the symbols recommended by the AMCA Code.

Details concerning the instrumentation used for torque measurement, rpm measurement, volume flow, and total and static pressure measurements can be found in Reference 10.

Calibrations

Details concerning the calibrations which account for the power absorbed by the bearing forward of the torque pickup and for the pressure loss through the inlet duct are discussed in Reference 10.

CIRCULAR MODEL

Design of Model

Fan. The fan, model RD 20-70, was designed by Joy Manufacturing Company from data supplied by Aerophysics. Its full-scale counterpart is the basic air mover for the GEM machine which was the subject of the ONR-Marine Corps competition of the spring of 1961 (Reference 9). The same fan was also used in the Aerophysics Company entry to the Navy Bureau of Ships competition (Reference 8). The model fan used in the present program is about a one-sixth scale model of the full-scale fan.

The same full-scale fan was also used for the structural analysis study performed under the present contract and reported in Section V and for the design analysis reported in Section VI.

Computed performance of the fan (also labelled Model RD 20-.7-1.3-75°) at 1600 rpm is shown in Figures 12 and 13. The method of computation is discussed in Appendix I. A photograph of the constructed fan is shown as Figure 2.

Before being installed in the model in Washington, D.C., the fan was extensively tested for structural integrity, vibration-tested and stress-coated by Joy in New Philadelphia and Cleveland, Ohio. A discussion of these tests can be found in Reference 7.

Inlet Blades. Inlet blades were designed for the internal-flow model (as shown on Figure 4) but were never installed. They were of a shutter type, meaning that when at 90° to the entrance flow, they closed the inlet completely. Performance of the inlet vanes for the fan alone was predicted in Figure 52 (Appendix I). It was felt that performance of the inlet vanes would be independent of the GEM internal-flow configuration, that their performance could now be predicted accurately, and that therefore their incorporation in the model was of secondary interest.

Internal- Flow Ducting. As mentioned earlier in this report, the circular model first tested does not represent a practical GEM configuration. The circular model does represent, however, the internal-flow configuration with minimum losses and maximum overall efficiency. Also, it was believed essential to test it to prove or disprove the effectiveness of cutoff blades in the annular nozzle.

The general test setup is shown in Figure 3. Details of the circular model configuration are shown in Figure 4. The fan is mounted with its axis horizontal. Therefore, the machine is rotated 90 degrees from its normal operating position, the ground being assumed to be vertical. The flow enters the fan from the left, is turned 90° by the fan, flows radially through the radial delivery duct, and is finally turned inwards 120° by the peripheral nozzle.

As can be seen from Figure 4 two nozzle configurations were successively tested, the first one with a wider nozzle (0.937 inch) than the second one (0.375 inch).

The model was constructed mostly of wood. The outer casing of the radial delivery duct and the turning fillet were made of fiberglass. The depth of the delivery duct was adjustable (5.25 inches, 4.25 inches, and 3.25 inches). Adjustments for depth changes necessitated sliding of the fan and driveshaft, to insure that the fan would always be at the center of the duct.

The most important feature of the circular model is the straightener vanes, shown in view B-B of Figure 4. As will be seen from the test results, these vanes were completely effective. Therefore, no effort was made to test a configuration with vanes inside the delivery duct itself.

Circular Model Specifications. Specifications for the wide- and narrow-nozzle configurations are shown in Figure 4.

Schedule of Runs

The detailed schedule of runs is given only in summary form in Reference 10.

Results of Tests

Internal-Flow-System Performance. The performance of the internal-flow system is shown in Figures 9, 10, and 11. The basic variable in abscissa is

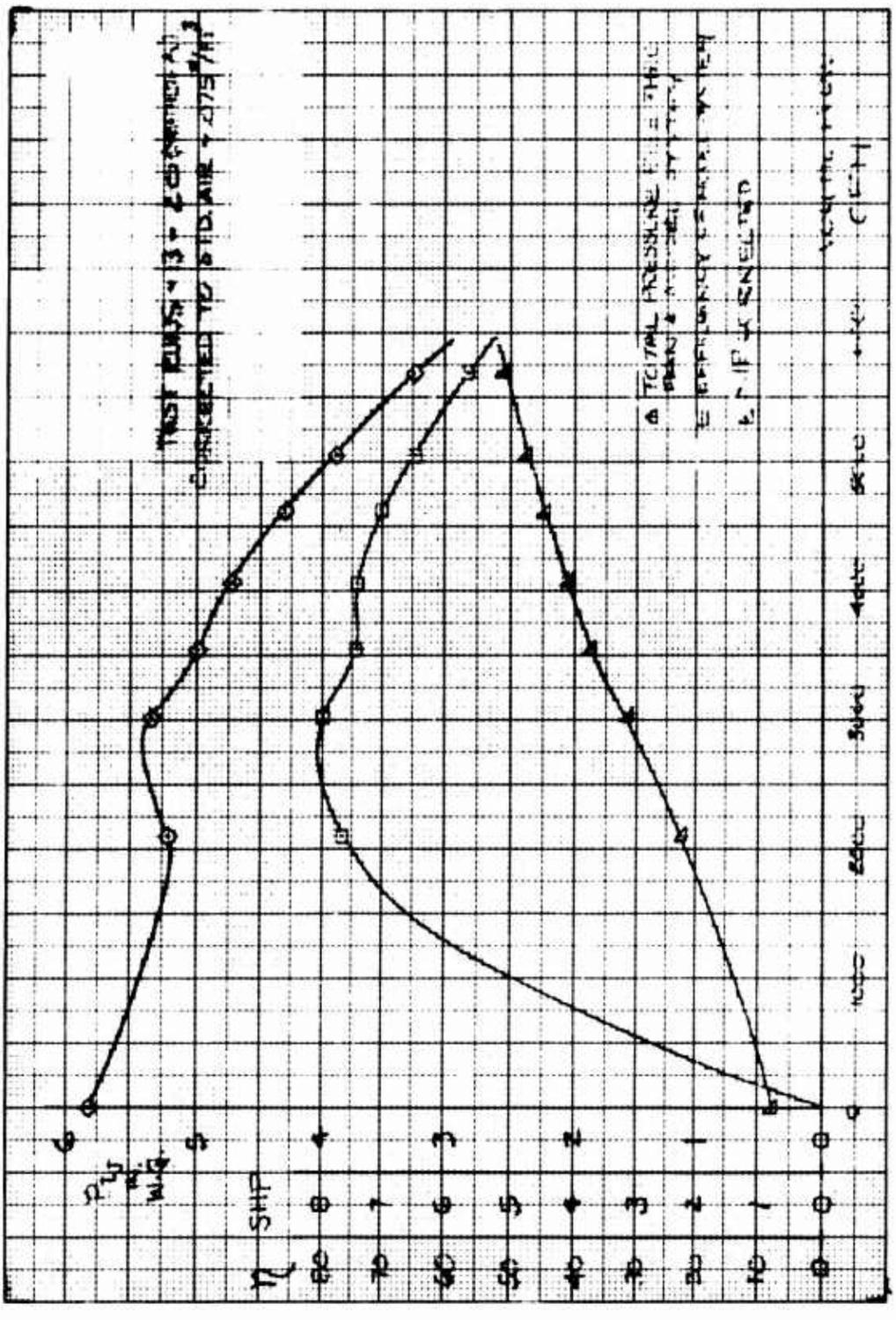

Figure 9: Measured Performance, Circular Model; Fan Speed, 1600 rpm; Delivery Duct Depth, 5.25 in.

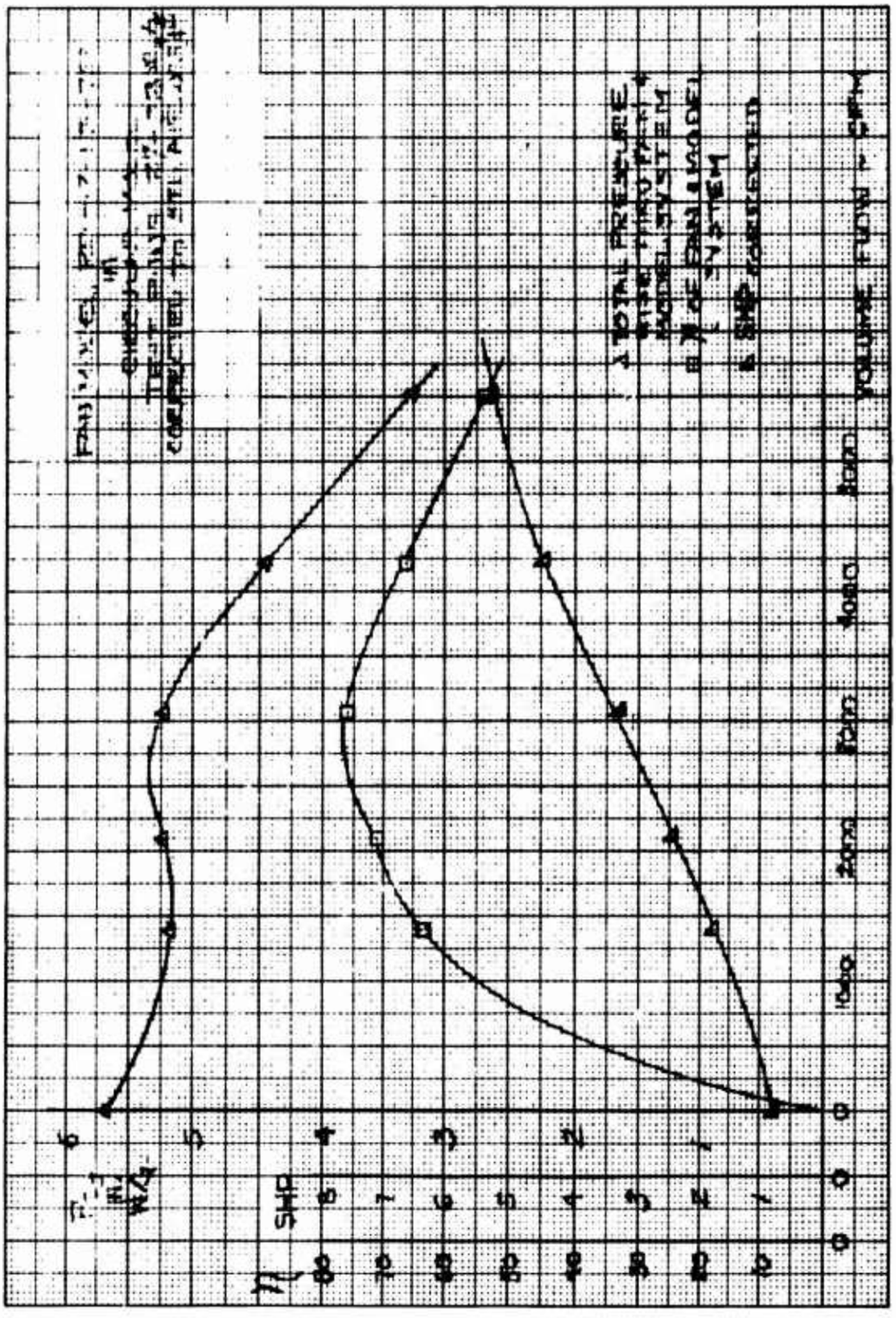

Figure 10: Measured Performance, Circular Model; Fan Speed, 1600 rpm; Delivery Duct Depth, 4.25 in.

Figure 11: Measured Performance, Circular Model; Fan Speed, 1600 rpm; Delivery Duct Depth, 3.25 in.

the volume flow or capacity. The volume flow was measured, as described earlier, by averaging the velocity distribution at a certain station in the duct ahead of the fan, using the standard AMCA method of Reference 1.

In ordinate are plotted the total pressure rise across the system, p_{t_j}; the total input power, SHP; and the overall system efficiency, η. These need to be described carefully.

The symbol p_{t_j} does not represent the pressure just downstream of the fan, but the total gage pressure at the peripheral nozzle exit. This pressure was measured at several locations along the periphery, and p_{t_j} is the pressure read at the nozzle, corrected for the pressure loss of the inlet calibration duct. Therefore, p_{t_j} corresponds to the total pressure rise across the fan, minus the pressure losses in the delivery duct and the turning losses in the nozzle. Therefore, p_{t_j} is the same total pressure in the jet which was used in the theoretical calculations of Appendix II. The total pressure just downstream of the fan was also measured, as well as the static pressure at various locations of the duct. They are not shown in this report, because they are not believed to be meaningful.

The input power, SHP, is essentially the product of the torque read on the strain gage recorder by the fan rotational speed, after allowance has been made as explained earlier for bearing frictional losses.

The efficiency is defined as the ratio of the air horsepower at the nozzle to the input horsepower:

$$\eta = \frac{q \times p_{t_j}}{550\ SHP}$$

Therefore, η is the system efficiency rather than simply the fan efficiency.

The results of the tests shown in Figure 9 for the wide delivery duct indicate the following:

BLANK PAGE

1. The maximum efficiency is 81 percent. A high efficiency is maintained over a wide range of deliveries: an efficiency higher than 70 percent is maintained over a range of deliveries corresponding to a ratio of 2.4 to 1.

   A corollary of this high efficiency is that the nozzle straightener does operate effectively and, therefore, is a desirable feature of the configuration.

2. The model fan is equipped with anti-surge (also called "modulating") vanes. These are effective, since the slope of the head-capacity curve remains positive all the way up to zero delivery. This feature is very desirable for a ground effect machine.

Figures 10 and 11 show the performance of the system for different delivery duct depths. It can be seen that the effect of reducing the depth of the delivery duct is to reduce slightly both pressure and efficiency. However, this reduction was found to be less than anticipated.

Note that the fan efficiencies obtained here would be raised by from three to five percent in a full-scale machine (say, 1000 HP), because of the scale effect.

It is concluded that system efficiencies of up to 85 percent can be obtained today, using an RD fan as air mover for a ground effect machine.

The results of Figures 9 to 11 are compared with the predicted results discussed under Phase II in Appendix I. The comparison is shown in Figures 12 and 13. It can be seen that the correlation is surprisingly good, for the circular model.

Cushion and Air Cushion Vehicle Performance. Limited performance results of the GEM air cushion were obtained, but they are not discussed here, since they have no bearing on internal-flow aerodynamics. (The interested reader is referred to Reference 10.)

OVAL MODEL

Design of Model

Two considerations were of paramount importance in the design of the oval model.

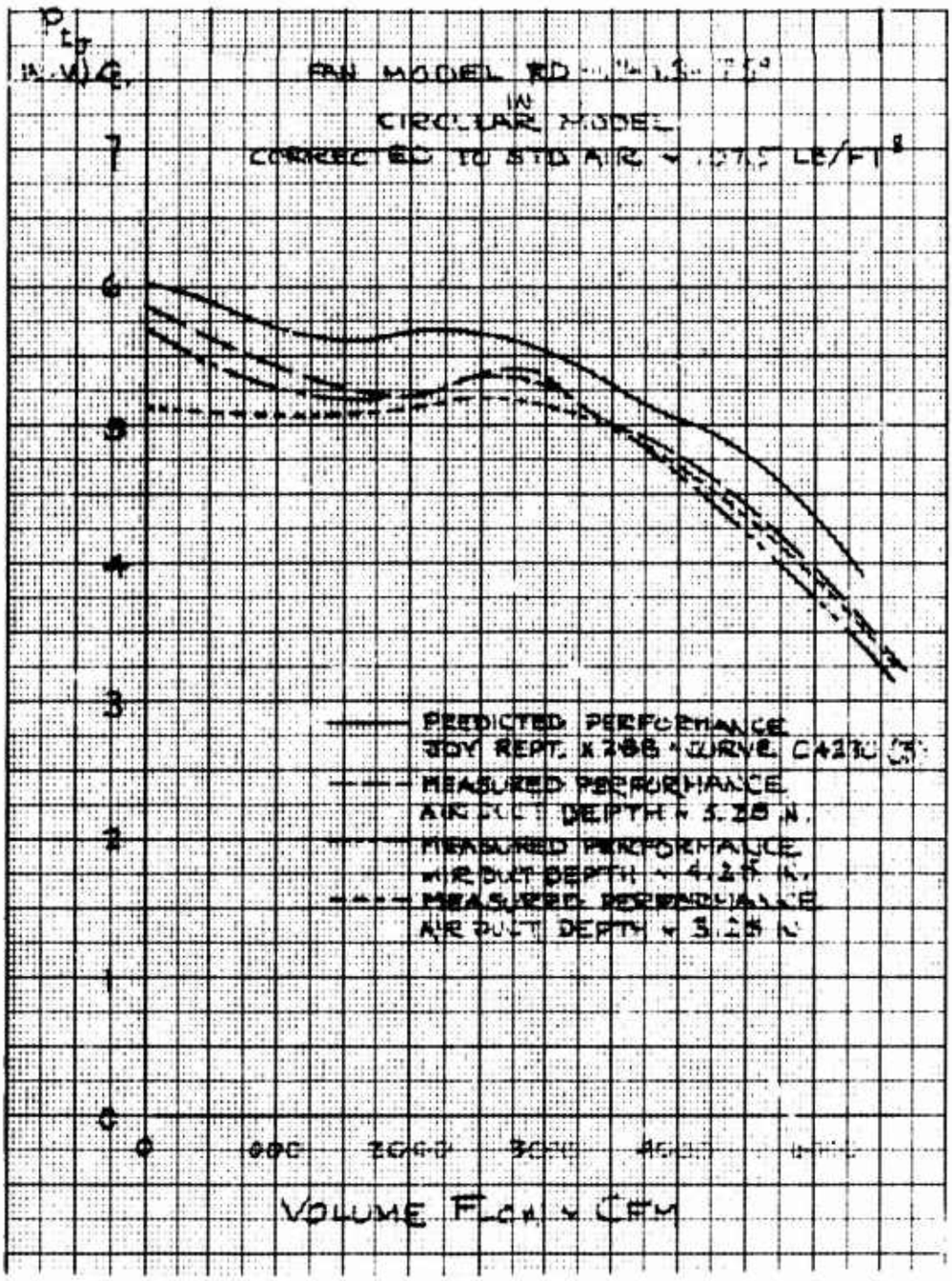

Figure 12: Comparison Between Predicted and Measured Fan Performance, Circular Model; Fan Speed, 1600 rpm; Total Head Against Capacity

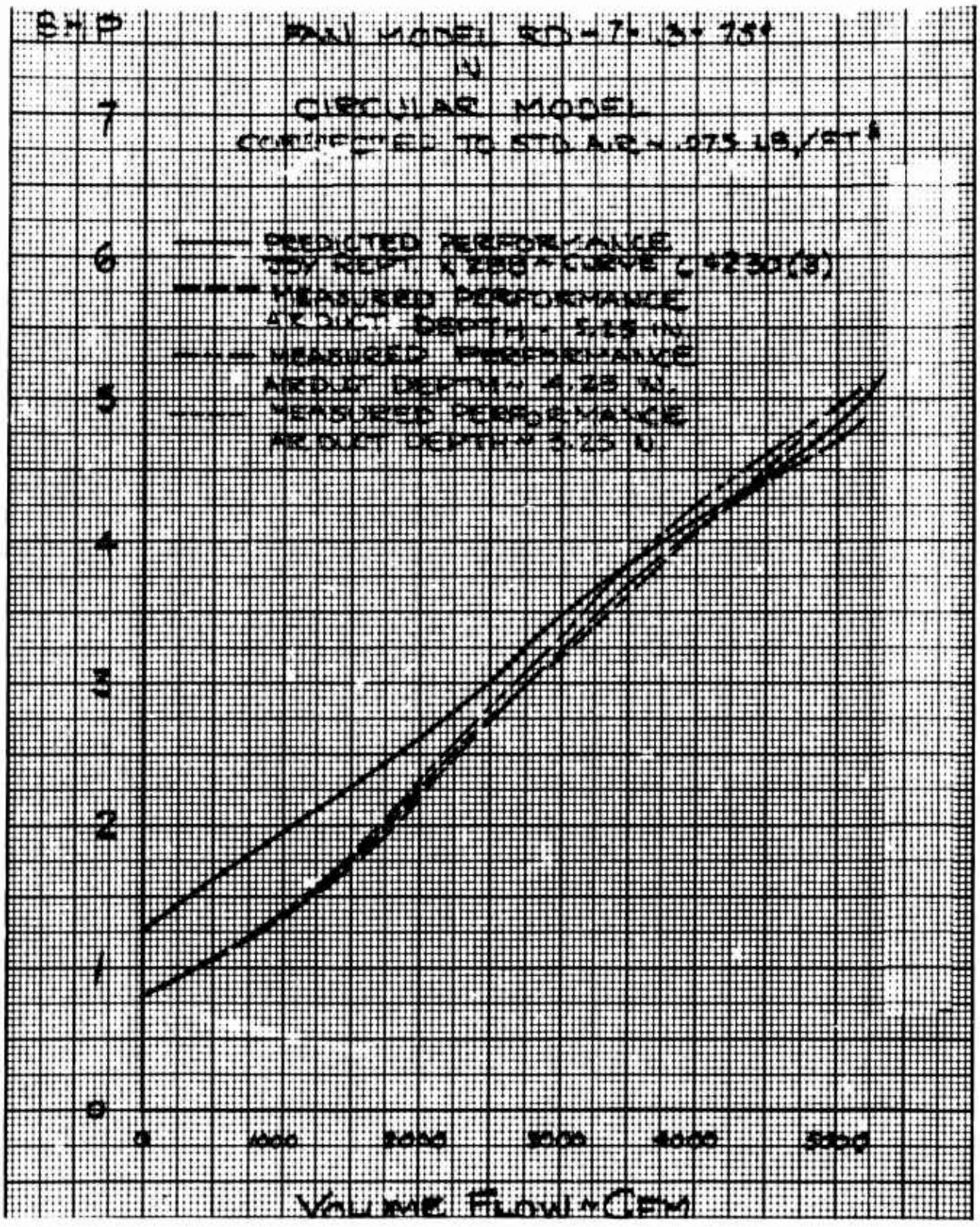

Figure 13: Comparison Between Predicted and Measured Fan Performance, Circular Model; Fan Speed, 1600 rpm; Horsepower Against Capacity

First, it was to be as similar as possible to the circular model; i.e., it was to use the same inlet, the same fan (tested at the same rpm), the same nozzle area, the same base area, etc. The only difference between the two models was to be in the planform shape of the peripheral nozzle.

Second, the planform shape was to resemble a useful configuration. Originally, it was intended to use a one-sixth scale of the Aerophysics ASG 4 model (proposal of Reference 9), as the internal-flow model. The shape finally used was that of the proposed Navy Bureau of Ships Hydroskimmer II, a model of which was currently being tested at the David Taylor Model Basin.

The oval model is shown in Figure 16. The model duplicates only one-half of the complete machine. Instead of a fully peripheral nozzle, one has an ogive. The second half of the machine is simulated by a wall which extends all the way to the ground.

Detailed design and fabrication of the oval model were started only after the circular model had already been extensively tested. Since the cutoff vanes in the peripheral nozzle had worked for the circular model, it was decided to use them for the oval model too. However, the flow in the circular model had axial symmetry, and the leading edges of the nozzle vanes were all set at the same angle, calculated to represent the local angle of the flow. The flow in the delivery duct of the oval nozzle is very far from having axial symmetry. It can therefore be anticipated that the leading-edge angle of the nozzle vanes must be set at different angles, depending upon the local flow characteristics. Since the flow cannot be theoretically predicted, one must make provision for the vanes to be fully adjustable. Access to the vanes inside the nozzle for this particular model would not be easy to provide. It was therefore decided to make a compromise and extend the vanes from the nozzle into the delivery duct. The vanes in the nozzle itself are fixed, but their leading-edge extension into the duct is adjustable, as can be seen from Figure 16.

The first runs were made with the vanes in the condition normally found in the peripheral nozzle. In successive runs, the vanes were bent by trial and error, the criterion for improvement being a smoothing out of the total pressure in the nozzle.

Since the oval model was built late in the program, only a limited number of tests were performed with it. An optimum vane angle distribution was never obtained, and one must talk more of trends than of definitive results.

The oval model was built mostly out of aluminum. No provision was made for varying the delivery duct depth; the largest depth of the circular model was used. The outside appearance of the model is shown in Figures 14, 15, and 16.

Model specifications can be found in Figure 16 and in Reference 10.

Test Results

Peripheral Distribution of the Nozzle Total Pressure. In the circular model, the total pressure in the peripheral nozzle p_{t_i} was found to be very uniform around the periphery of the nozzle.

As can be seen from Figure 17, this is very far from being the case for the oval model. Results of tests 46A, 47A and 16B, which are shown in Figure 17, were obtained at a constant nozzle height above the ground. In run 46A, the leading edges of the vanes were normal to the edge of the machine; in run 47A, they were slightly bent; in run 16B, they were bent some more. It can be seen that maximum pressure variations from the mean pressure, in the first case, were 30 percent. They are only 14 percent in the third case. Correspondingly, the mean pressure in the third case is mugh higher than in the first case.

It is concluded that adjustment of the nozzle vanes has a powerful influence on the peripheral nozzle total pressure distribution. By proper adjustment of the vanes, one can hope to approach a uniform pressure distribution, as with the circular planform model. Intuition suggests that one can hope, in such a case, to achieve efficiencies similar to those obtained with the circular model.

Internal-Flow System Performance. The performance of the internal-flow system is plotted in Figure 19, in the same form as was used for the performance of the circular model; i.e., pressure, power, and efficiency against volume flow. A substantial difference must be noted. The symbol p_{t_i} does not represent the nozzle total pressure, since it varies along the periphery. It is the arithmetic average of the pressure measured at 15 locations and shown on Figure 18. The calculation of the air horsepower at the nozzle, hence of the efficiency, is therefore approximate, since arithmetic averages were used instead of integration. The volume flow being measured upstream of the fan is not affected by the variations in total pressure. One way to check oneself is to verify that the volume flow calculated from the mean jet total pressure coincides with the measured volume flow. This was not done here.

Figure 14: Overall View of Test Setup, Oval Model

Figure 15: Overall View of Test Setup, Oval Model

BLANK PAGE

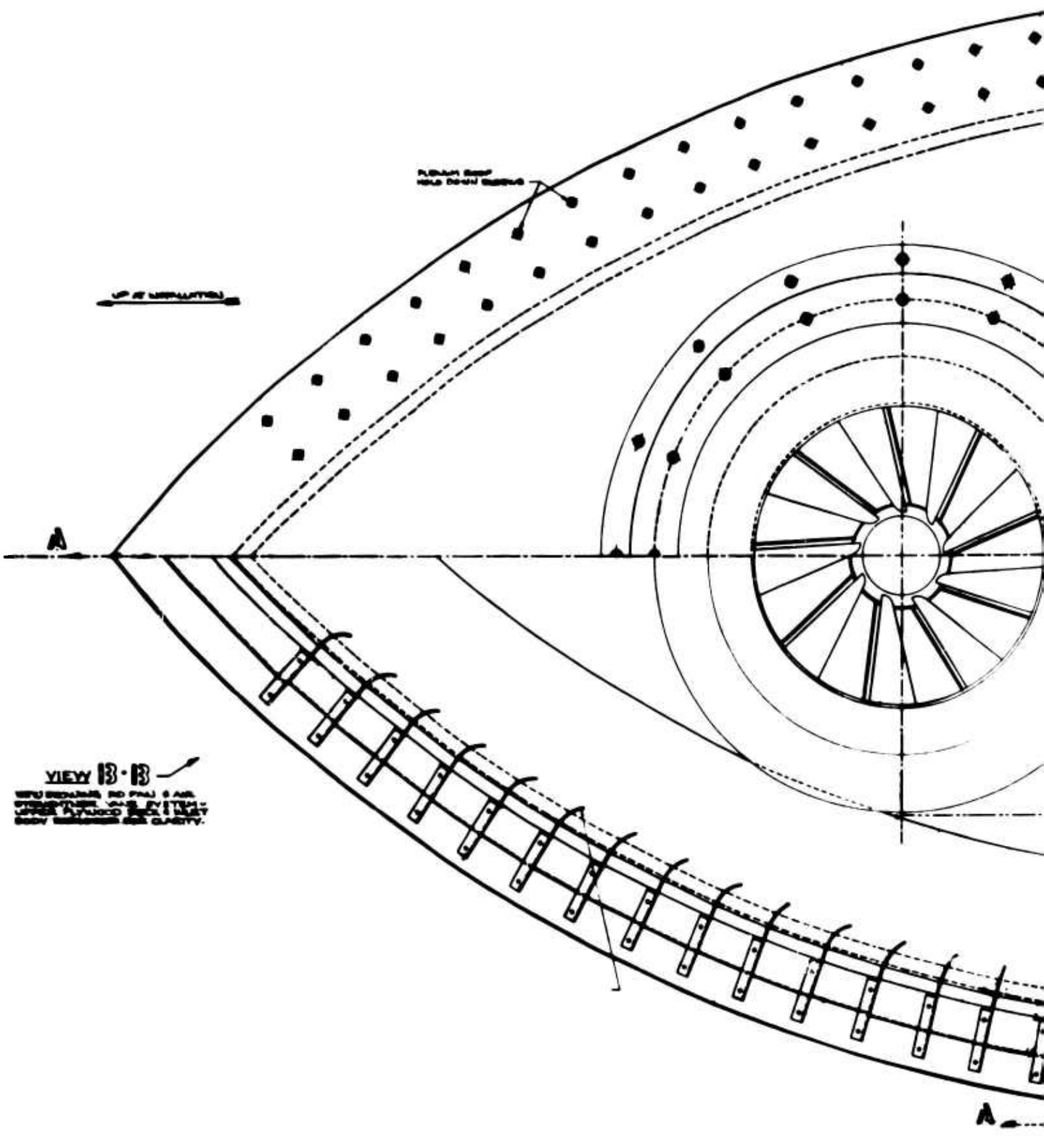

Figur

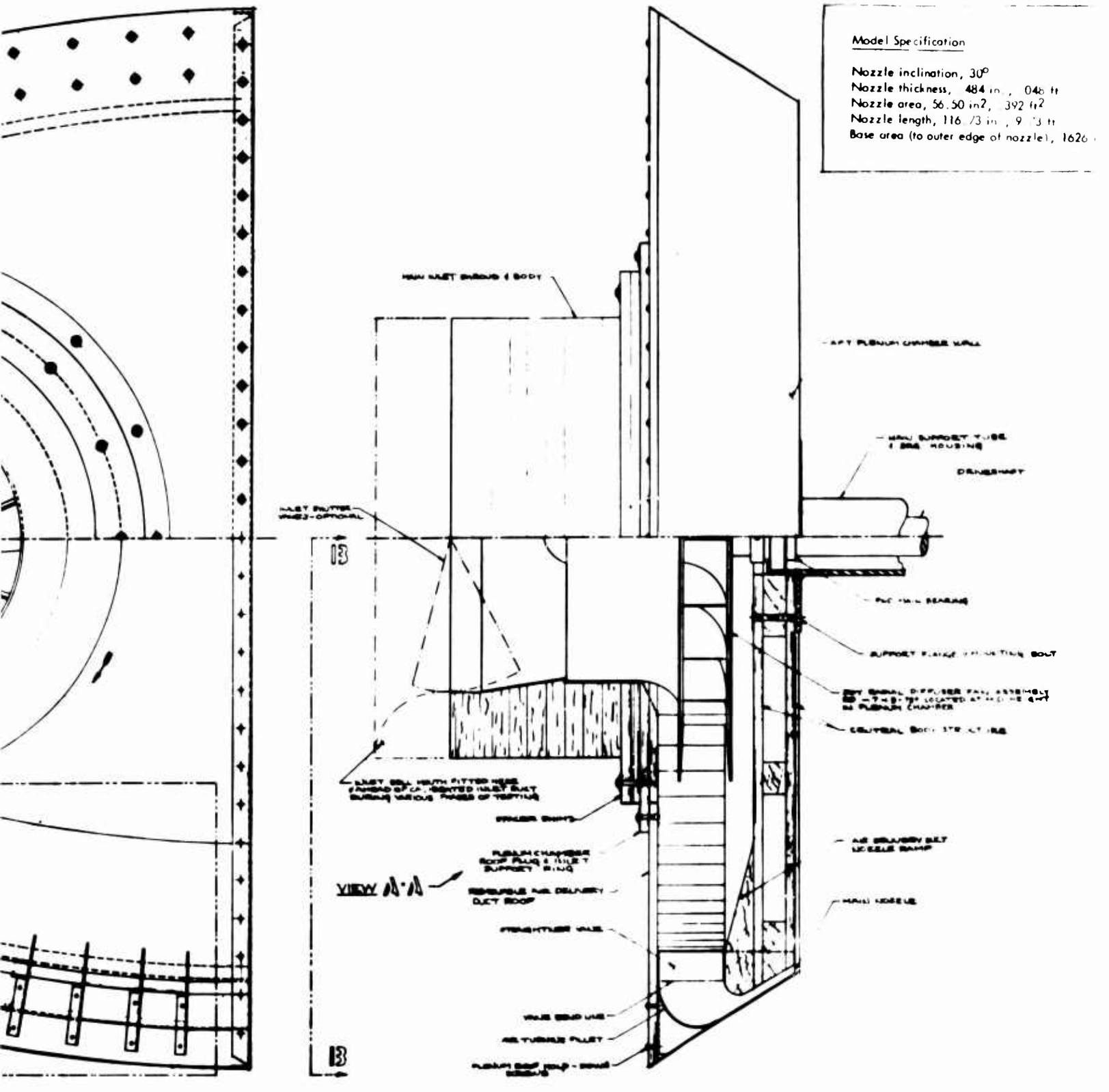

ure 16: Overall Oval Model Drawing

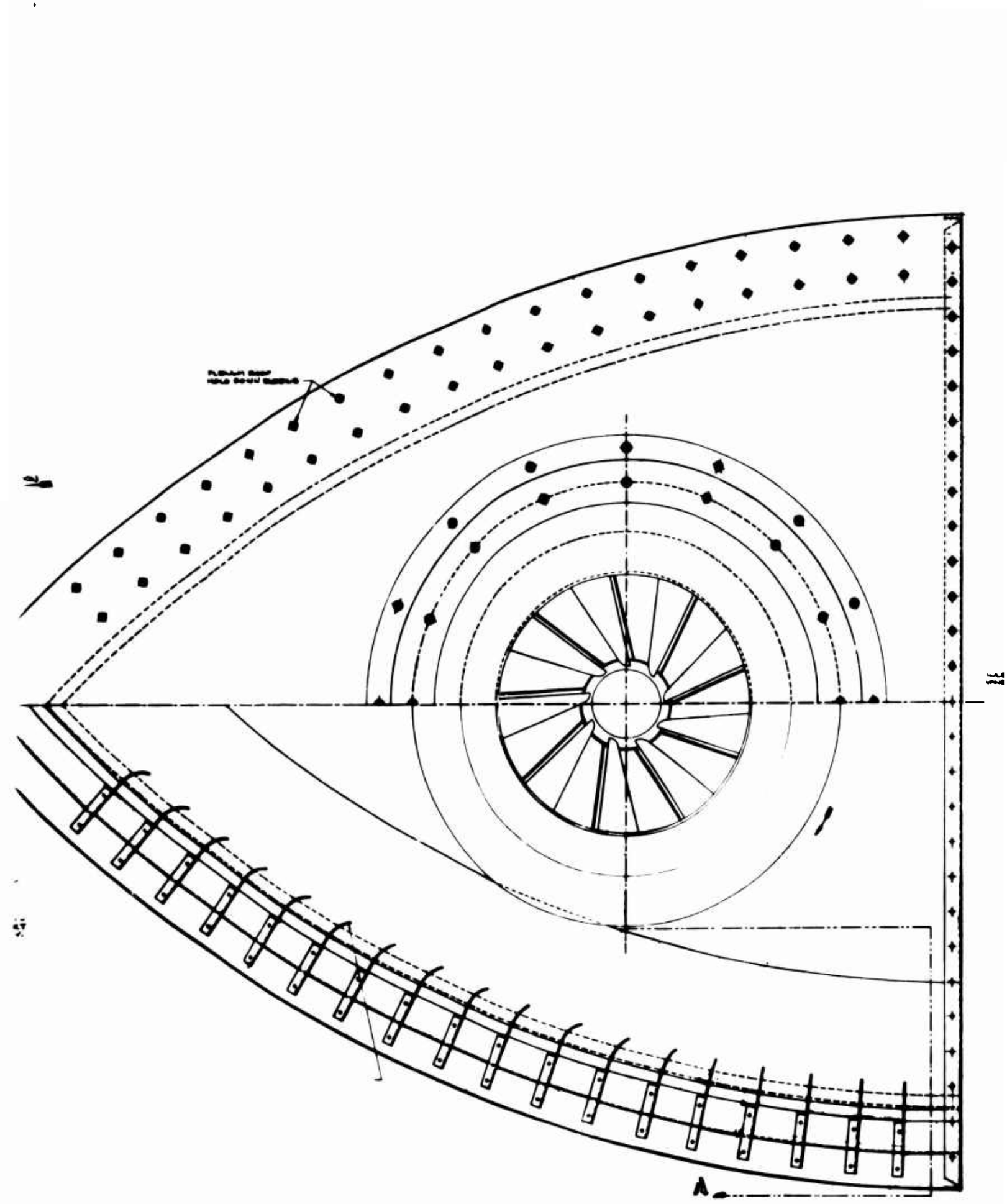

Figure 16: Overall Oval Model

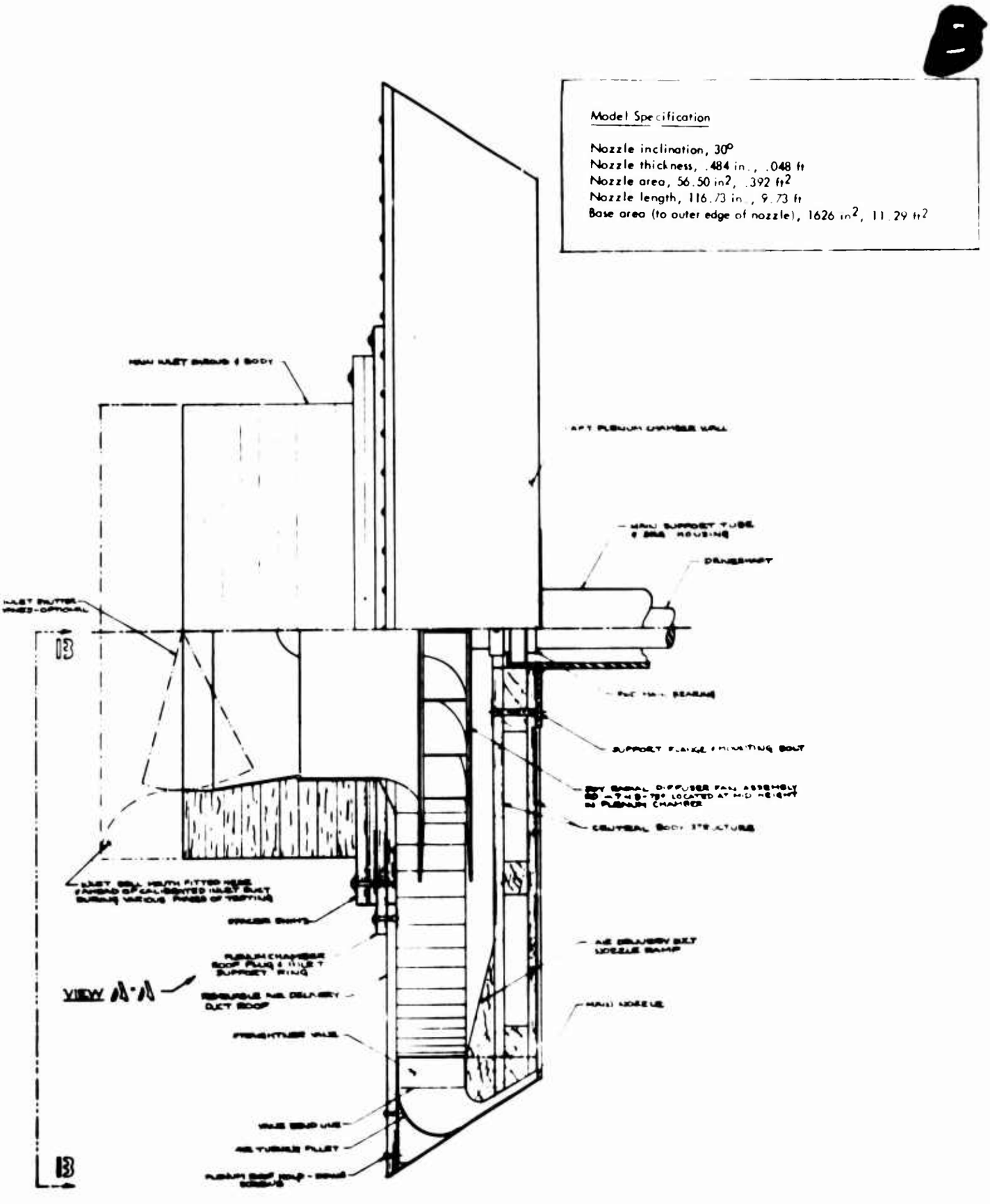
Model Specification
Nozzle inclination, 30°
Nozzle thickness, .484 in., .048 ft
Nozzle area, 56.50 in², .392 ft²
Nozzle length, 116.73 in., 9.73 ft
Base area (to outer edge of nozzle), 1626 in², 11.29 ft²
VIEW A-A

el Drawing

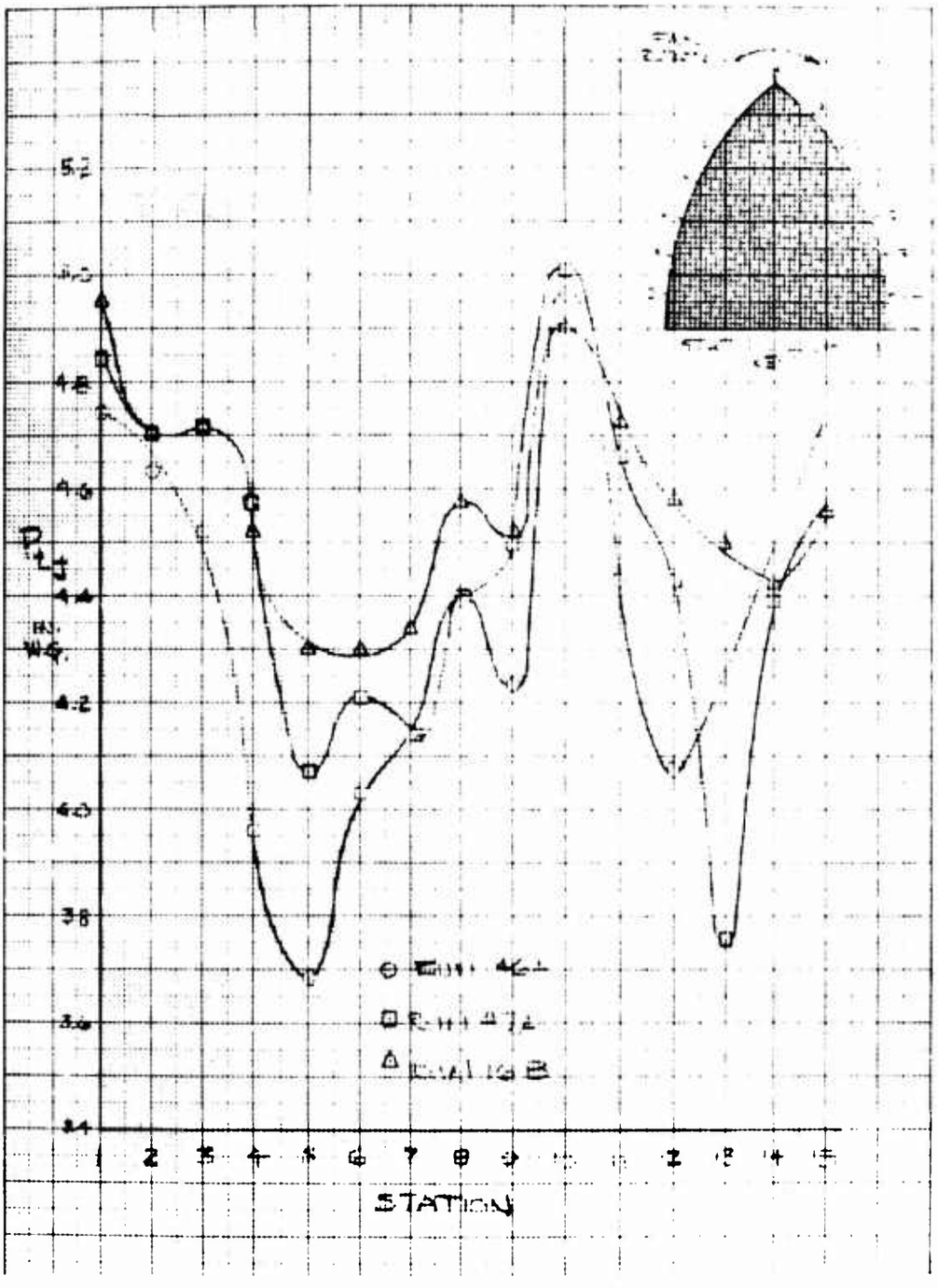

Figure 17: Peripheral Distribution of Nozzle Total Pressure for the Oval Model

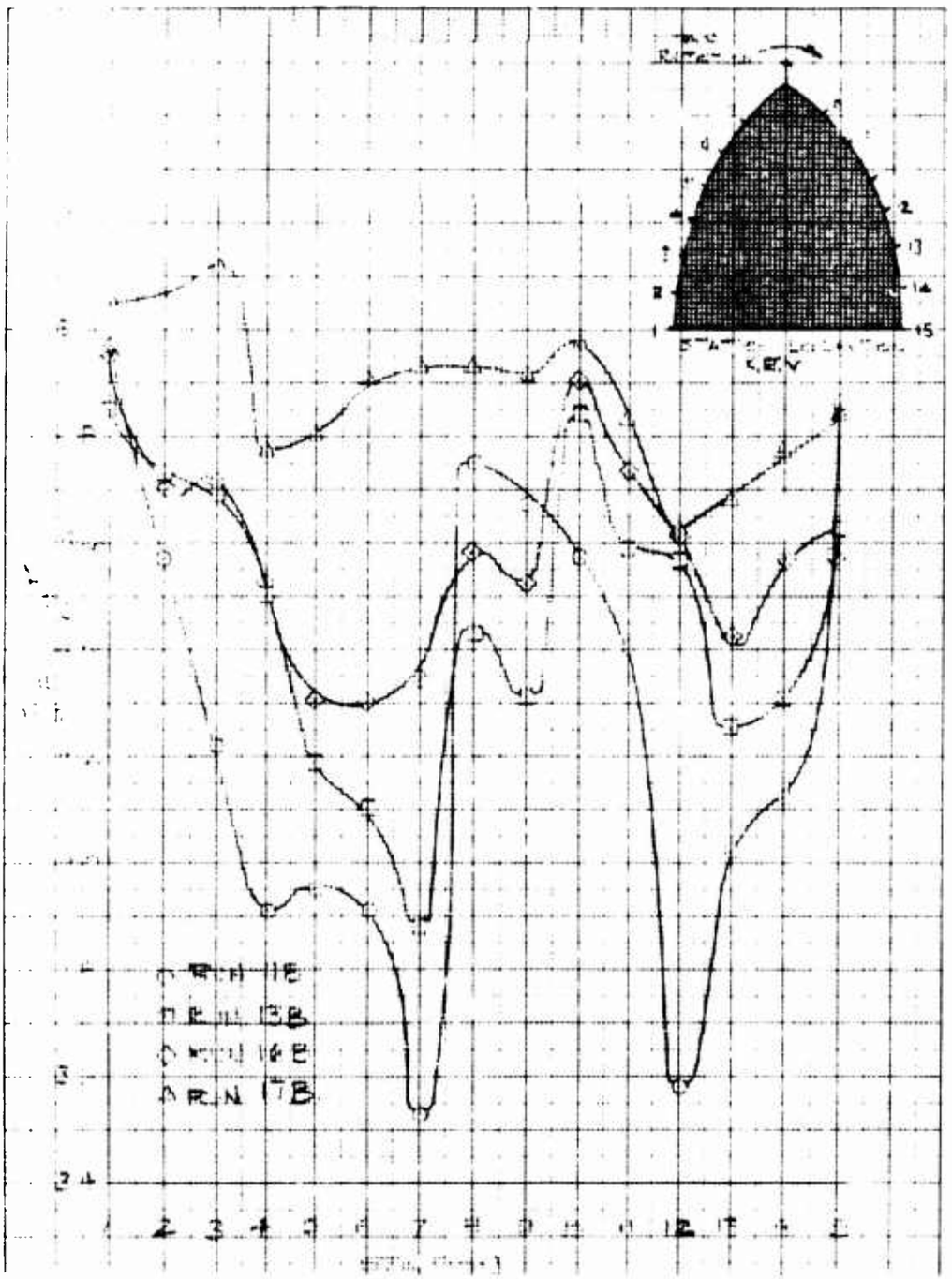

Figure 18: Peripheral Distribution of Nozzle Total Pressure for the Oval Model

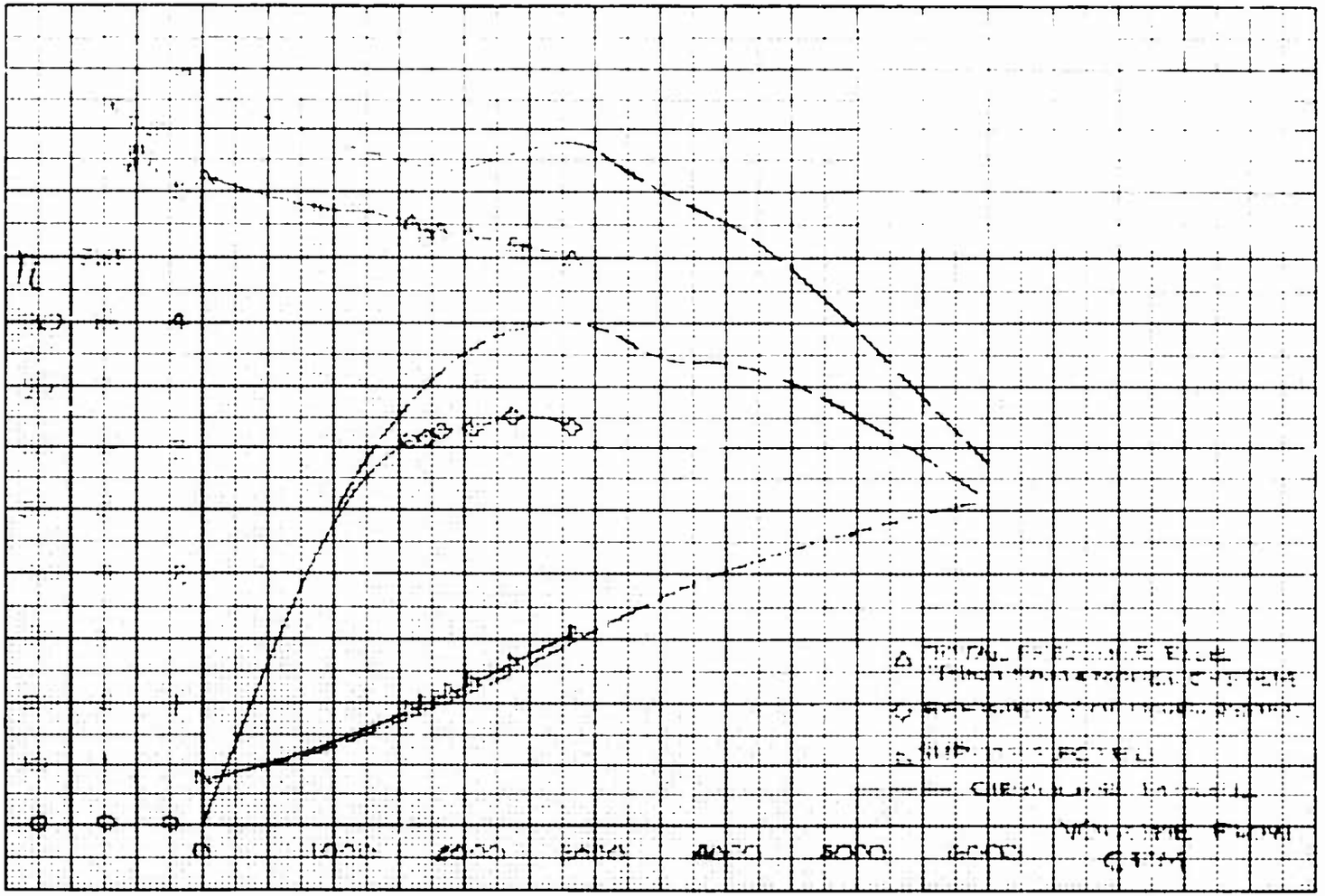

Figure 19: Measured Performance, Oval Model; Fan Speed, 1600 rpm; Delivery Duct Depth, 5.25 in.

The great interest of the performance results of Figure 19 comes from the fact that they are directly comparable with the results of the circular model testing, also shown on Figure 19. It can be seen that the losses due to the planform effect result in both a loss in jet mean pressure and in efficiency.

The most surprising feature is that the pressure loss is just as large at zero delivery as it is at the design point.

The loss in maximum efficiency is serious: from 81 percent to 66 percent. In comparison with other internal-flow systems, an overall efficiency of 66 percent, corresponding to an efficiency of 70 percent for the full-scale machine, is still quite good. There is no doubt whatsoever that these results can be improved by additional experimentation.

Critique of the Oval Model Experiment

Performance of the oval model at zero delivery is quite disconcerting. At zero delivery, corresponding to run 17B on Figure 18, it can be seen that the nozzle total pressure (upper curve with the triangles) is far from being constant. One would expect it to be constant and equal to the fan total pressure rise at shutoff. On the other hand, on Figure 19, the mean nozzle pressure is seen to be 14 percent lower than the corresponding pressure in the circular model. One would expect both pressures to be the same, since one uses the same fan at the same rpm.

A likely explanation of this phenomenon is the fact that the oval model is too small for its fan. It was preferred, in order to make the comparison possible, to use the same base area for oval and for circular models. Then, the circular model should have been larger, rather than the oval model smaller. There is a strong probability that an interference between the side wall of the delivery duct and the fan is causing the pressure loss. This matter can only be settled by building another larger oval model.

Also, some fairing should be used along the side which does not have a nozzle. Finally, as mentioned before, more time should be spent in attempts to optimize vane angles.

In conclusion, when the limited scope of the oval model program was considered, surprisingly encouraging results were obtained. There is no evidence that the efficiency obtained with the circular model cannot be obtained also with the oval model.

SECTION V

STRUCTURAL INVESTIGATIONS

APPLIED LOADS

In the absence of industry-wide, commonly accepted standards or government specifications for applied load criteria, as far as GEMs are concerned, it was necessary to preface the structural analysis by a state-of-the-art review of applied loads (see Appendix III). The investigation disclosed the existence of a surprisingly large amount of material, that this material could be fairly well rationalized, but that any suggested criteria had to be viewed with caution, considered only as tentative and updated at every available opportunity.

Naturally, load criteria for all types of GEMs cannot be identical. At the two extremes, small overland "demonstration" machines can be designed with very little thought being given to load criteria, while open ocean GEMs must be extremely sturdy.

From this standpoint, it is proposed that GEMs be separated into three classes, roughly based upon environment and size:

1. Overland GEM, fairly small size
2. Amphibious GEM, medium size
3. Open ocean GEM, fairly large size

Generally speaking, load criteria are the least stringent for the first category and the most stringent for the third.

It appeared reasonable that the typical RD fan of interest in this report would be usable in a fairly small machine (20- to 40-ton amphibian). Naturally, the applied loads for which the fan must be designed depend markedly upon the location of the fan within the machine. Then, tentative criteria must be given in a conservative fashion for the worst case of rotational acceleration in order not to restrict the choice of the designer to put the fan at what he believes to be the optimum location. The load criteria suggested in Appendix III for the design of the RD fan are as follows:

> Cruise or continuous operation, cyclic loads $\pm$ 1 g (limit) vertical, for an operating life of 20,000 hours.

Impact (primarily hydrodynamic) ± 4 g's vertical; ± 5 g's (limit) horizontal.

Crash conditions required of the fan bearing and bearing support structures: 10 g's (ultimate; ultimate loads are 1.5 times limit loads) applied horizontally and vertically.

Possible fan load alleviation is achieved by (1) increase of hover height; (2) protective structures (crushable material over the bow, for example); and (3) shock mounting of the propulsion system. (Details are discussed in Appendix III, "Applied Loads".) It is concluded that alleviation of dynamic loads, such as those created by the impact of waves at sea, can be achieved in several ways and that, when obtained, they can result in weight savings for the craft. For today's designs, however, a conservative approach, with no load alleviation, must be followed.

STRUCTURAL ANALYSIS

The structural analysis study of the Joy RD fans was made by Joy under subcontract to Aerophysics Company. The analysis is presented in Reference 7 and only its salient features will be discussed here.

First, Etablissements Neu and Joy Manufacturing Company have considerable experience in predicting the stress levels of a rotating-diffuser impeller. Such experience was gained experimentally, from extensive strain-gage results on wheels of all sizes. Correlation techniques were evolved that permit calculation of stresses on wheels of all sizes that are geometrically similar. In the present program, concerned with the application of RD wheels to GEMs, the reason for the stress analysis was twofold: (1) to permit the safe design and fabrication of the lightest possible structure, which is of paramount importance for an airborne application, while it is inconsequential for stationary applications; (2) to evaluate the possible effect of the dynamic loads encountered in airborne applications. It was found, therefore, that, for the present study, the application of the Neu-Joy routine stress-prediction method would not answer the above-mentioned objectives.

Second, the analytical determination of stresses in an impeller of the RD type is not an easy task, since the RD impeller is shrouded; therefore, the structure to be analyzed is indeterminate.

The stress analysis carried out in Reference 7 is an approximate one, in which tangential and radial stresses are calculated as if the shroud did not exist, using the constant-thickness ring method (Reference 19). It is assumed that the stresses are primarily the stresses induced by the centrifugal force of the disc itself and of

the parts supported by the disc. Since the effect of the redundancy is to reduce the displacements due to the tangential and radial stresses above, it is also to reduce these stresses. Therefore, an analysis which does not account for the presence of the shroud is a conservative analysis. Details of the analysis of Reference 7, which is quite lengthy, are not reproduced here.

The effect of g-loads applied statically on the RD rotor stresses is analyzed in Reference 7. It was found that this effect was not significant, since the g-loads are always small compared to the centrifugal loads. An analysis of the dynamic response of the fan under the action of the g-loads was not made.

The maximum stresses calculated from the determinate analysis described above were compared with available French test data and found to be in good agreement. The use of a safety factor of about two is recommended, however, primarily because of stress concentrations at the welds attaching the blades to the other structural parts.

Numerical calculations were carried out for a particular fan with a 156.75-inch outside diameter, designed to deliver about 310,000 CFM against a static pressure of 18 inches of water. The layout of this fan is shown on Figure 20, using conventional welded-aluminum fabrication techniques. It was concluded from the analysis of this fan that its structural soundness appeared excellent: "The Aerophysics full-sized RD rotor appears to be adequate for the intended application."

Recently, an indeterminate stress analysis for shrouded discs has become available (Reference 22). It was not possible to apply this method to the RD wheel within the scope of the present contract.

LIGHTWEIGHT FAN ANALYSIS

In the previous paragraph, the design and stress analysis of a specific fan were described. This design reflects the utilization of time-proven know-how relative to a welded structure of minimum weight. As a means of deriving some basis for subsequent weight reduction studies, the weight of the analyzed rotor (shown in Figure 20) appears in Table 1 (the impeller nomenclature is shown in Figure 21).

An immediate attempt may be made to reduce further the basic weight of 2074 pounds by questioning the geometric shape from an aerodynamic standpoint. This

Figure 20: Impeller Layout, Joy RD Fan 121-70

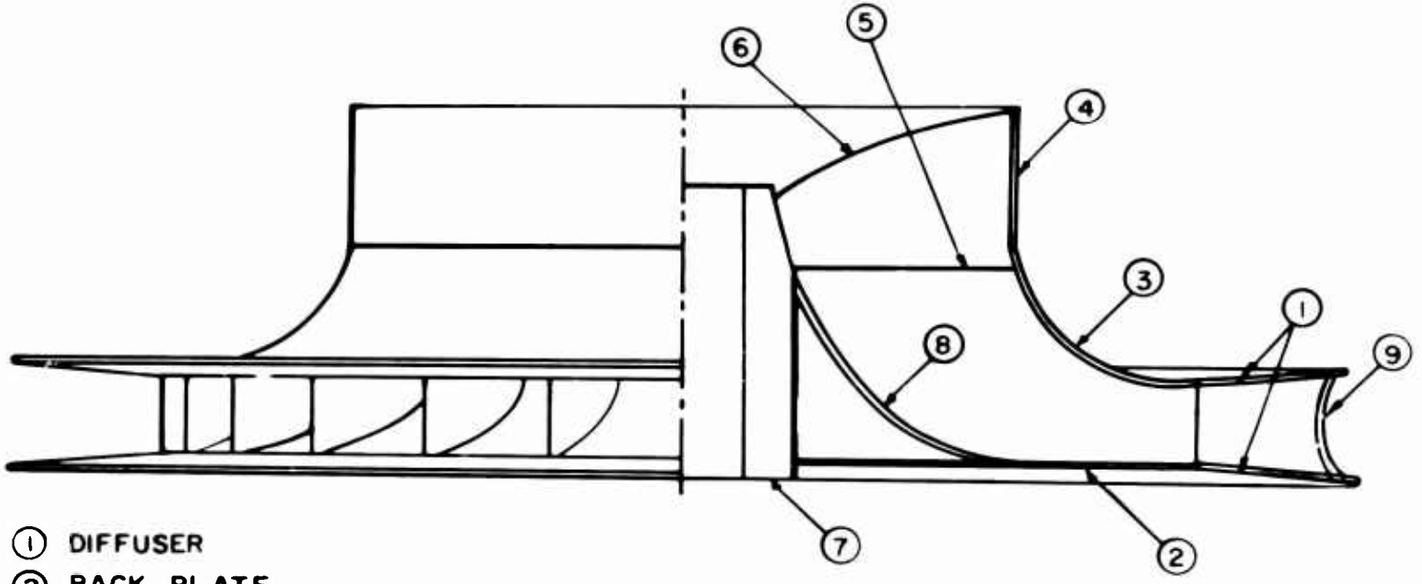

① DIFFUSER
② BACK PLATE
③ CONE
④ INLET CYCLINDER
⑤ BLADE
⑥ INDUCER
⑦ HUB
⑧ FAIRING
⑨ MODULATING VANE

①③④ FRONT SHROUD
①② BACK SHROUD

Figure 21: Impeller Nomenclature

approach indicates that the axial length of the inducer section (inlet) of the impeller could be reduced substantially without appreciably affecting aerodynamic performance. This change alone would institute a weight reduction of 164 pounds and would yield a new weight of 1909 pounds (see Table 2).

Further weight reduction could be accomplished through the utilization of absolute minimum sheet thicknesses as recommended by the Product Development Group at Alcoa, New Kensington, Pennsylvania. The two above recommendations are based solely on their experience with similar welded structures, with warpage and burnout being the sole consideration. The prime purpose for this study is to obtain a theoretical absolute minimum weight for the conventionally constructed rotor. The weight (1564 pounds) resulting from this study is shown in Table 3.

This absolute minimum weight could be carried one step further by replacing the aluminum with magnesium. However, the use of magnesium will dictate that careful attention be devoted to corrosion, stress corrosion, and residual stresses resulting from the joining operation. For further information on stress corrosion, see Joy Reports X-280 and X-284 included as part of Reference 7. Since the density ratio of magnesium to aluminum is .064/.096, or 0.66, the absolute minimum weight now becomes 1032 pounds (0.66 x 1564).

With the preceding considered as the maximum exploitation of weight reduction for the conventional design (welded structure), many alternative designs which utilize relatively new materials warrant examination and study.

The use of molded, reinforced plastics was expanded rapidly over the past several years with the choice of one molding being a major problem. The various methods selected for molding reinforced plastics usually depended upon physical properties and final cost. Strength, heat and cold resistance, weight, tolerances, and the like will largely determine selection of materials which, in turn, may dictate the type of molding.

From a weight standpoint, most reinforced plastics have a density and strength-weight ratio comparable to that of magnesium. Consideration of the geometric shape of the RD fan indicates that several components must be molded (shrouds and blades) independently and then attached by some efficient means. This point of attachment appears to be the major problem area which would limit the use of reinforced plastics. However, many adhesive bonding materials have been developed and could be used, or catalysts which would fuse the resins of the component parts at the junction points might be applicable. Joint strength in either of the above

methods would undoubtedly dictate increased section thickness. However, even if section thicknesses of the previously studied magnesium structure could be used, the resulting structural weight would be equivalent to that of magnesium, 1032 pounds.

One of the most appealing methods of construction from a weight standpoint would appear to be a "sandwich" construction, utilizing an aluminum skin and aluminum foil honeycomb core (see Figure 22). The selection of this type of construction and material is sound from any standpoint (cost, fabricability, strength, etc.).

Costs would be low since no extraordinary tooling would be required and the basic material costs are low and commercially available.

Fabrication would only necessitate the use of conventional metal working tools and related methods. From a strength standpoint, a knowledge of stresses in rotating discs indicates that stresses are unaltered as material thicknesses are decreased (neglecting boundary loads). Since the primary boundary load of the RD fan is imposed by a bending moment produced by the rotating diffusers, the skins of the sandwich in both front and back shrouds for component nomenclature may be ideally utilized to eliminate this bending moment.

The honeycomb core material would contribute the necessary material support for stiffness and overall rigidity of the thin skins.

The only remaining area requiring strict attention lies in the point of attachment of the component parts. Many adhesives for fabricating honeycomb sandwich construction have been developed to provide a bond with sufficient strength to satisfy the functional requirements in primary structures.

A detailed weight analysis of the rotor shown in Figure 22 is recorded in Table 4. The resulting weight of 655 pounds indicates that this type of construction for the purpose of weight reduction warrants much further study. The study should include the fabrication of a model of reasonable scale.

TABLE 1
WEIGHT ANALYSIS OF ALUMINUM ROTOR (IMPELLER ANALYZED)

Description	Number Required	Weight (lb.)
Inducer Blade	9	426
Radial Blade	9	275
Inlet Shroud Cylinder	1	160
Back Plate	1	389
Diffuser	2	228
Shroud Cone	1	244
Segment	18	99.5
Hub	1	243.25
Modulating Vane	17	7
Total Impeller Weight		2,073.75

TABLE 2
IMPELLER WEIGHT WITH REDUCED INDUCERS*

Description	Number Required	Reduction (lb.)
Inducer Blade	9	74.3
Inlet Shroud Cylinder	1	74.1
Hub	1	15.9
Total Impeller Weight Reduction		164.3
Total Impeller Weight with Reduced Inducers		1,909.45

* (See Figure 20)

TABLE 3
WEIGHT ANALYSIS OF ALUMINUM IMPELLER WITH MINIMUM ALLOWABLE MATERIAL THICKNESS

Description	Number Required	Weight (lb.)
Inducer Blade	9	321
Radial Blade	9	206
Inlet Shroud Cylinder	1	120
Back Plate	1	234
Diffuser	2	152
Shroud Cone	1	183
Segment	18	99.5
Hub	1	247.25
Modulating Vane	17	1.7
Total Impeller Weight		1,564.45

TABLE 4
WEIGHT ANALYSIS OF ALUMINUM IMPELLER WITH LAMINATED HONEYCOMB*

Description	Number Required	Weight (lb.)
Inducer Blade	9	81.9
Radial Blade	9	52.8
Inlet Shroud Cylinder	1	32.5
Back Plate	1	90.0
Diffuser	2	67.3
Shroud Cone	1	49.5
Segment	18	31.8
Hub	1	247.25
Modulating Vane	17	1.7
Total Impeller Weight		654.75

*See Figure 21

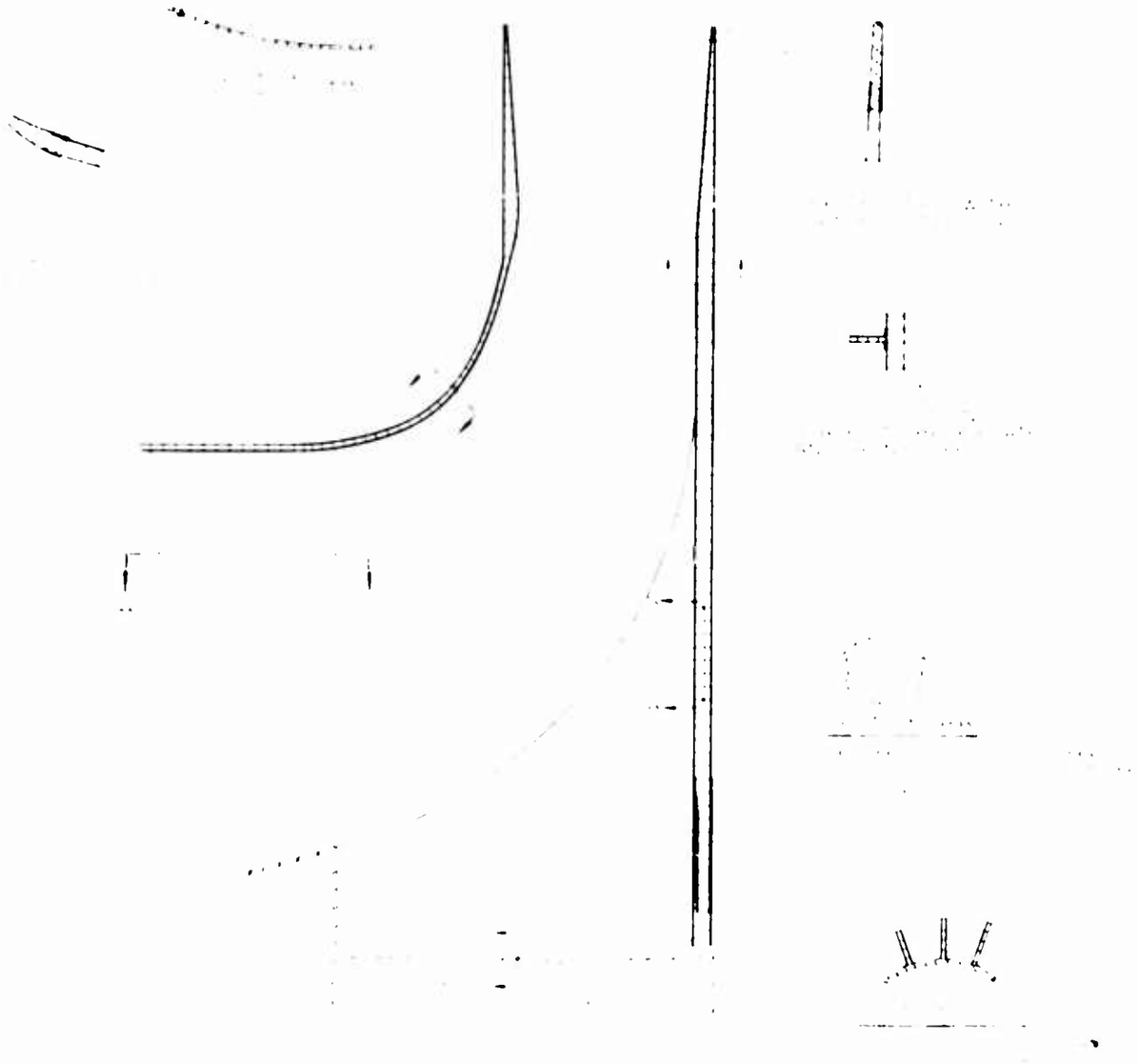

Figure 22: Impeller Layout, Proposed Redesigned Joy RD Fan 121-70, Lightweight Bonded Honeycomb-Aluminum Structure

SECTION VI

DESIGN STUDIES

SKIMMER I DESIGN STUDY

A substantial amount of information is available about the Bell Hydroskimmer I, which was constructed for the Bureau of Ships (see References 62 and 12 and Bell Aerosystems Company Report 2073-95001, dated February 28, 1962, for example). Hydroskimmer I is the outstanding example of an operating full-scale GEM in the United States. It was therefore logical to use Hydroskimmer I as a starting point for a design study in which the four axial-flow fans would be replaced by two rotating-diffuser fans.

To evaluate fairly two competing designs is difficult. An evaluation should not be made by the designer of one of the two craft but rather by an impartial observer. Also, it is not quite fair to compare a proposed new design with an older design; the designer of the latter one, if starting again, would certainly produce a higher performance machine. Finally, even though extensive tests have been performed on the Hydroskimmer I, the results of these tests have not yet been published, and one must rely on the calculated rather than the actual performance.

With all the above considerations in mind, it has been felt desirable in the present study to limit oneself to fairly general considerations and to avoid such things as a comparison on the basis of a mission profile, since the Hydroskimmer is a general research vehicle, which was not designed for a particular mission.

The newly-designed Skimmer I will be called Skimmer IB.

In the design of IB, as many of the features of Skimmer I as possible, with the exception of the fans, were preserved. The overall size is nearly the same. The planform shape is slightly different. The perimeter of the nozzle is the same, which gives design IB a larger base area than design I. The engines are the same. The forward propulsion unit is the same. The useful load is the same (for a given endurance, however, fuel weight is reduced because of high internal-flow efficiency).

Design IB can best be comprehended by looking at Figure 23. IB is so much like the first design that they hardly can be differentiated from the outside. Because of the location of the four engines in a rear engine compartment, IB has a slightly slimmer look than Skimmer I. An inboard profile key for design IB can be found in Figure 23.

A

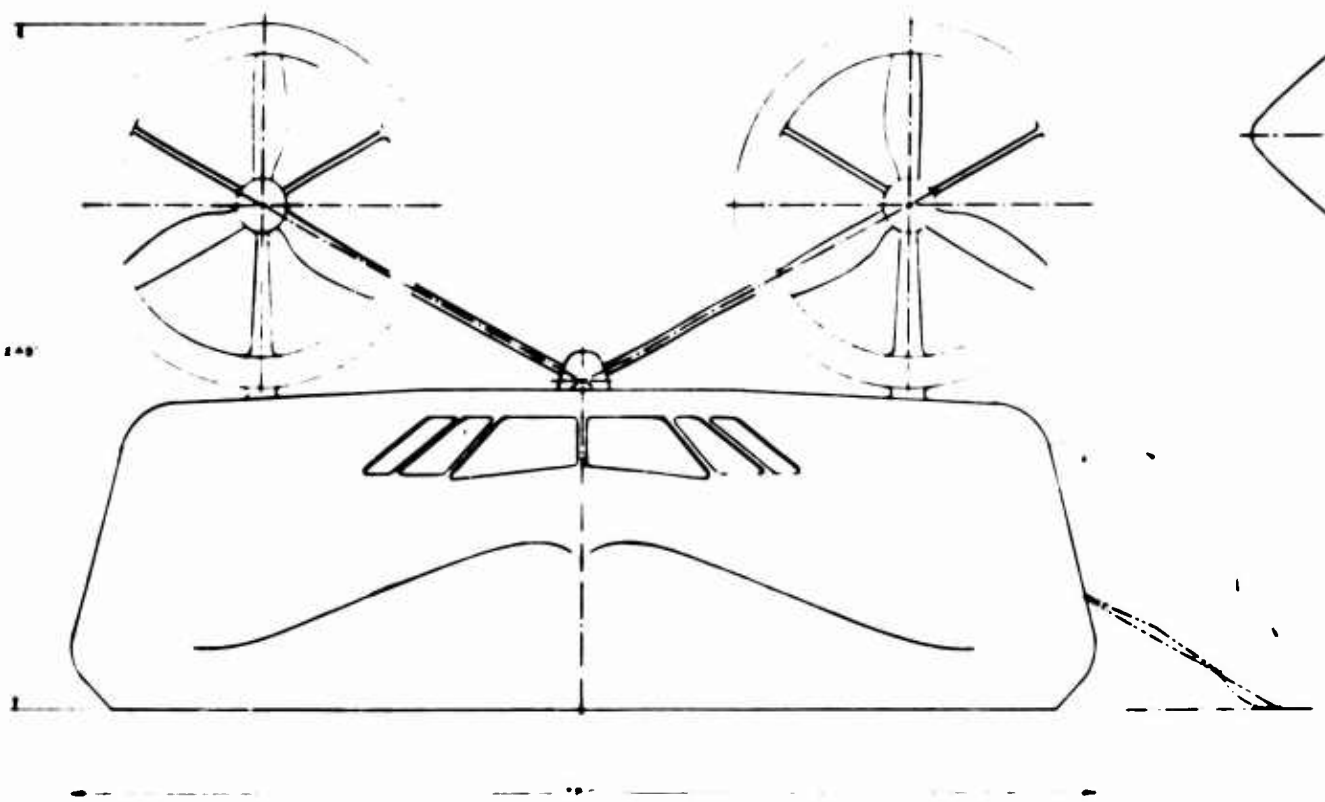

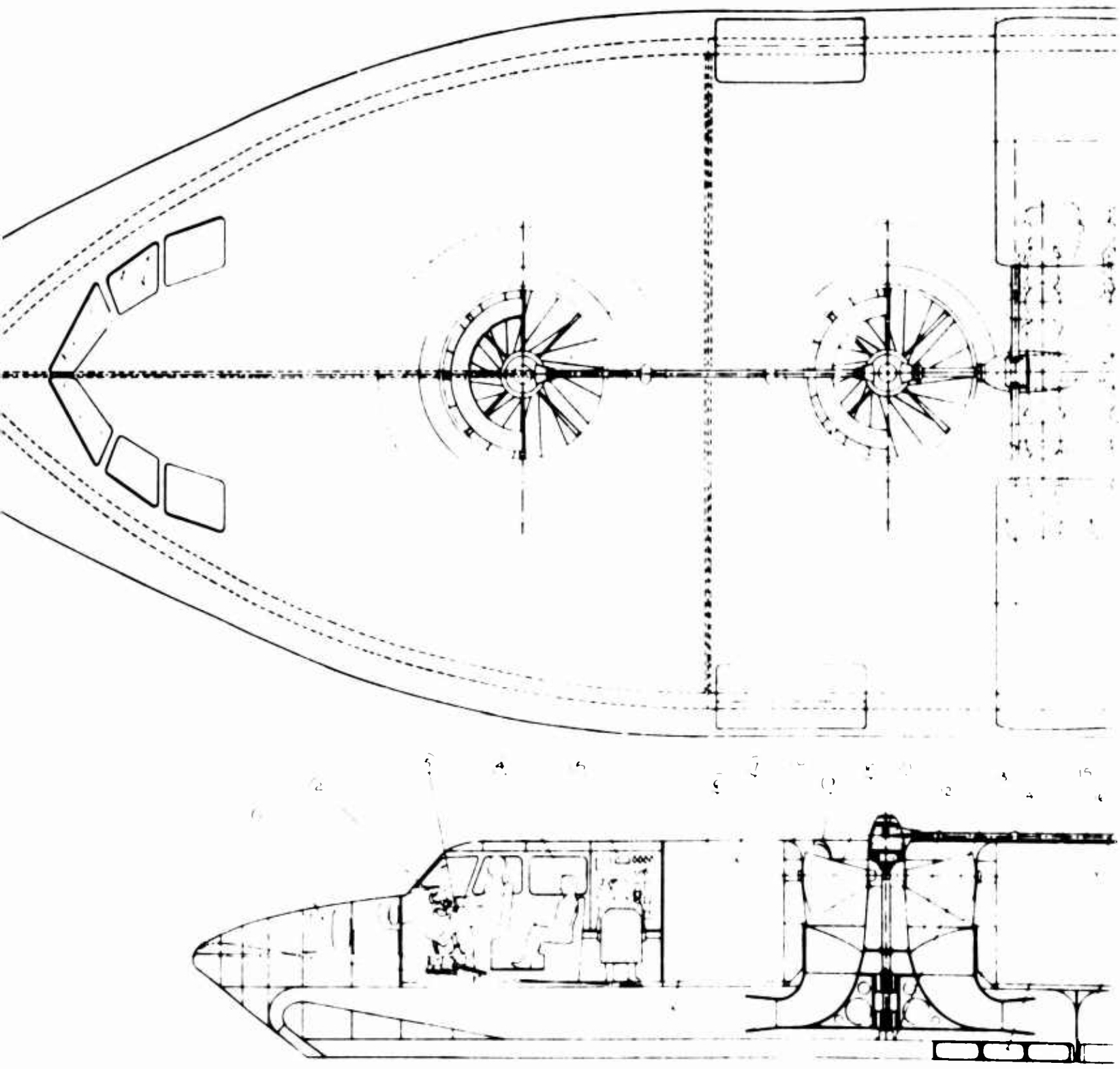

Figure 23: Design Study of a Hydroskimmer-I-Type GEM With Two RD Fans

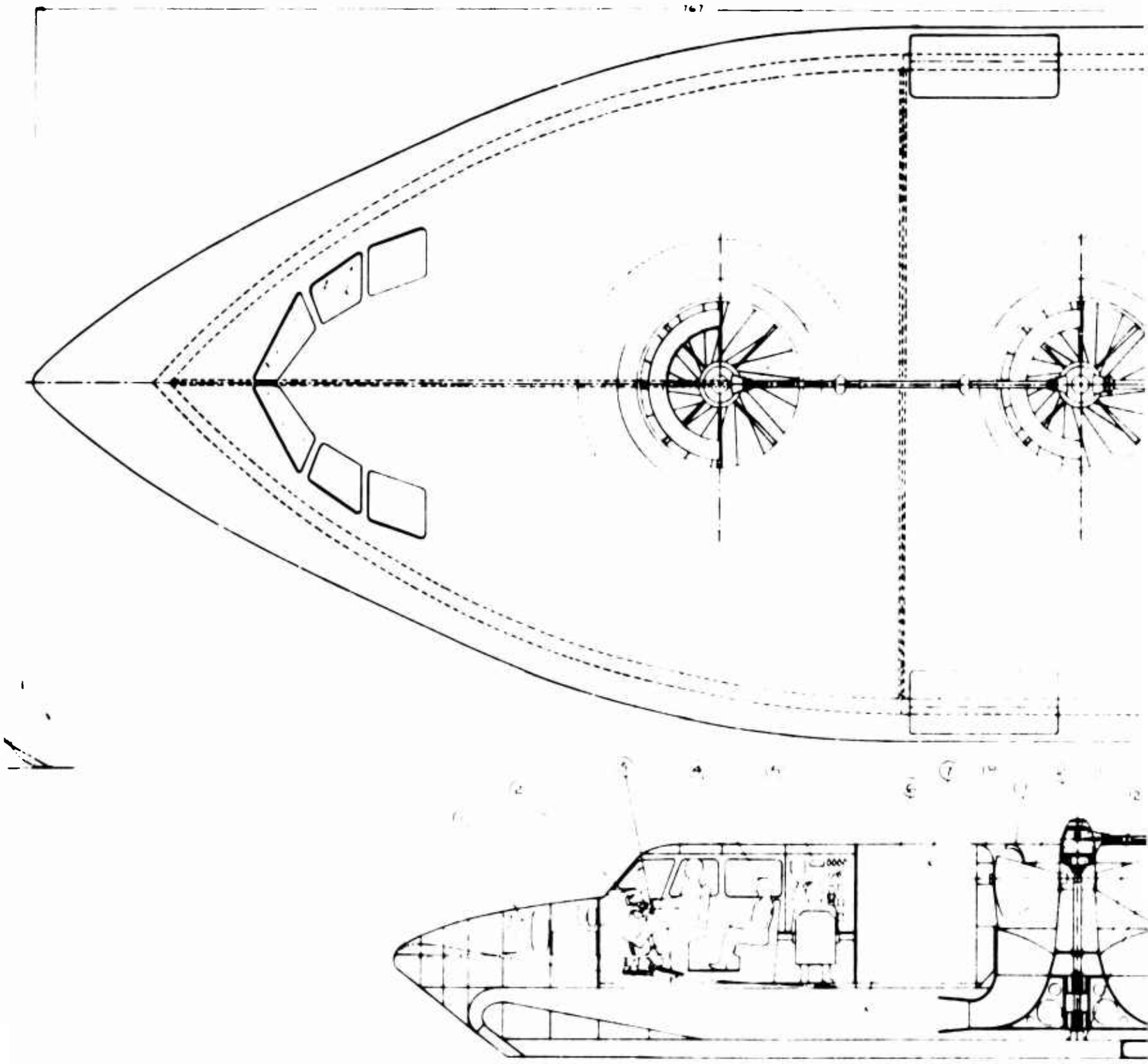

Figure 23: Design Study of a Hydroskimmer-I-Type GEM With Two RD Fans

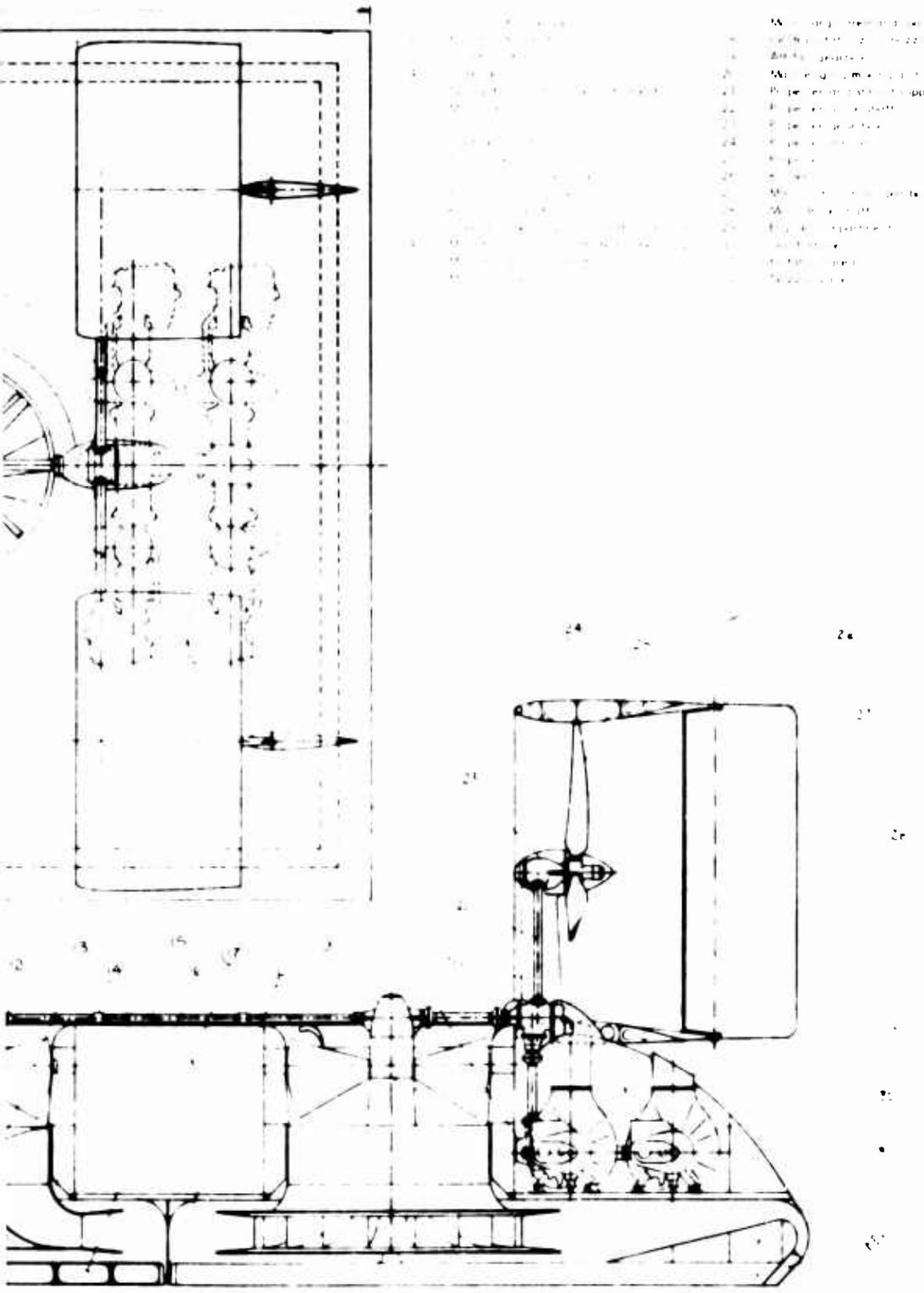

BLANK PAGE

An attempt at a weight comparison was made and is shown in Table 5. Taking advantage of the results of the previous section, it was assumed that a bonded-honeycomb-aluminum fan could be built at the weight quoted in Table 4 (this is presently beyond the state of the art). To everyone's surprise, one finds a slightly lighter lift-fan group weight for design IB than for design I. Propulsion group weights are the same. The gear box train of IB is lighter than that of Skimmer I, being much shorter. Having two fans instead of four, one can reason that the hull structure is slightly lighter. The other component weights are the same.

TABLE 5
EMPTY WEIGHT COMPARISON

	Design I (four axial fans)	Design IB (two RD fans)	Weight Difference I - IB
Lift Fan Group			
Fan	676	1310	- 634
Shroud, bell mouth, inlet guide vanes	1324	480	+ 844
TOTAL	2000	1790	+ 210
Propulsion Group			
Propellers	862	862	0
Shrouds	1434	1434	0
Rudders	145	145	0
TOTAL	2441	2441	0
Gearbox Group	3606	2371	+ 791
Hull Structure Group	24848	23000	+ 848
Power System Group	5207	6000	- 793
Electrical Group	1307	1000	+ 307
Control Group	201	225	- 24
Outfitting and Furnishings Group	661	450	+ 211
Auxiliary System	1248	1248	0
Manufacturing Variation	200	200	0
EMPTY WEIGHT	41719	38725	+2994

In conclusion, design 1B is no heavier, and it may even be lighter than design 1, though improvements in design 1 could close the gap. This came as a surprise, as it had been expected initially that an RD fan configuration would be heavier than the corresponding axial-fan configuration.

In initial design studies, it is believed that Bell assumed an overall internal efficiency of 60 percent. This ought to be an order of magnitude of the actual internal efficiency at the design point. It is believed that an internal efficiency of 70 percent can be achieved today with the RD fan in a Skimmer-type configuration (oval planform). As explained earlier, an internal efficiency of 80 or even 85 percent appears possible with additional research. This would therefore reduce the hourly fuel consumption of design 1B by from 10 to 20 percent with respect to design 1.

From Figure 23, it can be seen that the useful volume (for payload) of design 1B is larger than that of design 1, because of the reduced duct volume.

Significant advantages of design 1B over design 1 come from the features of the RD fan. Briefly, the RD fan is safer than an axial fan to personnel around the machine. It is more resistant to damage caused by ingestion of foreign objects or of water. Flutter properties of RD fans are unknown; they would appear good. The RD fan is quieter than an axial-flow fan, or than a conventional centrifugal fan.

In short, the RD fan is an attractive internal-flow air mover for GEMs. To a certain extent, however, the above claims are only realized if such a fan can be built as light as has been assumed possible. Also the full internal-flow efficiency potential has not yet been realized, and further research is needed.

ARMY GROUND MOBILITY DEVICE DESIGN STUDY

The second design in which the RD fan is applied to a GEM was conceived in answer to the following two questions: Can the RD fan be used for a GEM which is not of the annular jet type? Can the RD fan be used together with the delivery duct of circular planform, in which we know that we can, today, obtain an overall internal-flow efficiency superior to 80 percent?

Note in passing that the RD fan can be used for design concepts other than the two discussed in this report; see, for example, Reference 11.

The concept which was evolved, that of a rotating diffuser fan-skirted plenum chamber lifting pad, is shown in Figures 24 and 25. The basic unit is similar to the circular model discussed in Section IV, with an annular nozzle emerging normal to the ground, to which is added a peripheral flexible skirt. The ratio of the skirt radius to the fan inlet radius can be chosen at will to suit the designer. In the example of Figure 24, it is approximately three.

The pad by itself is pretty useless, since nobody would want a circular machine and, for large size machines, this would result in an excessively large fan. However, several pads can be combined together, as shown in Figure 26. In this concept of an Army ground mobility carrier, support of the machine is assured by eight pads. Steering is partially assured by the pads, partially by a front wheel (as was previously proposed by Bertin in France). Forward propulsion is assured by two wheels mounted rearward.

For such a machine, lifting power is minimum. Stability is good, since the pads operate independently. The main problem appears to be in skirt behavior in over-water operation. This intriguing concept is illustrated in Figure 26.

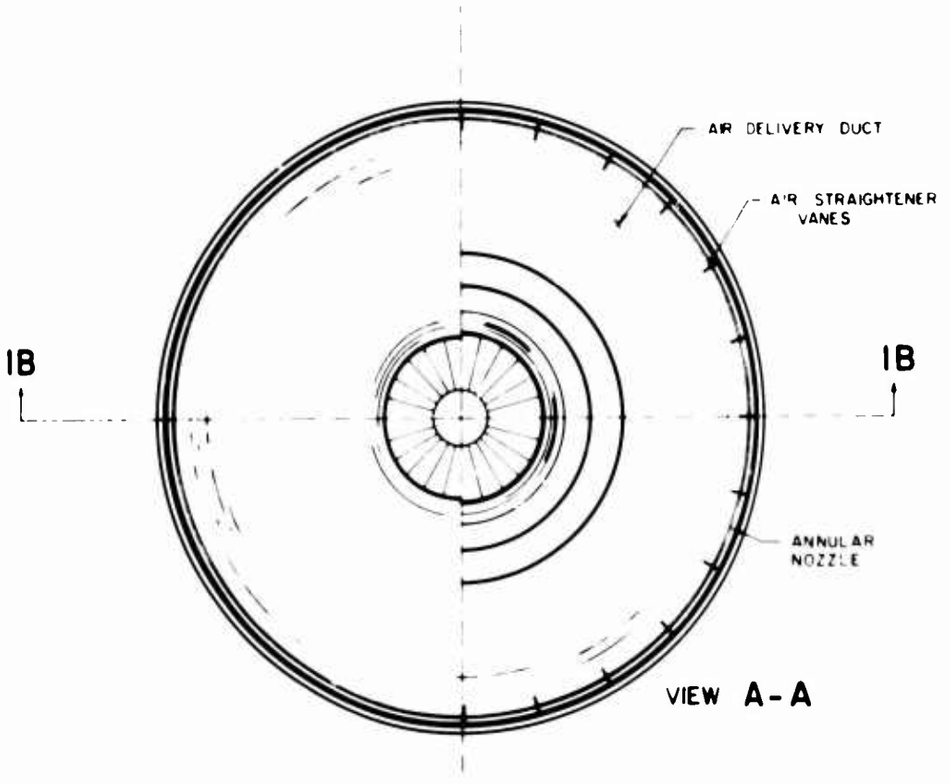

Figure 24: Radial-Diffuser Fan-Skirted Plenum Chamber Lifting Pad Concept, Top View

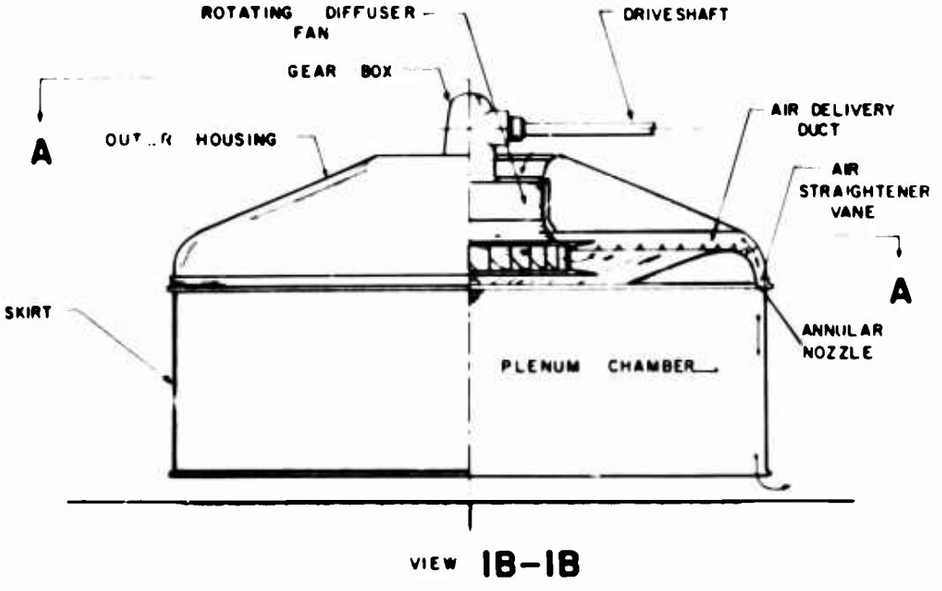

Figure 25: Radial-Diffuser Fan-Skirted Plenum Chamber Lifting Pad Concept, Side View

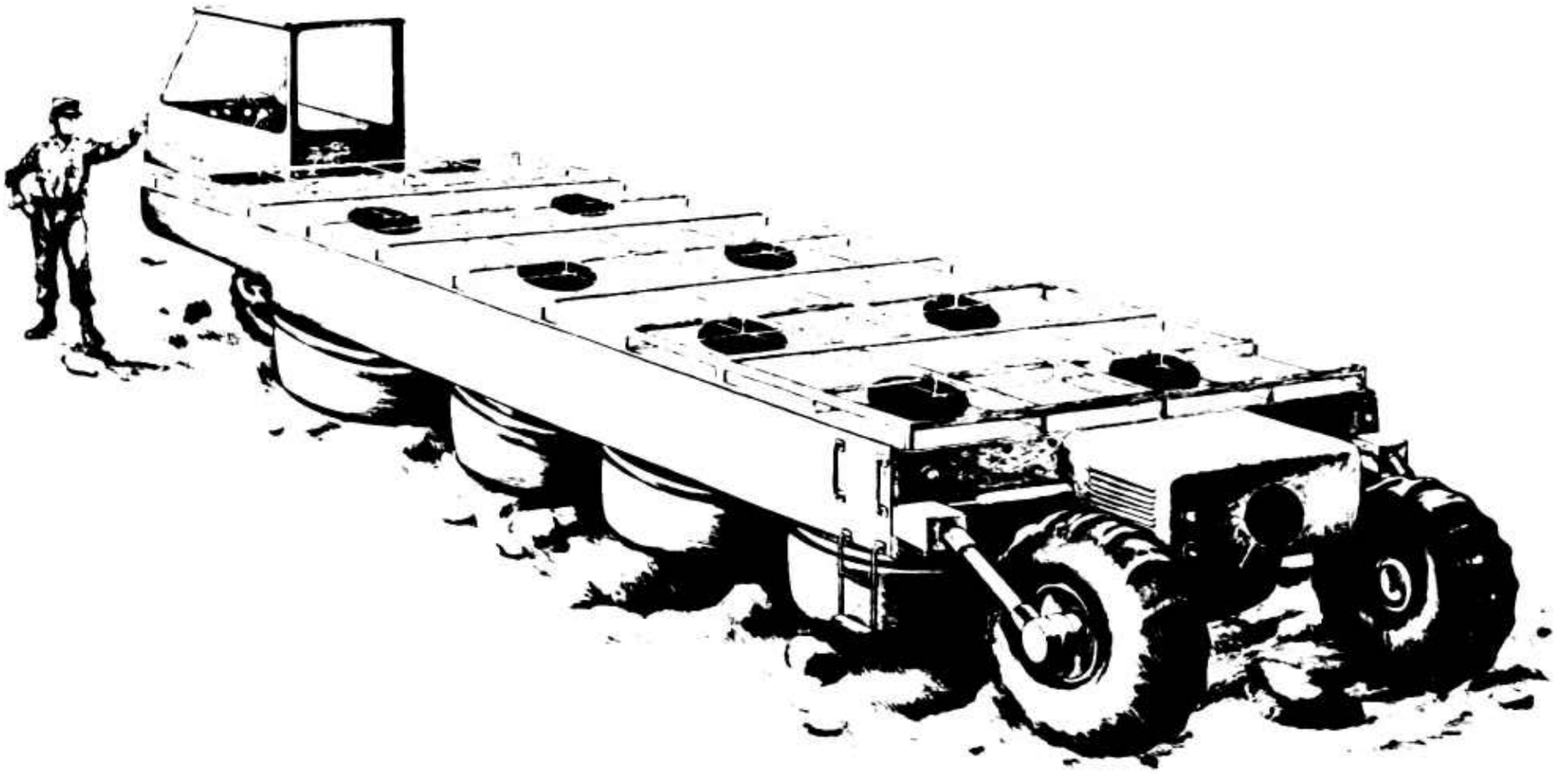

Figure 26: Army Ground Mobility Device Design Concept

REFERENCES

1. AMCA Standard Test Code for Air Moving Devices, Bulletin 210, The Air Moving and Conditioning Association, Inc., Detroit, Michigan, September 1960

2. MIL-A-8860 (ASG), Military Specification, Airplane Strength and Rigidity, general specification for, 18 May 1960

3. MIL-A-8862 (ASG), Military Specification, Airplane Strength and Rigidity Landplane Landing and Ground Handling Loads, 18 May 1960

4. MIL-A-8865 (ASG), Military Specification, Airplane Strength and Rigidity, Miscellaneous Loads, 18 May 1960

5. MIL-A-8866 (ASG), Military Specification, Airplane Strength and Rigidity, Reliability Requirements, Repeated Loads, and Fatigue, 18 May 1960

6. Civil Aeronautics Manual CAM 4b. Airplane Airworthiness, Transport Categories, Federal Aviation Agency, May 1, 1960

7. Balciunas, J.A., Lieser, J.E., Schwanke, W.P., and Olson, W.W., "A Study of Radial-Flow Fans for GEM Propulsion System Applications: Phase IV, Fabrication Techniques and Structural Design of Joy/RD Fan Impellers," Report No. X-295, Joy Manufacturing Company, New Philadelphia, Ohio, July 1963

8. Boehler, G., et al., Technical Dissertation for the Design of a Twenty-Ton Hydroskimmer Research Craft, Proposal to the Bureau of Ships, Aerophysics Company, Washington, D.C., June 1961

9. Boehler, G., et al., Design Study of O.N.R. - Marine Corps Amphibian GEM, Model ASG-4, Proposal to the Office of Naval Research, Aerophysics Company, Washington, D.C., May 1961

10. Boehler, G. and Foshag, W., "A Study of Radial-Flow Fans for GEM Propulsion System Applications: Phase V, Model Tests and Results," Aerophysics Company, Washington, D.C., September 1963

11. Boehler, G. and Foshag, W., "Preliminary Evaluation of the Ground Effect Machine (GEM) as Tractor Vehicle for Assault Minesweeping Duty," Report AR 62-02, (Prepared under Subcontract 81806 to Contract Nonr 3862(00)), Aerophysics Company, Washington, D.C., September 14, 1962

12. Booda, L., "Seaplane Rating Aids Hydroskimmer Pilot," Aviation Week and Space Technology, December 2, 1963

13. Carmichael, B.H., "Hovering Two-Dimensional Annular Jet Performance Experiments," Publication No. U-1053, Aeronutronic, A Division of Ford Motor Company, Newport Beach, California, November 1960

14. Cathers, L.E., Hirsch, A.A., and Walker, K.W., "Air Pressure Levitation," a paper presented at the February 25, 1960, meeting of the Chesapeake Section of the Society of Naval Architects and Marine Engineers, Washington, D.C.

15. Chaplin, H.R., "Design Study of a 29-Foot GEM," David Taylor Model Basin Report 1521, Aero Report 999, April 1961

16. Chappuis, R.C., "Progrès dans les ventilateurs centrifuges," Courrier des Etablissements NEU n° 17, Lille, France, February 1953

17. Chappuis, R.C., "Progrès dans les ventilateurs centrifuges," (Cont'd) Courrier des Etablissements NEU n° 19, Lille, France, October 1955

18. Chen, S.C.Y., and Kowalski, T., "An Experimental Study of the Longitudinal Seakeeping Characteristics of the Bureau of Ships Hydroskimmer," Report 904, Stevens Institute of Technology, Hoboken, New Jersey, June 1962

19. Church, A.H., Centrifugal Pumps and Blowers, John Wiley and Sons, Inc., New York 1944

20. Cutler, M.M. and Kossar, A.F., "Ground Effect Machine Applications in Mixed Terrains," SAE Transactions, Volume 70, 1962, pp. 122-135

21. "Research on the Longitudinal Seakeeping Characteristics of Ground Effect Machines," Status Report, Contract Nobs 84330, Davidson Laboratory, Stevens Institute of Technology, Hoboken, New Jersey, October 1961

22. Deutsch, E.J., "A Method of Stress Analysis for Shrouded Discs," Aerospace Engineering, Volume 21, Number 3, March 1962

23. Eckert, B., Axialkompressoren und Radialkompressoren, (Axial and radial compressors), Springer, Berlin, 1953

24. Fielding, P.G., "The Application of Inflatable Structures to the Ground Effect Machine (GEM), "TCREC Technical Report 62-40, prepared by Booz Allen Applied Research, Inc., for U.S. Army Transportation Research Command, Fort Eustis, Virginia, June 1962

25. Fielding, P.G., "The Application of Modular/Sectional Structures to Ground Effect Machines," TCREC Technical Report 62-41, prepared by Booz Allen Applied Research, Inc., for U.S. Army Transportation Research Command, Fort Eustis, Virginia, June 1962

26. Fielding, P.G., "The GEM in the Transportation Spectrum," Proceedings of the Ground Effect Machines Forum, presented at the I.A.S. 30th Annual Meeting, January 22-24, 1962. S.M.F. Fund Paper No. FF-32, pp. 4-11

27. Fisher, L.J. and Hoffman, E.L., "Ditching Investigations of Dynamic Models and Effects of Design Parameters on Ditching Characteristics," NACA Report 1347, National Advisory Committee for Aeronautics, Langley Field, Virginia, 1958

28. Fredericks, R.R., "Automobile Crash Research," a paper prepared for presentation at the SAE Detroit Section Meeting, Ford Motor Company, Detroit, Michigan, November 12, 1962

29. General Dynamics/Convair Report ZP-346

30. Gwinn, Jr., J.T., "Stop Overdesigning for Impact Loads," Machine Design, August 3, 1961

31. Hopkins, R.M. and Ramsey, J.C., "Study of Impact Loads and Motions of Ground Effect Machines," Report to Contractors' Meeting, 16-18 November 1960. Convair San Diego Report No. ZP-319

32. A.R.B./H.D.C. draft report, British Civil Hovercraft - Safety Requirements

33. Hughes, S.R., "The V.A. Series of A.C.V.'s," Hovering Craft and Hydrofoil, Volume 2, Number 3, December 1962, pp. 18-22

34. Hughes, S.R., "The Engineering Design of a Commercial Hovercraft," S.M.F. Fund Paper No. FF-32, pp. 14-24

35. Hughes, S.R., Vickers-Armstrong's (South Marston) Limited Hovercraft Lecture 3; a lecture presented to the Northern Development Conference in September 1961

36. Judet de la Combe, A., "Le calcul des soufflantes sur ordinateur IBM," Le Courrier des Etablissements NEU, No. 24, Lille, France, June 1962

37. Lamb, H., Hydrodynamics, Cambridge University Press, 6th Edition, 1932

38. LeBaron, A.D., "Structural Design Study of a Ground Effect Machine for Amphibious Support," Report 62 B 009, Ryan Aeronautical, San Diego, California, February 16, 1962

39. Le Manach, J., "Analyse des pertes dans les différents organes d'un compresseur centrifuge," Bulletin de l'Association Technique Maritime et Aéronautique, Session 1958, Paris, France

40. Ljungstrom, O., "GEM Design Philosophy for an Over-Water, Over-Ice Vehicle," I.A.S. paper No. 61-47, January 1961

41. Loomis, F.B. and Schwanke, F.B., "Aerodynamic Computation for Test Wheel RD 20-.7-1.3-75°. Curve 4230. Curve 4233," Joy Manufacturing Report No. X-288, Joy Manufacturing Co., New Philadelphia, Ohio, March 8, 1963

42. Loos, J.E., "Feasibility of Ground Effect Airborne Logistics Vehicles," Proceedings of the Symposium on Ground Effect Phenomena, Princeton University, Princeton, New Jersey, October 21-23, 1959, pp. 303-324

43. Mankuta, H., "Ground Effect Machines Morphology Study," Report No. 2017-945002, Bell Aerosystems Company, Buffalo, New York, January 1961

44. Nixon, W.B., "Maneuvering Capability of an Annular Jet Ground Effect Machine," Report No. 515, Department of Aeronautical Engineering, Princeton University, Princeton, New Jersey, May 1960

45. Norman, L.W., "Ground Effect Machine Propulsion System Design Consideration," IAS Paper No. 61-48, presented at IAS 29th Annual Meeting, January 23-25, 1961

46. Oakley, O.H., "Hydrofoils, A State of the Art Summary," Aerospace Engineering, Volume 21, Number 12, December 1962, pp. 10-28

47. Perlmutter, A.A., "An Experimental Investigation of the Response Characteristics of Two Man-Carrying Ground Effect Machines," TCREC Technical Report 62-28, prepared by Kellett Aircraft Corporation for U.S. Army Transportation Research Command, Fort Eustis, Virginia, April 1962

48. Perrone, G.L., Senoo, Y. and Dussourd, J., "Design and Test of a Fan Diffuser Bend System Suitable for a Ground Effect Machine," SAE Preprint No. 588 C, a paper presented at the National Aerospace Engineering and Manufacturing Meeting, Los Angeles, California, October 8-12, 1962

49. Rawlings, W.L. and Seiveno, D.H., "State-of-the-Art Summary, Air-Cushion Vehicles," Revision 1, TCREC Technical Report 61-108, prepared by Aeronutronics, for U.S. Army Transportation Research Command, Fort Eustis, Virginia, August 1961

50. Rijken, H. and Vossers, G., "Structural Tests with Ground Effect Machinery While Ditching Into Still Water and Into Waves," Netherlands Ship Model Basin Publication No. 207, April 1961

51. "A Study of Ground Effect Machine Structures," Informal statement of progress of the work performed under Office of Naval Research Contract No. Nonr-3068(00), Amendment No. 1, Ryan Aeronautical Company. Prepared for presentation at GEM Contractors' meeting of August 15, 1961

52. "Final Report, Ground Effect Machine Structures Study," Contract Nonr-3068(00), Report No. G-42-62, Ryan Aeronautical Company, San Diego, California, November 10, 1960

53. Senoo, Y., "GEM Propulsion System," Progress Report of Contract Nonr-3024, Report No. AP-5051-R, AiResearch Manufacturing Division, Phoenix, Arizona, December 1, 1961

54. Senoo, Y., "Considerations on the Lifting Fan-Duct Systems of Ground Effect Machines," Proceedings of the national meeting on hydrofoils and air cushion vehicles, September 17-18, 1962. Published by IAS

55. Senoo, Y., "Progress Report on Navy Contract Nonr-3024, GEM Propulsion Design Study," AiResearch Manufacturing Division, Garrett Corporation, Phoenix, Arizona, Rept No. AP-5062-R, December 7, 1962

56. Silverstein, B.L. and Schmidt, A.W., "A Study of a Commercial Application of Ground Effect Vehicles to Passenger Service," paper prepared for the High-Performance Ship Task Group of the Hydrodynamics Committee of SNAME, 5 April 1962

57. Southcote, M.F. and de Vault, R.G., "Requirements for Research Test GEMs," S.M.F. Fund Paper No. FF-32, pp. 46-50

58. Stanitz, J.D. and Ellis, G.O., "Two-Dimensional Flow on General Surfaces of Revolution in Turb -machines," Report NACA-TN-2654, National Advisory Committee for Aeronautics, March 1952

59. Stanton-Jones, R., "The Development of the Saunder-Roe Hovercraft SR-N1," Proceedings of the Symposium on Ground Effect Phenomena, Princeton University, Princeton, New Jersey, October 21-23, 1959, pp. 183-192

60. Stanton-Jones, R., "Some Design Problems of Hovercraft," IAS Paper No. 61-45, January 1961

61. Stark, R.E. and Winter, D.H., "Structural Load Criteria for Navy Hydroskimmer Air Cushion Vehicles," proceedings of the meeting concerning hydrofoils and air cushion vehicles, Washington, D.C., September 17-18, 1962, pp. 111-113

62. Stark, R.E. and Gauthey, J.R., "The SKMR-1 Research Hydroskimmer Program," Paper 697 E, Society of Automotive Engineers - American Society of Naval Engineers meeting, Washington, D.C., April 8-11, 1963

63. Stepanoff, A.J., Centrifugal and Axial Flow Pumps. Theory, Design and Application, John Wiley and Sons, Inc., New York, 1948

64. Stepanoff, A.J., Turboblowers, John Wiley and Sons, Inc., New York, 1955

65. Strand, T. and Fujita, T., "Internal Flow for Ground Effect Machines," Report No. 6, Vehicle Research Corporation, Pasadena, California, October 15, 1960

66. Strand, T., Royce, W.W. and Fujita, T., "Performance Theory for High Speed Ground Effect Machines," Report No. 11, Vehicle Research Corporation, Pasadena, California, June 1, 1961

67. Tulin, M., "The Hydrodynamics of High Speed Hydrofoil Craft," 3rd ONR Symposium on Naval Hydrodynamics, September 1960

68. Uyeda, S.T., "Study of Loads and Motions of Two Types of Ground Effect Machines," Report No. ZH-150, Hydrodynamics, General Dynamics/Convair, San Diego, California, July 1961

69. Walker, N.K., "Preliminary Stability, Control and Handling Criteria for Ground Effect Machines (GEMs)," IAS Paper No. 61-69, January 1961

APPENDIX I. PERFORMANCE OF AN RD WHEEL

List of Symbols

Coordinate system (Figure 50)

r	radial coordinate
s	curvilinear abscissa along a streamline on a mean surface of the flow
x	distances measured parallel to axis of fan

Symbols*

a	local speed of sound
a_{*_o}	critical speed of sound, $\sqrt{\frac{2(\gamma - 1)\, c_p\, T_{i_o}}{\gamma + 1}}$
A_o	area of the impeller eye
c	absolute velocity of flow
c_m	component of absolute velocity normal to peripheral velocity
H_c	total work of compression, based on assumption that air follows curvature of channel; increase in total enthalpy per unit mass
J	mechanical equivalent of heat
m	c/a
m_*	c/a_{*_o}
M_*	w/a_{*_o}
$\mathcal{M}_*$	u/a_{*_o}
p	static pressure

* Inasmuch as practical, all notations conform to Stepanoff's, Reference 64. Unless otherwise specified, units are assumed to be in the MKS system.

p	static pressure
pd	dynamic pressure
pt	total pressure rise of the fan
P	total (stagnation) pressure
$\mathcal{P}$	shaft power of the fan
q	volume flow of air through the fan
qu	recovery coefficient; ratio of static pressure to total pressure at impeller discharge
r_1	radius of inside wall at station 1
R_1	radius of outside wall at Station 1
$\bar{r}_1$	$\sqrt{(r_1^2 + R_1^2)/2}$
R_2	radius of outside wall at station 2
S	slip factor, ratio of the average absolute tangential velocity at the impeller tip to the impeller tip speed, c_{u_2}/u_2

Also called the head coefficient by Stepanoff (Reference 64). The value of the head coefficient is determined semi-empirically (see, for example, Figures 6-12 of Reference 64) as a function of β_2.

For $\beta_2 = 90^\circ$, Eckert (Reference 23) proposes

$$S = \frac{1}{1 - \frac{k\pi}{2z(1 - \bar{r}_1/R_2)}}$$

$k = 0.7$ is a parameter taking into account the friction and separation in the channels between the blades ($k = 1$ in a perfect fluid)

T	static temperature
T_i	stagnation temperature
u	peripheral velocity of impeller, ωR

w	relative velocity of flow
z	number of blades of impeller
α	angle between absolute velocity and axial velocity
β	angle between relative velocity and normal to axial velocity. In Figures 45 and 46, if the flow discharged parallel to the vanes, β_2 would be 90° and 45°, respectively. The discharge flow is deflected with respect to the vanes, so that in this case the angle between relative velocity and normal to axial velocity is $\beta_2' \neq \beta_2$
β^*	angle of the tangent to the camber line at the leading edge of the guide vanes with the normal to the axial velocity
γ	ratio of specific heats for normal air
δ	$\beta - \beta'$ (Figures 45 and 46)
ζ	hydraulic loss coefficient
η	fan efficiency, $\frac{Cd \times Cp}{75\ Cw}$
ϖ	specific weight of air
$d\varpi$	elementary hydraulic loss
ρ	flow density
τ	applied torque
ω	angular velocity of impeller
c_p	specific heat at constant pressure
Cd or cd	capacity factor, $q/\omega R_2 A_o$
Cp or cp	pressure coefficient, $pt/(\omega R_2)^2$
Cw or cw	power coefficient, $P/(\omega R_2)^3 A_o$

Subscripts

u	tangential components of relative and absolute velocities

Stations (Figure 50)

0	the state of rest upstream

1	entry to impeller
1'	plane of exit from the guide vanes and entry into the radial rotor
2	discharge from the impeller and entry into rotating diffuser
3	exit from the rotating diffuser

INTRODUCTION

The purpose of this appendix is to present a state-of-the-art review of our knowledge of RD fans in their industrial configuration, i.e., equipped with conventional volutes. This study is a prerequisite for the later study of the system performance of a GEM internal-flow system incorporating an RD fan.

The RD fan concept is not new. RD fans have been developed, as a proprietary commercial item, by Etablissements Neu of Lille, France, and are manufactured under license in the United States by Joy Manufacturing Company. It is safe to say that, until a year ago, practically all of the information available on RD wheels and RD fans had been generated by and was in the exclusive possession of Etablissements Neu. Therefore, when early in 1962 the Aerophysics Company proposed to the Army a development program for the application of the RD concept to GEMs, it felt privileged to obtain the participation in the program of Joy Manufacturing Company and, indirectly, of Etabliseements Neu. This appendix, therefore, does not represent original Aerophysics work, but a compilation of information on the RD fan obtained at various times from Neu and from Joy. Joy and Neu have been equally generous with advice concerning the subsequent phases of the program.

In the appendix, a review of the development of RD fans by Etablissements Neu is first made; next, the basic flow mechanics features of RD fans are reviewed. Third, the analytical formulation of the head-capacity relationship for an RD wheel, needed for the complete analytical formulation of the GEM-RD fan internal-flow system presented elsewhere in this report, is discussed. Fourth, the predicted performance of a 20-inch-diameter RD wheel, using the Joy-Neu performance method, is given. This performance is compared in the body of the report with the measured performance obtained by Aerophysics as part of the experimental program discussed in Section IV of the report.

REVIEW OF THE DEVELOPMENT OF RD FANS BY ETABLISSEMENTS NEU

The history of the development of the RD fan by Etablissements Neu was reported by Monsieur Chappuis, who was responsible for their development, in the "Courrier des Etablissements Neu," in 1953 (Reference 17). This reference is used extensively in what follows.

Neu became interested in research on centrifugal fans toward the end of World War II. The first attempts at performance improvement were made by using theoretical methods. They failed.

A program of systematic testing of centrifugal fans was then started by Neu in 1949. Between 1949 and 1952, tests on 86 configurations were performed. From one test to the next, only one parameter was varied. It was thus possible to obtain a precise understanding of the flow phenomena inside the fan.

EARLY TESTS

The results of a series of early tests of a centrifugal fan with radial blades are shown in Figures 27 through 30. In all cases, the variable plotted in abscissa is the volume flow coefficient.

In Figures 27 and 28 the results of test 791-26 (performed on January 26, 1952) are compared with those of older tests (Farcot, 1900; Neu N26, 1926; and Neu N 36, 1936) and with the theoretical result obtained by applying Euler's equation to a fan with radial discharge angle.

The differences between fan design 791-26 and earlier designs are in the vanes (extreme care is taken in shaping the vanes of the more recent design), in the meridional shape of the wheel, and in the addition of a fixed vaneless diffuser.

It can be seen in Figures 27 through 30 that the changes resulted in an improvement over older configurations, but only a moderate one. The head-capacity curve (Cp against Cd) moves slightly toward the right. The power-capacity curve (Cw against Cd) differs little from the curve N36 for Cd larger than 0.3 but shows an improvement for Cd between 0 and 0.3. In general, the efficiency is improved, but its maximum value is only 72 percent. Also, one is very far from approaching the theoretical curves.

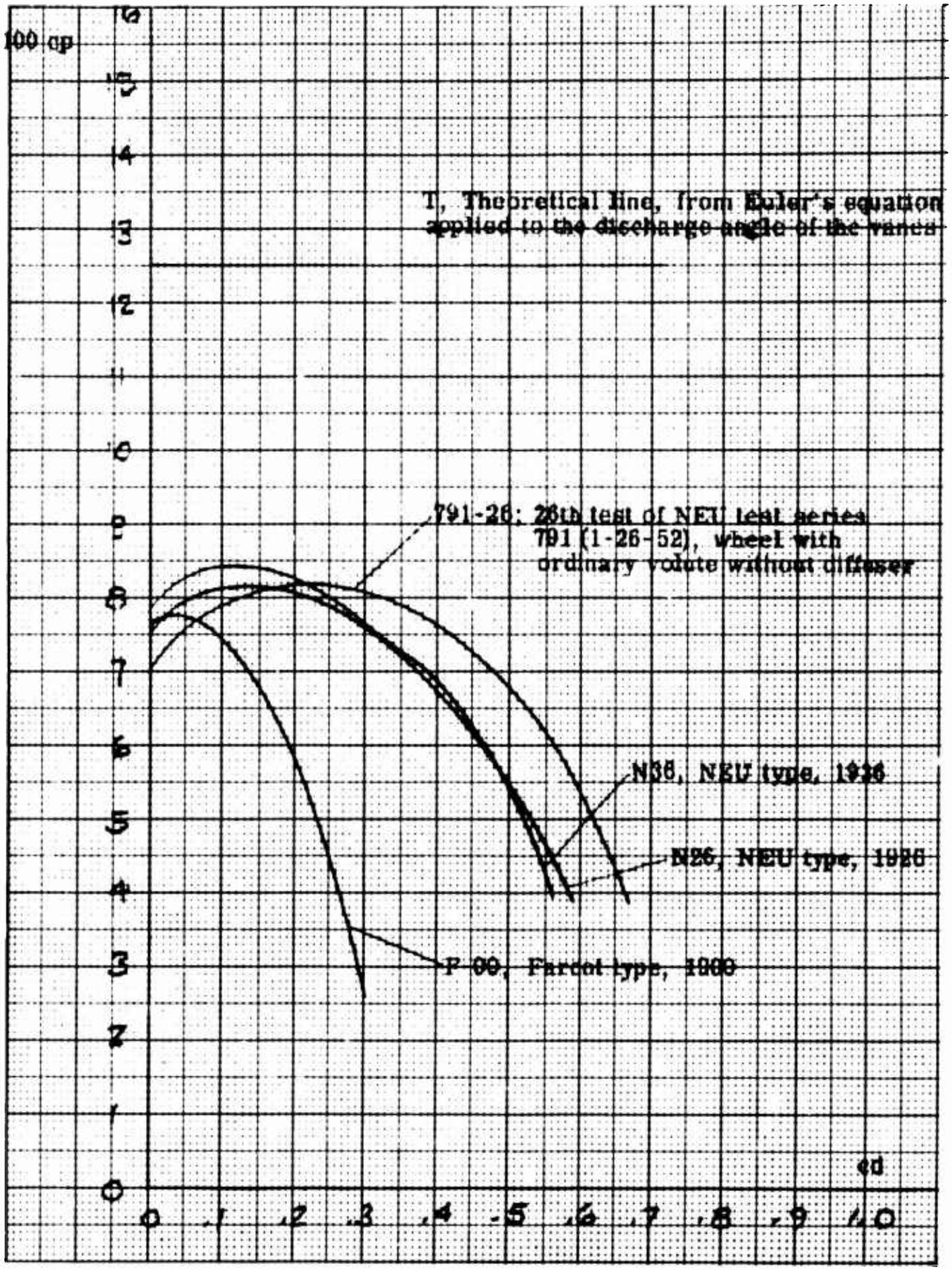

Figure 27: Comparative Characteristics of Several Types of Conventional Centrifugal Fans with Radial Vanes, of Proportion 0.5. Pressure Coefficient Cp as a Function of Capacity Coefficient Cd

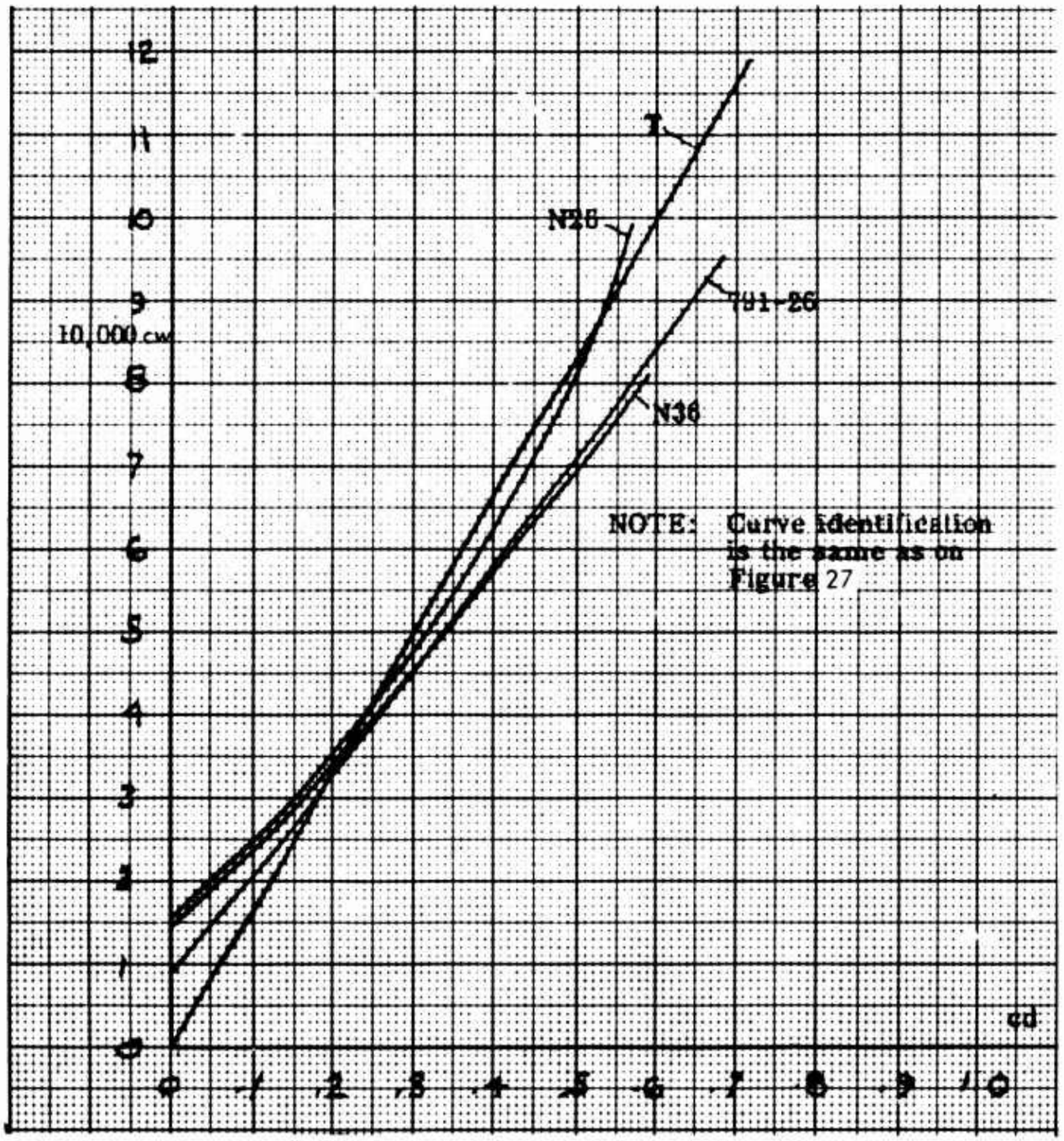

Figure 28: Comparative Characteristics of Several Types of Conventional Centrifugal Fans with Radial Vanes, of Proportion 0.5. Power Coefficient Cw as a Function of Capacity Coefficient Cd

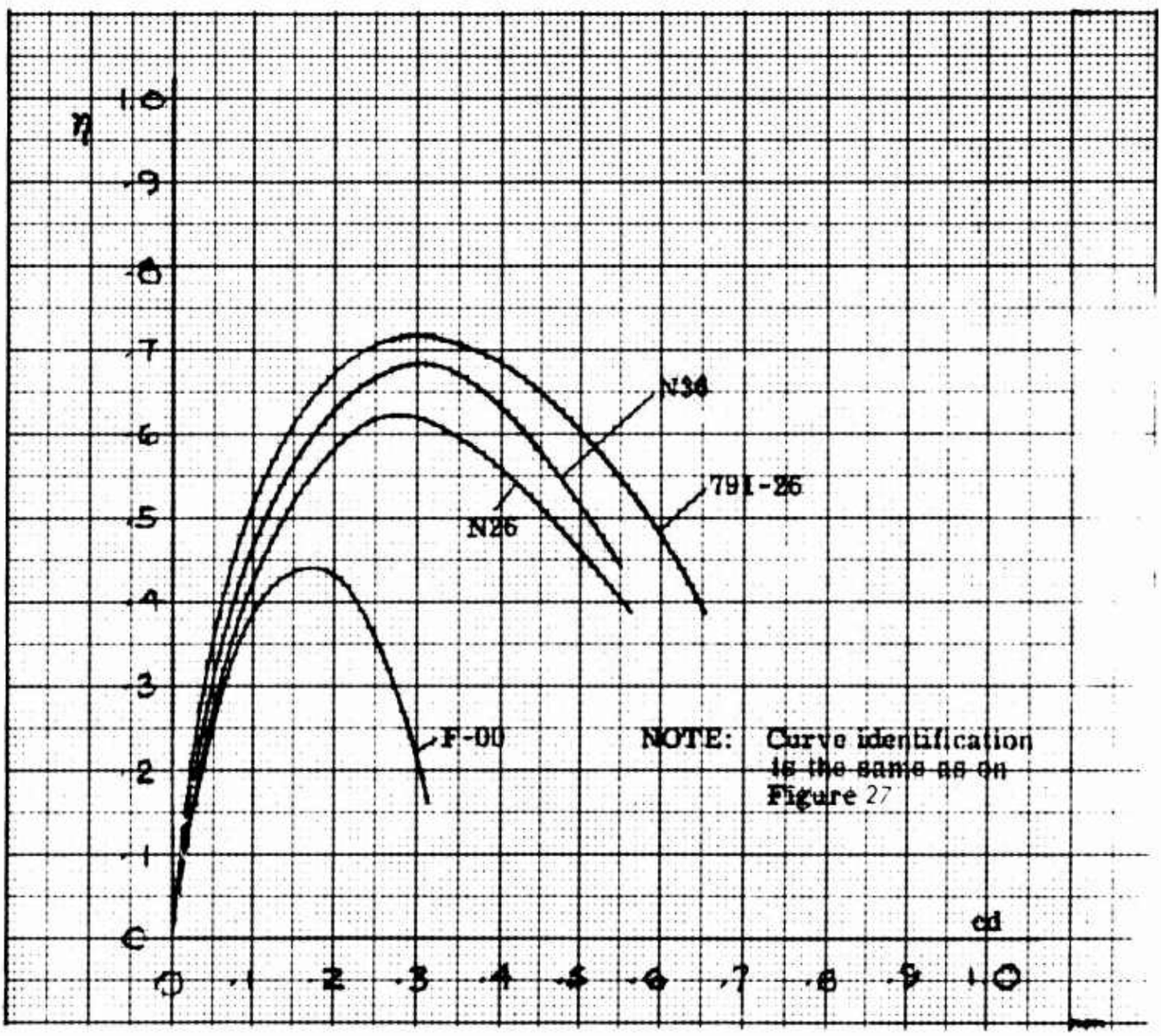

Figure 29: Comparative Characteristics of Several Types of Conventional Centrifugal Fans with Radial Vanes, of Proportion 0.5. Efficiency η as a Function of Capacity Coefficient Cd

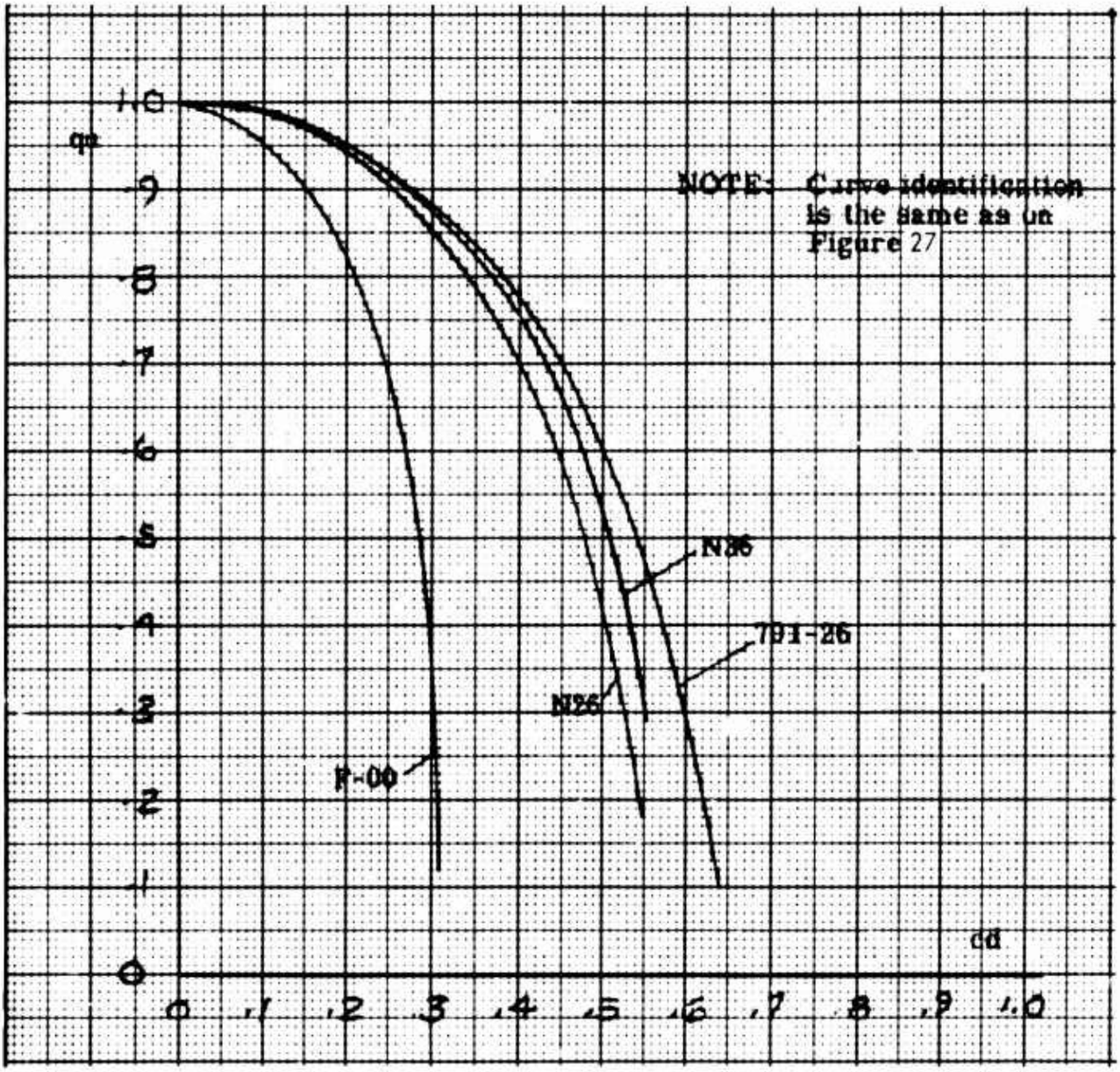

Figure 30: Comparative Characteristics of Several Types of Conventional Centrifugal Fans with Radial Vanes, of Proportion 0.5. Recovery Coefficient qu as a Function of Capacity Coefficient Cd

These results are disappointing, since they are accompanied by an aggravation of surging phenomena (positive slope of the head-capacity curve at small volume flows).

EARLY ROTATING-DIFFUSER WHEELS

At the end of tests 791-26, Neu was getting ready to try to improve the results by adding vanes to the vaneless diffuser. First, out of curiosity, a rotating diffuser was added to the wheel. There ensued spectacular results.

To show the improvement between the vaned diffuser test and the rotating diffuser test, performance characteristics of both are plotted in Figures 31 through 34. The curves labeled 791-27 correspond to the fan with rotating diffuser. It can be seen that the head increases sharply when one passes from test 791-26 to 791-27. The efficiency also increases sharply, passing from 72 to 78 percent. The power curve is slightly raised.

Also, the fan can operate efficiently at much higher capacities, as can be seen from the shift to the right (higher capacities) of the efficiency curve. The maximum efficiency corresponds now to Cd = 0.4 instead of Cd = 0.3 in the vaneless diffuser tests.

In addition, the surging trend at low capacities has completely disappeared, the head - capacity curve being nearly flat in the neighborhood of the origin.

Further improvements to the 791-27 configuration were made. In particular, attempts were successful in further improving the performance of the fan at high capacities, not only by shifting the maximum efficiency point to higher capacities but also by simultaneously increasing the recovery coefficient. This was obtained by increasing the size of the volute.

Typical results corresponding to this series of tests are also shown in Figures 31 through 34 -- tests 791-45. It can be seen that, in this test, the efficiency was increased from 78 to 84 percent (the adiabatic efficiency is 86 percent), and the maximum efficiency takes place at Cd = 0.55 instead of Cd = 0.40. Also, the power required is slightly decreased.

However, these performance improvements were accompanied by a reappearance of surging, as can be seen from the strongly positive slope of the head-capacity curve between Cd = 0 and Cd = 0.1. This is usually a minor disadvantage only, since surge usually takes place quite far from the capacity range for optimum efficiencies. However, additional research was carried out to attempt to eliminate surge without compromising performance.

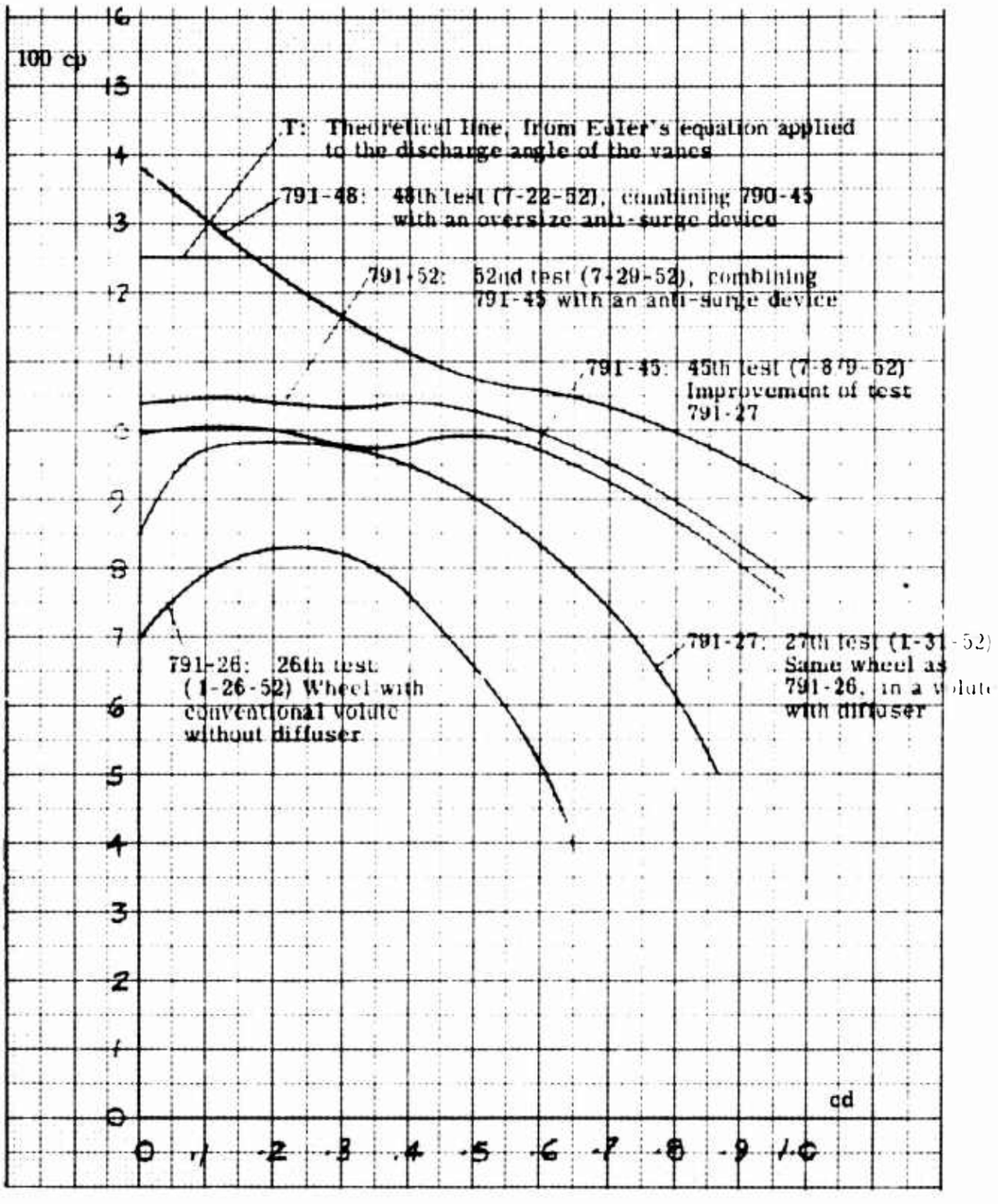

Figure 31: Comparative Characteristics of Several Wheels of Neu Series 791, with Radial Vanes, of Proportion 0.5. Pressure Coefficient Cp as a Function of Capacity Coefficient Cd

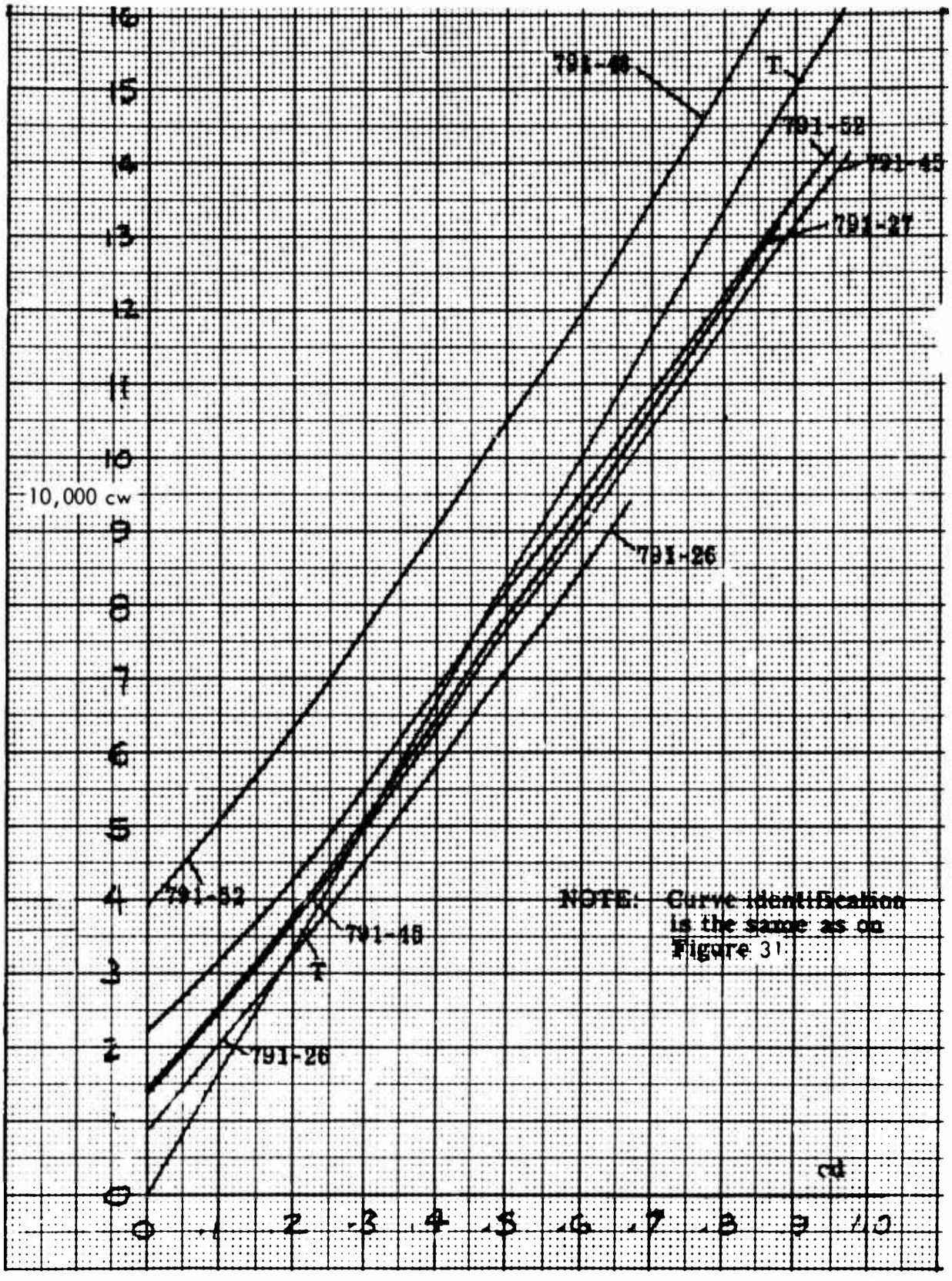

Figure 32: Comparative Characteristics of Several Wheels of Neu Series 791, with Radial Vanes, of Proportion 0.5. Power Coefficient Cw as a Function of Capacity Coefficient Cd

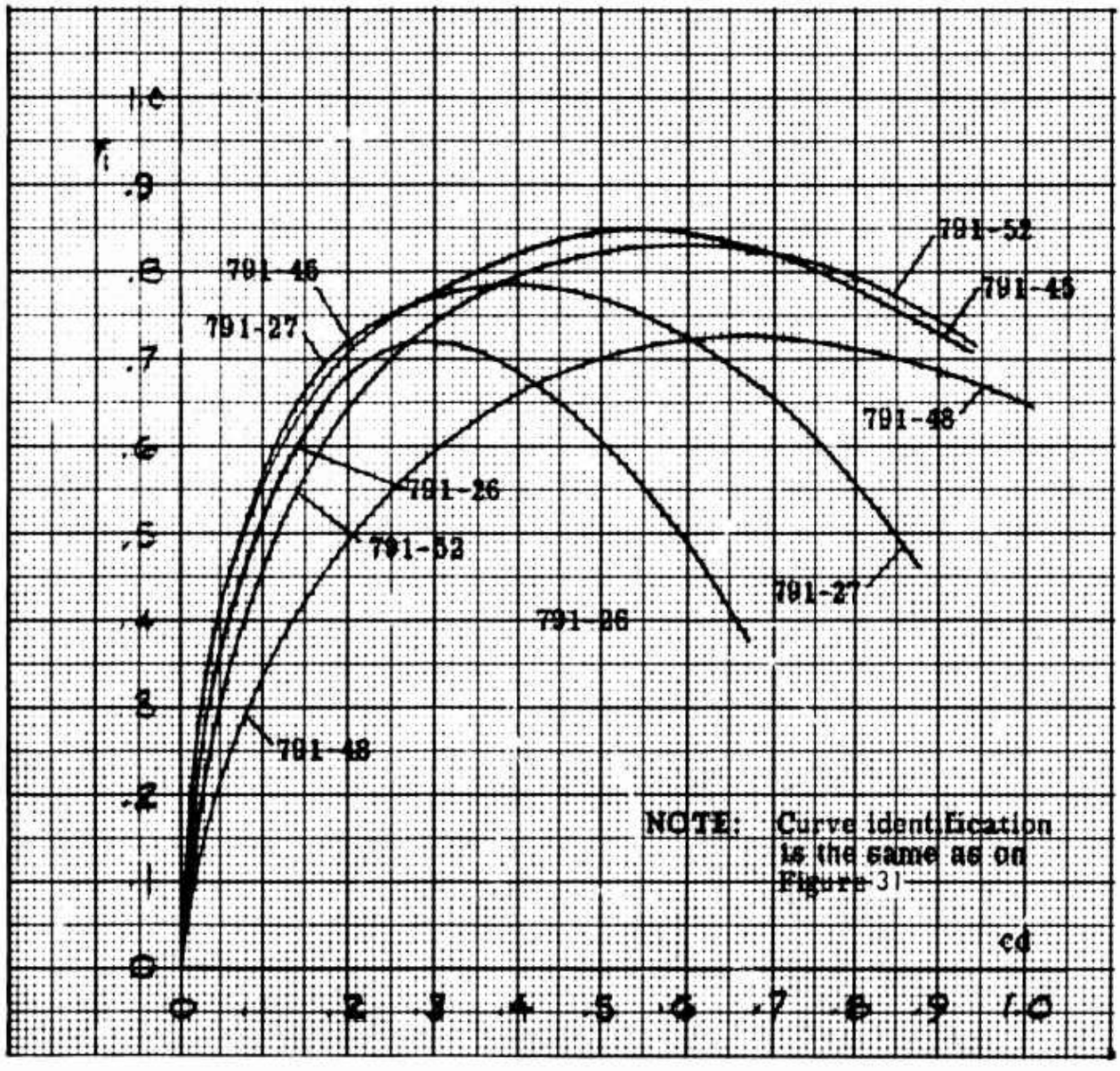

Figure 33: Comparative Characteristics of Several Wheels of Neu Series 791, with Radial Vanes, of Proportion 0.5. Efficiency η as a Function of Capacity Coefficient Cd

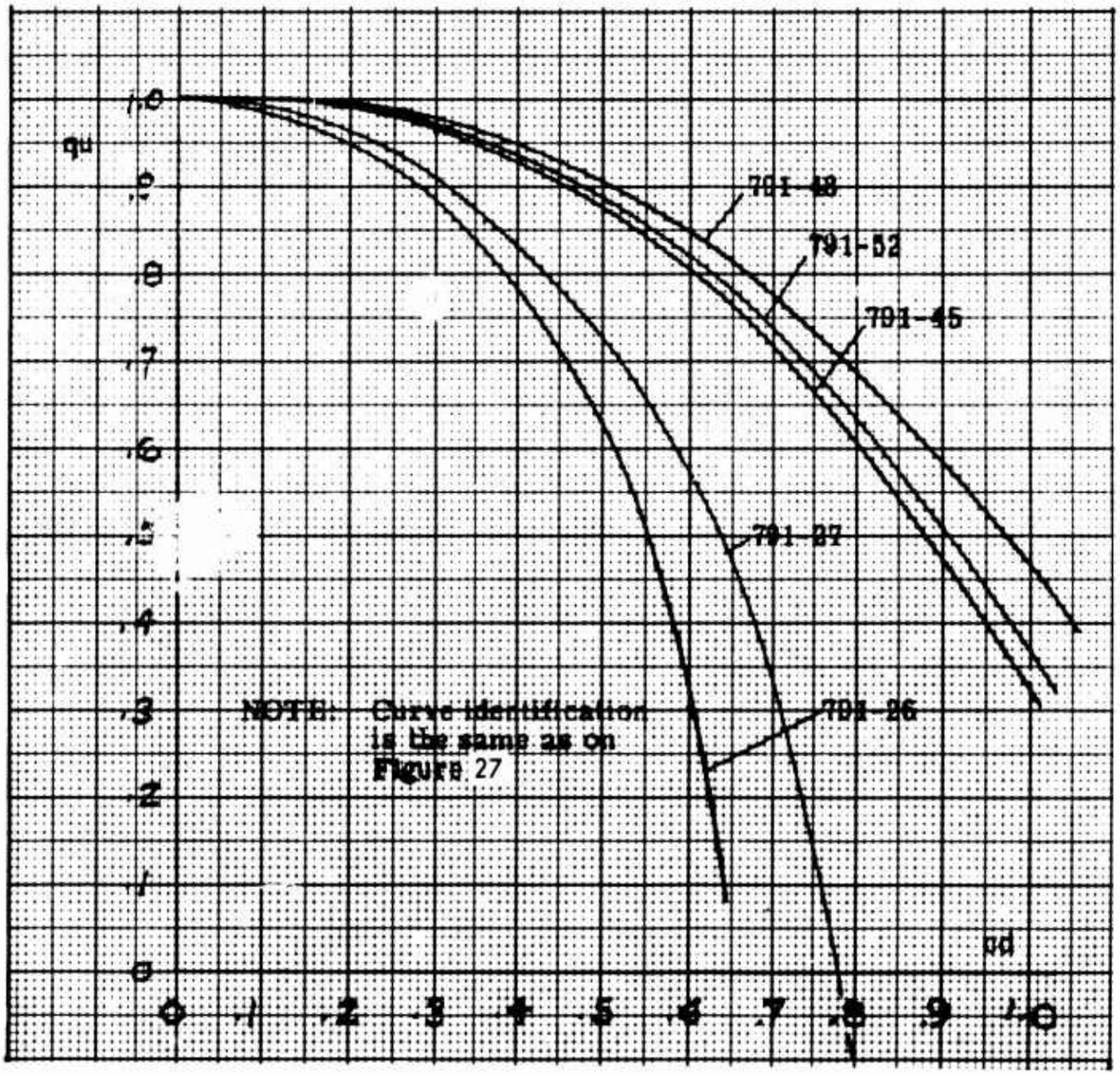

Figure 34: Comparative Characteristics of Several Wheels of Neu Series 791, with Radial Vanes, of Proportion 0.5. Recovery Coefficient qu as a Function of Capacity Coefficient Cd

ROTATING DIFFUSER WHEELS WITH ANTISURGE DEVICES

A very effective antisurge device was designed, as witnessed by the results of tests 791-48 and 791-52, which are shown in Figures 31 through 34.

The results of configuration 791-52 show a good compromise since the fan operates at the limit of surge. The head-capacity curve is practically flat at the origin. The cost to be paid is a slight decrease in efficiency, from 84 to 82.5 percent.

If one installs an over-powerful antisurge device, as in configuration 791-48, the performance of which is also plotted in Figures 31 through 34, one witnesses substantial increases in both the head and the power required. One can even obtain, at low capacities, values of the head larger than those predicted by Euler's equation. This is only paradoxical on the surface. However, the efficiency of configuration 791-48 is substantially lower than that of configuration 791-52, down from 82.5 percent to 72 percent. But, maximum efficiency takes place at a cd of 0.63, which is larger than for any of the other tests.

The ability of the rotating-diffuser fan to operate at larger and larger capacity coefficients is therefore increased by the addition of antisurge devices. Operation at a cd larger than 1 appears even feasible. Let us recall that cd = 1 means that the velocity of the fluid entering the wheel is equal to the tangential tip velocity.

COMPARISON OF RD WHEELS WITH FIXED DIFFUSER WHEELS

The comparison between an RD fan (Model 791-45) and two Neu centrifugal fans with fixed diffusers (Models TDA1 and TDA2) is made in Figures 35, 36, and 37. The fixed diffuser fans, as compared with the RD fan, have (1) lower heads; (2) lower efficiencies; (3) more restricted capacity; and (4) more noise. Finally, the fixed diffuser fans have a strong tendency to surge.

Not only is the RD fan less noisy than the fan with fixed diffuser, but it is also less noisy than the conventional centrifugal fan. All high frequencies have disappeared, and there only remains a wafty sound similar to that of the wind in the trees of a forest. During recent RD fan tests made by Aerophysics, the timing belt used to transmit the shaft power to the fan was more noisy than the fan itself.

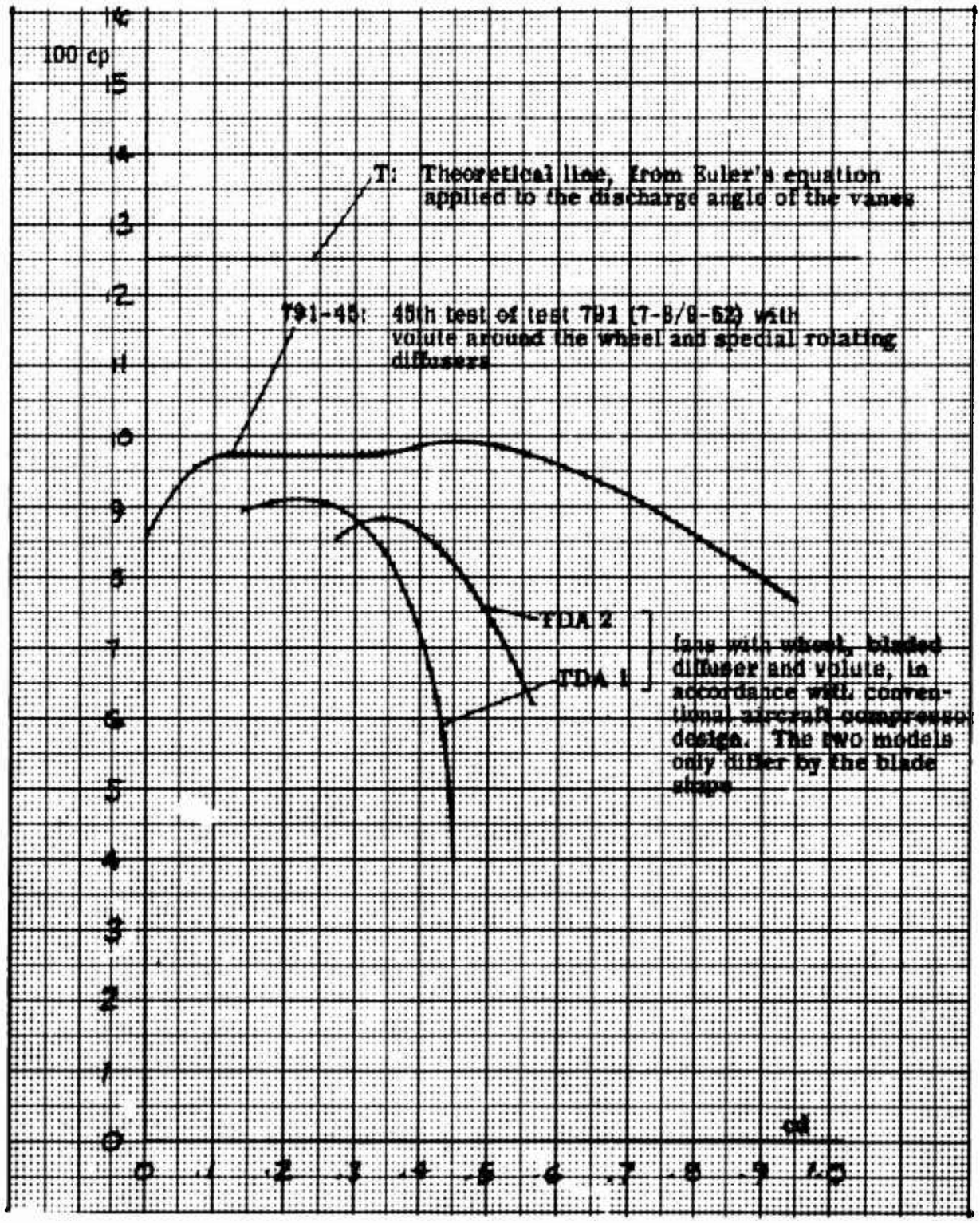

Figure 35: Comparative Characteristics of Three Types of Neu Centrifugal Fans with Radial Vanes, of Proportion 0.5, Having Different Diffusers. Pressure Coefficient Cp as a Function of Capacity Coefficient Cd

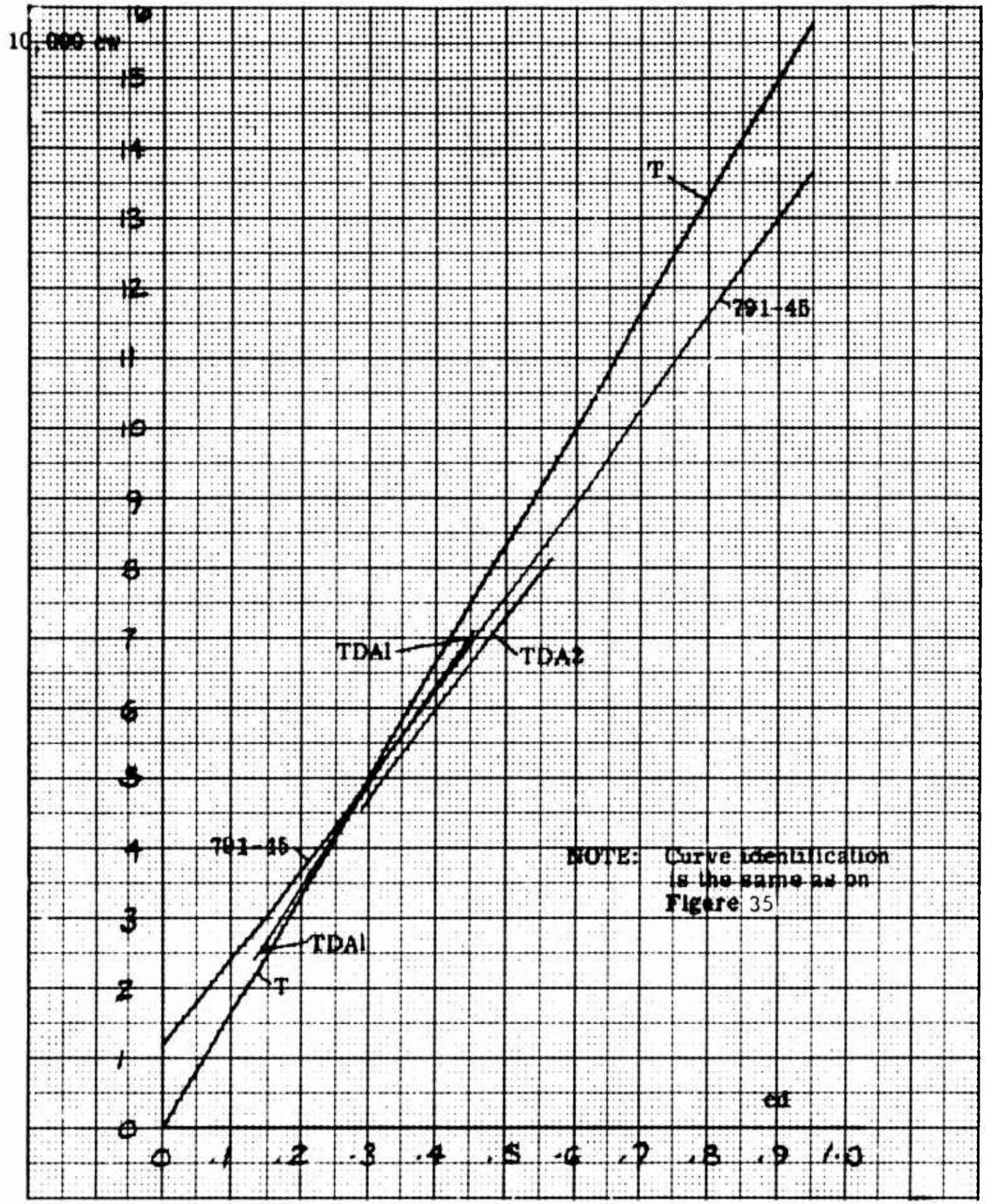

Figure 36: Comparative Characteristics of Three Types of Neu Centrifugal Fans with Radial Vanes, of Proportion 0.5, Having Different Diffusers. Power Coefficient Cw Against Capacity Coefficient Cd

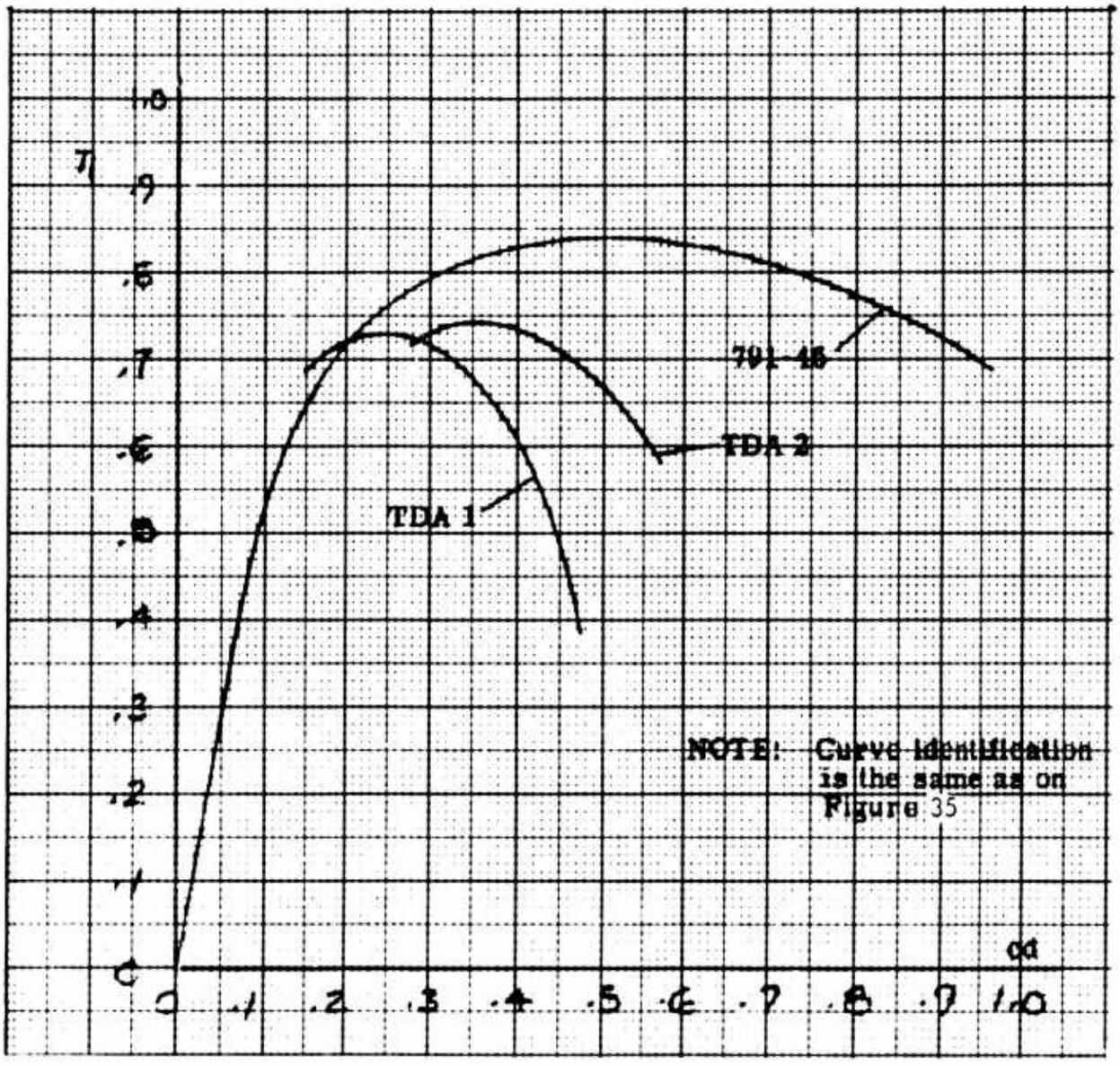

Figure 37: Comparative Characteristics of Three Types of Neu Centrifugal Fans with Radial Vanes, of Proportion 0.5, Having Different Diffusers. Efficiency η as a Function of Capacity Coefficient Cd

EFFECT OF THE IMPELLER DISCHARGE ANGLE ON RD FAN PERFORMANCE

In the tests of the series 710, a wheel of proportion 0.5, with a discharge angle of 63°, instead of 90°, was built and tested. The blades were designed according to a lifting-surface theory. The results of these tests are shown in Figures 38 to 41.

It can be seen that the improvements in performance resulting from the use of a rotating diffuser and of antisurge vanes still exist but are less substantial than for a fan with radial blades. One can observe a general increase of the head and of the efficiency, and a shift toward the right of the head-capacity curve.

One should not conclude from that, however, that the rotating diffuser used in the series 710 is any less effective than when used on an impeller with radial blades. What happens here is that the Euler head-capacity curve is now inclined over the horizontal axis (it intersects the horizontal axis at Cd = 1.96). The zone of operation of the fan, instead of extending to infinity to the right, is considerably narrowed down, and the experimental curves must therefore crowd into a smaller space.

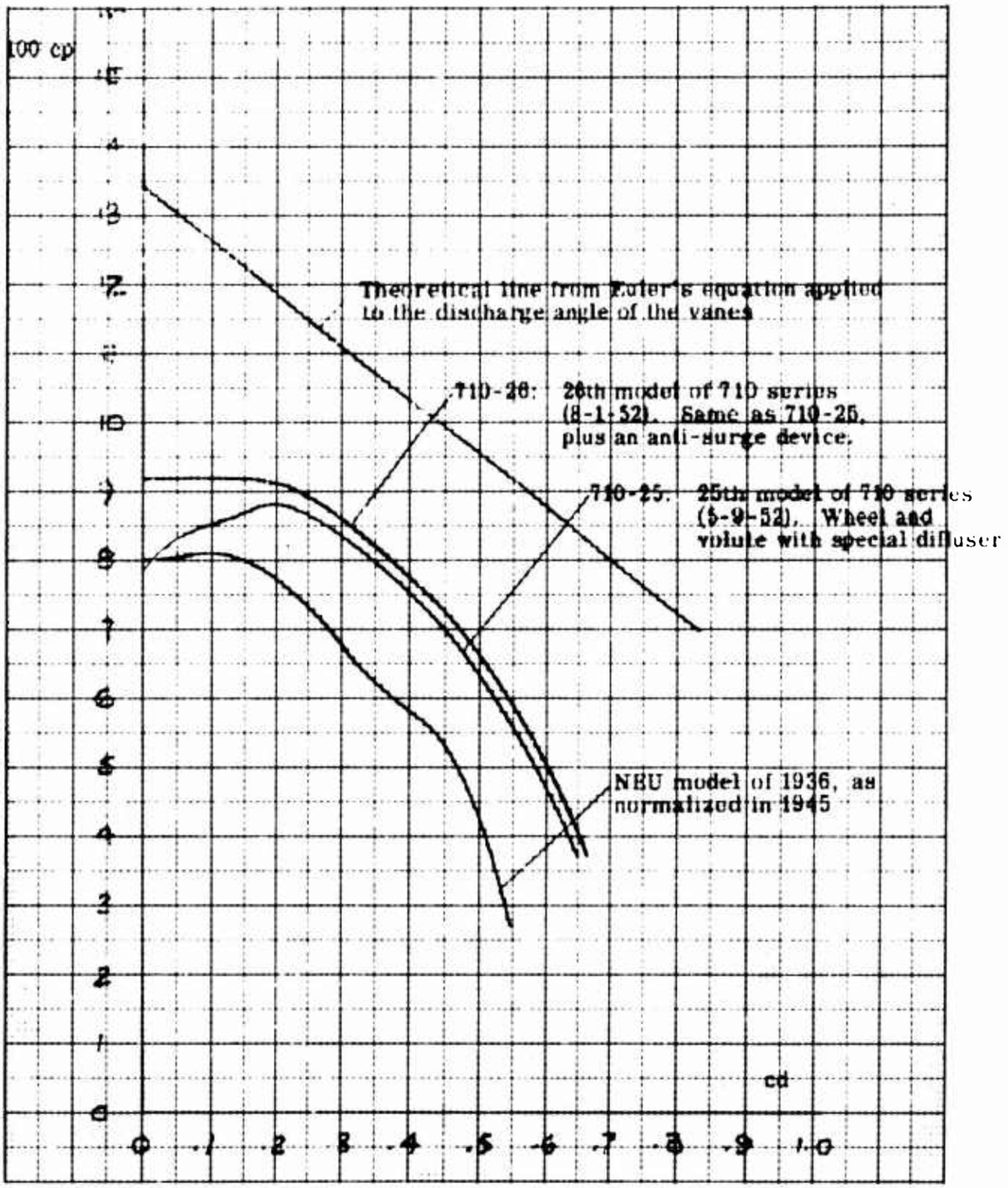

Figure 38: Comparative Characteristics of Several Neu Centrifugal Fans with 63° Vane Discharge Angle, of Proportion 0.5. Pressure Coefficient Cp as a Function of Capacity Coefficient Cd

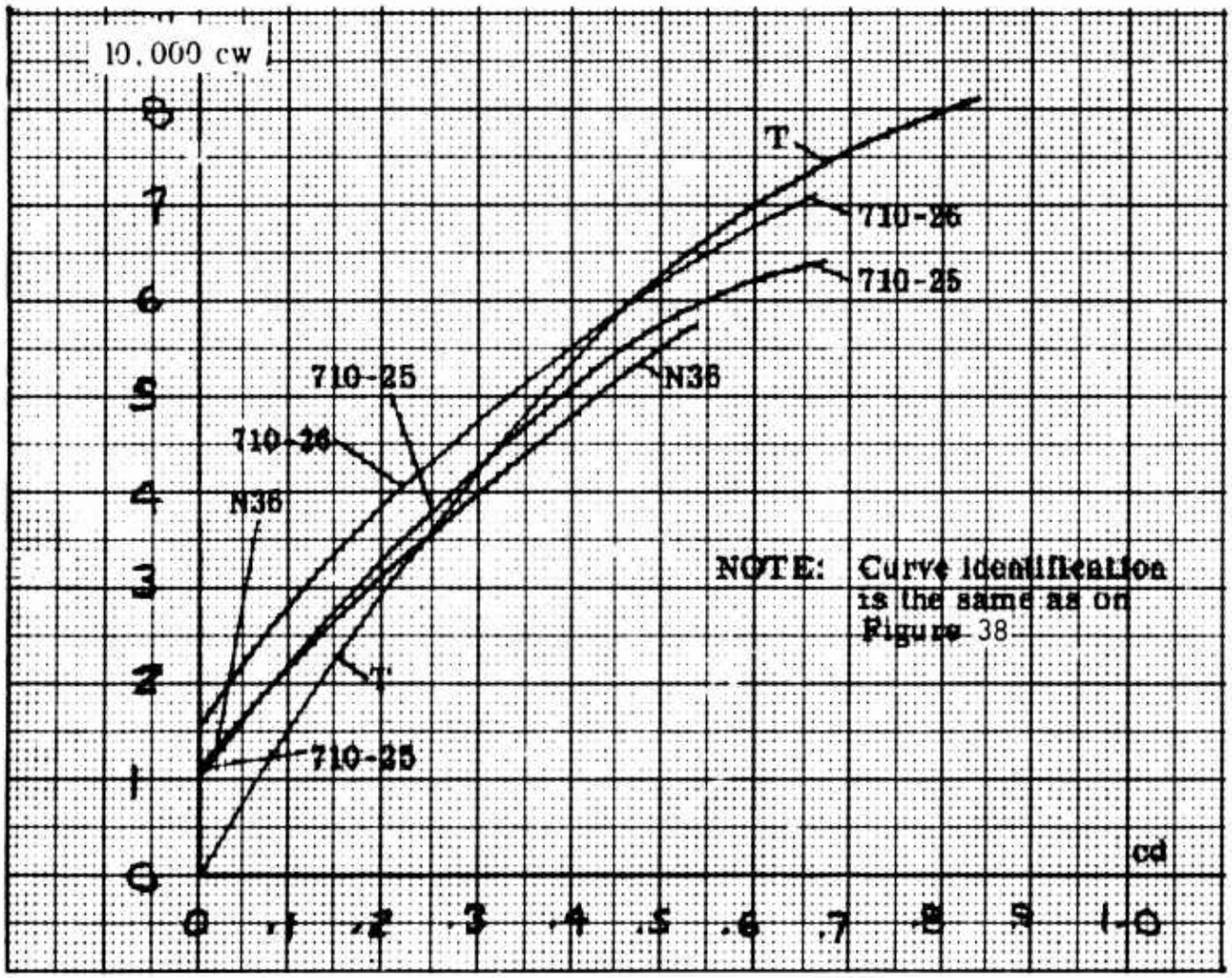

Figure 39: Comparative Characteristics of Several Neu Centrifugal Fans with 63° Vane Discharge Angle, of Proportion 0.5. Power Coefficient Cw as a Function of Capacity Coefficient Cd

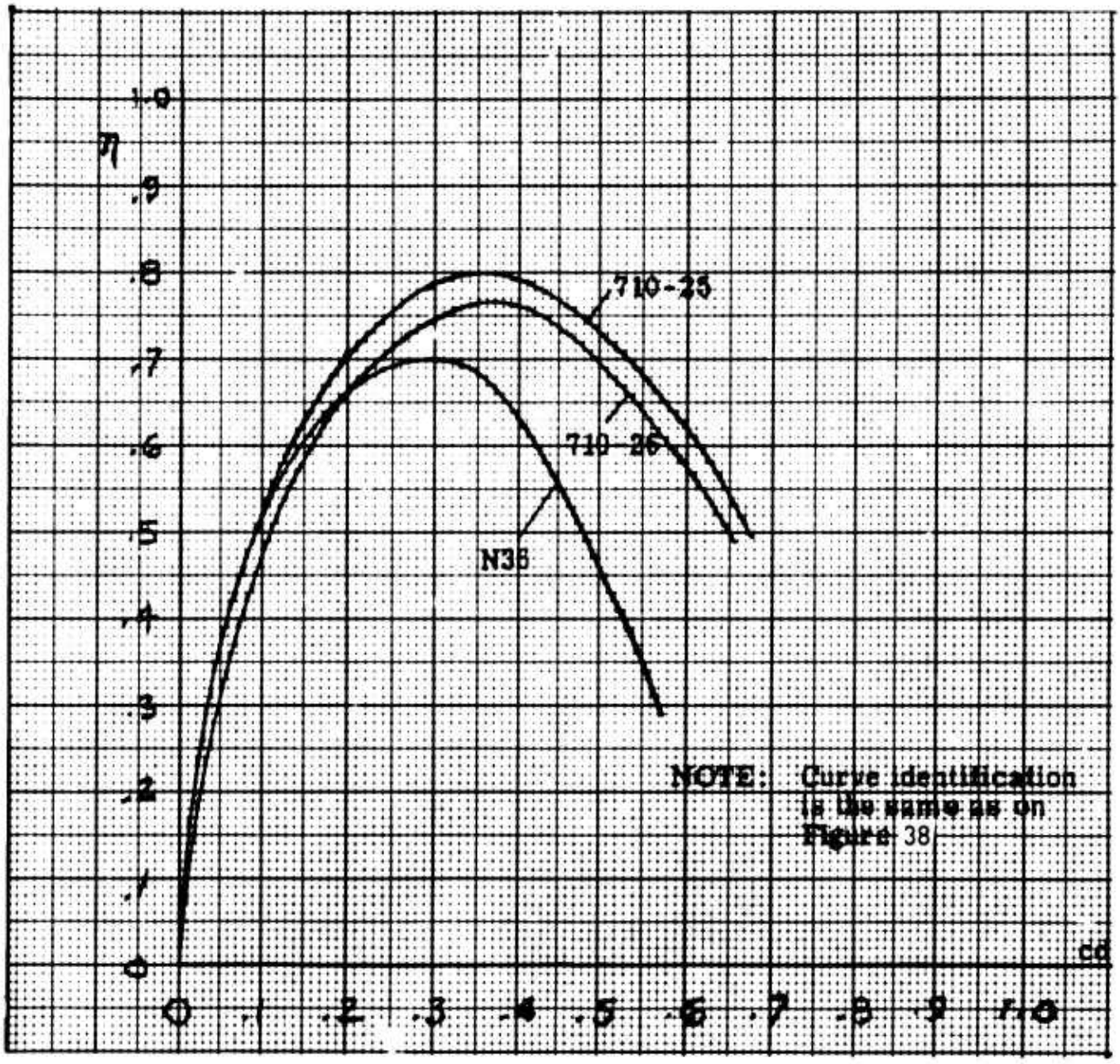

Figure 40: Comparative Characteristics of Several Neu Centrifugal Fans with 63° Vane Discharge Angle, of Proportion 0.5. Efficiency η as a Function of Capacity Coefficient, Cd

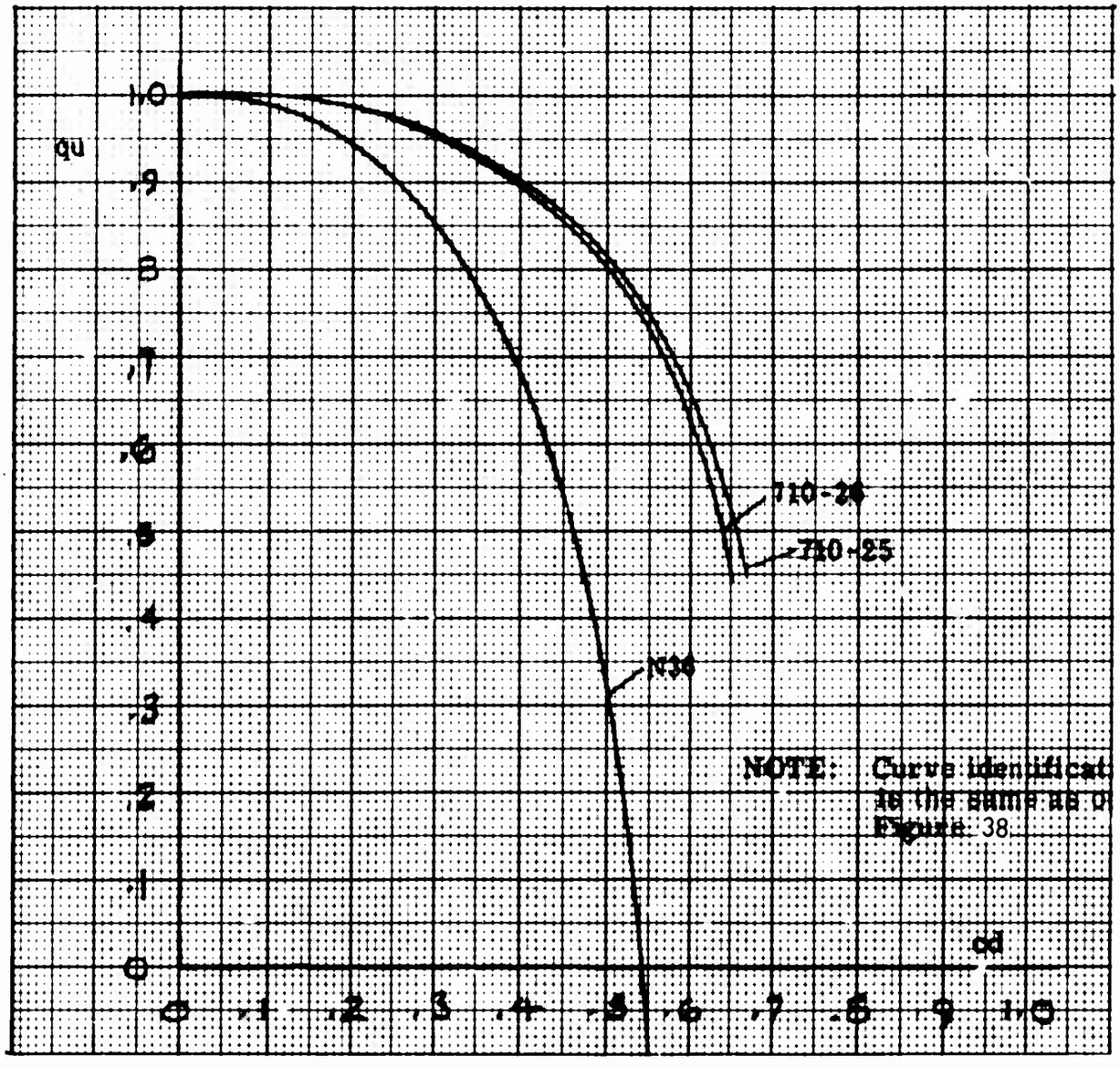

Figure 41: Comparative Characteristics of Several Neu Centrifugal Fans with 63° Vane Discharge Angle, of Proportion 0.5. Recovery Coefficient qu as a Function of Capacity Coefficient Cd

BLANK PAGE

AN ELEMENTARY UNDERSTANDING OF THE OPERATION OF AN RD WHEEL

The material in this chapter is borrowed from a paper by Monsieur Chappuis, published in the "Courrier des Etablissements Neu," in 1955 (Reference 17). Related information can also be found in Reference 64.

THE THREE CLASSICAL TYPES OF CENTRIFUGAL FANS

Let us consider successively and compare the three classical types of centrifugal fans, each assumed to be designed in accordance with the best state of the art. In Figure 42 we show a cross-section of a conventional centrifugal fan of an industrial type. In Figure 43 is shown a centrifugal fan with fixed vaneless diffuser, and in Figure 44 a fan with vaned diffuser.

Each one of these configurations has certain advantages and, conversely, disadvantages with respect to such factors as cost, size, efficiency, range of operation, and noise.

Experience teaches that the first configuration (Figure 42) is the cheapest and most compact, but it has the lowest efficiency. The third configuration (Figure 44) has the highest efficiency, but is the most expensive, noisiest, and has the narrowest range of operation (see, for example, curves TDA 1 and TDA 2 of Figures 35 and 37). Finally, the second configuration is intermediary as far as cost and efficiency are concerned, but is the most bulky one.

Simple theoretical considerations can explain the above differences.

Let us first assume that all three fans have radial blades. The impeller vane discharge angle is therefore $\beta_2 = 90^\circ$. But the discharge flow can never be exactly parallel to the vanes, and there exists between the mean discharge angle of the flow β_2' and the angle β_2 a deviation δ_2:

$$\delta_2 = \beta_2 - \beta_2'$$

The deviation is maximum when the capacity is zero and decreases to zero when the capacity increases. Let us assume for this discussion that $\delta = 15^\circ$.

Let us also assume that the peripheral speed u_2 is $u_2 = 150$ ft/sec and that the meridian component c_{m_2} of the discharge velocity is $c_{m_2} = 60$ ft/sec.

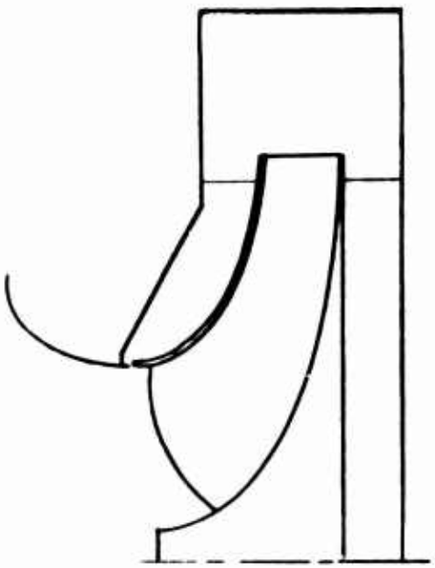

Figure 42: Conventional Centrifugal Fan Without Diffuser

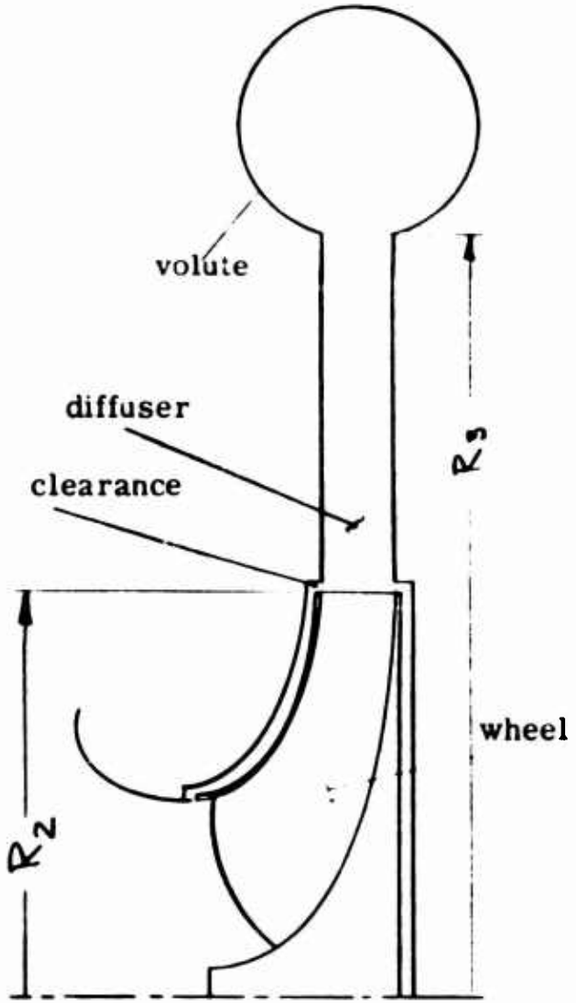

Figure 43: Conventional Fan With Vaneless Diffuser

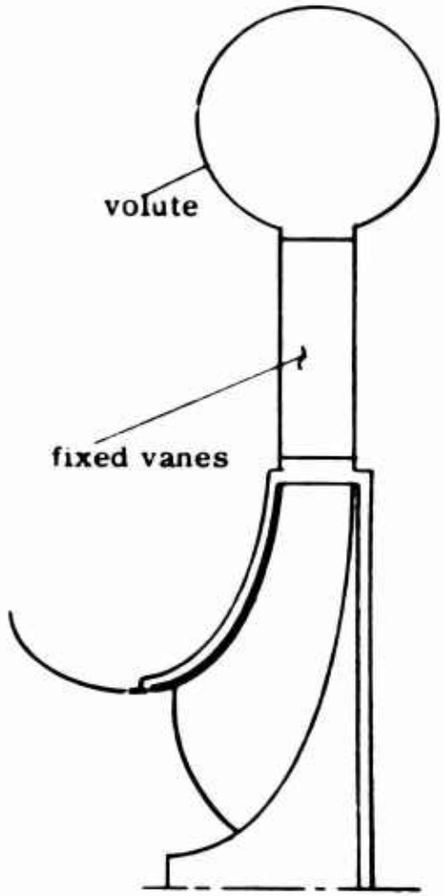

Figure 44: Conventional Fan With Vaned Diffuser

An observer turning with the wheel will see the fluid discharge at the angle β'_2. He will not be conscious of the velocity u_2, so that, for him, the flow is the resultant of a radial flow along c_{m_2} and of a rotation along

$$u_2 - c_{u_2} = \frac{c_{m_2}}{\tan \beta'}$$

One finds:

$$c_{u_2} = 134 \text{ ft/sec.}$$

The above tangential velocity is that of the rotation of the flow, as seen by an observer sitting on the fan casing. It is of great importance, since it characterizes the theoretical pressure rise of which the fan is capable.

From Euler's theorem (see, for example, Reference 64, Chapter 3) the theoretical head of the fan is given by:

$$P_{th} = \frac{\gamma(u_2 c_{u_2} - u_1 c_{u_1})}{g}$$

Assuming that the fluid enters the impeller without a tangential component, Euler's equation reduces to:

$$P_{th} = \frac{\gamma u_2 c_{u_2}}{g}$$

Because of hydraulic losses, the actual available total head is related to the input head by:

$$\eta = \frac{P}{P_{th}}$$

For the above example, one finds $p_{th} = 11.2$ in. H_2O, and, assuming an efficiency $\eta = 0.80$, $p = 8.9$ in. H_2O.

The dynamic pressure of the discharging flow is:

$$pd_2 = \frac{\gamma}{2g}\left(c_{m_2}^2 + c_{u_2}^2\right)$$

One finds presently:

$$pd_2 = 1 + 5 = 6 \text{ in. } H_2O.$$

It can be seen that the dynamic pressure of the air coming out of the fan is quite high.

Consider now the example of Figure 46, in which we assume $\beta = 45^\circ$, $\beta' = 35^\circ$, $c_{m_2} = 60$ ft/sec, $u_2 = 150$ ft/sec. One finds: $c_{u_2} = 64.2$ ft/sec, $p_{th} = 5.34$ in. H_2O, with $\eta = 0.80$ and $pd_2 = 1 + 1.1 = 2.1$ in. H_2O.

In the case of Figure 45, it will be necessary to diffuse the flow very substantially in the volute, to convert most of the dynamic pressure into static pressure from 6 in. H_2O to 1 in. H_2O, while in the case of Figure 46 the required diffusion is much less, only from 2.1 in. H_2O to 1 in. H_2O. One can thus perceive that the manner in which the conversion from dynamic to static pressure is effected has an important effect on the efficiency of the fan. The diffusion must take place in the volute, and the volute must be designed for efficient diffusion. The volute design is therefore an order of magnitude more complicated and more critical for the first configuration (Figure 45) than for the second one (Figure 46).

One can thus perceive that a simple volute, such as the one schematized in Figure 42, may result in an acceptable efficiency for the second fan configuration (Figure 46), but poor efficiency for the first configuration (Figure 45), because of its inability to handle efficient, extensive diffusion. It is well known that, in industrial applications, this is indeed the case, and simple volute fans are built with small discharge angles ($\beta_2 \approx 25^\circ$). For a typical fan, the difference in fan efficiency

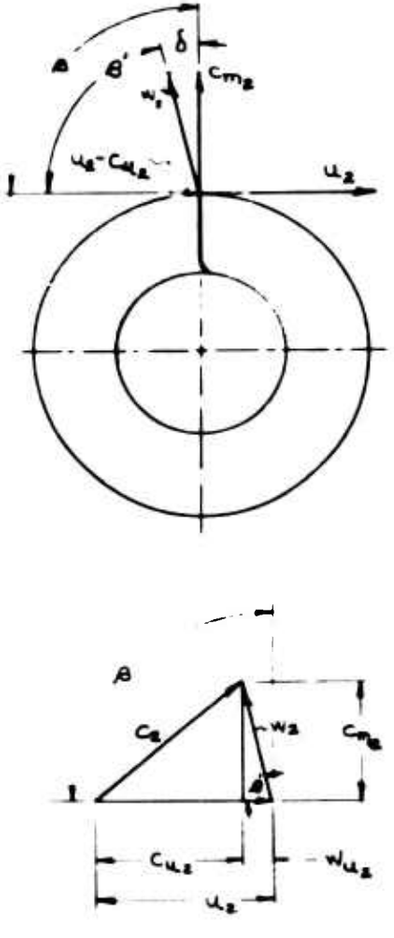

Figure 45: Discharge Flow and Velocity Diagram for a Wheel with Radial Vanes, $\beta = 90^{o}$

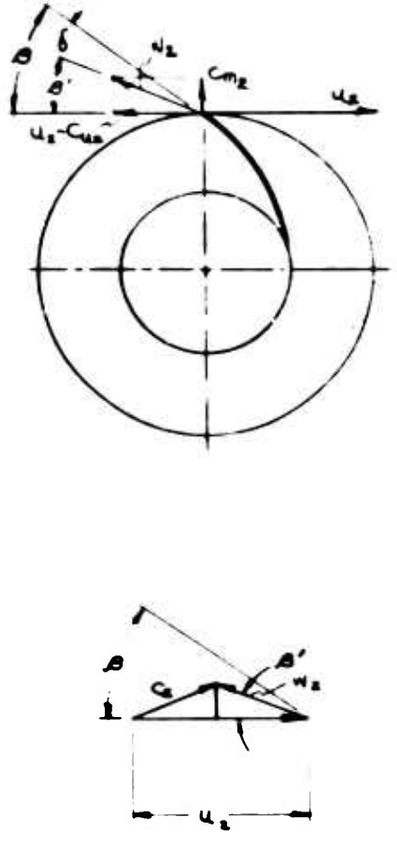

Figure 46: Discharge Flow and Velocity Diagram for a Wheel with Inclined Blades, $\beta = 45^{o}$

may be of the order of five to ten points for $\beta_2 = 25^\circ$ and $\beta_2 = 90^\circ$, or about 1 point for each five degrees.

Now, if one adds between the wheel and the volute a fixed diffuser with parallel walls, as shown in Figure 43 the results should be better, at least theoretically.

Let us assume the fluid perfect and that the vortex law applies; i.e., that one has a free vortex flow. The variation of the tangential velocity is given by:

$$c_{u_3} r_3 = c_{u_2} r_2$$

On the other hand, the diffuser is assumed to have parallel walls, hence a constant depth, and the flow exhaust area also increases linearly with the radius. Hence,

$$c_{m_3} r_3 = c_{m_2} r_2$$

Assume, for example, $r_3 = 2r_2$. Then, $c_{u_3} = c_{u_2}/2$ and $c_{m_3} = c_{m_2}/2$.

Therefore, the exhaust dynamic pressure at the end of the diffuser is reduced by a factor of four. In the previous numerical example, for the wheel of Figure 45, the dynamic pressure is reduced to 1.5 in. H_2O; for the wheel of Figure 46, it is reduced to 0.53 in. H_2O. In the first case, the dynamic pressure is still larger than the desired one, which is 1 in. H_2O; therefore, a diffusion from 1.5 in. H_2O to 1 in. H_2O can take place in the volute that surrounds the diffuser. This diffusion is small and can be effected under relatively good conditions. In the second case, the dynamic pressure at the entrance of the volute is smaller than the desired one, and the volute must have a convergent, not a diffuser. This indicates that in the latter case the outer radius of the diffuser must be reduced.

From the above discussion, it can be concluded that the centrifugal fan with a vaneless diffuser can be very efficient, if the actual laws of variation of meridional and tangential velocities do not differ too drastically from the theoretical law. However, such a fan could be quite bulky.

Experience indicates, however, that the true variation of the velocities differs very substantially from the theoretical one. There are two reasons for this that will now be discussed.

The first reason is that the clearance between the rotor and the stator diffuser introduces important perturbations in the flow. Friction between the fluid layer emerging from the wheel and the fluid outside the wheel creates two effects, both unfavorable.

The first effect is a local deflection of the flow angularity rearward with respect to the direction of rotation. This results in a decrease of the angle β, i.e., indirectly of both theoretical and actual head. The second effect is an energy loss which, by reducing the dynamic head of the moving fluid, results in a decrease of efficiency, hence of actual head.

Besides, frictional losses result in the creation of local vorticity and, hence, in a poor velocity distribution at the entrance of the diffuser. It is well known that the efficiency of a diffuser is critically affected by the velocity distribution at the entrance of the diffuser, mostly by the local distribution in the neighborhood of the walls. Therefore, the efficiency of a diffuser within the configuration of Figure 43 is not good.

The second reason why the efficiency of a diffuser associated with a centrifugal fan is poor is the existence of large frictional losses along the walls of the diffuser. The deceleration of the tangential velocity is larger than the theoretical one, without the corresponding static pressure rise. There is a destruction of dynamic pressure.

Vaned diffusers, as shown in the configuration of Figure 44, have been known for a long time. Their use makes possible a much more rapid deceleration of the tangential velocity than with a free vortex. The frictional losses are therefore reduced, and the efficiency increased. However, this remains true only for a very narrow capacity range, that for which the aerodynamic design of the vanes is correct. On the other hand, the proximity of a moving-vane system to a fixed-vane system causes an unpleasant aerodynamic noise.

The above analysis of the three classical types of centrifugal fans reveals that all three solutions are unsatisfactory in many respects. This leads us to a discussion of the rotating-diffuser fan.

THE ROTATING-DIFFUSER CENTRIFUGAL FAN

A further examination of Figure 43 suggests the apparently trivial modification which consists in making the diffuser rotate with the wheel rather than remain

stationary. Actually, this change turns out to be very significant: with a rotating diffuser, most of the disadvantages of the configuration of Figure 43 listed above completely disappear.

First, there is no clearance problem any more between rotor and diffuser; thus, the flow at the entrance of the diffuser can be more uniform than before. Second, since the walls of the diffuser turn with the wheel, the frictional forces between the diffuser wall and the flow are substantially decreased, since the relative velocity is smaller. Actually, in many cases, the relative velocity even changes direction, so that the tangential frictional forces result in a tractive, rather than a retarding force. In the radial direction, the boundary layer along the walls is contained by centrifugal action, and therefore interferes less with the diffusion process.

Finally, the rotor diffuser constitutes a very effective "buffer" element between the wheel and the volute, and contributes to the damping of flow variations associated, in a given vane channel, with the one-per-revolution passage in front of the exhaust orifice. This damping action also allows the wake flows behind the vanes to die down before reaching the exhaust orifice, thus eliminating one of the main causes of fan noise.

The second advantage listed above for the rotating diffuser has its counterpart. The relative velocity of the inside wall of the diffuser with the flow is reduced, as compared with a stationary diffuser, but the friction of the outside wall of the diffuser with the surrounded fluid is added. This effect is so much more important that the diameter of the rotating diffuser is larger.

One can thus intuitively feel that a design compromise must be found, in each application, between diffuser diameter and shape, to insure that the power saving resulting from more efficient diffusion is always larger than the power expended due to the friction of the outside wall of the diffuser with the surrounding medium.

From the earlier discussion, it is obvious that the rotating diffuser design depends upon the vane discharge angle. It also depends upon a number of other factors, such as the wheel discharge to inlet area ratio, fan operating condition, etc.

Extensive systematic tests are required to find the best compromise between fan geometry and flow condition. The incorrectly designed RD fan could easily be ten points off in efficiency, as compared to the properly designed fan. For the

usual capacity range, a family of optimum fans has been designed by Etablissements Neu for a range of area ratios between 0.35 and 0.84 and the vane discharge angles between 45° and 105°. These design characteristics are of a proprietary nature, and are not discussed further here. A typical example of application of the Neu design charts, applied to a fan independently tested by Aerophysics Company as part of its GEM internal flow program, is discussed in a subsequent paragraph.

DISCUSSION OF SURGING AND SHUT-OFF HEAD

The zero-flow condition is a regime which many fan designers tend to ignore. However, it is well known that it is associated with the phenomenon called surging, which can be a very disagreeable one. Also, ground effect machines operating over water have to operate at lift-off under zero-flow conditions. It is important that they do so under good conditions of operation of the fan.

Consider, for example, the results of test 791-45 (Figures 31 and 35). At low capacities, the head curve dips. In this region, the slope of the curve is positive and operation of the fan is unstable (correspondingly, it could be shown that the ground effect machine would be unstable). The flow is characterized by large fluctuations in pressure and capacity. These fluctuations can be large enough to cause back-flow. They are accompanied by noise and vibrations. This is the phenomenon called surging.

It is therefore desirable to devise an anti-surge device. The pressure curve with such a device can be seen on Figure 31: Test 791-52, for example. Consider an impeller shaped as shown on Figure 47. Let us apply to it Euler's equation discussed above. If the capacity is zero, $c_{u_2} = u_2$ whatever the value of the angle β. This is the equation representing a solid gyration, called solid gyration of the fluid in the wheel, the fluid behaving as if it were frozen, and rotating at the same speed of rotation as the wheel. One can show (see, for example, Reference 64) that the theoretical pressure consists then of two equal parts: a static pressure rise between the axis of the fan and the periphery equal to $\frac{\gamma}{2g} u_2^2$ and a dynamic pressure difference between the axis and the periphery also equal to $\frac{\gamma}{2g} u_2^2$. If the machine were perfect, one should have a complete recovery of dynamic pressure into static pressure in the volute; hence, a total pressure equal to

$$\frac{\gamma}{2g} u_2^2 .$$

Experience indicates that the measured pressure (under zero-flow conditions), if the eye area remains open, is hardly larger than half the above theoretical pressure.

A visualization of the flow by means of tufts reveals trajectories as shown on Figure 47. There is indication that secondary currents inside the wheel do not exist. The fluid does rotate as a solid, as was postulated in the above theoretical analysis.

A pressure survey indicates that, along the wall DE (Figure 47), there is a static pressure rise equal to $\frac{\gamma}{2g} u_2^2$. However, this does not hold for the wall AC. Indeed, at point A, the tangential velocity is $u_1 < u_2$ and the increase in static pressure between A and C due to the solid gyration inside the wheel is only $\frac{\gamma}{2g} (u_2^2 - u_1^2)$. It would appear that the static pressures are not in equilibrium, which is in contradiction with the fact that there are no internal secondary currents.

The missing pressure must be created somehow. It is actually created by the outside air motions described in Figure 47. The solid gyration will create a certain static pressure difference between the axis and the periphery of the eye in front of the wheel. Also, the shape of the impeller vanes will induce a certain pressure distribution. Altogether, one can expect that these effects will reduce the theoretical static pressure by about 10 percent.

Let us consider now what happens downstream of the impeller. At different radii away from the impeller, one can measure static and dynamic pressures, from which one can calculate the tangential velocities.

The results of this test are shown in Figure 48 for a conventional centrifugal fan. The first curve shows the ratio of measured static pressure to theoretical static pressure (assuming a free vortex). The second curve shows the variation of measured tangential velocity to theoretical tangential velocity.

If the flow were perfect, both curves should be straight lines parallel to the horizontal axis, going through the ordinate 1.0. One is very far from perfection,

but, in the neighborhood of the impeller, the static pressure is about 9/10 of the theoretical static pressure, as was mentioned before should be the case.

One can notice mainly a very rapid decrease of the velocity curve, indicating a rapid destruction of dynamic pressure by friction.

Finally, the pressure against the opening of the volute is $0.52 \frac{\gamma}{g} u_2^2$ with respect to atmosphere, and $0.58 \frac{\gamma}{g} u_2^2$ with respect to point D. Therefore, $0.42 \frac{\gamma}{g} u_2^2$ has been destroyed. In other terms, 84 percent of the dynamic pressure at the impeller exit was destroyed.

Consider now a similar test with an impeller to which is attached a rotating diffuser. The results are shown in Figure 49. One can notice a very substantial improvement. Inside the diffuser, the velocity curve decreases much more slowly than before; therefore, there is more dynamic pressure recovery, and one finds, against the volute, a static pressure equal to $0.7 \frac{\gamma}{g} u_2^2$ with respect to atmospheric and $0.75 \frac{\gamma}{g} u_2^2$ with respect to point D. The destruction of dynamic pressure is only 0.5 times its value at the periphery of the wheel.

One can thus conceive that, by varying the diameter of the rotating diffuser, one may reduce, then eliminate, surge. This is vividly demonstrated in Figure 31.

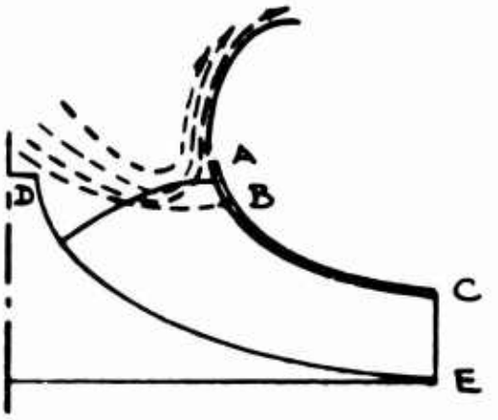

Figure 47: Flow at the Entrance of an Impeller Vane at Shutoff Condition

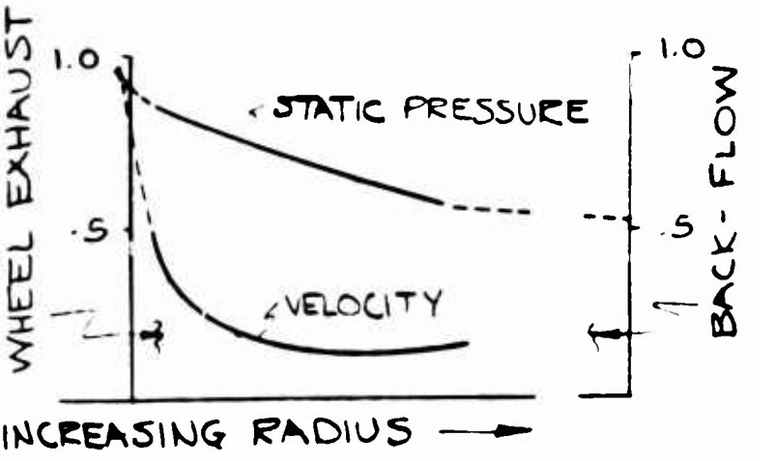

Figure 48: Degradation of Tangential Velocity and of Pressure at Exit of Impeller without Diffuser

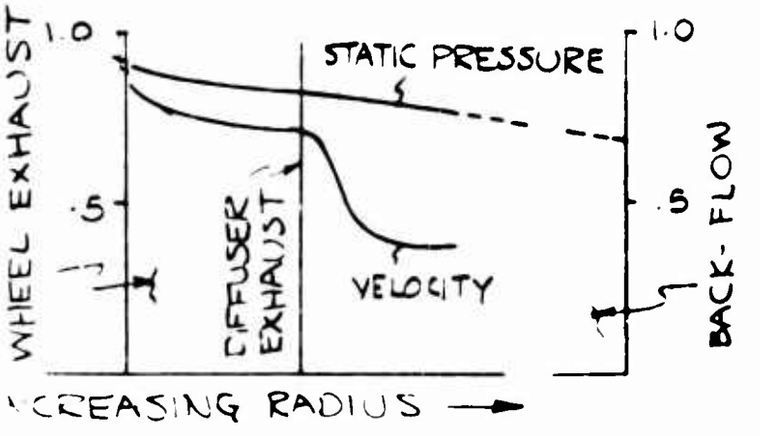

Figure 49: Degradation of Tangential Velocity and of Pressure at Exit of Impeller with Rotating Diffuser

ELEMENTS OF A THEORY OF THE RD WHEEL

The characteristics of various types of centrifugal fans in terms of the Euler equation only having been just discussed, a more complete analytical formulation of the flow equations of a centrifugal fan with or without rotating diffuser will now be made.

The inviscid analysis for two-dimensional flow on general surfaces of revolution in turbomachines with arbitrary blade shapes was developed in Reference 58. Such an analysis is very useful as a guide to impeller design, but cannot under any circumstances be used for an analytical determination of the head-capacity curve of a real fan. Such a determination is attempted here, following the method of Reference 39. This is done by carefully defining the hydraulic losses through the fan and expressing them in terms of nondimensional coefficients that can be obtained experimentally. At the beginning of the Aerophysics development program of application of RD fans to GEM propulsion systems, it was believed that these hydraulic loss coefficients had been obtained as part of the extensive Neu development program. It turned out that such is not the case. Neu's own method of performance prediction of RD fans is discussed briefly later in this appendix and proceeds along different lines. The RD fan test program of the Aerophysics Company, which is discussed in Section IV of this report, could, with the proper extension of scope, lead to a numerical estimation of the hydraulic loss coefficients. Until such an estimation has been made, however, the method discussed below will not lend itself to numerical applications.

THE ENERGY EQUATION OF A CENTRIFUGAL FAN

It is assumed that the flow is nonviscous and that the machine is thermally insulated. A meridian section of the fan being analyzed is shown in Figure 50 and the reference numbers denoting the cross sections are discussed in detail in the list of symbols. The significant velocity triangles are also shown in Figure 50. As mentioned in the list of symbols, notations conform to Stepanoff's (Reference 64) inasmuch as possible.

The energy at the impeller entrance is:

$$\frac{\gamma}{\gamma - 1} \frac{p_1}{\rho_1} + \frac{c_1^2}{2g} = c_p J T_{io}$$

The energy added to the impeller (per pound) is:

$$H_c = \tau\omega = \frac{u}{g} c_u$$

The energy at any point on the impeller is:

$$\frac{\gamma}{\gamma - 1} \frac{p}{\rho} + \frac{c^2}{2g}$$

Adding up the first two energy terms to the third one above gives:

$$c_p J T_{io} + \frac{u}{g} c_u = \frac{\gamma}{\gamma - 1} \frac{p}{\rho} + \frac{c^2}{2g} \tag{1}$$

On the other hand, the equation of state gives:

$$p = \frac{(\gamma - 1)}{\gamma} J c_p \rho T \tag{2}$$

Substituting into (1), one finds:

$$c_p J T + \frac{c^2 - 2u c_u}{2g} = c_p J T_{io} \tag{1'}$$

One can express $c^2 - 2u c_u$ in another form:

$$c^2 - 2u c_u = (u - w_u)^2 + w^2 - u w_u^2 - 2u(u - w_u)$$

$$= w_u^2 - u^2$$

Therefore, one also has:

$$c_p J T + \frac{w^2}{2g} - \frac{u^2}{2g} = c_p J T_{io} \tag{3}$$

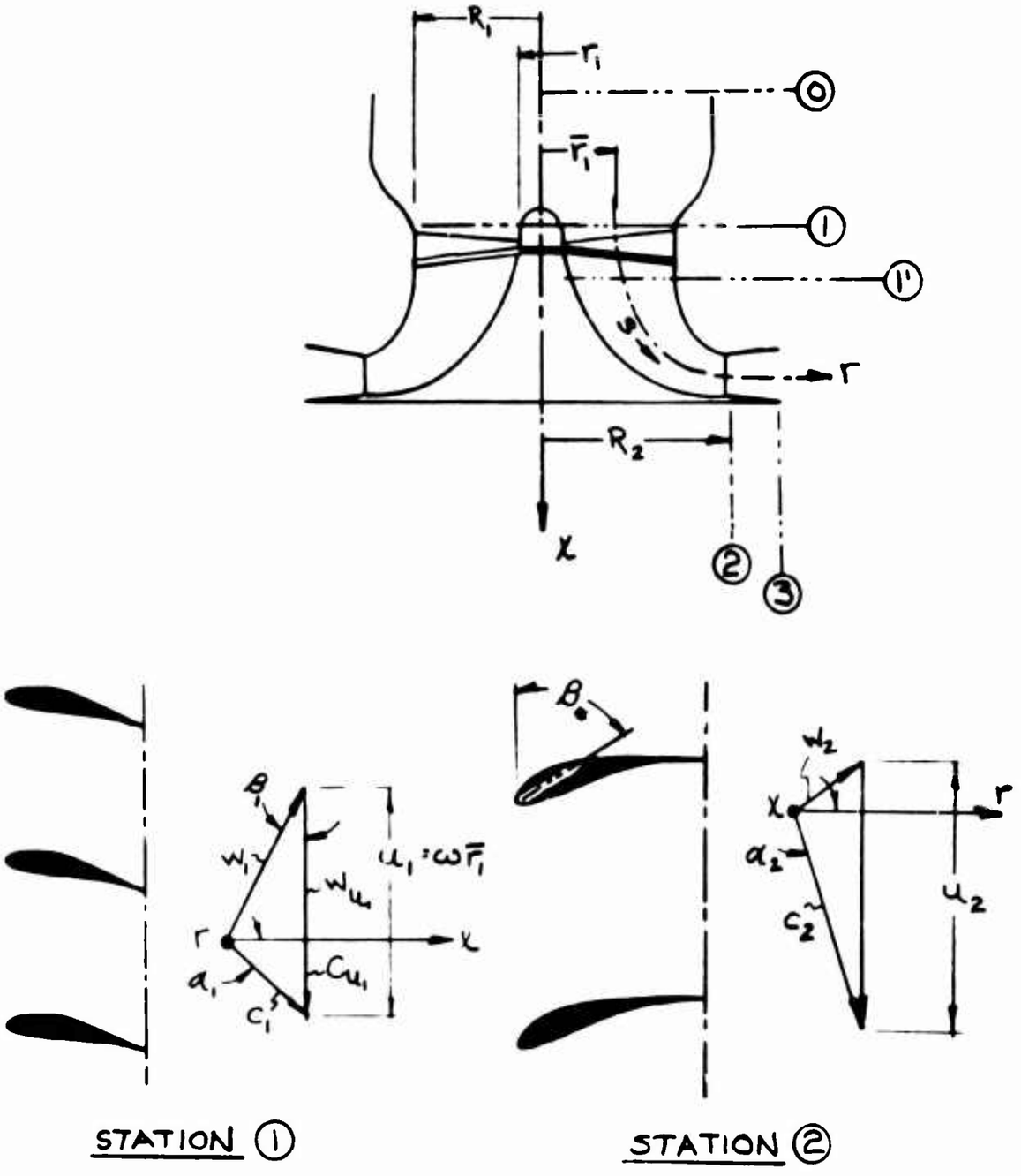

Figure 50: Schematic of Stations for RD Fan Analysis and Velocity Triangle at Two Stations

One has: $c_u = c \sin \alpha$

Therefore, equation (1') can be written as follows:

$$c_p J T + \frac{c^2 - 2\omega r c \sin \alpha}{2g} = c_p J T_{io} \qquad (4)$$

Applying equation (4) at station 2, one finds:

$$c_p J T_2 + \frac{c_2^2 - 2\omega r_2 c_2 \sin \alpha_2}{2g} = c_p J T_{io} \qquad (4')$$

But: $$T_{i_2} = T_2 \left(1 + \frac{\gamma - 1}{2} \frac{c_2^2}{a_2^2} \right)$$

and $$a_2^2 = g \gamma R T_2$$

Hence:

$$T_{i_2} = T_2 + \frac{\gamma - 1}{2g \gamma R} c_2^2$$

Substituting the expression of T_{i_2} into equation (4'), one finds:

$$c_p J T_{i_2} - \frac{J c_p (\gamma - 1)}{2g \gamma R} c_2^2 + \frac{c_2^2}{2g} - \frac{\omega r_2 c_2 \sin \alpha_2}{g} = c_p J T_{io}$$

By definition,

$$R = \frac{\gamma - 1}{\gamma} J c_p$$

Therefore, the terms in c_2^2 cancel out, and one has left:

$$g\, c_p\, J(T_{i_2} - T_{io}) = \omega r_2 c_2 \sin \alpha_2 \qquad (5)$$

Equation (5) can also be written as follows:

$$g\, J\, c_p\, (T_{i_2} - T_{io}) = u_2\, w_{u_2} \qquad (5')$$

Expressing the velocities in terms of Mach numbers and introducing a slip factor S (see References 39 and 23 and the list of symbols), the energy equation becomes:

$$g\, J\, c_p\, (T_{i_2} - T_{io}) = a_*^2\, S\, M_{*_2}^2 \qquad (6)$$

THE EQUATION OF THE FLOW

Consider on a mean surface of the flow the motion of a fluid particle along a streamline (the curvilinear abscissa being s). The intrinsic equation of the motion (Bernoulli) can be written introducing elemental hydraulic losses $d\varpi$, as follows:

$$\frac{dp}{ds} = -\rho \frac{d}{ds}\left[\frac{w^2 - u^2}{2}\right] - \frac{d\varpi}{ds} \qquad (7)$$

In this particular flow equation, the velocity square term is $w^2 - u^2$, instead of c^2. The same substitution was found with the energy equation (3):

$$g\, J\, c_p\, T + \frac{w^2 - u^2}{2} = c_p\, J\, g\, T_{i_1} \qquad (3)$$

THE THEORETICAL AND THE REAL COMPRESSION RATIOS

Combining the equation of state (2) with equations (3) and (7), one finds:

$$\frac{dp}{p} = \frac{\gamma}{\gamma - 1} \frac{dT}{T} - \frac{d\omega}{p} \tag{8}$$

By integration, one obtains:

$$\frac{p}{p_o} = \left(\frac{T}{T_{io}}\right)^{\gamma/\gamma - 1} \exp\left(-\int_o^s \frac{d\omega}{pds}\, ds\right) \tag{9}$$

For any point of the flow, one also has:

$$\frac{p}{P} = \left(\frac{T_i}{T_{io}}\right)^{\gamma/\gamma - 1}$$

Hence:

$$\frac{p}{p_o} = \left(\frac{T_i}{T_{io}}\right)^{\gamma/\gamma - 1} \exp\left(-\int_o^s \frac{d\omega}{pds}\, ds\right) \tag{10}$$

This is the actual compression ratio.

The theoretical compression ratio is defined as:

$$\left(\frac{p}{p_o}\right)_{th} = \left(\frac{T_i}{T_{io}}\right)^{\gamma/\gamma - 1} \tag{11}$$

For the special case of an incompressible flow, it is well known that:

$$p = p_{th} - \int_o^s \frac{d\omega}{ds}\, ds \tag{12}$$

The theoretical compression ratio can be expressed in terms of the velocity, using equations (6) and (11):

First, one has:

$$T_{i_2} = T_{io}\left[1 + \frac{2(\gamma - 1)}{\gamma + 1}\right] S M_{*_2}^2 \qquad (13)$$

Then:

$$\left(\frac{P_2}{P_o}\right)_{th} = \left[1 + \frac{2(\gamma - 1)}{\gamma + 1}\right] S M_{*_2}^2 \qquad (14)$$

DEFINITION OF THE COEFFICIENTS OF HYDRAULIC LOSS

A study of the losses in centrifugal blowers is important for one of the following reasons: (1) information about the nature and magnitude of losses may indicate the way to reduce these losses; (2) if the losses are known, it is possible to predetermine the head capacity of a new machine by first assuming, or establishing in some other manner, the head-capacity curve of an idealized blower; (3) since the head-capacity curve of an idealized blower is a straight line, the shape of the head-capacity curve of an actual blower is determined by the hydraulic losses. Thus, it would seem possible, when something is known about the losses, that one could change the shape of the head-capacity curve to suit some special requirement.

Very little exact knowledge is available on the exact losses of centrifugal blowers. The progress in design has been accomplished mostly in an experimental way, the gross efficiency being the only criterion of improvement in performance. The losses are usually grouped under the following headings: hydraulic, leakage, mechanical, and disk friction. Only hydraulic losses will be discussed in this paragraph.

A great many factors contribute to hydraulic losses. In general, hydraulic losses are caused by (1) skin friction and (2) eddy and separation losses due to changes

in direction and magnitude of the flow. The latter group includes the so-called shock loss and diffusion loss.

In the channels from the inlet to the discharge nozzle, there is not a single stretch of the path where either the direction of flow or the shape and area of the channel is constant; besides, part of the channel is rotating, thus upsetting the velocity distribution and further complicating the study of hydraulic losses. Under such conditions, it is impossible to calculate the friction loss through the machine with a degree of accuracy sufficient to serve any useful purpose.

It is sufficient in practice to estimate the global hydraulic loss between two of the fan stations defined in Figure 50 as being proportional to certain nondimensional groupings of aerodynamic variables which characterize adequately the origin of the losses incurred between the stations under consideration. The combination used in the evaluation of the integral of the hydraulic losses (equations 10 and 12) are shown in Table 6, following Reference 23. The experimental values of the coefficients ζ of hydraulic losses remain to be determined experimentally. This task remains to be accomplished for RD fans. Therefore, the present analysis will not lend itself to numerical applications until these coefficients have been obtained experimentally. In the meantime, a practical method to predict RD fan characteristics, developed by Etablissements Neu, is discussed on page 112.

ANALYTICAL EXPRESSIONS FOR THE HYDRAULIC LOSSES

The hydraulic losses can be most conveniently expressed in terms of "capacity coefficients" ($\varphi = \tan \beta$, and $\varphi_* = \tan \beta_*$), which in turn can be simply related to the volume flow q. Assuming that, at the impeller entrance, $\alpha_1 = 0$, one has:

$$\varphi = \tan \beta_1 = \frac{c_m}{\omega \bar{r}_1} = \frac{A_1 q}{\omega \bar{r}_1}$$

where A_1 is the flow area at station 1.

The coefficients defined in Table 6 can be substituted in the integral

$$\int_o^s \frac{d\omega}{pds} ds = \delta\omega$$

TABLE 6
DEFINITION OF HYDRAULIC LOSS COEFFICIENTS
($\alpha_1 = 0$)

Origin of Loss of Pressure	Reference Velocity	Nondimensional Form
Shock at Entry to Guide Vanes	$\omega \bar{r}_1 \left(1 - \frac{\tan \beta_1}{\tan \beta_*}\right)$	$\zeta_{sh} \left(1 - \frac{\tan \beta_1}{\tan \beta_*}\right)^2 M_{*1}^2$
Radial Deflection of Flow	c_1	$\zeta_d \varepsilon^2 M_{*1}^2$
Friction in Moving Rotor	w_1	$\zeta_f (1 + \varepsilon^2) M_{*1}^2$
Wall Friction (parietal)	ωr_2	$\zeta_r \left(\frac{r_2}{\bar{r}_1}\right) M_{*1}^2$
Friction in Diffuser	c_3	$\frac{\zeta_D m^2 {}_{*3}}{1 + \frac{2(\nu - 1)}{\nu + 1} S M_{*2}^2}$
Shock at Entry to Diffuser	$c_3 \sin \alpha_3 \left(1 - \frac{\tan \alpha_3}{\tan \alpha_*}\right)$	$\frac{\zeta'_{sh} S^2 M_{*2}^2 \left(1 - \frac{\tan \alpha_3}{\tan \alpha_*}\right)^2}{1 + 2\left(\frac{\nu - 1}{\nu + 1}\right) S M_{*2}^2}$

for each coefficient, using mean values for approximate integration. One finds the following:

Shock at entry of the guide vanes

$$\delta\varpi = \frac{\gamma - 1}{\gamma} \frac{\rho(\omega \bar{r}_1)^2}{2} \zeta_{sh} \left(1 - \frac{\varphi}{\varphi_*}\right)^2$$

Radial deflection of the flow

$$\delta\varpi = \frac{\gamma + 1}{\gamma} \frac{\rho(\omega \bar{r}_1)^2}{2} \zeta_d \varphi^2$$

Friction in the moving rotor:
From station (1) to (1'):

$$\delta\varpi = \frac{\gamma + 1}{\gamma} \frac{\rho(\omega \bar{r}_1)^2}{2} \zeta_f (1 + \varphi^2)$$

From station (1') to (2):

$$\delta\varpi = \frac{\gamma + 1}{\gamma} \frac{\rho(\omega \bar{r}_1)^2}{2} \zeta_f' (1 + \varphi^2)$$

Wall friction (parietal)

$\delta\varpi = 0$ (The RD fan is of the enclosed type, the walls rotating with the flow)

Friction in the rotating diffuser

$$\delta\varpi = \frac{\gamma + 1}{\gamma} \zeta_D \rho \frac{c_2^2}{2}$$

Shock at entry to the diffuser

$\delta\varpi = 0$

Hence:

$$\psi\varpi = \frac{\gamma + 1}{\gamma} \frac{\rho(\omega \bar{r}_1)^2}{2} \left[\zeta_d \varphi^2 + (\zeta_f + \zeta_{f'})(1 + \varphi^2) + \zeta_{sh} \left(1 - \frac{\varphi}{\varphi_*}\right)^2 \right] + \frac{\gamma + 1}{\gamma} \zeta_D \rho \frac{c_2^2}{2}$$

If the flow is incompressible, the above expression for $\delta\varpi$ can be used in equation (12). If the flow is compressible, equation (10) must be used. For

most applications concerning the RD fan, incompressible equations are satisfactory.

The two following remarks concerning the hydraulic losses are of interest:

1. One essential difference between the bladed diffuser and the rotary diffuser is that for the bladed diffuser, one has both frictional losses and large shock losses at entry (for example, $\zeta_{sh} = 0.95$). These chock losses increase rapidly as soon as one departs from the matching conditions. For the rotary diffuser, the shock losses are essentially zero, and hence, the performance superiority of the rotary diffuser.

2. It was mentioned earlier that disk friction losses could be important for an RD fan. In an investigation reported in Reference 39 and in Table 6, it is noted that the reference velocity that has to be used for the rotating diffuser losses is not the relative velocity at the exit of the rotor, but the absolute velocity. In relative magnitude, the losses due to the external friction of the rotor rotating inside a fixed casing are larger than those corresponding to the friction of the fluid against the side walls of the diffuser. As the external friction of the disk is a function of its peripheral velocity, and this is directly connected with the absolute velocity of the flow, it is suspected that here lies the reason for referring the total loss coefficient of a rotary diffuser to the absolute exit velocity rather than to the relative velocity.

The analysis of the centrifugal fan with rotating diffuser has been carried out in sufficient detail to show the possibility of a complete mathematical representation of the fan. This formulation is in terms of experimental coefficients, which are not presently available with any amount of reliability. Therefore, the rest of the analysis, which relates the above equations to the geometry of the fan and involves nothing more than the repeated use of the equation of continuity, will not be discussed here. Instead, a practical method of prediction of RD fan performance, evolved by Etablissements Neu during the past 10 years, will be discussed in general terms and illustrated.

ACTUAL PREDICTION OF THE PERFORMANCE OF AN RD WHEEL

METHOD

The performance prediction by Neu for RD fans of arbitrary size and characteristics is based on the proper exploitation of an intensive series of model tests (on standardized 500 mm diameter wheels), supplemented by selected full-scale tests used to obtain scale effect factors.

Model tests were made over the years by Neu and complete performance was recorded in terms of two parameters: R_1/R_2 and β_2. As was indicated earlier, optimum designs were obtained for a range of values of R_1/R_2 (from 0.35 to 0.84; for example, the fans of Figures 27 to 41 correspond to 0.5; the model fan used by Aerophysics in its GEM internal-flow test belongs to the 0.7 series) and a range of values of β_2 (between 45° and 105°; for example, the Aerophysics-tested fan corresponds to 75°.

For each of the above combinations of R_1/R_2 and β_2, performance of the tested model fan can be plotted (see Figures 27 to 41) in the form of pressure coefficient, Cp; power coefficient, Cw; or recovery coefficient, qu, as a function of the capacity factor, Cd. These coefficients were first introduced by Monsieur Chappuis (References 16 and 36).

The efficiency of the basic model fan is then given by:

$$\eta = \frac{Cd \times Cp}{.75\ Cw}$$

Consider now a fan belonging to a certain family (defined by the two digits R_1/R_2, β_2), for which test model results are available. This fan is assumed to have all dimensions homothetic of those of the model fan. In first approximation, the unknown characteristics of the fan (assumed operating under standard atmospheric conditions) will be given by:

$$q = Cd \times u_2 \times A_o$$

$$pt = Cp \times u_2^2$$

$$\mathcal{P} = Cw \times u_2^3 \times A_o$$

$$\eta = \frac{Cd \times Cp}{75\ Cw}$$

The size and rotor tip speed of the machine do not appear in the above expression of the efficiency. This means that one implicitly assumes that all machines of a given family will have the same efficiency.

It is well known that this is an erroneous oversimplification. A strong scale effect, which depends upon a number of complex factors related to the flow characteristics of each particular unit, exists for centrifugal fans.

The originality and merit of the Neu method is that it accounts thoroughly and accurately for scale effects. The method will be described only briefly, since details of the method, as well as basic model test results, are proprietary to Neu.

For a given capacity, the scale effect results in a correction to the pressure coefficient (for example, $\Delta_1 Cp$) and a correction to the power coefficient (such as, $\Delta_1 Cw$), which can be either positive or negative. These coefficients can be calculated and controlled by means of tests, and then are tabulated for each family of fans.

In a similar fashion, such elements as (1) inlet vanes, (2) modulating vanes, (3) pressure losses downstream of the rotating diffuser, etc., will modify the basic performance of a fan, and this will result in additional correction factors, such as $\Delta_2 Cp$, $\Delta_2 Cw$, $\Delta_3 Cp$, $\Delta_3 Cw$, etc.

The exact performance of a fan, accounting for scale effect, vane effect, and miscellaneous pressure losses can then be expressed as

$$q = Cd \times u_2 \times A_o$$

$$pt = (Cp + \Delta_1 Cp + \Delta_2 Cp + \Delta_3 Cp + \cdots) \times u_2^2$$

$$p = Cw + \Delta_1 Cw + \Delta_2 Cw + \Delta_3 Cw + \cdots) \times u_2^3 \times A_o$$

$$\eta = \frac{Cd \times (Cp + \Delta_1 Cp + \Delta_2 Cp + \Delta_3 Cp + \cdots)}{75(Cw + \Delta_1 Cw + \Delta_2 Cw + \Delta_3 Cw + \cdots)}$$

For a given family of fans, the efficiency is not constant any more.

A discussion of the effect of inlet vanes, modulating vanes, etc., is beyond the scope of this appendix. The reason why they were introduced here is that they appear in the numerical calculations of the next paragraph.

The above calculations assume incompressible flow. If the flow is compressible, it can be shown (Reference 36) that the method can be extended. Recently, Neu completed the programming and solution of the compressible flow problem on an IBM 7090 computer.

APPLICATION TO A 20-INCH TEST FAN

As part of the program of application of RD fans to ground effect machines discussed in this report, a 20-inch-diameter rotating-diffuser fan was designed analytically and built by Joy Manufacturing Company for testing by Aerophysics (see section IV of the report for a discussion of the experimental program).

The tabular calculations submitted by Joy to Aerophysics (Reference 41) were made in accordance with the Neu method described above. The calculations of Reference 41 consist of 6 tables. These tables are not reproduced here, since Joy feels that the details of the method are proprietary. Results of the calculations are shown, however, as Figures 51 and 52. Note that the Aerophysics test wheel of the present program is the same size as the standard Neu test wheel; therefore, there is no scale effect.

The fan model shown on Figures 51 and 52 is labelled: RD 20-.7-1.3-75°. The nomenclature can be read as follows: RD stands for rotating diffuser; 20 means $2R_2 = 20$ inches; .7 means $R_1/R_2 = .7$; 1.3 means $R_3/R_2 = 1.3$. Finally, $\beta_2 = 75°$.

The different curves shown on Figures 51 and 52 represent several cases, as follows:

1. The solid curve on Figure 51 shows the performance for a standard industrial RD fan, used in conjunction with a conventional volute.

2. The second curve on Figure 51 represents the estimated performance for an RD wheel in a plenum chamber, with the volute removed, the cutoff being replaced by a series of peripheral vanes located at some distance downstream of the rotating diffuser. The losses associated

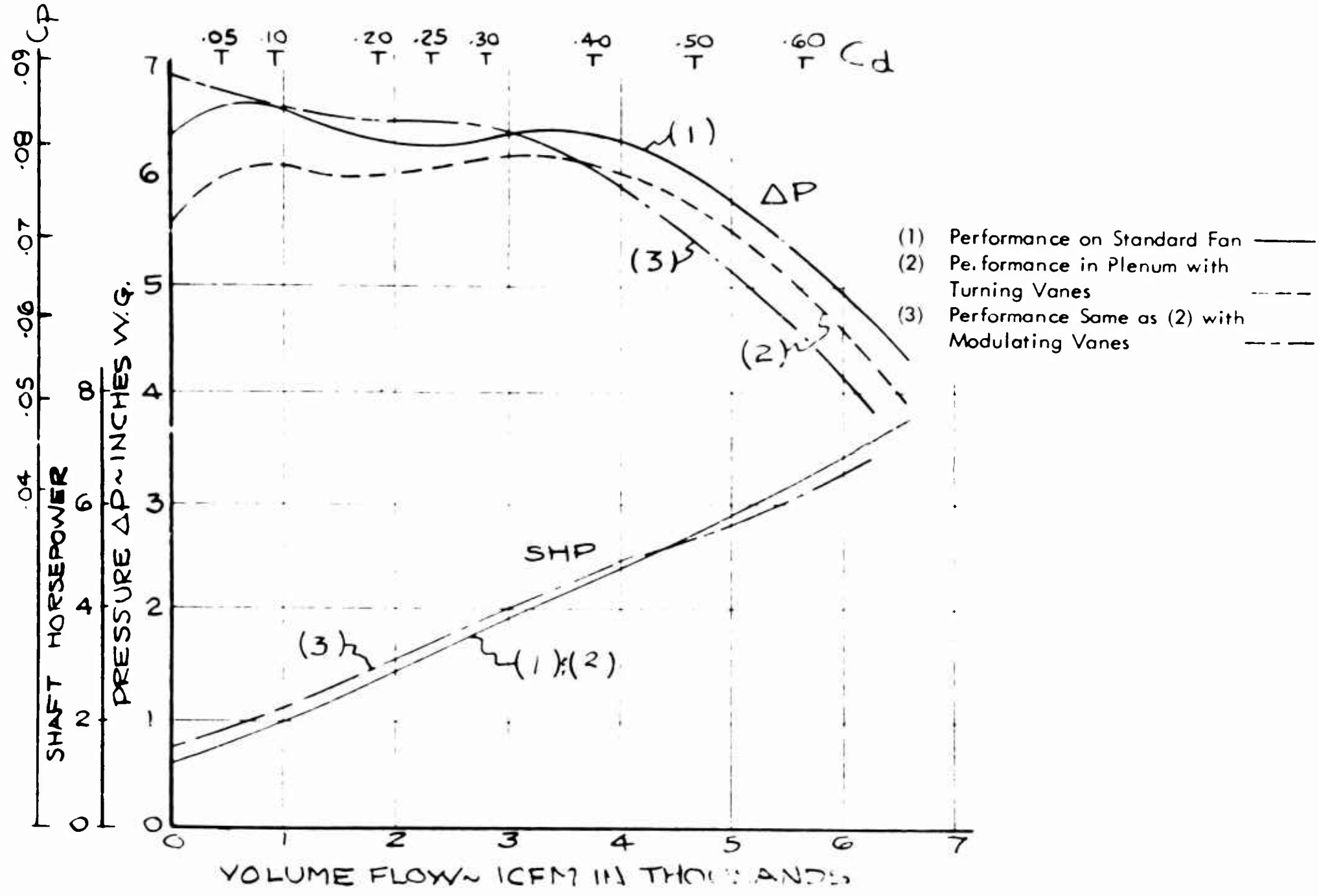

Figure 51: Joy Curve C-4230. Computed Performance, Fan Model RD 20-.7-1.3-75°; Fan Speed, 1700 rpm

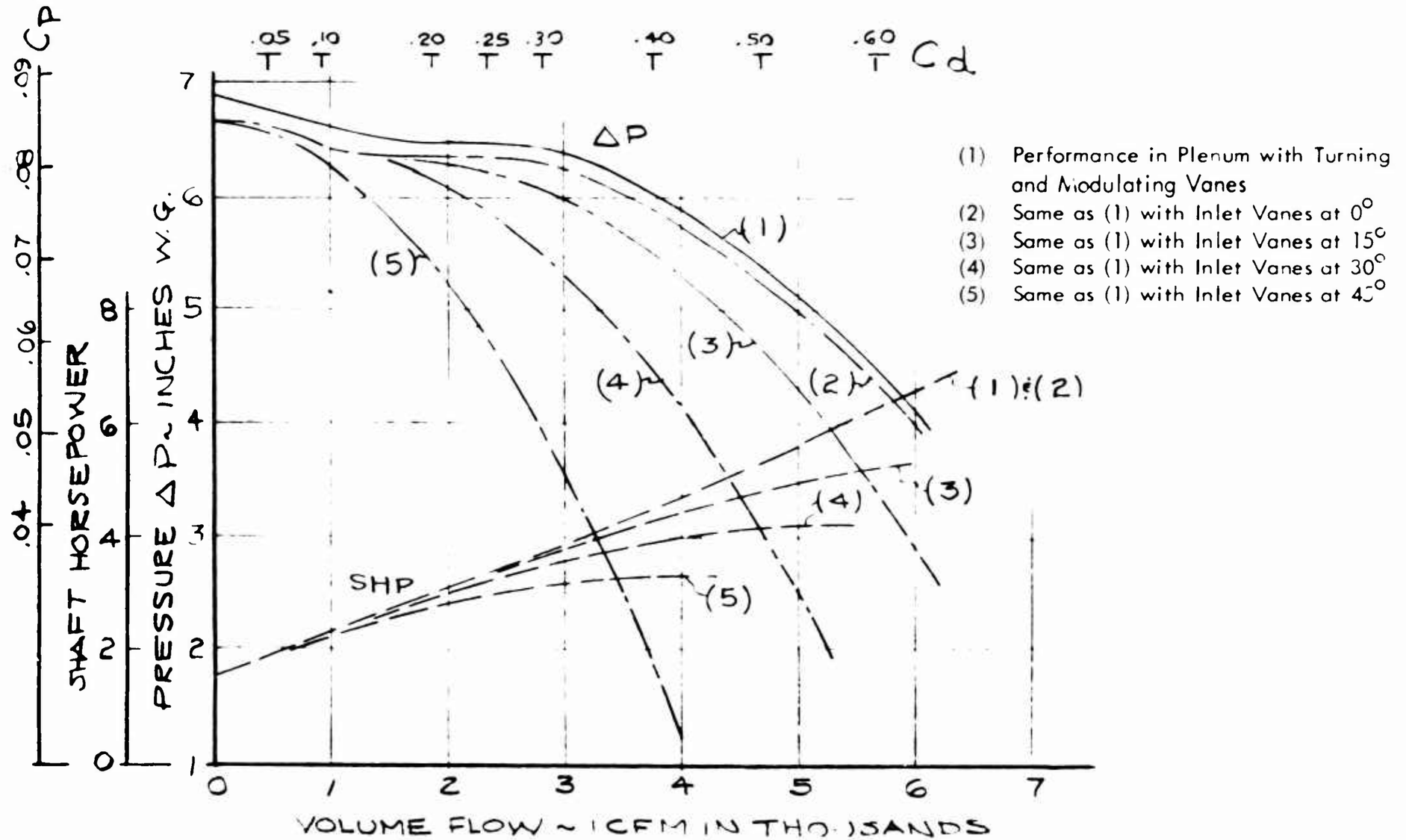

Figure 52: Joy Curve C-4233. Computed Performance, Fan Model RD 20-.7-1.3-75°, Fan Speed, 1700 rpm

with the turning vanes are estimated from past Neu model tests. This curve is expected to represent closely the behavior of the RD fan as part of a GEM internal-flow system.

Naturally, at all capacities, the second curve lies everywhere under the first one, since the radial-delivery duct with turning vanes is intuitively felt to be less efficient than the volute.

3. The third case represents the same configuration as the second one, with the addition of modulating vanes. As explained earlier, the modulating vanes prevent surge at low capacities. It can be seen that this is paid for by a slight pressure decrease near the operating point.

4. Several curves are shown on Figure 52 to indicate the pressure drop corresponding to several inlet vane angles.

EVALUATION

1. Thanks to the pioneering work of Etablissements Neu and of Joy Manufacturing Company, the flow mechanics of RD fans are fairly well understood and their performance can be predicted very accurately.

2. The operation of an RD fan as part of a GEM internal-flow system may be radically different from its operation as a conventional industrial fan. The knowledge of the factors discussed in this report will be invaluable, however, for an understanding of the operation of an RD fan with a GEM internal-flow system.

3. Fundamental research into the detailed flow mechanics of RD fans (for example, the behavior of the boundary layer along the walls of the diffuser) would be of great theoretical and practical interest and would represent an advance to the state of the art of rotating machinery.

APPENDIX II. INTERNAL-FLOW REQUIREMENTS DICTATED BY AIR CUSHION AERODYNAMICS

List of Symbols

c	perimeter, measured at the nozzle center line in the nozzle exit (the nozzle exit is taken normal to the jet discharge direction)
h	altitude, measured from the surface to the lower edge of the nozzle exit
J	scalar total jet momentum flux
L	total lift
M	figure of merit, defined as $\frac{1}{2\sqrt{\rho S}} \frac{L^{3/2}}{P}$
p	static pressure inside the jet
Δp	effective base pressure (gage): total base pressure lift, accounting for the static pressure over the nozzle exit, divided by $(S - \frac{tc}{2})$
p_{t_i}	weighted-average jet total pressure (gage) measured at the nozzle exit, the pressure at a point being weighted proportional to the normal velocity at that point
P	air horsepower at nozzle exit, in pound-feet per second
HP	horsepower $HP = \frac{P}{550}$
Q	volume flow at the nozzle exit per unit time
R	radius of curvature of the jet, usually assumed constant
S	reference area: plan area enclosed by outer edge of nozzle exit
t	nozzle width; usually also curved jet width

t_∞	jet width at infinity (Figure 53)
U	variable velocity in the jet
U_o	jet velocity at infinity (Figure 54)
V_i or $\overline{V_i}$	average jet velocity measured at the nozzle exit
W	vehicle weight
x	thickness over height ratio parameter = $\frac{t}{h}(1 - \sin\theta)$
y	coordinate in a direction normal to flow at or near jet exit
η_A	Chaplin's augmentation efficiency factor
θ	jet discharge angle measured from vertical at the nozzle exit; negative for an inward-inclined jet
ρ	air density

INTRODUCTION

The internal-flow requirements for a ground effect machine are commonly expressed in terms of the total head at the nozzle exit and the volume flow rate through the nozzle. The total head and the volume flow are expressed in terms of the desired vehicle characteristics.

The assumptions under which the analysis is made are limitative and therefore must be specified carefully. The assumed geometry of the nozzle with respect to the ground is shown in Figure 53. All symbols used in this appendix are defined on page 119.

Figure 53 shows two-dimensional flow. It is known that the two-dimensional theory represents accurately the performance of a three-dimensional machine. However, this is only true if the total pressure of the jet, p_{t_j}, is constant around the periphery of the jet. In this paragraph, the only comparison to be made between theory and experiment is concerned with two-dimensional experimental data, where p_{t_j} is always constant around the periphery. However, for any three-dimensional data such as those discussed in Section IV of this report for a machine of oval planform, p_{t_j} is far from being constant along the periphery of the nozzle, and it is not correct to state, for example, that the total volume flow is the product of the volume flow per unit length by the peripheral length. Only two-dimensional, inviscid theories will be reviewed here. The aim of this study is to choose, among the simple available theories of inviscid static peripheral jets, that which satisfies best existing two-dimensional data; one then assumes that such a theory will best represent the internal-flow requirements of a GEM. The best available experimental data to date are those of Reference 13.

In previous internal-flow studies, Vehicle Research Corporation and AiResearch initially used the thin-jet momentum theory (References 65 and 45, respectively). In a subsequent study (Reference 66) Vehicle Research used the exponential theory (also known as the Stanton-Jones theory). These theories and modifications thereof will be reviewed in what follows.

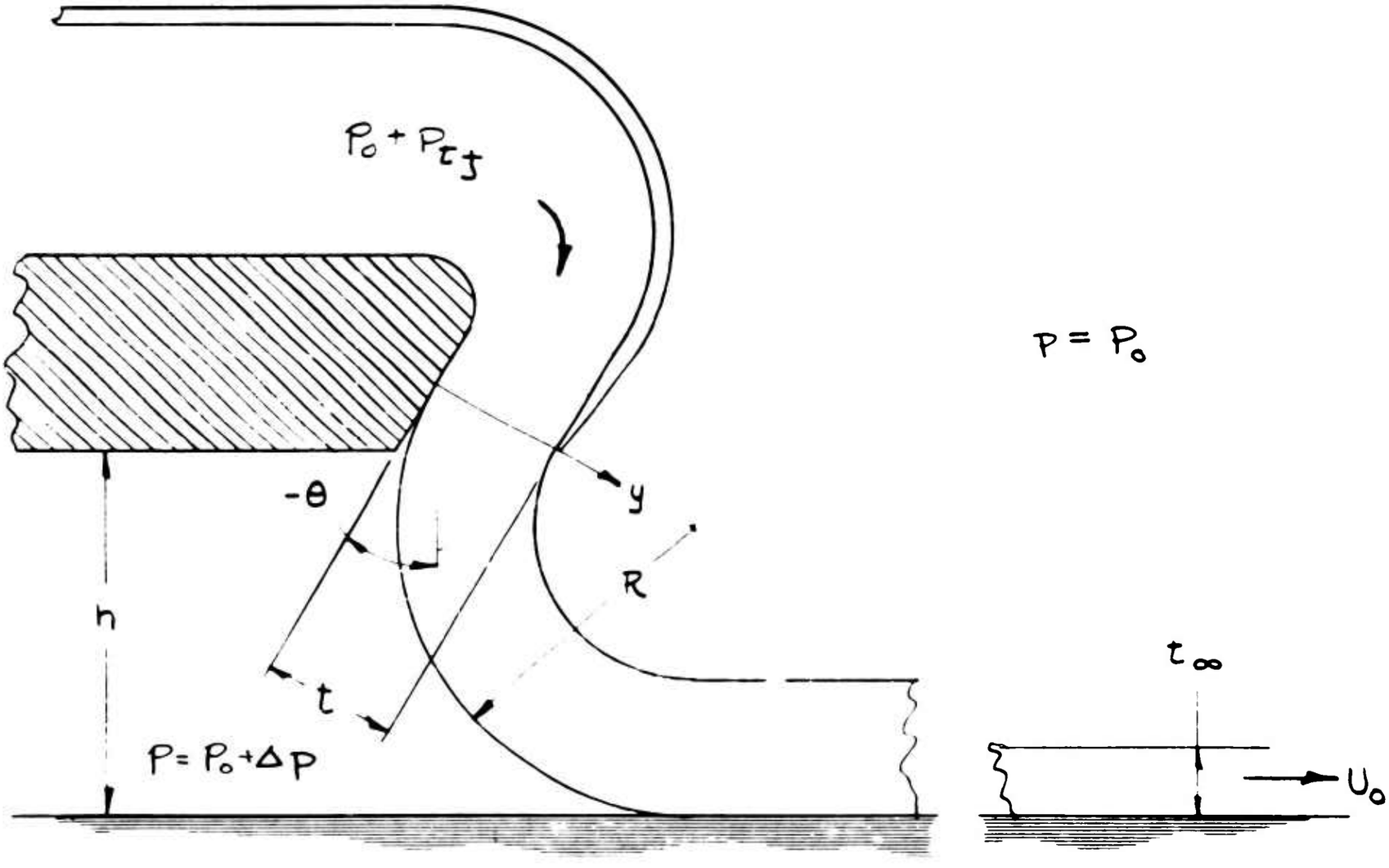

Figure 53: Peripheral Jet in Two-Dimensional Flow

Summary of Momentum Theory Results

The jet exit velocity, assumed to be uniform across the jet, since the jet is assumed infinitely thin, is given by:

$$V_i = \sqrt{\frac{2\,p_{t_i}}{\rho}} \sqrt{\frac{1}{1 + \frac{t}{h}(1 - \sin\theta)\tau_A}} \tag{1}$$

The volume flow is given by:

$$Q = t\,c\,V_i \tag{2}$$

The ratio of base pressure to total pressure in the jet is given by:

$$\frac{\Delta p}{p_{t_i}} = \frac{2\frac{t}{h}(1 - \sin\theta)\,\tau_A}{1 + \frac{t}{h}(1 - \sin\theta)\,\tau_A} \tag{3}$$

Following Reference 65, the GEM internal-flow requirements can be plotted in the form of total head parameter $\tau_A\, p_{t_i} \Big/ W \Big/ S$ against $(\tau_A)^{1/2}\, \frac{Q}{S} \Big/ \left(\frac{W}{S}\right)^{1/2}$

Such a plot is shown in Figure 54 for $\theta = 45^\circ$. The only additional equation required to obtain the plot is that expressing vertical equilibrium:

$$W = \Delta p\,(S - \tfrac{tc}{2}) + J\cos\theta \tag{4}$$

Hovering performance can best be expressed in terms of the figure of merit

$$M = \sqrt{\frac{\frac{t}{h}}{\frac{S}{hc}}} \cdot \frac{\left[\cos\theta + (1 - \sin\theta)\left(\frac{S}{hc} - \frac{t}{2h}\right)\tau_A\right]^{3/2}}{1 + (1 - \sin\theta)\frac{t}{h}\,\tau_A} \tag{5}$$

Results of the momentum theory (assuming $\tau_A = 1$) are plotted in Figure 56 and compared with the experimental data of Reference 13.

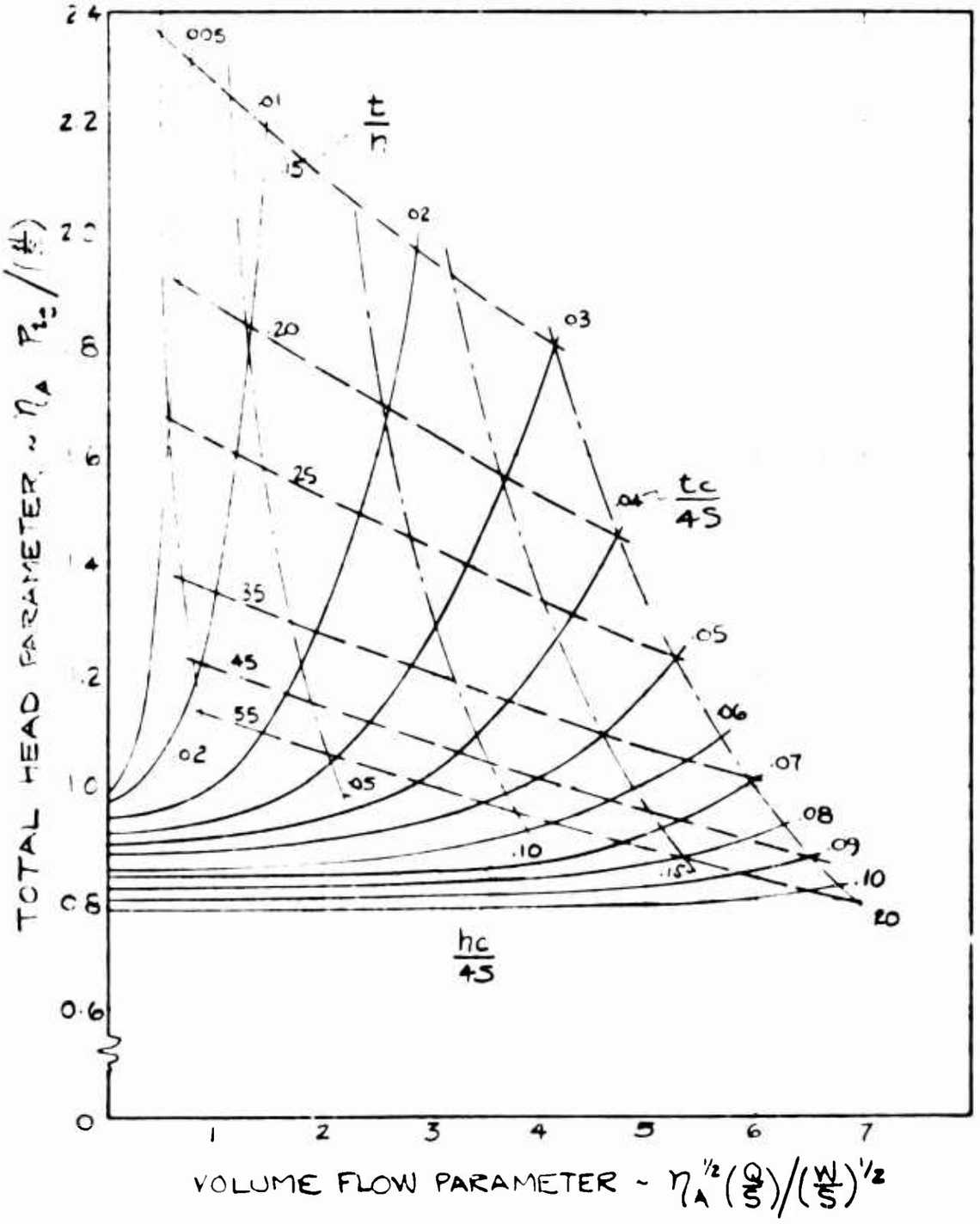

Figure 54: Volume Flow and Jet Exit Total Head, Calculated from Momentum Theory ($\theta = -45^{\circ}$, S.L. Standard Day, Static Condition)

Chaplin's Modified Momentum Theory

In the spring of 1963, Chaplin proposed a partially empirical correction to the momentum theory to bring it into better agreement with experimental data. This was done as part of an academic exercise at Catholic University of America and the resultant data are published for the first time here.

It is first noted, from Figure 56, that the agreement between momentum theory and experiment is good at low values of $x = \frac{t}{h}(1 - \sin\theta)$, but not very good at large values of x. One can attempt to improve the theory by seeking a solution which is valid at large values of x, and then can attempt to modify the theory so that it is relatively unchanged at moderate x but approaches the correct asymptotic limit.

Consider an extreme case:

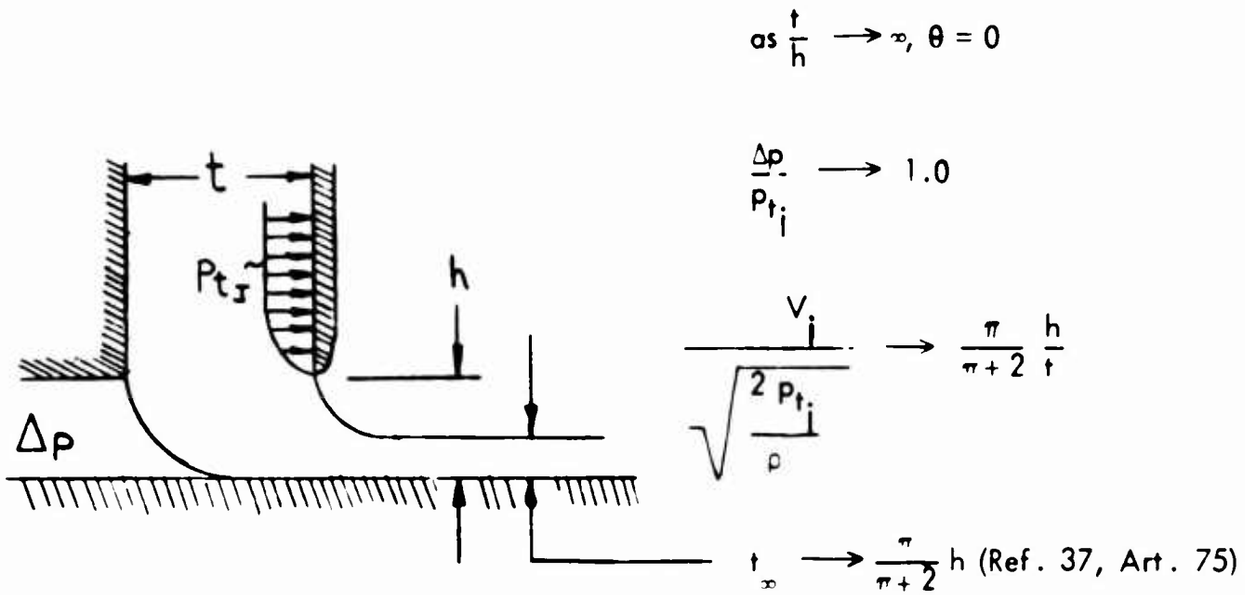

FIGURE 55: NOZZLE FLOW AT VERY LARGE VALUES OF x

A momentum theory formulation (equation 3), namely,

$$h\,\Delta p = 2\,p_{t_i}\,t_\infty$$

would give $t_\infty/h = 1/2$, an incorrect result. It is necessary to put

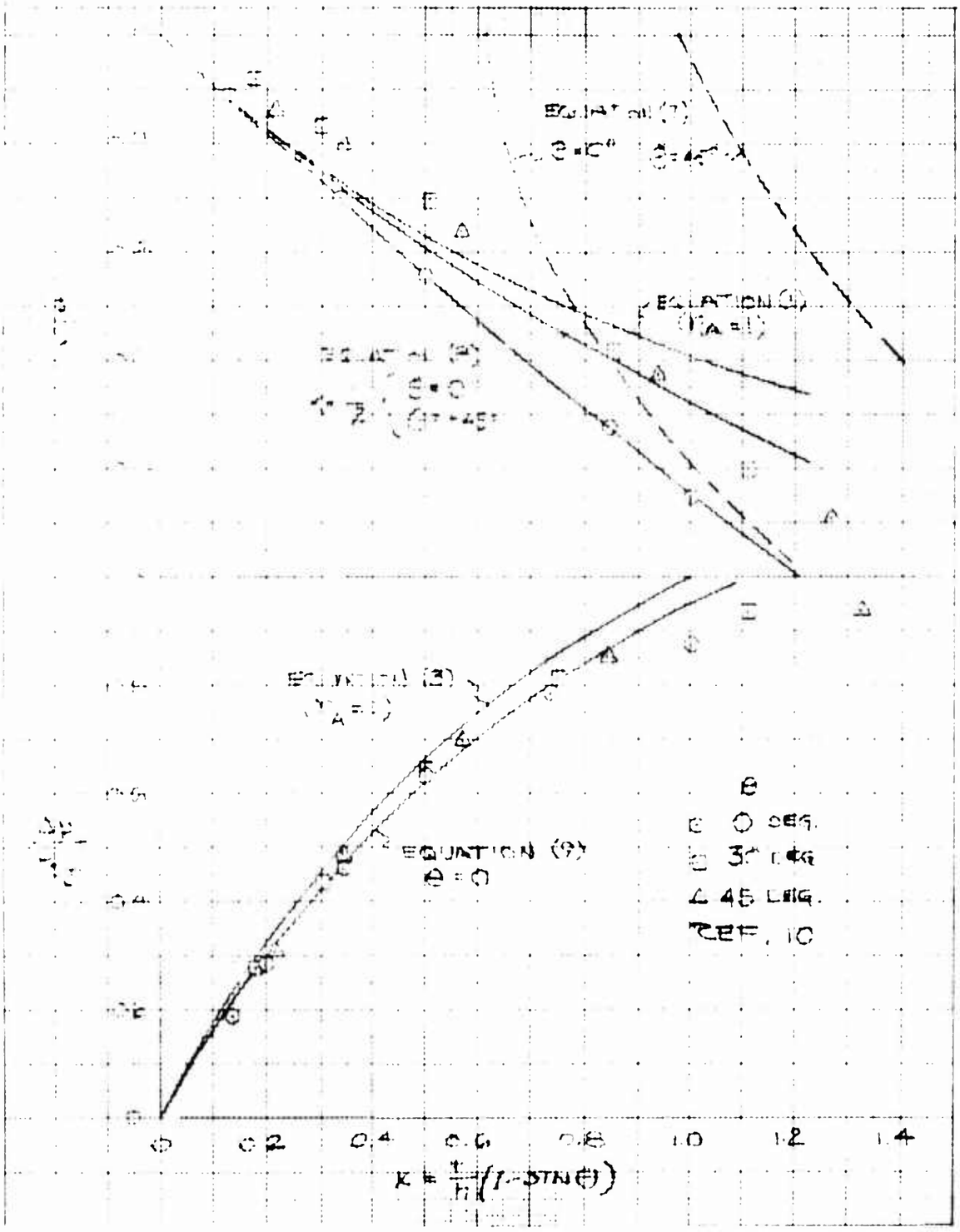

Figure 56: Jet Velocity and Base Pressure Variation Against x: Momentum Theory and Modified Momentum Theory

$$h(1 + a)\,\Delta p = 2\,p_{t_i}\,t$$

to account for the fact that the pressure begins to drop along the outer lip of the nozzle before the exit is reached, so that the pressure acts across the nozzle over an effective height of $(1 + a)h$, where "a", comparing with Lamb's result (Reference 37), is:

$$\frac{1 + a}{2} = \frac{\pi}{\pi + 2}, \quad \text{or} \quad a = \frac{\pi - 2}{\pi + 2}.$$

It is reasonable to assume that, with $\theta < 0$, we can put

$$\Delta p\,(1 + \frac{\pi - 2}{\pi + 2}\cos\theta)h \quad 2\,p_{t_i}\,t, \quad x \to \infty,$$

with small error. In any event, this expression approaches the correct limit as $\theta \to -90^\circ$, namely, $t \to +1/2$ (Reference 37, Art. 74).

For $-90^\circ < \theta < 0$, $x \to \infty$, we then have

$$\frac{V_j}{\sqrt{\frac{2}{\rho}\,p_{t_i}}} \quad \frac{1}{2}\left[1 + \frac{\pi - 2}{\pi + 2}\cos\theta\right] \frac{h}{t} \tag{6}$$

as our asymptotic form. This may be written:

$$\frac{V_j}{\sqrt{\frac{2}{\rho}\,p_{t_i}}} \quad \frac{1 + \frac{\pi - 2}{\pi + 2}\cos\theta}{2x}\,(1 - \sin\theta), \quad x \to \infty \tag{7}$$

Equation (7) is plotted in Figure 56 for $\theta = 0$ and $\theta = -45^\circ$. On an empirical basis, one can try

$$\frac{V_j}{\sqrt{\frac{2}{\rho}\,p_{t_i}}} = \left[1 + \frac{t}{h}(1 - \sin\theta) + (1 - e^{-K\frac{t}{h}(1 - \sin\theta)})\,\frac{4(\frac{t}{h})^2}{\left(1 + \frac{\pi - 2}{\pi + 2}\cos\theta\right)^2}\right]^{-1/2} \tag{8}$$

Equation (8) will give the correct forms at $t/h \ll 1$ and at $t/h \gg 1$, the constant K to be determined by comparison with experiment. On Figure 56, equation (8) is plotted for $\theta = 0^\circ$ and $\theta = 45^\circ$, compared with formula (1).

The equivc'ent formula for $\Delta p/p_{t_j}$ can be found by writing the force equilibrium in the horizontal direction:

$$\Delta p \left(1 + \frac{\pi - 2}{\pi + 2} \cos\theta\right) h = 2\, p_t \frac{V_j}{\sqrt{\frac{2}{\rho} p_{t_j}}}\, t - \sin\theta\, \rho\, V_j^2\, t$$

or

$$\frac{\Delta p}{p_{t_j}} = 2\,\frac{t}{h}\,\frac{\dfrac{V_j}{\sqrt{\frac{2}{\rho} p_{t_j}}} - \left(\dfrac{V_j}{\sqrt{\frac{2}{\rho} p_{t_j}}}\right)^2 \sin\theta}{1 + \dfrac{\pi - 2}{\pi + 2}\cos\theta} \qquad (9)$$

where

$\dfrac{V_j}{\sqrt{\frac{2}{\rho} p_{t_j}}}$ in formula (9) is taken from formula (8).

Formula (9) has the correct property of giving a $\Delta p/p_{t_j}$ which approaches unity asymptotically as $t/h \longrightarrow \infty$.

Formula (9) is plotted for $\theta = 0^\circ$ on Figure 56. The agreement is seen to be very good. However, the agreement would not be so good for $\theta = -45^\circ$.

Exponential Theory

In the exponential theory, the velocity across the jet, assumed to be thick, can vary according to:

$$p + \frac{1}{2}\rho U^2 = p_{t_i} + p_o$$

where p_{t_i} is assumed constant. For a simple solution to be possible, one must assume that the thickness of the jet is constant and equal to the nozzle thickness and that the curvature of the jet is constant and given by the oversimplified formula:

$$R = \frac{h}{1 - \sin\theta}$$

The static pressure inside the jet is found to be, after integration:

$$\frac{p - p_o}{p_{t_i}} = 1 - e^{-2(1-\sin\theta)\frac{y}{h}}$$

if $y = t$, $p - p_o = \Delta p$

Hence:

$$\frac{\Delta p}{p_{t_i}} = 1 - e^{-2(1-\sin\theta)\frac{t}{h}}$$

or

$$\frac{\Delta p}{p_{t_i}} = 1 - e^{-2x} \qquad (10)$$

The velocity of the jet at infinity is defined from:

$$p_{t_i} = \frac{1}{2}\rho U_o^2$$

The jet velocity cannot be calculated as for the momentum theory. One must first calculate the volume flow by integration across the jet width:

$$Q = c\int_o^t U\, dy \qquad (11)$$

The jet velocity is defined as a mean velocity $\overline{V_j}$, obtained, for example, by non-dimensionalizing the volume flow, using the jet velocity at infinity U_o and the nozzle area c t:

$$\frac{\overline{V_j}}{U_o} = \frac{Q}{ct}$$

Substituting the values for U and dy in terms of p and dp and integrating, one finds:

$$Q = \frac{ch}{1 - \sin\theta} \sqrt{\frac{2}{\rho} p_{t_j}} \left[1 - e^{-x}\right] \tag{12}$$

and

$$\frac{\overline{V_j}}{U_o} \quad \frac{Q}{U_o c t} = \frac{1}{x} (1 - e^{-x}) \tag{13}$$

Formulas (10) and (13) are plotted in Figure 57. A comparison with experimental data indicates good overall agreement. However, formula (10) does not show the dependency upon the jet angle, θ, which is observed experimentally.

The figure of merit can be calculated as follows:

First, one easily shows:

$$M = \frac{1}{2tc\sqrt{S}} \cdot \frac{1}{V_j/\sqrt{p_{t_j}}} \left(\frac{\Delta p}{p_{t_j}}\right)^{3/2} \left[tc\cos\theta \frac{V_j^2}{p_{t_j}} \frac{p_{t_j}}{\Delta p} + \left(S - \frac{tc}{2}\right)\right]^{3/2}$$

Then V_j^2/p_j can be obtained from a combination of equations (13) and (12), and $\Delta p/p_{t_j}$ can be obtained from formula (10).

Selected Theory for Internal-Flow Requirements

It is felt that Chaplin's modified momentum theory (equation 8) presently represents best the experimental data, as far as the jet velocity is concerned. For a calculation

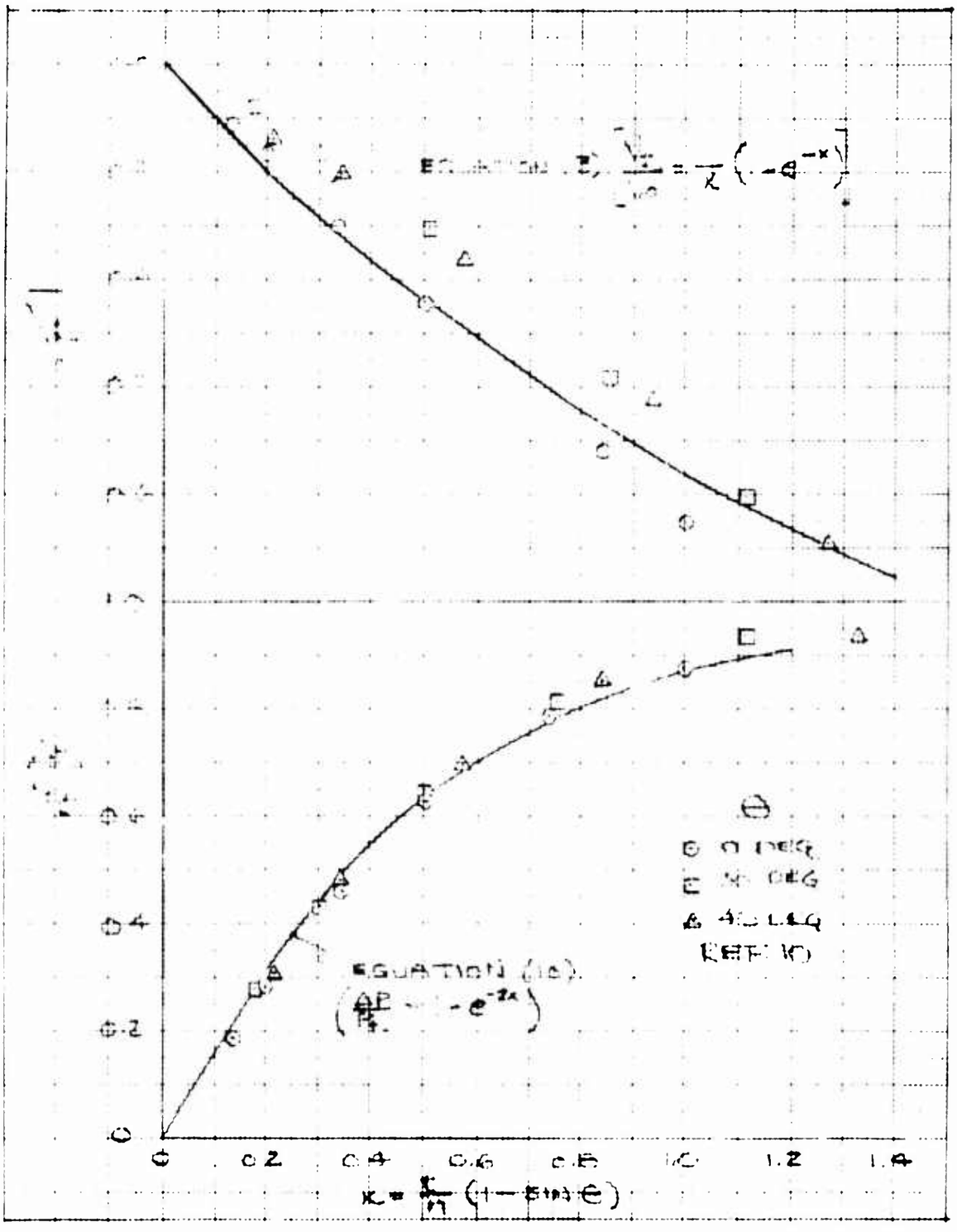

Figure 57: Average Jet Velocity and Base Pressure Variation Against x: Exponential Theory

of base pressures, Chaplin's equation (9) is more complicated and less satisfactory than equation (10) obtained from the exponential theory. The best representation for jet velocity and total pressure is therefore given as follows

$$\begin{cases} \dfrac{V_j}{\sqrt{\frac{2}{\rho} p_{t_j}}} = \left[1 + x + (1 - e^{-0.5x}) \dfrac{4(t/h)^2}{\left(1 + \frac{\pi - 2}{\pi + 2} \cos\theta\right)^2} \right]^{-1/2} \\ \dfrac{\Delta p}{p_{t_j}} = 1 - e^{-2x} \end{cases}$$

The two formulas are plotted on Figure 58.

From these two equations, it is a simple matter to draw a plot similar to that of Figure 54.

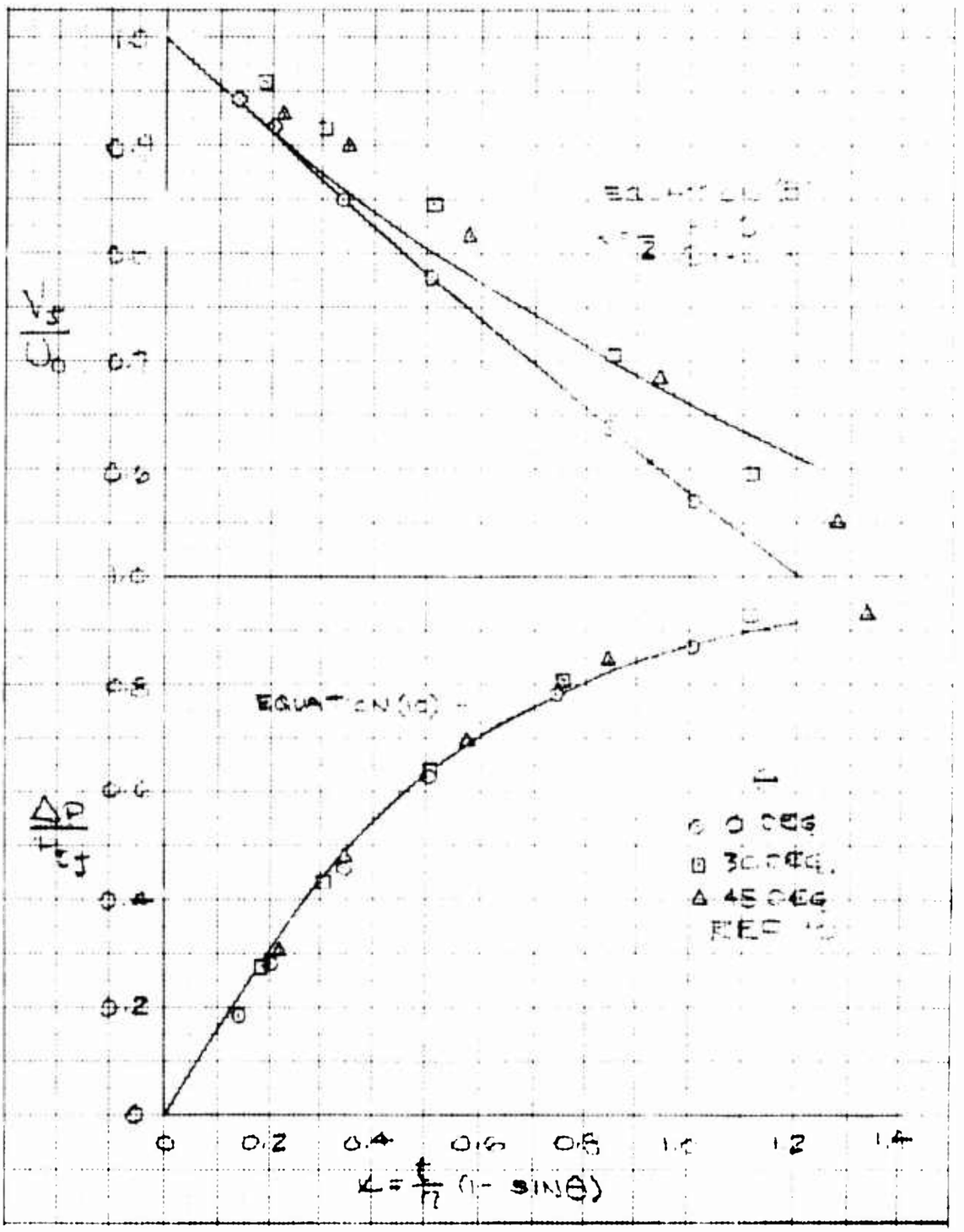

Figure 58: Jet Velocity and Base Pressure Variations Chosen as Input for Internal Flow Requirement Calculations

APPENDIX III. APPLIED LOADS

STATE OF THE ART

DEFINITIONS

In the discussion of structural criteria for GEMs, certain definitions are required. Many are standard in aircraft design; others had to be formulated for this report.

Reference System of Coordinates

The reference system of coordinates is a system of body axes, consisting of three mutually perpendicular axes centered at the center of gravity of the machine, with the positive x (longitudinal) axis directed forward, the positive y (transverse) axis directed to the left, or port side of the vehicle, and the positive z (vertical) axis directed upwards.

Load Factor, n

The load factor, n, is a ratio of a given load to the weight with which the load is associated. If used, a subscript designates the direction of the load.

Translational Acceleration

If the machine experiences only a translational acceleration, a, and if g denotes the acceleration of gravity, one has:

$$n = 1 + \frac{a}{g}$$

In other terms, the combined inertia and gravity forces are considered in the analysis in the same manner as weights which are multiplied by the load factor, n.

From the above, $n = +1$ corresponds to $a = 0$, i.e., unaccelerated flight. Hence, positive vertical accelerations are upward accelerations and correspond to load factors $+n_z$ larger than 1. Negative accelerations are directed downwards and correspond to the load factors $-n_z$ smaller than 1.

Translational load factors are expressed in g's, i.e., in ft/sec^2. A positive longitudinal acceleration causes the vehicle to increase its speed. Therefore, longitudinal load factors, n_x, are positive forward and negative aft.

Rotational Accelerations

Rotational load factors corresponding to rotational accelerations are expressed in rad/sec^2. They are defined as follows:

Rotational load factor in pitch: n_α, positive, up at the bow; negative, down at the bow.

Rotational load factor in roll: n_ϕ, positive, up at the left or port side; negative, down at the right or starboard side.

Rotational load factor in yaw: n_ψ, positive, turn to starboard side; negative, turn to port side.

In most of the loading conditions for military or commercial airplanes, the angular accelerations can be disregarded. They usually are considered in the design of Navy airplanes. Similarly, certain over-water load conditions for GEMs will force a consideration of angular accelerations, which can be disregarded in all other cases.

Limit Load or Limit Load Factor

A limit load, or limit load factor, establishes a strength level for the design of the GEM and its components and is the maximum load factor normally authorized for operations.

Ultimate Loads

Except for loading conditions for which specific ultimate loads are delineated, the ultimate loads are obtained by multiplying the limit loads by the ultimate factor of safety. Failure shall not occur at the design ultimate load. The ultimate factor of safety to be used for the design of the structure shall be 1.50.

Impact

Impact is considered to be the sharp encounter with a deformable medium (water, soft earth, sand, brush, etc.), resulting in an applied load with subsequent yielding of said medium and/or GEM structure.

Crash Loads

These loads (specified as ultimate loads) are applicable to the design of crew seats, passenger seats, litters, etc., and to the attachment of equipment items, cargo, engines, fuel tanks, etc. These loads need not be considered unless they are for those items whose failure would result in injury to personnel or prevent egress from the crashed vehicle.

CLASSIFICATION OF GEM MISSIONS

Classification From 1959-1960 ONR Program

Proposed missions for GEM vehicles were set up by Bell as part of the 1959-1960 ONR program (Reference 43). Mission requirements and mission characteristics are reproduced from Reference 43 as Tables 7 and 8, respectively. This classification into five missions does not, however, provide for a convenient way to define applied loads. Hence, in the next paragraph a classification is proposed which is based upon a consideration of the environment in which the machine must live, rather than upon the specific mission of the machine.

TABLE 7
GEM MISSION REQUIREMENTS*

Mission	Environment	Payload lb	Height ft	Cruise V_o Knots	Range n.mi.	Max Width ft	Operator Type	Stability
1 amphibious support vehicle	surf, beach	10,000	3	60	200	45	unskilled	inherent
2 anti-sub warfare platform	open sea	10,000	4	100	-	45	skilled	automatic
3 utility barge	sheltered waters	40,000	1	60	300	45	unskilled	inherent
4 reconnaissance car	land, rivers flat terrain	1,000	5	100	100	12	skilled	automatic, manual
5 ocean transport	ocean	2,000,000	15	100	4,500	-	-	-

*Bell Aersystems Company, Report No. 2017-945002, p. 9

TABLE 9
SUMMARY OF MILITARY GEM CHARACTERISTICS

Type	Class	Size		Operating Height Required by Surface		% of Year Operation is Feasible	% of Land & Water Surface Vehicle Can be Used	Slope Capability Required	Surface Treatment Required before Operating Vehicle	Relative Vulnerability Similar to			Relative Maintenance Level		Transportability Possible by	
		Length ft.	Width ft.	Normal	Max.					Ship	Truck	Aircraft	Truck	Aircraft	Aircraft	Ship
Marine	I	40	20	1	1.5	Year round	Coastal waters and inland waterways	5-10	GEM beaching ramps		x		x		x	x
	II	60	30	1.5	2.5	Year round		5-10			x		x			x
	III	100	50	2.5	4	61	80% of ocean	5-10			x		x			x
	IV	150	75	4	6	70	80% of ocean	5-10			x		x			x
	V	200	100	6	10	84	80% of ocean	5-10			x		x			x
Amphibious	I	40	20	1.5	2.5	Year round	10% of beaches 10% inland	10	none		x		x		x	x
	II	60	30	2	3	Year round	40% of beaches 25% inland	15	none		x		x			x
	III	80	40	3	5	Year round	70% of beaches 40% inland	15	none		x		x			x
	IV	100	50	3	5	Year round	70% of beaches 55% inland	15	none		x		x			x
	V	150	75	4	6	Year round	50% of beaches 30% inland	15	none		x		x			x
Overland	I	20	10	1	2	Year round	60% grassy plain and	15			x		x		x	x
	II	40	20	2	4	Year round	10% of land mass	20-30	trim trees and bulldoze path		x		x		x	x
	III	60	30	3	6	Year round	34% of land mass	30			x		x			x
	IV	80	40	3	6	Year round	32% of land mass	30	clear path		x		x			x
	V	100	50	3	6	Year round	25% of land mass	30			x		x			x

* Fielding, P. G., I.M.F. Fund Paper No. FF-32, January, 1963, Table 10

Proposed Classification

The proposed classification to be used here follows very closely that proposed in References 26 and 57. It divides GEMs into three categories, based upon the environment:

1. Overland GEM: "GEMBUS"
2. Amphibious GEM: "GEMTRUCK" or "GEM FERRY"
3. Open Ocean GEM: "MARINE GEM" or "HYDROSKIMMER"

Applied loads for GEMs will be discussed in this appendix for each of the above categories. This classification is, naturally, arbitrary, but it has the advantage of indicating distinct load criteria for each category.

The summary of Fielding's characteristics of military GEMs corresponding to the above Reference 26 is given in Table 9. Note that the open ocean GEM defined here would correspond to Fielding's marine category V, or possibly a new category VI that would provide for year-round use over the ocean, instead of Fielding's restriction to 9-month operation.

GENERAL BASIS FOR STRESSING OF GEMS

Since this is a survey, the stress criteria for GEMs published in the literature will all be discussed. Quite obviously, for the early projects, stress criteria were quite inadequate, and part of the information presented is obsolete. It is believed useful to present it here, however, since this information has never been put together before.

The Aeronautical Heritage

As in the case of hydrofoils (Reference 46) aircraft technology has had and continues to have a strong influence on the development of ground effect machines. In particular, aircraft structural techniques are used for the design and construction of GEMs. In England, aircraft practice forms the basis of requirements now being drafted for British Civil Hovercraft (References 34 and 32). As for an aircraft, the primary structure of a GEM must be designed to attain required strength and rigidity at minimum weight.

It has often been suggested that certain GEMs should be designed through the proper marriage of aircraft and ship-building techniques, aircraft techniques

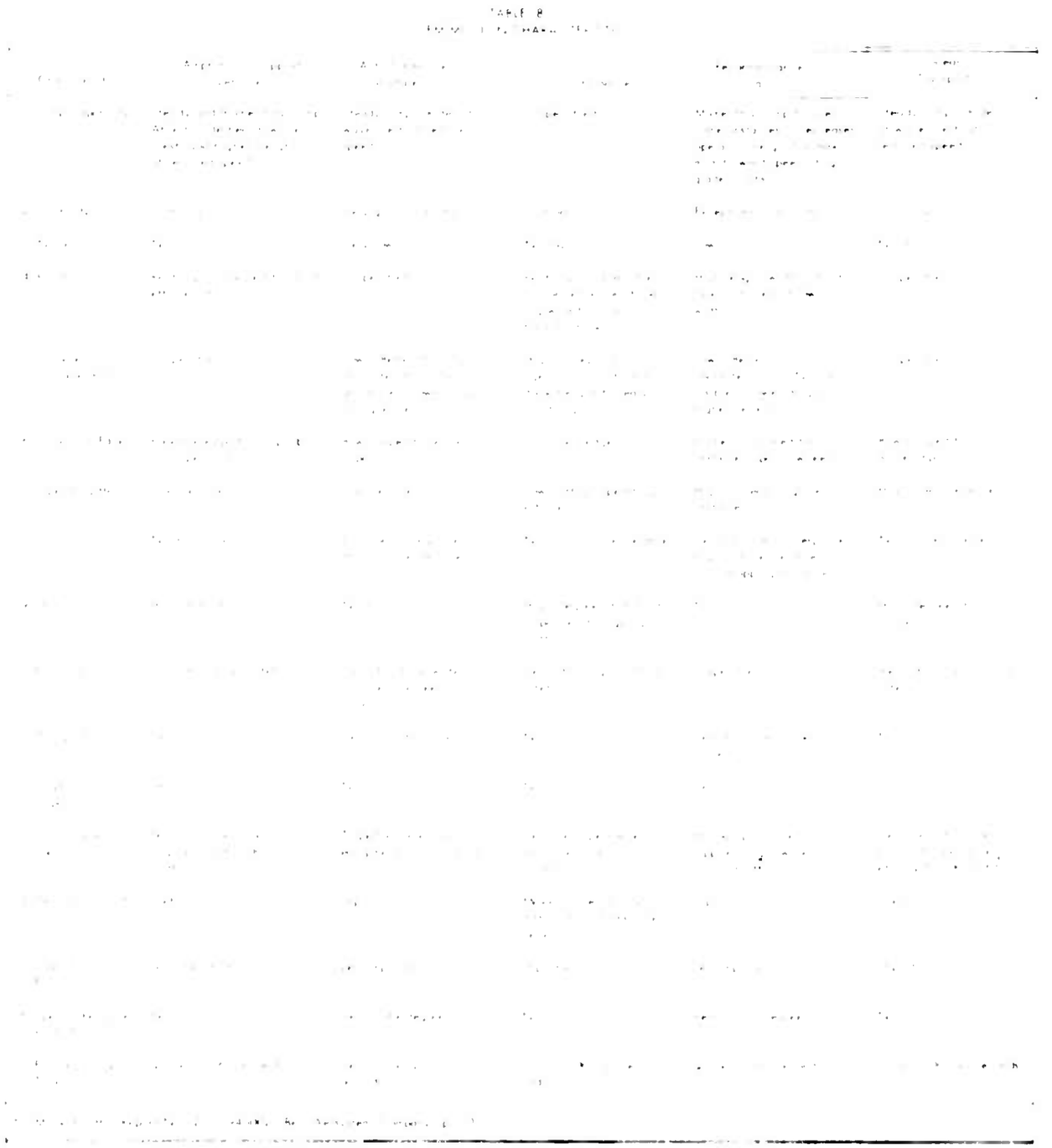

resulting in intolerably expensive construction. At this time, however, loading criteria and stress analysis methods for GEMs resemble more aircraft than nautical practice.

Strength Factors

In conformity with aircraft practice, the cases for strength assessment are based, unless otherwise stated, on limit conditions.

The factors provided on limit conditions are:

Proof factor	1.0
Ultimate factor	1.5

The ultimate factor of 1.5 is used in all cases except crash cases.

Loading Conditions

For overall strength assessment, the craft is considered in a number of representative conditions and placed in equilibrium under applied loads and reactive gravity and inertia loads. For each of these conditions, the load distribution along the machine can be determined; from these determinations the shear and moment curves can be obtained by successive integrations. The structure is then analyzed to withstand the applied loads and then weighed.

Clearly, the normal, substantially unaccelerated, operating conditions provide no basis for strength with factors of the order proposed. It is envisaged that in adverse operating conditions a variety of water impacts with appropriate reactive forces will occur. In the cushion-borne conditions, this system of forces is additive to the steady unit air and gravity loads. These conditions are as follows:

Water and ground impact
Collision and emergency ditching
Beaching, jacking, and slinging
Towing and mooring
Maneuvering and control system loads.

SOURCE OF DATA

The data discussed in this appendix are taken from open literature, which, with one exception (Ljungstrom, Reference 43), is entirely of British or American origin.

All available British information comes from the Hovercraft Club (H.D.L., Westland and Vickers-Armstrong) and can be fairly well summarized in the British Civil Hovercraft Safety Requirements (Reference 32); nothing is available from either Denny or Norman-Britten. The information from the U.S. comes from the following:

Office of Naval Research
Bureau of Naval Weapons
Bureau of Ships
U.S. Army Transportation Research Command
National Aeronautics and Space Administration

These data consist of (1) analytical or computer predictions, (2) design studies, (3) model tests, and (4) full-scale tests of testbeds.

APPLIED LOADS FOR OVERLAND GEMS

Testbeds of the Past

Most ground effect machines built before 1961 can be labeled "overland GEMs." Because of their low ground clearance, they could not be operated over typical cross-country terrain where crash hazards would be prevalent. With the possible exception of the Folland GERM machines, they were all built without any considerations being given to rational structural design criteria. In particular, the air-moving units were designed for stationary duty. There is no recorded history showing that these procedures were not satisfactory nor showing any catastrophic failure of any one of the early GEMs. The reason, naturally, is that these machines were never put through environmental conditions generating high loads. Two of the machines (the P-GEM and the Hula-Hoop test bed) were tested extensively for maneuvering loads (References 47 and 44). Little more than an order of magnitude for maneuvering loads can therefore be obtained from a study of the testing of the early machines. For the sake of completeness, the machines referred to are listed below:

Bertelson Aeromobiles
Curtiss-Wright Aircars
Gyrodyne Co., Model 55
National Research Associates - Marine Corps GEM 1
National Research Associates - Marine Corps GEM 3
Princeton University P-GEM
Folland Aircraft GERM

Design Criteria

Very few papers have been devoted primarily to the overland GEM as opposed to the marine GEM. In one such paper (Reference 20), it is noted that "operation over land in close proximity to the ground introduces problems such as bumping into obstacles and landing on uneven surfaces where the vehicle might not be evenly supported." Also: "structural design is dictated by the nature of the applied loads, allowable deflections and the ever-present requirement for minimum weight. One of the difficulties here is the lack of adequate design criteria for this type of vehicle." In view of this, an attempt is made in the following to propose design criteria suitable for overland GEMs. Some design criteria are specific to overland vehicles; however, as will become abundantly clear later on, others (crash load criteria, for example) are similar for different types of machines.

Normal Operating Loads

It is proposed in Reference 51 to use a "slight positive vertical load factor, assumed to be 1.25 (limit) and a small thrust load factor, 0.13 (limit)" for normal operating loads. These loads are not likely under any circumstances to be critical for design and are also within the maximum allowable load level for passenger comfort.

Impact Loads

Impact load conditions are distinguished from crash load conditions inasmuch as it is assumed that, following an impact, the machine is still operative, while, following a crash, it may be demolished. Impact loads may be classified under two types, cyclic impact and obstacle impact.

Cyclic Impacts: Cyclic impacts occur as repeated low-order load-factor impacts. Such impacts can occur when a moving vehicle strikes small, regularly spaced, local obstacles, such as hummocks, sand dunes, etc., or when it rides wave crests over lakes. (A more familiar form of cyclic loads is recognized in the action of automobile tires striking the expansion joints on a concrete highway.) Cyclic impacts of such nature do not normally constitute a loading hazard for overland GEMs.

Obstacle Impacts: Obstacle impacts would result from occasional severe contact with unavoidable obstacles in the path of a moving vehicle, such

as unforeseen stumps, rocks, etc., hidden by grass or brush. Other situations likely to cause severe impact would be the occasion of a vehicle crossing a gully where the possibility of striking the vehicle nose or stern on the ridges of the gully is likely to occur (somewhat analogous to an auto tire passing over a pot-hole in the surface of a highway). Such conditions are likely to inflict minor damage or deformation to the vehicle structure, but should not disable it. Such conditions were tested experimentally in Reference 47.

The tests of Reference 47 concern the P-GEM which was tested at various forward speeds over individual ditches up to 4 feet wide by 4 feet deep. During the crossing of such a ditch, the machine front and rear ends collided with the ground, resulting in 0.1 g values of rearward acceleration (Figure 20 of Reference 47) for a forward speed of 10 feet per second. No data are available in Reference 47 for speeds greater than 26 feet per second.

In Reference 51, a longitudinal collision load factor of 3.0 g (limit) is proposed.

Crash Loads

In the event of a crash, it is assumed that the vehicle may sustain severe damage or be completely demolished. However, the safety of the crew and passengers must be achieved under any circumstances. Crash data for automobiles and aircraft are discussed in a recent paper (Reference 28), where typical incidents are presented. Vehicle velocity and deceleration histories for typical automotive crashes are reproduced in Figure 59.

Regulations from the Federal Aviation Agency specify the following ultimate accelerations tolerable for the occupants, under crash conditions, for normal and utility aircraft:

Upward	3.0 g
Forward	9.0 g
Sideward	1.5 g

Regulations for military airplanes (Reference 24) specify typical longitudinal load factors for seat installations of 20 g for the flight-deck crew and 10 g for the passengers and troops.

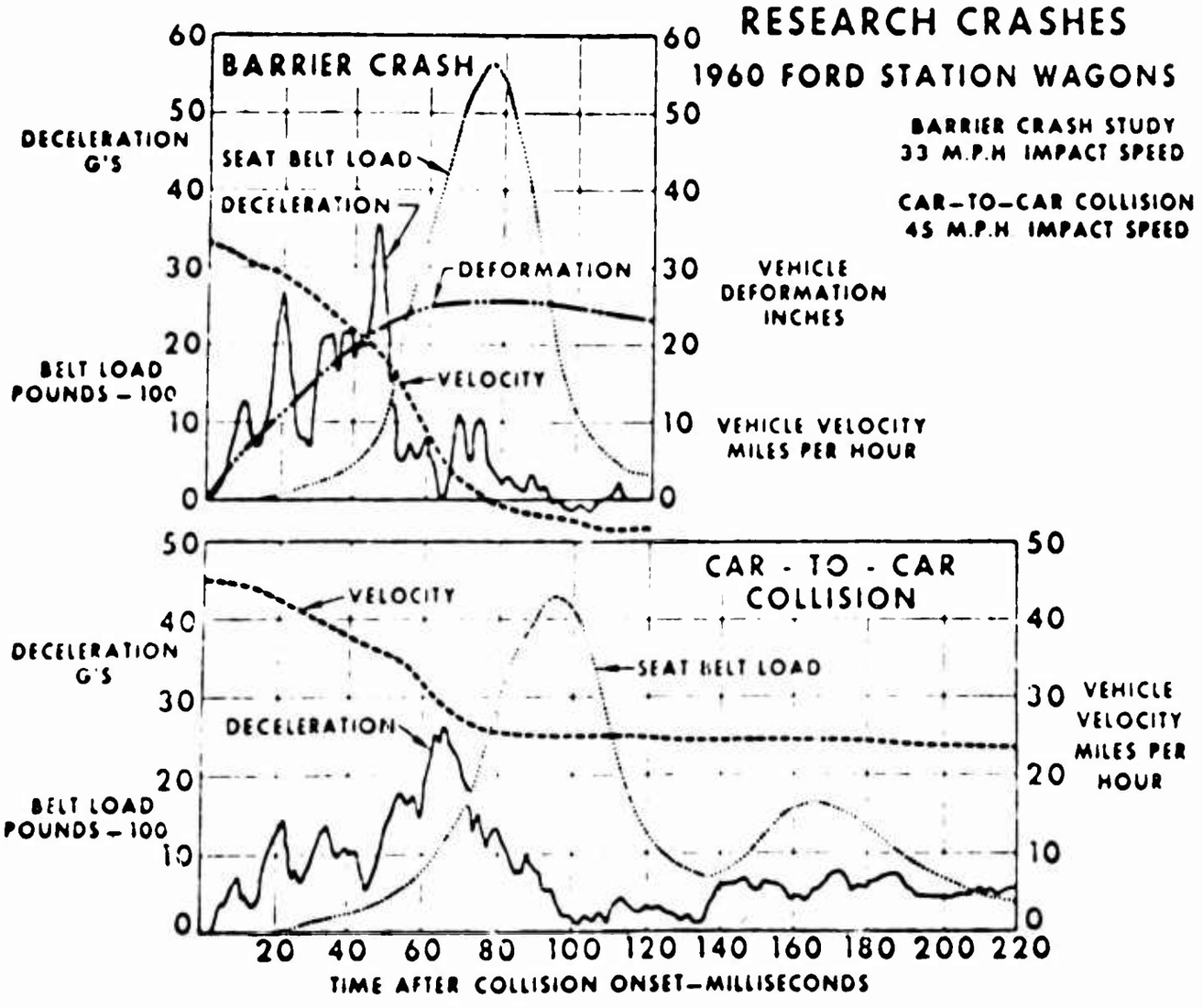

Figure 59: Typical Automobile Crash Loads (Reference 28)

The same regulations of Reference 24 specify that for cargo, engines, etc., the following minimum load factors (ultimate), acting separately, shall apply:

Longitudinal	8.0 g forward, 1.5 g aft
Lateral	1.5 g to right and to left
Vertical	4.5 g down
	2.0 g up

Finally, the British Civil Hovercraft requirements (Reference 32), and the British designs (References 34, 24, and 35) have settled for the following crash criteria (ultimate loads):

4 g downwards to 3 g upwards
6 g forwards to 3 g rearwards
zero to 3 g sideways
maximum resultant 6 g

Landing Loads

Following Reference 51, it is assumed for the determination of landing loads that, because of the low operating heights and because a finite time is required for the ground cushion to deteriorate, a landing load factor of 2 is sufficient for design purposes.

For solid surface landings, the landing legs are assumed extended and are the points of load reaction. The three cases considered are shown pictorially in Figure 60.

Handling Loads

Typical military specifications, such as Reference 3, are applicable. In particular, the vertical component for hoisting will correspond to a load factor of 2, the machine being assumed to be in the level attitude. Towing loads will depend upon the particular machine's configuration.

Maneuvering Loads

To a large extent, maneuvering and gust loads determine the structural design of an airplane. It is unlikely that gust loads will have much significance for GEMs, and therefore their consideration is not warranted. Man-

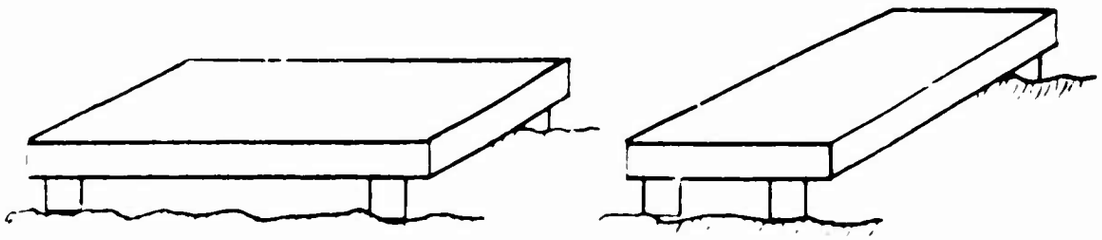

CASE I

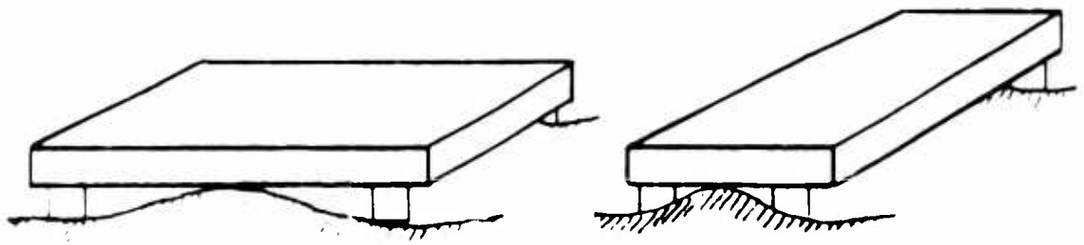

CASE II

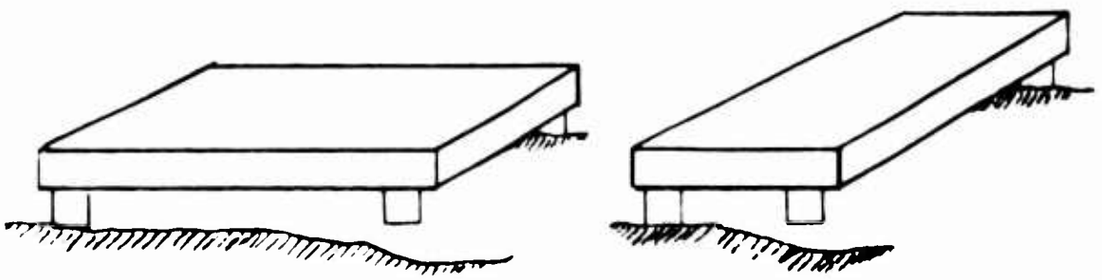

CASE III

Figure 60: Landing Load Cases for Solid Surface Landing (Reference 51)

euvering loads are also likely to be less significant for GEMs than for airplanes, because of the lower forward speeds and because of the difficulty in generating the large moments necessary to obtain a maneuverable GEM. The maneuvering capability of a typical GEM by using successively three general methods of control has been assessed in Reference 44. A comparison with other surface vehicles is made in Reference 44 and is reproduced in Table 10. The maximum overland centripetal acceleration to be encountered by a GEM is taken as 0.15 at high speed.

TABLE 10
MANEUVERING LOADS FOR VARIOUS SURFACE VEHICLES*

Vehicle	Accelerations $\frac{a}{g}$		
	Start	Turn	Stop
Navion	.17 (take off)	.40	.23 (roll out)
HUP-1	.26 - .20	.36	.26
Automobile	.18	.26 (15 mph) .22 (70 mph)	.2 (casual) .5 (emerg.)
Jeep (casual)	.0.	.21	.17
(snappy)	.17	.30	.50

* Nixon, W.B., Report No. 515, Dept. of Aero. Eng., Princeton University, p. 40

Tentative maneuvering criteria, which apply to amphibious as well as to overland GEMs, were proposed for GEMs in Reference 69. In particular, a "standard maneuver" is defined. The standard maneuver, which is equal to the desired maximum lateral acceleration in the hover mode, is equal to "h/a" gravities, where h is the height of the machine above the ground and a is its width. The standard maneuver gives greater agility (for example, 0.25 g) to the small reconnaissance GEM than to the larger cargo carrier (for example, 0.05 g). A proposed target requirement is that the primary jet control system of a GEM shall be capable of giving the machine a lateral acceleration of at least one standard maneuver "h/a" gravities in the

hovering mode, with no forward thrust. In forward flight, a suggested minimum requirement is a total of three standard maneuvers at maximum speed.

All of the above accelerations are much larger than those proposed in Reference 25, Table VI-2 (lateral acceleration of 0.075).

APPLIED LOADS FOR AMPHIBIOUS GEMS

There is a greater availability of applied load criteria for amphibious GEMs than for any other type of GEMs. The reason is that the major interest of the 1959-1960 Office of Naval Research program was centered around such a type of machine (References 51 and 11, for example); the more recent interest of the Transportation Corps has been centered over the LOTS (logistics over the shore) mission (References 24 and 25, for example). Finally, the British presently have several full-scale machines in operation that are truly amphibious (Westland N2, Vickers-Armstrong VA 3).

The main difference between overland and amphibious GEMs, as far as structural design criteria are concerned, is that the amphibious GEM must be designed for a seakeeping environment. It then turns out that the structure of the machine is essentially designed by the loads resulting from wave impact. It is generally felt sufficient to design the vehicle for operation in Sea State 3.

The load factors proposed in the early studies (1959, Convair, for example) are significantly different from those used more recently (1962 for the ONR design study, for example). It is worthwhile to review the major structural design criteria proposed in the past and then to discuss the typical stressing conditions for the amphibious GEMs as was done for the overland GEM. A review of loads and structural criteria for amphibious GEMs similar to the present one was made in Chapter IV of Reference 25.

Review of Proposed Strength Criteria

The logical way to design a GEM is similar to that by which an airplane is designed. Applied loads are postulated. A minimum weight structure is then designed that will withstand these loads. However, for preliminary design studies, one step can be skipped and the structural weight of the machine assumed at the start. When the state of the art is sufficiently advanced, it should be possible, for each type of machine, to correlate applied loads and structural weight. However, a review of the literature, such as those studies described below, indicates that today it is

a very hazardous task. The structural weight of a GEM has been seen to vary from 3 to 30 pounds per square foot of cushion area.

Ryan Study, August 1961 (Reference 51)

The Ryan design loading conditions for the amphibious ONR GEM are reproduced in Table 11. The landing load conditions over land are shown in Figure 60. The landing load conditions over water are shown in Figure 61. These loading conditions are in substantial agreement with those found

TABLE 11
RYAN DESIGN LOADING CONDITIONS*

Component	Design Condition	Limit Load Factor n_x	n_y	n_z
Primary Structure (Basic Framework Including Bow)	Gross Weight, Flight	+2.00	±1.00	± 1.25
	Gross Weight, Landing	0	0	± 2.00
	Gross Weight, Collision	- 3.00	±1.33	0
Engine Pods and Supports	Maximum Loads Acting Simultaneously	+2.00	-	+ 2.00
		- 3.00	±1.33	- 1.25
Secondary Structure (Enclosures, etc.)	Maximum Loads Acting Separately	+2.00	-	+ 2.00
		- 3.00	±1.33	- 1.25
Crew and Personnel Safety Structure	Minor Crash Loads Acting Simultaneously	- 6.00	±1.00	- 2.00
Ducting, Nozzles and Air Pressure Loaded Structure	Maximum Calculated Pressure	1.33 x calculated pressure		
Flotation Hull	Landing Pressure	No factor applied to calculated pressure		
Exposed Deck	Water Pressure	No factor applied to calculated pressure		

* Ryan Aeronautical Company, "A Study of Ground Effect Machine Structures," August 15, 1961

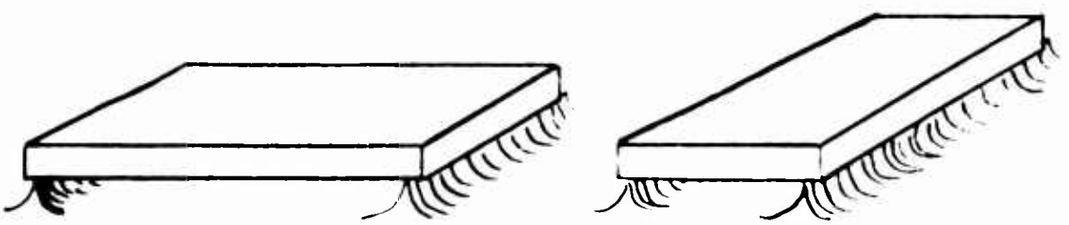

CASE I

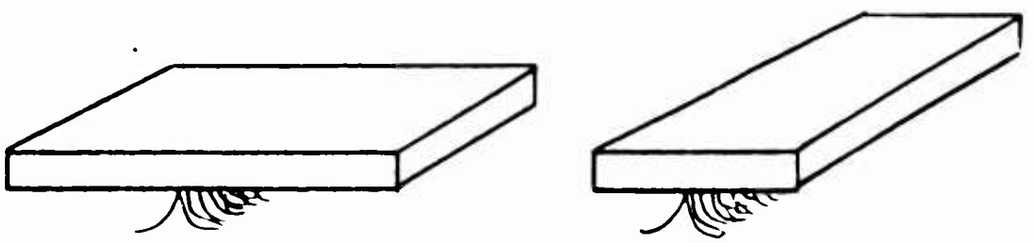

CASE II

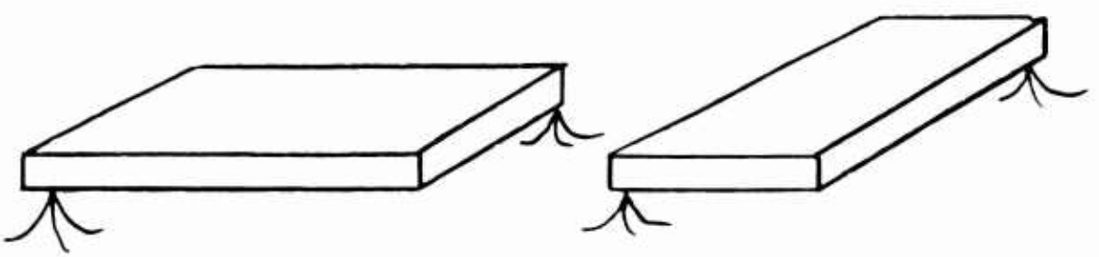

CASE III

Figure 61: Landing Load Cases for Water Landing (Reference 51)

in the earlier Ryan study (Reference 52). Ryan did not find that introducing any condition of water impact with rotation of the craft was necessary. Probably because of this, the structural weight of the machine is relatively low. Reference 49 summarizes a study made by Ryan and presented in Reference 52. The summary indicates that the ratio of structural weight to planform area for an amphibious assault vehicle will be about 3 to 5 pounds per square foot, depending upon the structural material. The design study of Reference 51 shows a structural weight of 5.1 pounds per square foot of planform area.

Convair Studies, 1958-1961 (References 42, 68, and 31)

In an early study of the feasibility of ground effect airborne logistics vehicles (Reference 42), a limit design load factor of 1.5 was selected by Convair. Three design conditions were considered: flight; alighting on land; and alighting on water. However, no wave impact condition was considered. The calculated structural weight of the machine was fairly large, 10 pounds per square foot of planform area, or 30 percent of the gross weight; this was not due to the severity of the loading conditions, but to the large size of the machine (about 450 feet in diameter).

More recent tests were made by Convair on an annular jet configuration in the towing tank of the General Dynamics/Convair Hydrodynamics Laboratory (Reference 68). The purpose of these tests was to determine the dynamic behavior of a GEM during normal operation and in various regular wave conditions. The tests were therefore made using dynamically similar models of several full-scale configurations. The full-scale machines of interest were fairly large ones, with gross weights between 600,000 and 1,120,000 pounds. A secondary purpose of the tests was to provide input data for an analytical study of loads and motions performed on an analog computer (References 31 and 29). Drop tests (power on and power off) were also made.

The results of the tests indicated that GEMs operating over waves are subject to heaving and pitching motions and accelerations. Overall model length was 100 inches, and accelerations were measured with two accelerometers placed 30 inches on each side of the center of gravity. Hence, both forward accelerations and center-of-gravity accelerations could be measured. The peak forward accelerations were of the order of 2 g. The peak center-of-gravity accelerations were approximately 1.70 g. Peak

accelerations occurred at the critical heave frequency and were maximum for the longest wave length tested (wave length over model length equal to 2).

These accelerations are not as large as some accelerations discussed later in this appendix (originating from References 61 and 21). The reason is that they are accelerations experienced by the vehicle while skimming over the wave tops, not impacting them. Under certain conditions, vehicles operating over waves are subject to critical heaving and pitching motions and accelerations. Usually, however, the wave impact conditions generate higher accelerations than the above one.

Results of power failure impact tests indicated load factors of the order of 3 g's at a simulated forward speed of 87.5 knots. These are not very high loads; it is believed that this is due to the way the tests were conducted. The model, initially operating at constant speed in waves, had its fan turned off and was released; after it impacted the first wave, the fan was turned on again. The procedure was used to prevent the possible destruction of the model but probably resulted in an alleviation of the water ditching loads. Anyway, the model was totally destroyed after six test runs.

ONR - Netherlands Ship Model Basin Tests, 1961 (Reference 50)

Ditching tests were run at Wageningen (Reference 50) under ONR sponsorship to determine pressures and accelerations on the flat bottom of a circular and an ogive planform model. These models had no air cushion. The vertical accelerations for the ogive model varied from 5 to 30 g's.

The results of these tests have led to the conclusion that the loading condition corresponding to emergency ditching without cushion is unrealistic and should be eliminated from consideration in the future.

Full-Scale Experiences

As pointed out in Reference 25, very little information has been accumulated in this category because of the small number of craft in operation.

The first published information concerns the Saunders-Roe SRN-1 machine (Reference 59). "The maximum g that we recorded during the trial was 0.6 g, when we inadvertently ran into the wake of the 'America' as she

was steaming down the Solent." Also, Stanton-Jones notes in Reference 60: "On the SRN-1 the peak bow acceleration which has been recorded at speeds of 40 knots is approximately 4 g, but the acceleration rarely exceeds 1.5 g when operating in 12 inch to 18 inch choppy conditions in the Solent with a clearance height of only 4 inches."

Recently, the results of testing of the Vickers VA 3 have been reported (Reference 33): "Most of the overwater operation during the first trials of VA 3 was in the random short crested waves which are found in sheltered waters . . . continuous trace records from six accelerometers have been made on VA 3 during thirty-eight ditchings . . . The records of vertical acceleration at the bow, centre, stern and beam have shown peak acceleration of only short duration (about 1/30th second). Vertical accelerations at the centre were between 0 and 1.3 g in excess of the equilibrium condition . . . The mean values of the upward accelerations of the centre in excess of the equilibrium condition are shown in Figure 9." Figure 9 of Reference 33 is reproduced in this appendix as Figure 68.

Westland Load Criteria for the N 1 and N 2 Machines

The design stress criteria for the N 1 and N 2 machines are discussed in detail in References 59 and 60. The original stress criteria for the N 1 machine are discussed in Reference 59 and are reproduced here. It was assumed that there would be a sudden engine failure when the machine was operating at 40 miles per hour forward speed over waves of critical length that were two feet high from trough to crest. This led to the two main conditions which are shown in Figure 62.

The first is the condition where the machine has been rotated by striking a wave with its stern in such a way that the maximum slamming load comes on to the bow. This leads to about 8 g acceleration on the pilot, which is equivalent to a load approximately equal to 1.25 of the weight of the machine acting right on its bow. Furthermore, it was assumed that this could apply to angles of yaw up to 45°. This stressed the attachment point of the outer rims and the engine mounting.

The other case is the condition where the machine just dives over one wave and plows over the next, so that one gets a maximum longitudinal acceleration of about 1.5 g.

CASE 1.

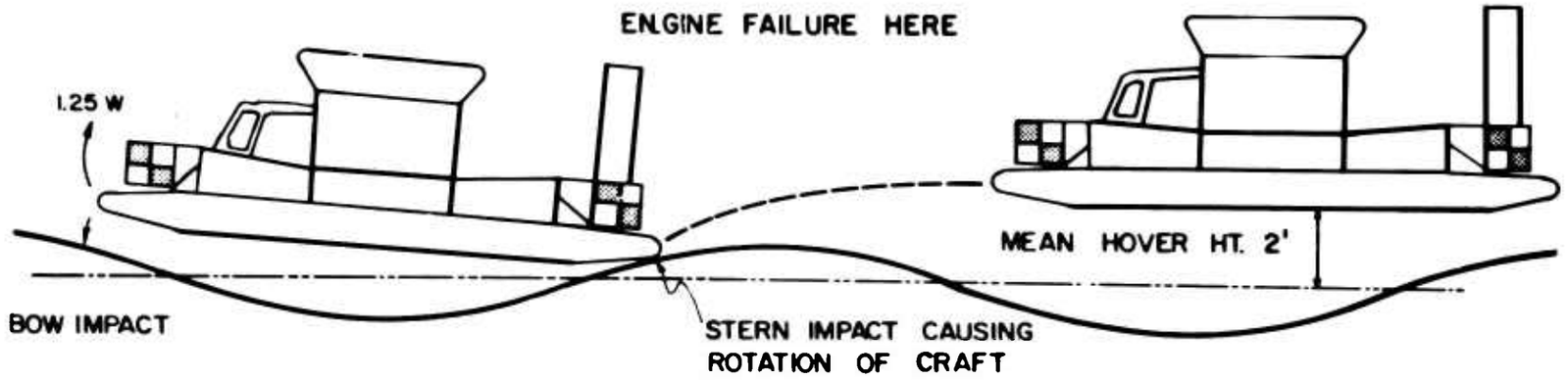

WAVE HT. 2' ~ WAVE LENGTH/CRAFT LENGTH 1:1.5 ~ FWD. SPEED 40 KNTS.

CASE 2.

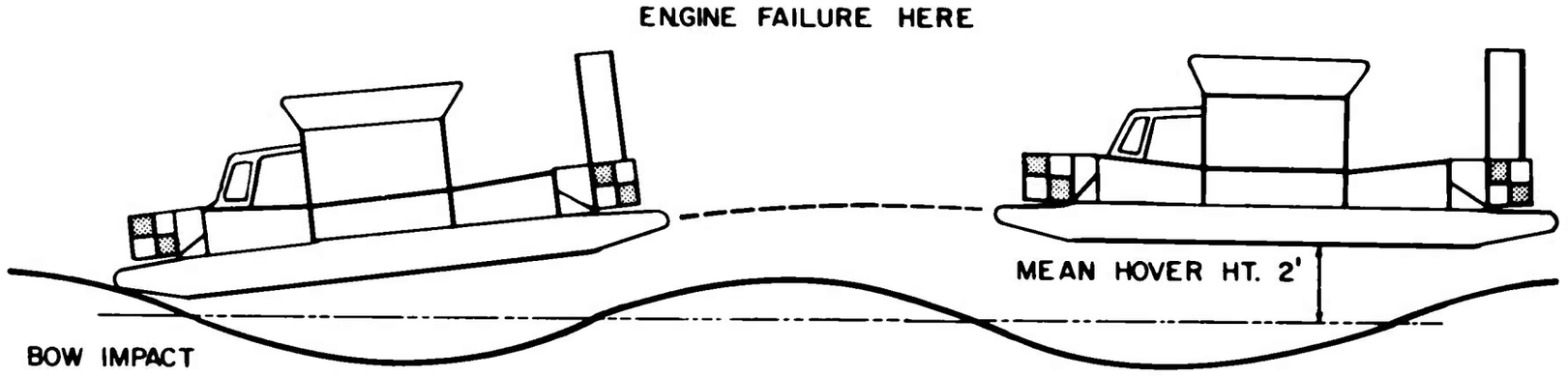

Figure 62: SRN 1 Stressing Conditions (Reference 59)

BLANK PAGE

The engine attachments of the N 1 craft were also stressed to withstand a crash condition, where it was assumed that the craft would hit a log of wood so that the front structure would crumple, the maximum deceleration being about 4 g.

The remarkable conclusion drawn from the test of the N 1 machine was that it was much overstrength for the speeds which it could achieve. It was estimated that the design for a maximum acceleration at the bow of 8 g was more appropriate to speeds of from 70 to 90 knots than to speeds of from 30 to 40 knots. Therefore, the figures of the 8 g (limit) impact at the bow were retained for the design of the N 2. It is noted in Reference 60 that this acceleration is approximately equivalent to a force equal to the gross weight of the craft distributed over the bow area.

It is also noted in Reference 60 that on nearly all forms of passenger vehicles the design stressing condition is approximately equal to the gross weight of the craft applied at its extremities and that the ground effect machine seems to fall into the same pattern.

The results of the design studies, reported in Reference 60, made in connection with machines of the same family as the N 2, indicate an overall structural weight per square foot of planform area of the order of 20 pounds per square foot. This corresponds to a structural weight equal to 30 - 35 percent of the vehicle's gross weight.

Saunders-Roe "Test Computation"

Stanton-Jones describes in detail in Reference 60 how the model testing for the N 1 program was complemented by a dynamic analysis, using an analog computer, of the motion over waves. The main purpose of the model testing was the determination by experiment of certain coefficients needed for the analysis. The match between test results and computation was excellent. This investigation did disclose, as the similar Convair investigation also had (Reference 68), the possibility of substantial accelerations, e.g., as follows:

	With Impact	Without Impact
Acceleration of c.g.	6.0 g	0.3 g
Acceleration of bow	18.0 g	0.4 g

Vickers-Armstrong Stress Criteria (Reference 34)

The stress criteria discussed by Hughes in Reference 34 appear to be very close to those being drafted for British Civil Hovercraft (Reference 32), which are presently unpublished. They therefore warrant an extensive discussion.

The loading cases for an amphibious machine considered by Hughes, which are of special interest, concern water impact. The idealized water impact conditions discussed below are considered to cover all cases of water impact. These conditions will arise from the relative vertical and horizontal velocities between the craft and the water when alighting at high speed or encountering waves in adverse conditions.

The following cases describe conditions of water impact without rotation of the craft (see Figure 63):

CASE I: One-wave water impact vertically below center of gravity (c.g.). A water force of twice the weight of the craft and corresponding inertia reactions are applied to a local circular area vertically below the c.g. These forces are combined with a steady cushion lift balancing the weight of the craft. The total unfactored inertia force on each mass is thus three times its weight. This case gives rise to longitudinal and transverse "hogging" bending.

CASE II: Two-wave impact. Two water forces, together equal to twice the weight of the craft, are applied to local areas, one at the bow curtain and the other at the stern curtain, together with corresponding inertia reactions. This case gives rise to longitudinal "sagging" bending.

CASE III: Two-wave impact inclined to the vertical. Two water forces, together equal to twice the weight of the craft, are applied to local areas, one at the bow and the other at the stern curtains, and inclined to the vertical, up and aft, together with corresponding inertia reactions. These are combined with the steady vertical cushion lift balancing the weight. The inclination of the straight line joining the bow impact position with the c.g. to the vertical through the c.g. is represented by θ degrees.

CASE IV: Two-wave impact at side curtains. Two water forces, together equal to twice the weight of the craft, are applied along the sidewall.

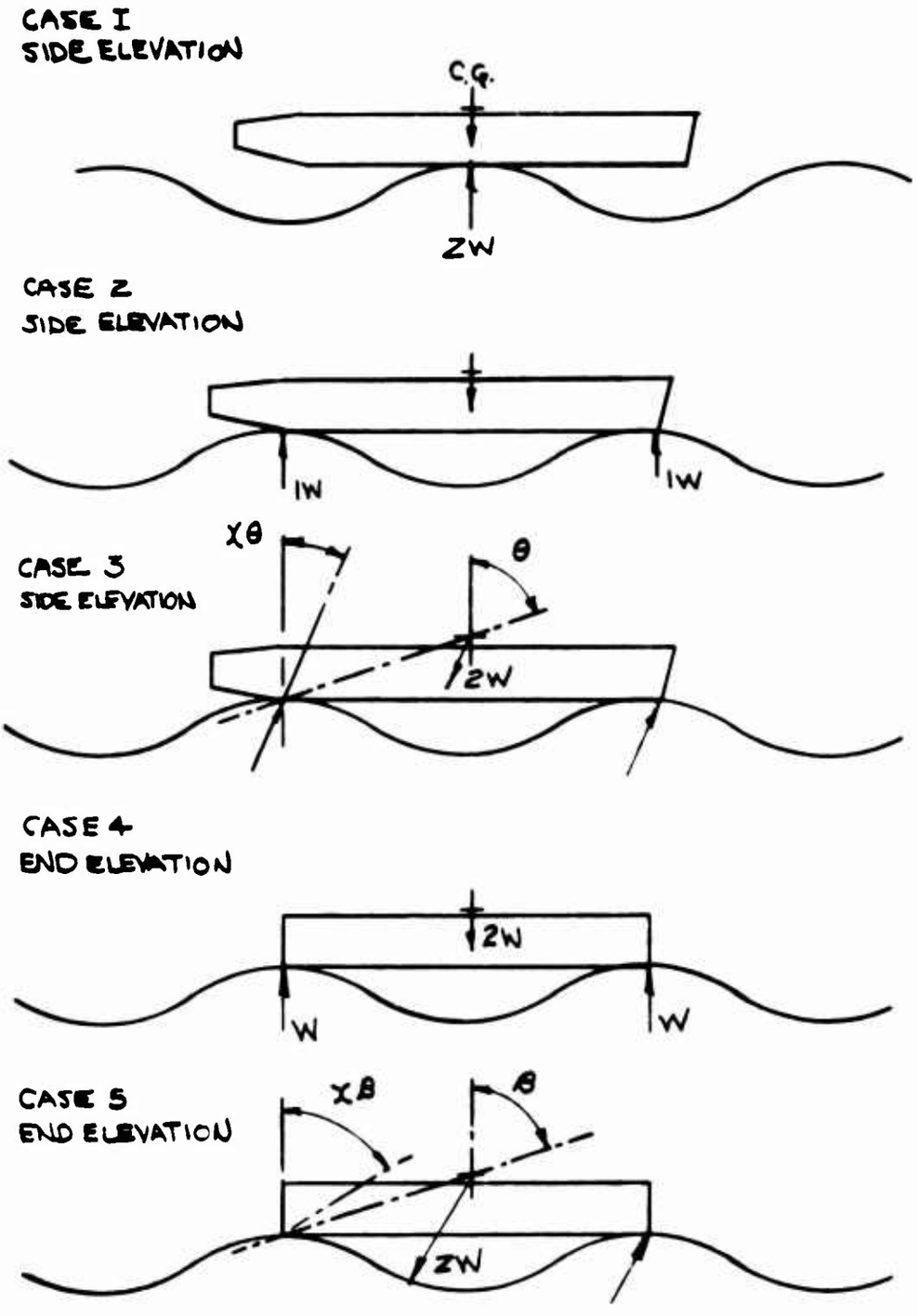

Figure 63: Water Impact Load Without Rotation (Reference 34)

CASE V: Two-wave impact inclined to vertical. Two water forces are inclined to the vertical, up and sideways, together with corresponding inertia reactions. These are combined with the steady cushion lift balancing the weight. This case gives rise to side and vertical loads on the masses.

The inclination of the straight line joining the sidewall impact position with the c.g. relative to the vertical is represented by β degrees.

The following cases describe conditions of water impact with rotation of the craft (see Figure 64):

CASE I: One-wave vertical water impact at forward curtain. A vertical water force is applied to the forward curtain of such magnitude as to give a maximum acceleration of 8 g, immediately above the force. The reactive vertical force on a mass immediately over the applied force is eight times its weight, and elsewhere the vertical reactive force may be obtained. Additional fore-and-aft forces on the masses may arise due to the horizontal component of the component of the rotational inertia.

The above loads are combined with steady cushion lift balancing the weight of the craft.

CASE II: One-wave vertical water impact at rear curtain. Same as for Case I except that the impact force is applied to the rear curtain.

CASE III: One-wave water impact at all positions between the forward and rear curtains. A vertical water force is applied at any position along the fore-and-aft centerline of the craft, between the forward and rear curtains.

CASE IV: Single vertical water impact to one side of c.g. A vertical force is applied along one side curtain of such magnitude as to give a vertical acceleration of 4 g immediately above the force. The impact force and reactions are combined with cushion lift and weight.

The relationship between translational accelerations at the c.g. ($a_{c.g.}$) and at the bow (a_{bow}), for example, is as follows (Reference 25):

$$a_{bow} = a_{c.g.} + r_1 \alpha = \frac{F g}{W} \left(1 + \frac{r_1 r_2}{r_g^2}\right)$$

CASE 1
SIDE ELEVATION

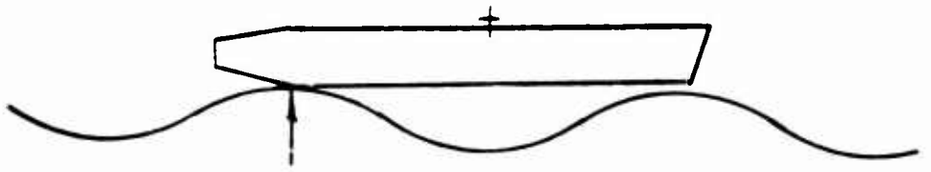

CASE 2
SIDE ELEVATION

CASE 3
END ELEVATION

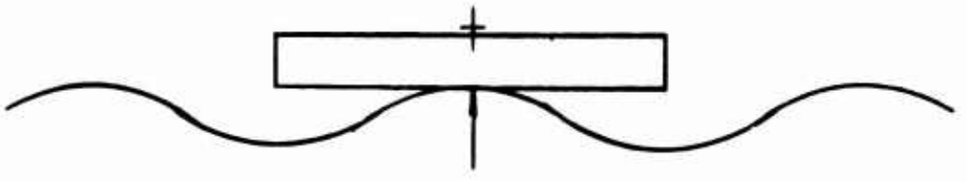

CASE 4
END ELEVATION

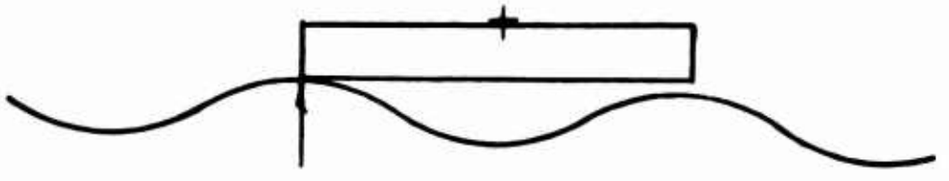

Figure 64: Water Impact Loading Cases with Rotation (Reference 34)

where: r_1 is the distance between c.g. and bow

F is the force generated by bow slamming and producing the acceleration

r_2 is the distance between c.g. and force location

r_g is the radius of gyration of the craft

a is the rotational acceleration, in radians per second square

Saab Aircraft Stress Criteria (Reference 40)

Two types of loads are discussed in Reference 40 toward an application to an over-water, over-ice vehicle: the maneuvering loads and the water impact loads:

Maneuvering Loads: A range of typical maneuvering load factors is proposed. For the typical GEM discussed in Reference 40 (ferry over an archipelago route around Stockholm), the following maneuvering capability is proposed:

Average acceleration	0.10 g
Average braking ability	-0.20 g
Lateral acceleration in turns	±0.10 g

Water Impact Loads: It is proposed to use as criteria for water impact loads those obtained from experience in the design and operation of flying boats. Specifically, the loads specified in the U.S. Civil Aeronautics Manual 4b (Reference 6) for seaplanes are used to compute water impact loads. It is recognized that since, for practical reasons, the bow of a GEM must normally be quite blunt in shape compared to a flying boat, higher bow impact load factors can be expected. The water impact loads for a 30-ton GEM at speeds of up to 100 knots are reproduced from Reference 40 in Table 12.

It is also mentioned in Reference 40 that, when a sudden cushion failure occurs over perfectly smooth water around 80 knots, the hydrodynamic friction drag may cause decelerations above 1 g, if the bottom is flat. On the other hand, for normal operation with passengers, not more than 0.3 - 0.4 g deceleration is acceptable. Provisions should therefore be incorpor-

TABLE 12
WATER IMPACT LOADS FOR A 30-TON GEM
AT SPEEDS UP TO 100 KNOTS*

GEM Speed V, Knots	40	60	80	100
A. Near Vertical Bow Impact				
Limit Load $P_z/W = n_z$ =	1.5	1.5 h = 0.5 m critical	1.7	2.6
Angular Acceleration in Pitch ϵ_y, rad/sec^2	7.4	7.4	8.0	12.5
Maximum Local Water Pressure on Bow Structure, p kg/cm^2	0.7	1.6	2.9	4.5
psi	10	23	41	64
B. Symmetric Water Landing				
Limit Load $P_{z\ c.g.}/W = n_z$ =	2.3	2.3 h = 0.5 m critical	2.5	3.9

* Ljungstrom, O., IAS Paper No. 61-47

ated, either by properly shaping the bottom of the machine or by incorporating extendable water-braking flaps, for example, to achieve soft braking over water.

The crash landing loads suggested in Reference 40 are especially severe because of the nature of the particular operation, i.e., operation in archipelagoes in bad weather and over ice. An ultimate longitudinal crash load factor of at least 15 g is proposed.

BAARINC LOTS Mission Design Criteria (Reference 25)

These mission design criteria are quoted verbatim, since they are self-explanatory.

> "Without bow slamming, the accelerations experienced by a GEM, even in rough water, will not be enough to influence structural design."
>
> "With bow slamming, the accelerations may appear high when measured at the bow but for probable proportions the greater component of the acceleration is rotational and less severe than normal accelerations."
>
> "Cargo handling operations 'in the stream' and exceptional hazards to the vehicle can, according to numerical engineering estimates, easily exceed the load conditions carried over directly from aeronautical practice."

Structural Weight Assumptions for Various Designs and Design Studies

A review of structural weight assumptions for typical amphibious GEMs is made in Reference 25. The three figures summarizing the results of the review are reproduced as Figures 65 to 67. In Figure 65 are shown plots of the gross weight required for structure; structure, in this case, includes all primary and secondary structures, as well as the ducting where ducting constitutes an integral part of the total structure.

In Figure 66 is shown a plot of structural weight per square foot of cushion area against gross weight of the machine.

Finally, in Figure 67 is shown a plot of the structural weight against the total surface area of the enclosed structure.

An attempt at predicting the structural weight of a GEM as a percentage of total gross weight for an amphibious machine is made in Reference 43. Figure 13 of Reference 43 is reproduced as Figure 68.

In Reference 11, a design study is made of the ONR Marine Corps amphibian GEM of the 1961 ONR competition. A structural analysis is made,

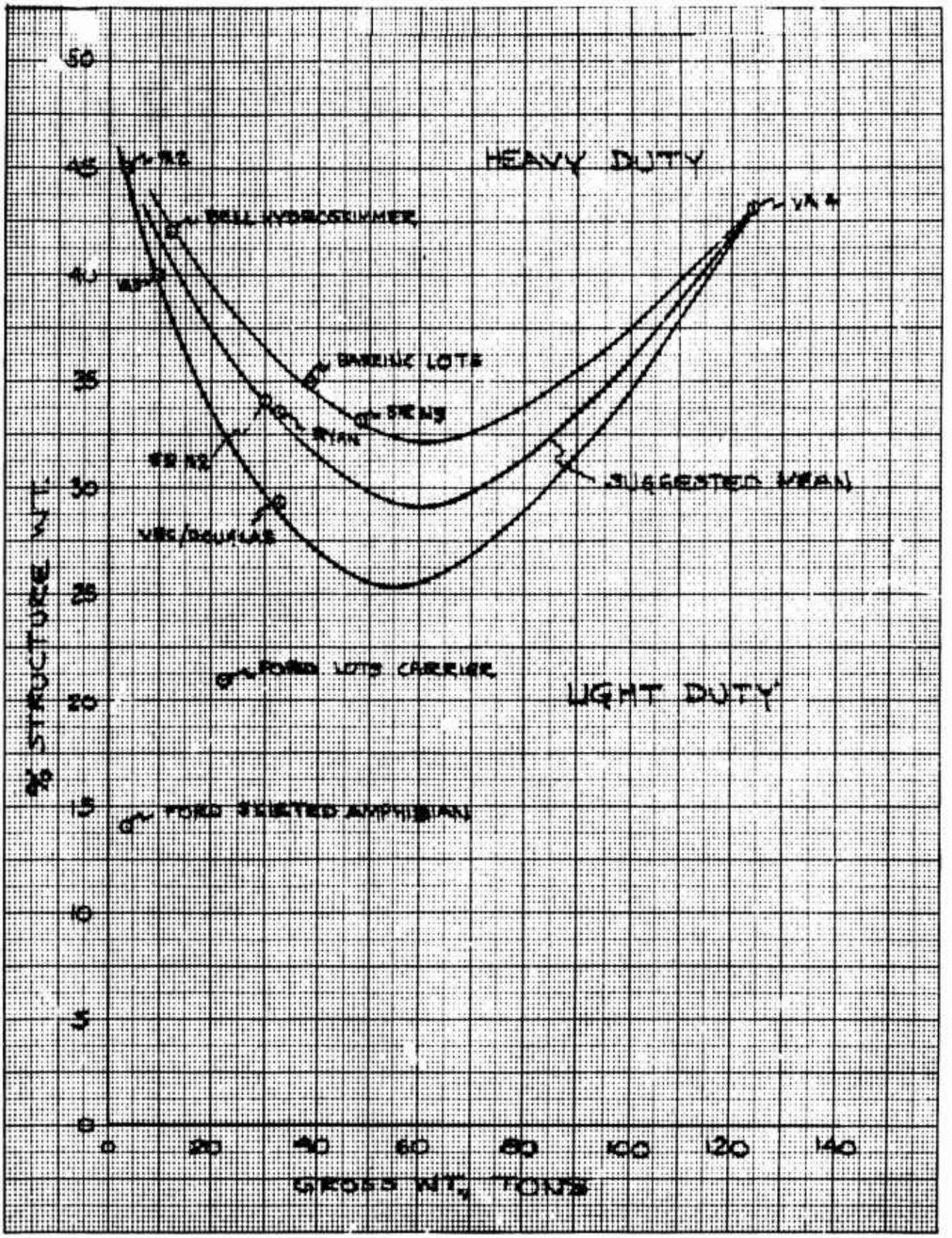

Figure 65: Percent of Structure Weight vs. Total Weight (Reference 24)

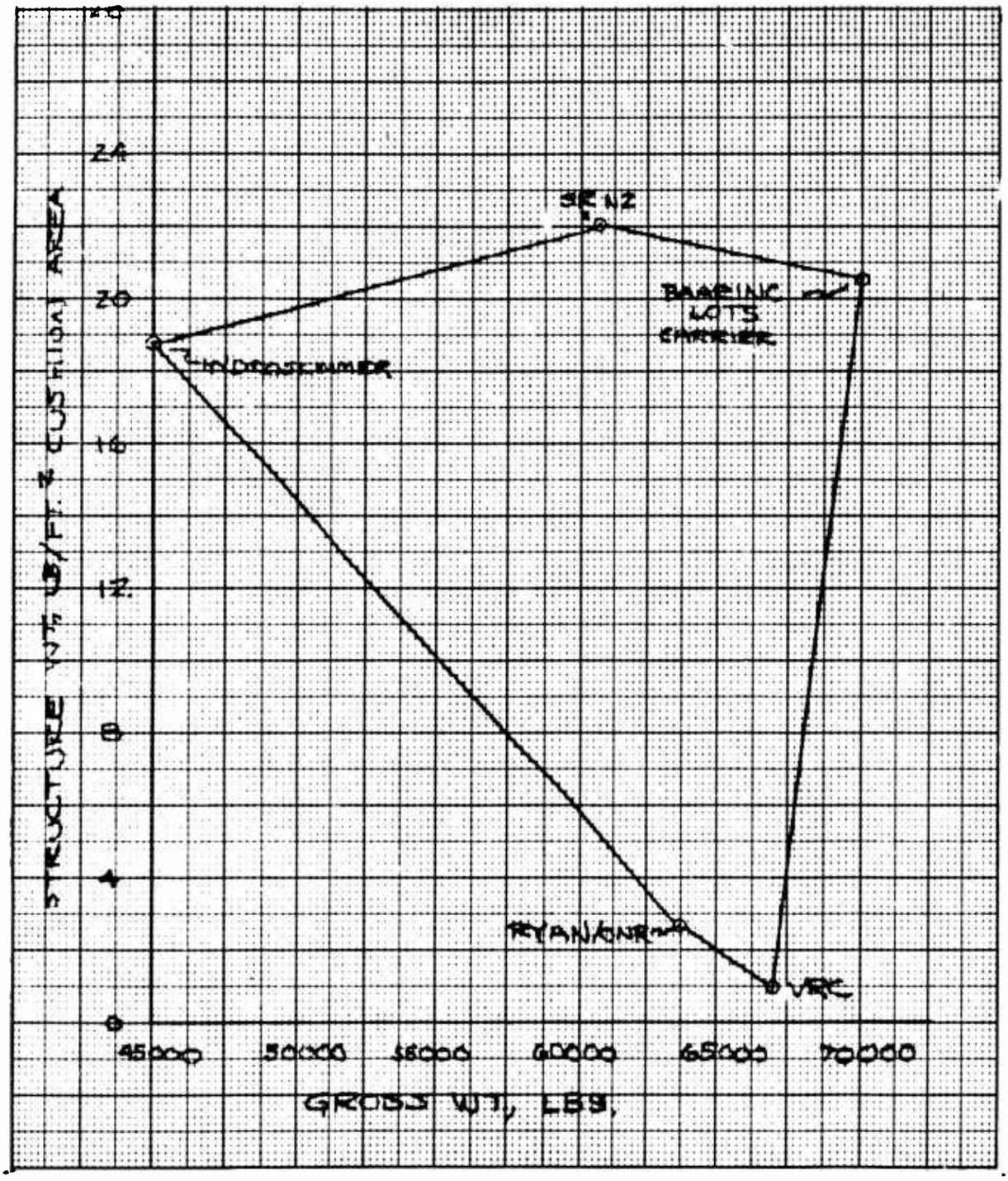

Figure 66: Structure Weight Variation for Similar GEMs (Reference 24)

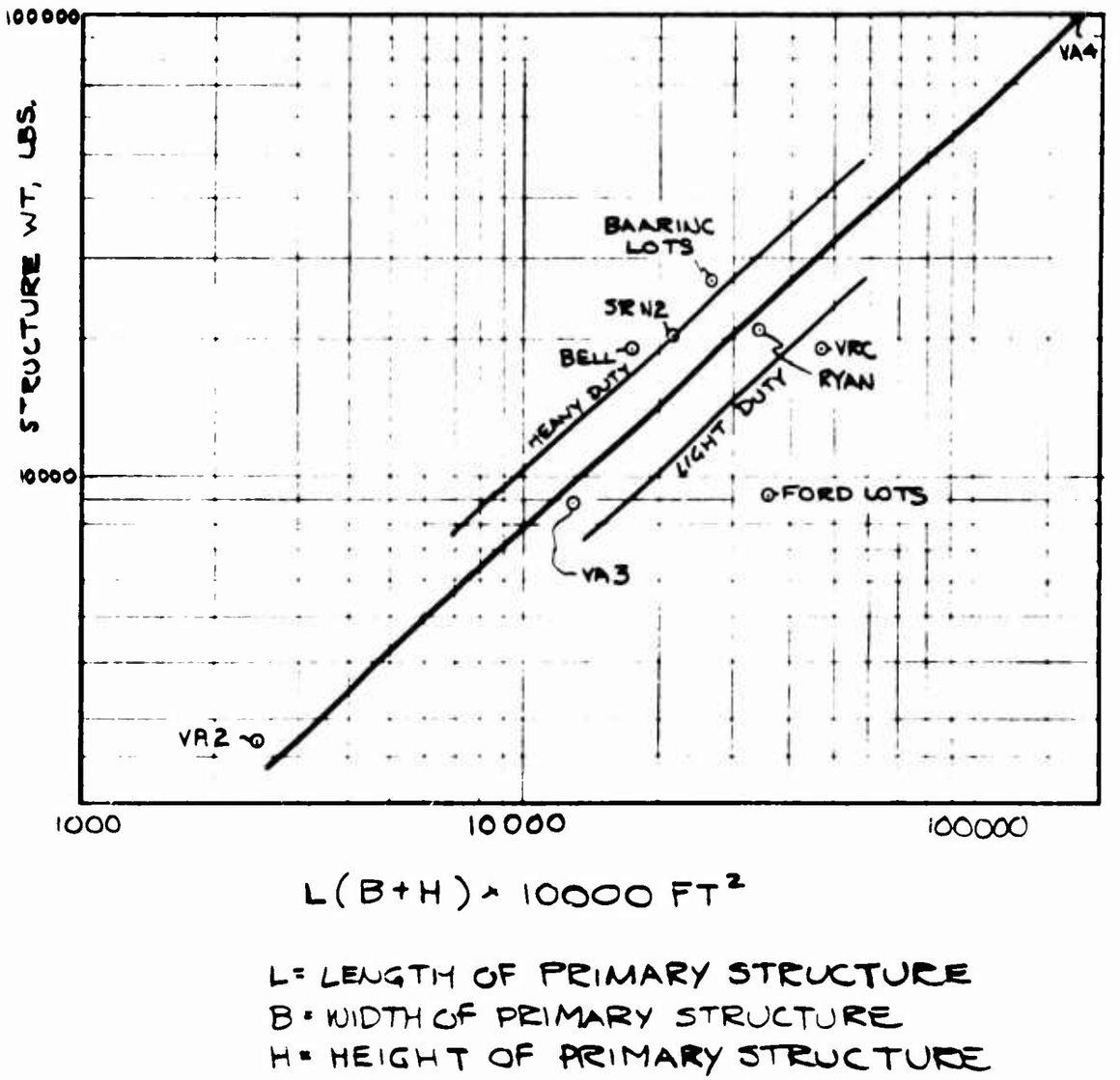

Figure 67: Structural Weight vs. Total Wetted Area of Primary Structure (Reference 24)

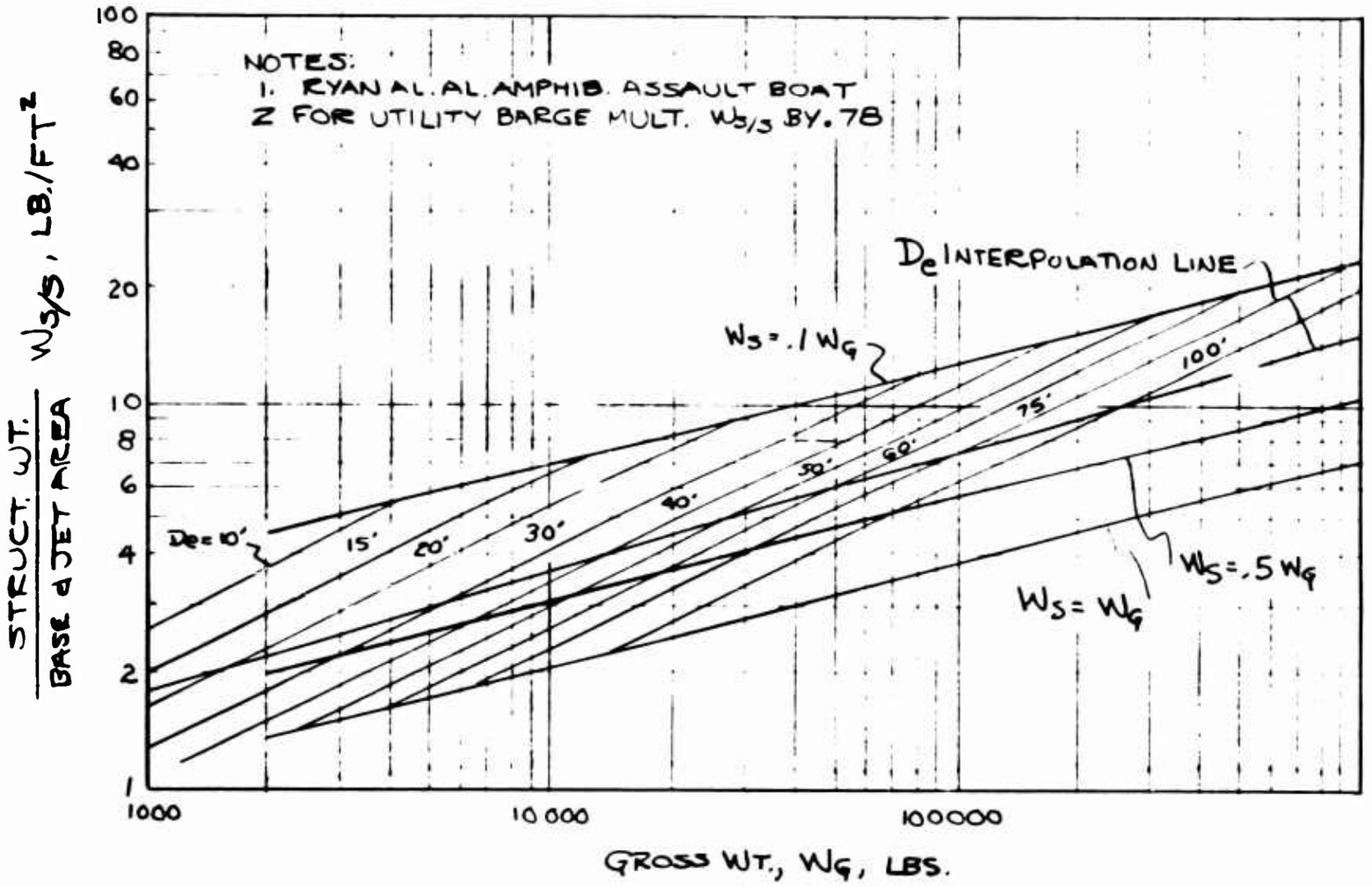

Figure 68: Structural Weight Variation with Gross Weight and Size (Reference 43)

from which a weight analysis is evolved. It is found that the structural weight is 16 percent of the gross weight, or equal to 11 pounds per square foot of cushion area.

Reference 15 discusses a design study of a 29-foot GEM to be used as a lightly-loaded crash boat, communications launch, personnel launch, and light-cargo launch. The structural weight is assumed to be 14 pounds per square foot of reference area, which corresponds to a structural weight equal to 43 percent of the total weight.

Reference 14 discusses the design of a high-speed passenger ferry to be used in the Chesapeake Bay. The assumed structural weight is 12 pounds per square foot of cushion area, corresponding to a structural weight of 29 percent of the design gross weight.

Reference 56 discusses the design of a passenger ferry boat to be used on the Miami-Nassau run. The hull weight is assumed to be 14 pounds per square foot of planform area and is increased by 2 pounds per square foot for each additional 25 feet of length. The authors feel this assumption to be optimistic rather than pessimistic.

The result of a series of preliminary studies is reported in Reference 26. The purpose of these studies was to compare several types of GEM vehicles in terms of their general utility and applicability to commercial operations. For all vehicles, a structural weight of 20 pounds per square foot of cushion area is assumed. The corresponding cushion pressure is assumed to be 70 pounds per square foot.

Design Criteria

The discussions on pages 142 and 145 concerning normal operating loads and landing, handling, and maneuvering loads for overland vehicles also applies to amphibious vehicles. Normal loads are always minor compared to impact loads and are strictly limited by the demands of passenger comfort.

Impact Loads

Cyclic Impacts: Cyclic impacts are of special significance for amphibious GEMs, which may operate frequently in regular or irregular wave conditions. The dynamic behavior of a GEM under regular wave conditions has been

extensively investigated by Convair (see page 151) and Saunders-Roe (see page 155). As noted in the discussion on overland GEMs, the accelerations due to the waves, without impact, are minor (0.3 g at the c.g., 0.4 at the bow). The accelerations due to impact can be very severe. Specifically, the reader is referred to Figures 26 to 29 of Reference 60 which are not reproduced in this report. Accelerations in excess of 16 g at the bow can be predicted if the vehicle is allowed to operate at speeds over waves corresponding to certain frequencies of encounter where resonance with the pitch or heave natural frequency can occur. It would be unrealistic to try and design any GEM for resonance conditions, i.e., for regular sinusoidal waves. Fortunately, most sea conditions are random and not regular. However, no general conclusions can be obtained at this time, based on theoretical considerations of the dynamic behavior of a GEM in a seaway. Further, the situation may vary from machine to machine, depending upon the damping of the machine, its bow design and the distance between the solid structure and the waves.

Stress criteria for water impact can then be obtained realistically by using the idealizations discussed by Vickers-Armstrong, which are summarized on pages 156 and 158.

Recorded accelerations during wave impacts obtained during tests of the VA 3 machine are reported in Reference 33 (Figure 9) and plotted in Figure 69.

Obstacle Impacts: There are three types of obstacle impacts: either over-water minor impacts from unforeseen or unavoidable contact with flotsam and jetsam small objects, logs, etc., or impacts due to the loading operations, or surf impacts. Very substantial loads can be created because of the first two types of obstacle impact. These can be estimated, as in Reference 25 on the basis of rigid-body dynamics. For example, an impacting velocity of 10 feet per second applied over one-tenth of a second would correspond to an acceleration of 10 g's. Such figures are completely unrealistic for design purposes, since such impacts can easily be cushioned by fenders and bumpers. Therefore, obstacle impact acceleration criteria are not significant, except for surf impacts. For surf impacts, it is proposed in Reference 25 to use a deceleration of 2 g's.

The discussion of crash loads for overland vehicles (see page 143) also applies for amphibious vehicles.

The discussion on landing loads for overland vehicles on page 145 applies in the present case.

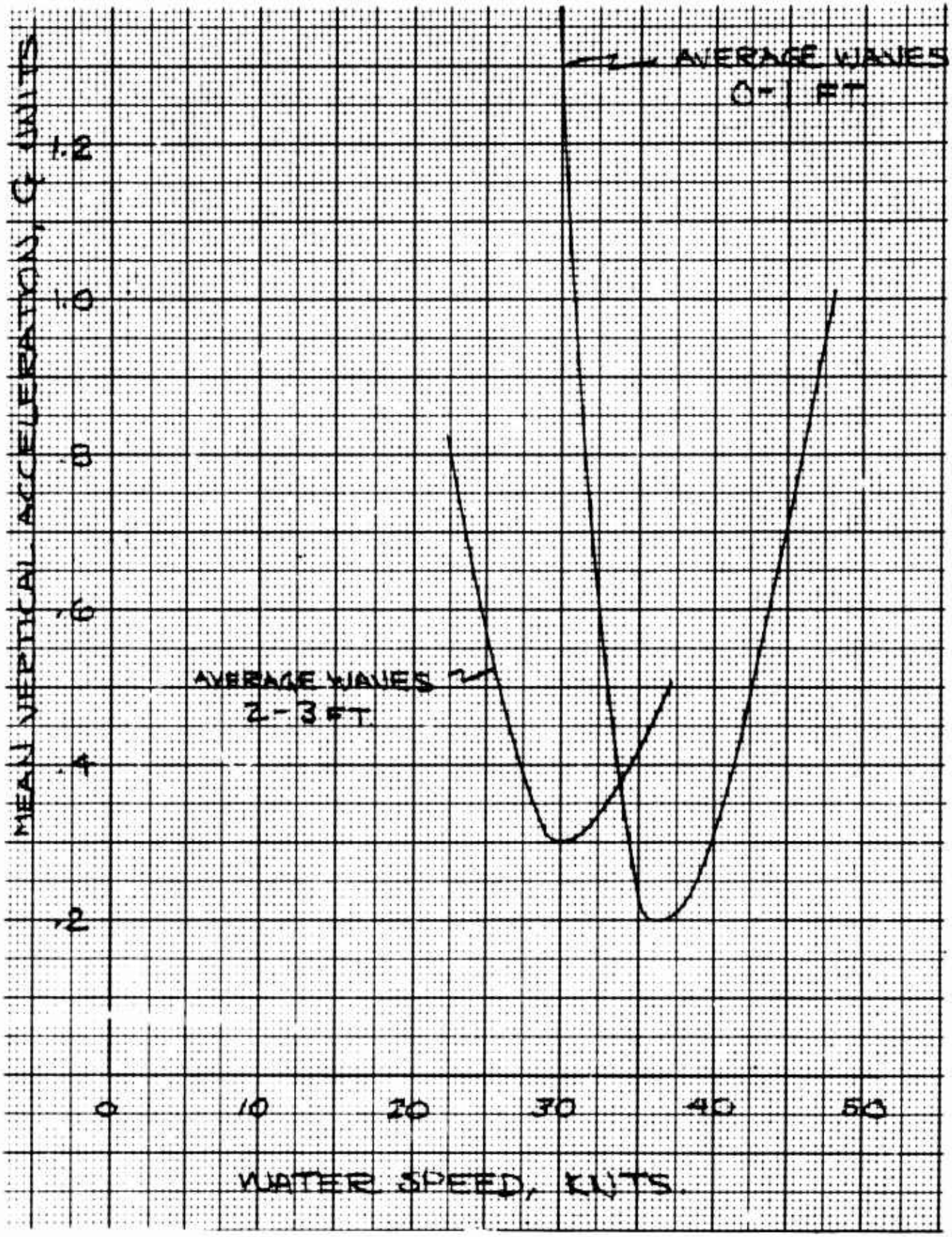

Figure 69: Mean Vertical Acceleration of VA 3 Craft Center Due to Random Waves vs. Water Speed (Reference 33)

The discussion on handling loads for overland vehicles on page 145 applies in the present case.

The discussion on maneuvering loads for overland vehicles on page 145 also applies in the present case.

APPLIED LOADS FOR OPEN OCEAN GEMS

The development of a GEM for open water operation all through the year is the goal of the Bureau of Ships Hydroskimmer program. It is obvious that the wave conditions encountered over the open ocean dictate a craft of larger size than those described earlier, to keep the structural loads to a reasonable value. Irrespective of size, it can be anticipated that applied load criteria will be more severe for this type of craft than for either of the two discussed previously. This is due to the proximity of the sea surface.

In Reference 67, quoted in Reference 46, Tulin made a comparison of the near-surface sea and the atmosphere with respect to turbulence in the two media. He concluded that the sea is a much more "hostile" environment in which to fly. Figure 70 taken from Reference 67, illustrates the situation by comparing the acceleration loadings of two transport airplanes with typical hydrofoils under comparable average conditions of air turbulence and sea state. As pointed out in Reference 46, in this case the loadings are not quite realistic because no craft or control-surface response is postulated. The wings are assumed to be fixed in attitude and are constrained to a flat trajectory. The loadings do, however, give a feel for the relative forces at work and support Tulin's assertion concerning the hostility of the sea.

Structural load criteria for the U.S. Navy Bureau of Ships Hydroskimmer test bed are discussed in Reference 61. The Tulin philosophy that the open sea is a hostile environment is accepted. Based on the model tests of References 68 and 21 and allowing a generous margin for conservatism, a set of water forces to be used as design criteria for the machine is proposed. These loads are reproduced as Figure 71. The relationship between translational and rotational accelerations was shown on page 158 of this report.

It will be noted that the structural loading of this section is significantly more severe than that of the two previous sections. Therefore, the loads of this section cannot be used in lieu of those discussed earlier without severe penalties being accrued.

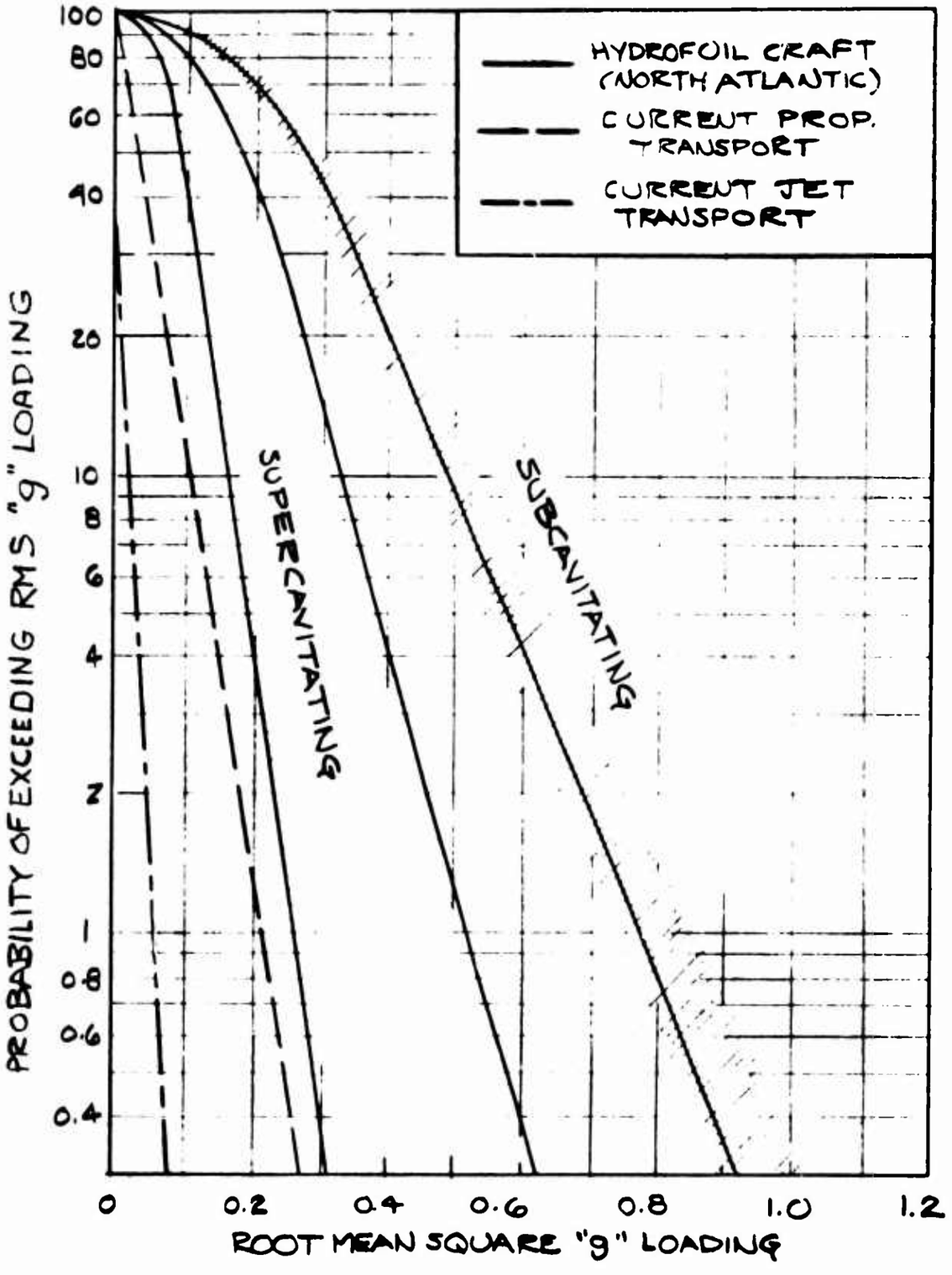

Figure 70: Statistical Dynamic Loading for Seacraft and Aircraft (Reference 46)

CASE	DIAGRAM	VERT. REACTIONS LBS.			TRANSLATIONAL 'G', FT/SEC^2			ROTATIONAL ACCL. RAD/SEC^2		
		BOW	MIDSHIPS	STERN	VERTICAL	LONGIT	TRANS.	PITCH	ROLL	YAW
1		67500	0	0	2.5	-1.0	0	6.0	0	0
2		45000	0	0	2.0	0	0	3.3	0	0
3		90000	0	0	3.0	0	0	6.0	0	0
4		67500	0	0	2.5	-1.0	±1.0	6.0	±2.0	±0.2
5	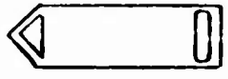	45000	0	45000	3.0	-1.0	0	0	0	0
6	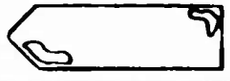	45000	0	45000	3.0	-0.5	0	0	0	±0.5
7		0	0	45000	2.0	-0.1	0	-3.0	0	0
8	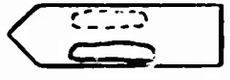	0	45000	0	2.0	-0.1	±0.5	0	±5.0	0
9		0	45000	0	2.0	-0.1	0	0	0	0
10	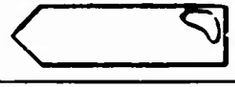	0	0	45000	2.0	-0.1	0	-3.0	±2.0	0

Figure 71: Forces and Acceleration on SKMR-1 (Reference 61)

The conclusions reached in Reference 61 were to a large extent based upon the results of Reference 18.

EVALUATION

General Structural Design Criteria

Most British and American designers have held the position that GEM design criteria and techniques are derivable from aircraft structural practice. This philosophy has been embodied in England in the tentative formulation of the British Civil Hovercraft Safety requirements. On the other hand, with the growing involvement of the U.S. Navy Bureau of Ships in the Hydroskimmer program, compromises between the aircraft practice and ship design practice can be expected.

The state of the art can be expected to grow very rapidly in this field in 1964, because of the availability of several machines (U.S. Navy SKMR-1, Vickers VA2 and VA3, Westland SR N2) for full-scale testing. It is not unreasonable to expect, therefore, that a set of specifications will be developed in the U.S. by some regulatory agency in the not-too-distant future.

Operating Life of a GEM

Estimates for the desired operating life of a GEM range from 2500 hours to 20,000 hours. The life of prototypes built until now has been considerably less than this figure.

Service life for structural design of transport aircraft is specified in Reference 5 as 20,000 flying hours and 15,000 flights and landings.

In Reference 26 the economics of a GEM are based upon an annual utilization of 3,000 hours yearly and an amortization period of 10 years.

In Reference 34, also for economic analyses, the assumption is made that the craft has a utilization of 2,000 hours yearly (at a block speed of 60 knots) and a service life of 10 years.

In conclusion, it appears justified to select a design life of 20,000 hours for a GEM.

LOAD ALLEVIATION

EXPECTED LOADING

The foregoing information concerning applied loads indicates that the open sea military GEM is expected to encounter twice the loadings expected to be encountered by the current generation of commercial passenger-carrying craft operating in sheltered areas. Indeed, the open sea conditions, except for crash situations, would be more severe than overland operating conditions. But regardless of the conditions encountered, whether on land or sea, all means must be continually developed and adapted to reduce impact. This effort would result in a reduction in design criteria, a consequent saving in structural weight with attendant increases in GEM payload, range, and general performance.

LOAD ALLEVIATION

Increase of Hover Height

Whether on land or at sea, an increase in the vehicle's hover height would decidedly reduce the frequency of encounter with obstacles over land and of wave impact at sea; either circumstance could cause serious applied loading conditions.

At the same time, however, an increase in hover height increases the chances for greater impact loadings during a crash by virtue of permitting higher forward speeds; also, if the engine fails, there is a greater (perhaps even uncontrolled) gliding range on a decaying cushion and a higher dropping distance if there is a sudden and complete loss of cushion pressure. Nevertheless, hover height increases should be sought, and some increase can be obtained through the use of skirts or trunks and through improvements in cushion system efficiencies.

Load alleviations may also be sought through improvements in bottom hull and bow design. Proper application of flare and dead-rise angles could be effective in minimizing cyclic impact with heavy seas. Finally, attention must be given to craft attitude prior to and during wave encounter. Pitch trim during cruise and especially during power failure conditions can be expected to influence impact loads at the bow.

Protective Structures

To reduce to some extent the impact forces which are likely to result from head-on collision on land or sea, from docking, or from lateral forces resulting from boarding or loading operations at sea, the use of bumper material, solid or pneumatic,

about the vehicle periphery seems advisable. Crushable material utilized over the bow area could alleviate numerous collision impacts expected during land operations by absorbing the impact energy and by reducing the local g loads. In addition to impact absorption, the force distribution over a larger area could neutralize the tendency for relatively sharp obstacle impact to puncture the bow plating, a condition least desirable during over-water operations. Perhaps a possibility exists in combining the concept of a peripheral pneumatic bumper with the skirt system. Crash padding on the inside is, of course, recommended for the protection of the vehicle's occupants.

Because GEM operations over land are largely to be conducted on unprepared surfaces, some sort of skid or pad-type multipoint suspension system would seem desirable for landing. Unless perhaps the bottom of the vehicle were solid and strong enough at all points to support the vehicle no matter how sharp the terrain and unless the bottom design were such as to permit the development of the lift cushion, the use of pneumatic-hydraulic oleo-type shock absorbers or even small rubber tires at landing support points would materially reduce any excess applied loads occurring at landing due to operator error or terrain hazard. For GEMs required to operate alternately from land and sea surfaces (i.e., amphibious GEMs), an inflatable-deflatable bag system would distribute and absorb the landing load impacts. This would be especially true at sea, where the bags would provide an added measure of buoyancy, plus support the vehicle structure somewhat above the sea surface, and thus prevent water from covering the cushion-producing nozzles or from entering the plenum and concurrently creating the initial volume beneath the vehicle for immediate cushion buildup.

Shock Mounting of Propulsion System

The loads applied to the main vehicle structure are transmitted to the vehicle propulsion system (i.e., to the engines, gearing, shafting, and the fans) if this system is mounted rigidly. Under the most severe conditions of wave impact, it is not unthinkable that these loads could impose design criteria on the fan which would result in excessively high fan weights. A possibility of reducing these loads, hence the fan weight, exists through the introduction of the proper shock mountings of the propulsion system. The discussion that follows is limited to a consideration of the possible alleviation of the loads applied on a radial fan system, such as the one described in this report.

Preliminary investigations indicated that not only would a "soft" mounting of the fan reduce the applied loads, but it would also eliminate dangerous resonance vibrations. A preliminary design made with the help of a representative from Lord Manufacturing Company indicated a load alleviation of up to 50 percent for transient loads. The particular design concerned a 12-foot-diameter fan, weighing an estimated 2000 pounds, rotating at 600 rpm; the applied load was 10 g at 5 - 10 cps for a 10-millisecond duration. It was found that each of the fan shock mounts selected to meet these requirements weighed 4 pounds. A 50-percent reduction of the applied loads at a cost of 16 pounds appears very attractive. This was accomplished without excessive excursions of the fan mass.

It is naturally impossible to draw general conclusions about the design of shock mounts for this type of application. Each design depends upon the particular configuration of the machine and the shape of the impact pulse. Some general rules for design are discussed in Reference 30. It is essential to know the duration of the impact. Very little information is presently available for GEMs. A very recent paper (Reference 33) states that the duration of the maximum recorded vertical accelerations on the Vickers VA 3 machine was 1/30th second.

Shock mounting appears attractive. There exists a trade-off between the fan system weight reduction and the applied load design criteria reductions resulting from the proper use and optimum choice of shock mounting.

Additional Considerations on Relief From Sea Impacts

With the open sea wave impact conditions likely to become the greatest and most serious contributor to applied loads, some means of load relief, in addition to those previously discussed, may be required. The condition of a GEM skimming over and perhaps contacting the tops of waves at very high speeds is not much different from the situation in which an aircraft finds itself when required to ditch at sea. Indeed the situation becomes even more analogous except for vehicle geometry and a reduction in forward speed if a GEM experiences power failure while moving at cruising speeds.

In Reference 27, NACA conducted ditching investigations with dynamic scale models of various aircraft configurations, both with and without the use of some ditching aids, as a means of improving ditching behavior. While this information is not directly applicable to open sea GEM operations, it nevertheless provides some trend information which the GEM engineer might consider from the standpoint

of possible reductions in the applied loads brought about by emergency conditions, during over-water operations.

The various aircraft models were tested in undamaged and simulated damaged conditions. Damage was simulated by the removal of parts (generally on the underside of the vehicle), such as access hatches, bomb doors, and landing gear doors. Under various conditions of speed and attitude, the simulated damaged models gave average longitudinal g loadings of double the loadings for the undamaged conditions and occasional maximum loadings of 4 times greater than the average in both the damaged and undamaged conditions.

The undamaged models generally pitched and ran smoothly, sustaining tolerable maximum longitudinal accelerations of up to 3 or 3.5 g's with the average from 1 to 1.5 g's except when in a low attitude and when presenting a rather blunt nose or jet airscoop. The damaged model not only sustained double the maximum and average g loads for the same speeds and attitudes but pitched, rebounded, dove, or turned abruptly in making its run. These differences and magnitudes in loadings and stability behavior would not normally be expected of flat-bottom GEMs as is reported in References 68 and 18. Some attention, however, must be paid to the design of the peripheral jet nozzles since they were found to act as scoops and thus to induce higher than average loading. Trends evident from aircraft ditching tests which contributed to reducing g loadings were:

1. Fuselages or appendages intact; no damage or loss of plating

2. Slower speeds on first contact

3. Higher attitudes in pitch on contact (not normally possible on GEMs but perhaps some form of control could be developed, i.e., sealing off rear cushion nozzles with complete reduction of air pressure while maintaining pressure from the forward nozzles only)

4. Incorporation of a hydroflap or hydroski at some position forward of the c.g. (maintains a pitch-up trim, reduces average longitudinal decelerations, reduces the number of stability motions essentially to one of pitch, reduces the length of run).

APPLIED LOADS ON RD FANS FOR DESIGN STUDIES

The previous chapter strongly suggests that identical load criteria should not be chosen for all types of GEMs. Small overland "demonstration" machines can be designed with little thought being given to load criteria, while open-ocean GEMs should be extremely sturdy.

Under the present contract, Aerophysics concentrated on the "median" size GEM, i.e., the 20- to 40-ton amphibian. Typical machines of interest in this category are shown schematically in Figures 72 to 74. Quite obviously, the applied load for which the fan must be designed will depend markedly upon the location of the fan within the machine. Since the fans are subjected to rotational as well as translational accelerations, the optimum location for the fans would be where the rotational accelerations subtract from translational accelerations. In most cases, this would correspond to a longitudinal location slightly aft of the center of gravity. Also, effects of roll would be minimized by placing the fans along the center line of the craft.

Under most circumstances, it is likely that considerations other than the minimization of the rotational accelerations will dictate the location of the fans within the machine. This should be taken into account in the determination of applied loads over the fan by assuming that the fan is likely to be within a certain area and that the applied loads correspond to the most extreme rotational accelerations within this area. In the present case, this area corresponds to the fan locations shown in Figures 72 to 74.

Using the information of this report, it is possible to establish tentative criteria for the applied loads for which the fans should be designed for an amphibious GEM in the 20- to 40-ton-gross-weight category. The load criteria suggested for the design of the RD fan are:

> Cruise or continuous operation, cyclic loads: $\pm$ 1 g (limit) vertical for 20,000 hours of operating life
>
> Impact (primarily hydrodynamic): $\pm$ 4 g's vertical; $\pm$ 5 g's (limit) horizontal
>
> Crash conditions required of the fan-bearing and bearing-support structures: 10 g's (ultimate) applied horizontally and vertically.

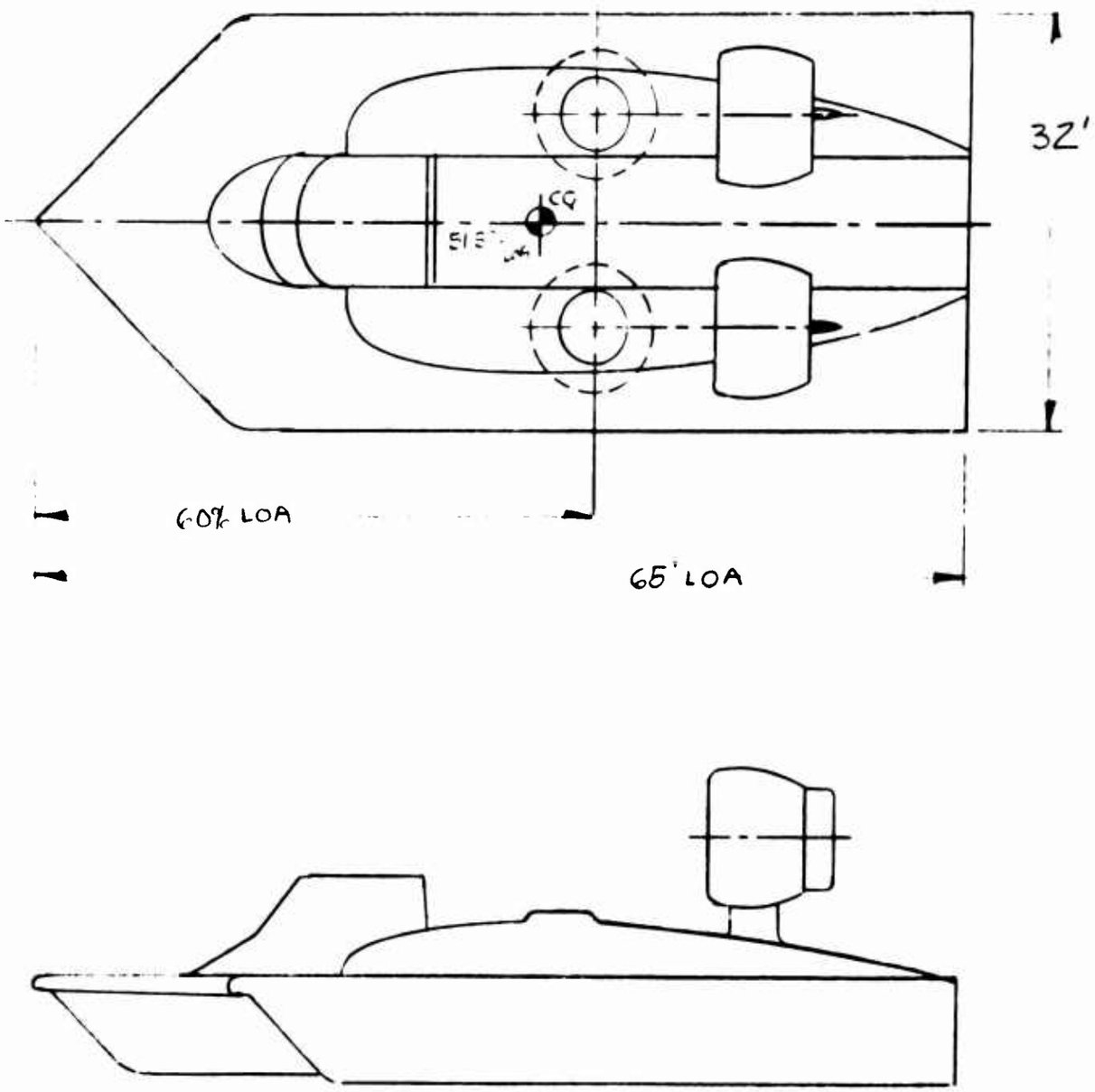

Figure 72: GEM RD Fan Arrangement, Based on Previous Design Studies, SKMR-1 Modified for 2 RD Fans

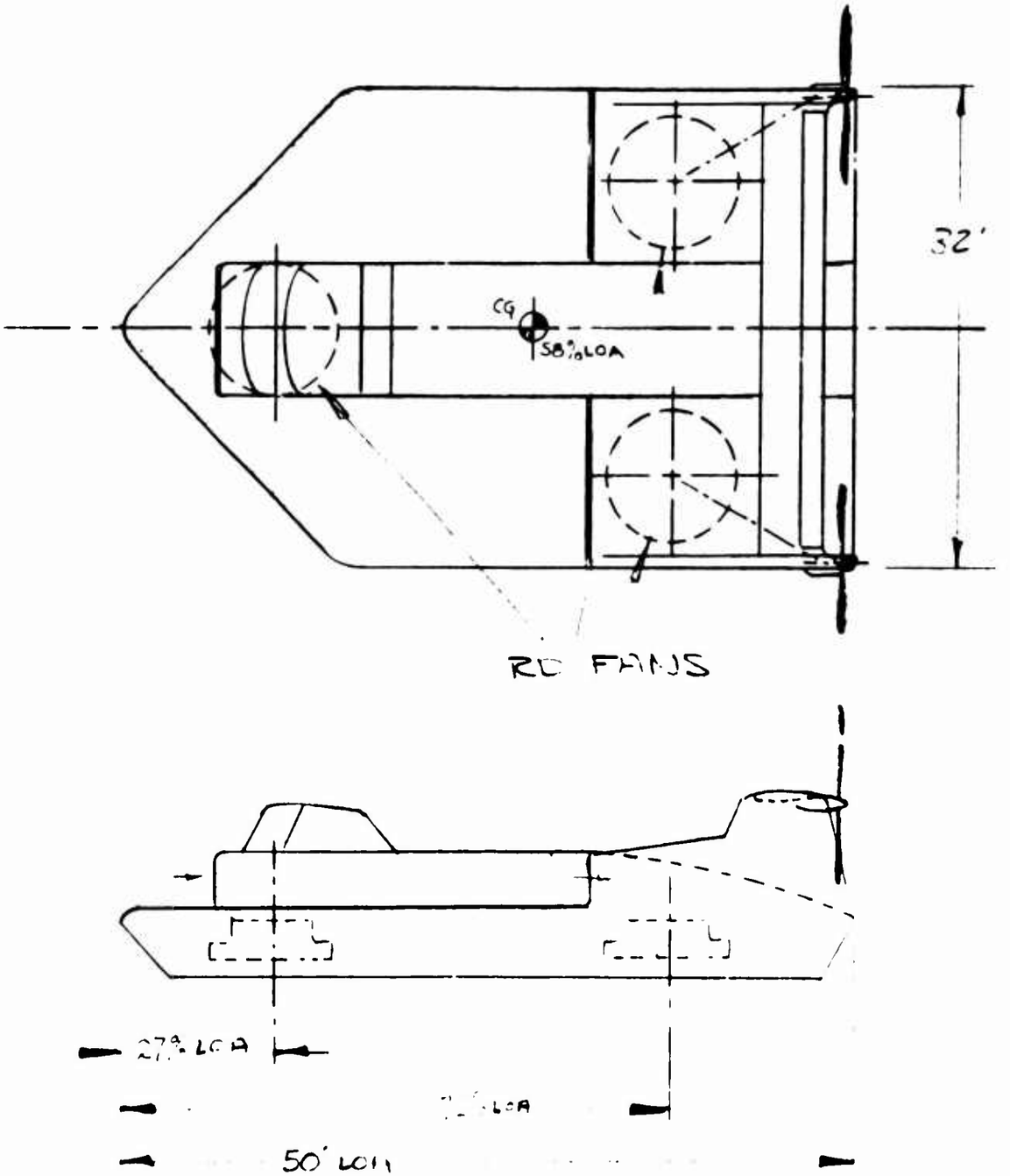

Figure 73: GEM RD Fan Arrangement, Based on Previous Design Studies, Amphibious Support GEM, 3 RD Fans

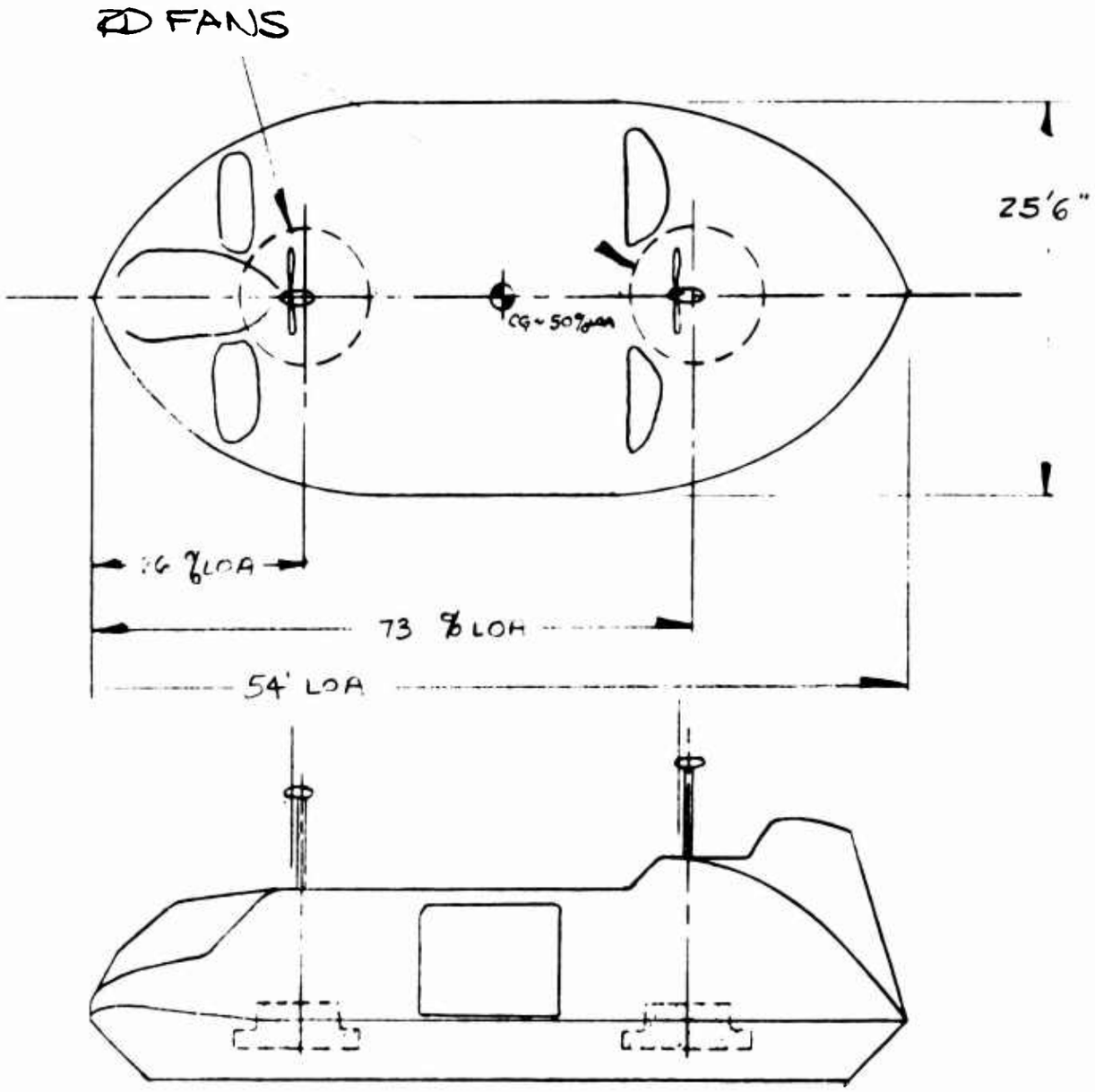

Figure 74: GEM RD Fan Arrangement, Based on Previous Design Studies, Amphibious Support GEM, 2 RD Fans

The above accelerations were obtained by adding linear and rotational accelerations. However, a secondary effect of rotational accelerations could be gyroscopic loads on the fan blades. Standard dynamic analyses which would account for the gyroscopic loads are not presently available. Therefore, at this time, gyroscopic loads are disregarded.

EVALUATION

1. In quality as well as in quantity, the amount of available information is going to continue to increase very rapidly in 1964, when the results of the tests of fairly large machines (U.S. Navy Hydroskimmer I, Vickers VA2 and VA3, Westland SRN2 and SRN3) will become available.

2. In spite of the great diversity in published applied load criteria and structural weights, it is possible to rationalize the design of GEMs by dividing them into three classes, based upon environmental and mission criteria.

3. Until more full-scale data become available, any presently-suggested criteria must be viewed with caution and updated at every available opportunity.

4. The establishment of specifications for structural design criteria either by governmental or by industrial groups is desirable and will probably be accomplished soon.

5. Alleviation of dynamic loads such as those created by the impact of waves at sea can be achieved in several ways and, when obtained, can result in weight savings for the craft.

RECOMMENDATIONS

It is recommended that:

1. Agencies or industry groups having a sincere interest in pursuing the development of ground effect machines for operational purposes establish or adopt, without excessive delay, a tentative and representative set of structural design criteria for their vehicles. (There are sufficient applied load data available to justify the present criteria. For GEM development in the United States to achieve future operational importance and economic practicality, this initial regulatory step is most important.)

2. All loads and load factors (except for the crash cases) for design criteria be specified as limit loads and that an ultimate load factor of 1.5 times the limit load factor be recommended.

3. Applied loads be determined for GEM vehicles in hover and in surface displacement condition on the basis of combined loading due to translational and rotational accelerations, for the maximum conditions of speed, vehicle attitude, and, when applicable, for sea-state and wave frequency encountered at or near the vehicle natural frequency in pitch and heave.

4. An operating life of 20,000 hours be established for the vehicle structure and the components of the lift and propulsion systems.

5. The first operational vehicles in their respective media be continuously instrumented to record "g" history in magnitude and duration, the results to be used in establishing the much-needed structural design criteria, because of the lack of present true applied-load information for either land or sea operations.

6. Vehicles be equipped with some system to achieve a quick controlled stop while settling to the surface on a decaying cushion, since GEMs tend to glide a good distance on cushion decay when engine failure occurs at high forward speed. Tail-first landings are desirable.

7. Specific analytic studies be initiated regarding the reduction of crash and severe impact forces. Proper bow and hull bottom design and the application of frangible or deliberately deformable surfaces and structures at the expected points of impact should materially reduce the forces transmitted to the occupants and components within the vehicle.

8. A series of high-speed ditching model tests be performed to determine the proposed vehicle's landing qualities in a given sea state under emergency conditions as part of future contractual requirements for amphibious GEMs.

9. Attention be directed to possible savings which can be effected through load alleviation in conjunction with vigorous programs of vehicle weight reduction.

DISTRIBUTION

U. S. Army Materiel Command	7
U. S. Army Mobility Command	4
U. S. Army Aviation Materiel Command	4
U. S. Strike Command	1
Chief of R&D, D/A	2
U. S. Army Transportation Research Command	69
U. S. Army Research and Development Group (Europe)	2
U. S. Army Engineer Research and Development Laboratories	4
U. S. Army Human Engineering Laboratories	1
Army Research Office-Durham	2
U. S. Army Polar Research and Development Center	1
U. S. Army Medical Research and Development Command	1
U. S. Army Engineer Waterways Experiment Station	1
U. S. Army Combat Developments Command Transportation Agency	1
U. S. Army War College	1
U. S. Army Command and General Staff College	1
U. S. Army Transportation School	1
U. S. Army Tank-Automotive Center	2
U. S. Army Arctic Test Center	1
U. S. Army General Equipment Test Activity	1
U. S. Army Airborne, Electronics and Special Warfare Board	1
Chief of Naval Operations	1
Bureau of Ships	1
Bureau of Naval Weapons	2
Bureau of Supplies and Accounts, N/D	1
U. S. Naval Supply Research and Development Facility	1
U. S. Naval Postgraduate School	1
David Taylor Model Basin	1
Marine Corps Landing Force Development Center	1
Marine Corps Educational Center	1
Ames Research Center, NASA	2
NASA-LRC, Langley Station	2
Lewis Research Center, NASA	2
NASA Representative, Scientific and Technical Information Facility	2
Human Resources Research Office	2
U. S. Army Standardization Group, Canada	2

Canadian Liaison Officer,	
U. S. Army Transportation School	3
British Army Staff, British Embassy	4
U. S. Army Standardization Group, U. K.	1
Defense Documentation Center	10
U. S. Government Printing Office	1

Aerophysics Company, Washington, D.C., 20036, A STUDY OF RADIAL-FLOW FANS FOR GEM PROPULSION SYSTEM APPLICATIONS - G.D. Boehler, W. Foshag, J.S. Karwoski, J.A. Balciunas, J.E. Lieser, W.P. Schwanke, and W.W. Olson. TCREC Technical Rept. 64-33, July 1964, 203 pp. (Contract DA 44-177-AMC-886 T) USA TRECOM Task ID 021701A 04809

Unclassified Report

The overall results of a study of the application of rotating-diffuser centrifugal

1. Radial-Flow Fans, Application to Ground Effect Machines
2. Internal Flow Aerodynamics, Ground Effect Machines
3. Ground Effect Machines
4. Contract DA 44-177-AMC-886(T)

Aerophysics Company, Washington, D.C., 20036, A STUDY OF RADIAL-FLOW FANS FOR GEM PROPULSION SYSTEM APPLICATIONS - G.D. Boehler, W. Foshag, J.S. Karwoski, J.A. Balciunas, J.E. Lieser, W.P. Schwanke, and W.W. Olson. TCREC Technical Rept. 64-33, July 1964, 203 pp. (Contract DA 44-177-AMC-886 T) USA TRECOM Task ID 021701A 04809

Unclassified Report

The overall results of a study of the application of rotating-diffuser centrifugal

1. Radial-Flow Fans, Application to Ground Effect Machines
2. Internal Flow Aerodynamics, Ground Effect Machines
3. Ground Effect Machines
4. Contract DA 44-177-AMC-886(T)

Aerophysics Company, Washington, D.C., 20036, A STUDY OF RADIAL-FLOW FANS FOR GEM PROPULSION SYSTEM APPLICATIONS - G.D. Boehler, W. Foshag, J.S. Karwoski, J.A. Balciunas, J.E. Lieser, W.P. Schwanke, and W.W. Olson. TCREC Technical Rept. 64-33, July 1964, 203 pp. (Contract DA 44 177-AMC-886 T) USA TRECOM Task ID 021701A 04809

Unclassified Report

The overall results of a study of the application of rotating-diffuser centrifugal

1. Radial-Flow Fans, Application to Ground Effect Machines
2. Internal Flow Aerodynamics, Ground Effect Machines
3. Ground Effect Machines
4. Contract DA 44-177-AMC-886(T)

Aerophysics Company, Washington, D.C., 20036, A STUDY OF RADIAL-FLOW FANS FOR GEM PROPULSION SYSTEM APPLICATIONS - G.D. Boehler, W. Foshag, J.S. Karwoski, J.A. Balciunas, J.E. Lieser, W.P. Schwanke, and W.W. Olson. TCREC Technical Rept. 64-33, July 1964, 203 pp. (Contract DA 44-177-AMC-886 T) USA TRECOM Task ID 021701A 04809

Unclassified Report

The overall results of a study of the application of rotating-diffuser centrifugal

1. Radial-Flow Fans, Application to Ground Effect Machines
2. Internal Flow Aerodynamics, Ground Effect Machines
3. Ground Effect Machines
4. Contract DA 44-177-AMC-886(T)

fans (RD fans) as air movers to peripheral-jet ground effect machines (GEMs) are presented. The overall investigation consists of aerodynamics, structural, fabrication, and design studies.

It is concluded that RD fans are well suited to GEM applications, because of high aerodynamic efficiency, low weight, and operational advantages such as sturdiness and quietness.

fans (RD fans) as air movers to peripheral-jet ground effect machines (GEMs) are presented. The overall investigation consists of aerodynamics, structural, fabrication, and design studies.

It is concluded that RD fans are well suited to GEM applications, because of high aerodynamic efficiency, low weight, and operational advantages such as sturdiness and quietness.

fans (RD fans) as air movers to peripheral-jet ground effect machines (GEMs) are presented. The overall investigation consists of aerodynamics, structural, fabrication, and design studies.

It is concluded that RD fans are well suited to GEM applications, because of high aerodynamic efficiency, low weight, and operational advantages such as sturdiness and quietness.

fans (RD fans) as air movers to peripheral-jet ground effect machines (GEMs) are presented. The overall investigation consists of aerodynamics, structural, fabrication, and design studies.

It is concluded that RD fans are well suited to GEM applications, because of high aerodynamic efficiency, low weight, and operational advantages such as sturdiness and quietness.